NEW INSIGHTS INTO THE BLADE MISTUNING PROBLEM

A thesis submitted for the degree of

Doctor of Philosophy

by

MARIJA NIKOLIC

MEng, BA, Engineering, University of Cambridge, 2002

Department of Mechanical Engineering

Imperial College London / University of London

August, 2006

Abstract

An attempt is made in this thesis to shed new light on the blade mistuning problem, which has defiantly opposed a ‘solution’. The fundamental problem with blade mistuning stems from the fact that small blade-to-blade variations, due to practically unavoidable manufacturing tolerances and wear, produce large uncertainty in the forced response levels of bladed discs. This is a phenomenon that often results in one or more blades experiencing excessive vibration levels, sometimes leading to catastrophic high-cycle fatigue failures. For this reason, the mistuning problem has been the focus of attention by many researchers for the past four decades. Although knowledge on mistuning has been continuously enriched since the late 1960s, the ill-effects of mistuning have still not been successfully eliminated.

This research commences by tracing the real roots of the mistuning problem by presenting a philosophical debate on mistuning. As a result, so-called “critical outstanding mistuning questions” are identified in an attempt to bridge the existing gap between academic and industrial concerns. The approach chosen in this study is to raise new questions to revisit old mistuning problems in a new, illuminating way. In the light of this, the work reported in this thesis is split into three parts. The first challenges the conventional belief commonly accepted in bladed disc analysis with regard to the effect of Coriolis forces in an effort to improve the fundamental model used in analysis. Experimental validation of predictions including the previously-neglected Coriolis effect using a carefully-designed testpiece serves to provide indisputable evidence of the influence of Coriolis forces. This result prompts a unique numerical study of mutual influence of Coriolis forces and blade mistuning on forced response characteristics, revealing that there are particular bladed disc designs where the Coriolis forces cannot be neglected due to their non-trivial impact on maximum amplification factors, contrary to a current belief.

With an aim of establishing whether the recent trends to relax manufacturing tolerances could be used effectively to reduce and control the maximum forced response levels, two strategies based on new “large mistuning” concept are introduced in the second part of the thesis. The first of them, involving a statistical study with extensive Monte Carlo simulations, demonstrates the benefits of such a scheme on an industrial bladed disc. Subsequently, a few favourable deterministic patterns of unconventionally large mistuning strengths are explored and their sensitivity and robustness assessed. It is shown that the latter is of utmost importance in gauging the usefulness of design.

The final part of the thesis attempts to make generalisations about bladed disc vibration problems by discussing lessons learned from the specific cases studied and by anticipating future developments, trends and philosophy. Results obtained provide solid ground for deeper understanding of the blade mistuning problem and for effective ways of preventing (rather than curing) it, which are believed to be beneficial for industry.

Acknowledgements

I am awed and pleasantly overwhelmed by the wealth of knowledge and inspiration provided by my supervisor, Prof. David J. Ewins, with whom it was my great honour and privilege to work with. I would like to thank him for giving me this unique opportunity to experience research, one of the most exciting journeys of my life. Not only his ideas and guidance throughout this endeavour, but also projection of his impeccable command of English language and his advice on lucid and concise writing, attention to detail and continuous enthusiasm that contributed appreciably to the accomplishment of this thesis.

I would particularly like to express my gratitude to Dr. Evgeny P. Petrov for his relentless eagerness to help and patience during the last few years, especially with the technical issues. His formidable expertise, active interest, invaluable time and incisive criticism provided constant impetus for this work and numerous possibilities to learn.

I am grateful to many past and present members of Imperial College Dynamics Section for their advice, fruitful discussions and favourable disposition. Among those, the contributions from Dr. S. Malpede, Dr. G. Chen and Mr. A. Stanbridge are duly recognised. Special thanks are also to our Section's technicians, Mr. J. Miller and Mr. P. Woodward, for their skills and assistance during brief experimental work. Mrs. M. Wright and Ms. N. Hancock are remembered for their friendliness and efficiency in administrative matters.

I wish to say a word of thanks to my colleague and friend, Mr. Dario Di Maio, for providing experimental results to validate theoretical predictions described in Chapters 4 and 5 of this thesis.

I am delighted to be among many good friends – Mr. Sen Huang, Dr. Enrique Gutierrez-Wing, Mr. Ivan Sladojevic, Dr. Hugo Elizalde Siller, Dr. Matthew Cand and Dr. Ibrahim Sever – who made my time at Imperial College especially memorable.

I would like to acknowledge technical support at various stages of this project from Rolls-Royce Plc. A valuable input from Mr. Norbert Kill from SAMTECH S.A. is appreciated in providing a numerical code for a study of effects of Coriolis forces in bladed disc vibration analysis.

Finally, I would like to thank my parents, Zivko and Dragica, for igniting in me a passionate pursuit of knowledge and emphasis on education, but above all, for their love and support.

Marija Nikolic

To my Parents,

with love and admiration

Contents

Nomenclature

Latin symbols

N	Number of blades in the assembly
t	Time
r , θ	Polar coordinates
n , s	Numbers of nodal diameters and nodal circles
$\{q\}$	Response of the system
$\{f\}$	Vector of applied forces
$[M]$	Mass matrix
$[K]$	Stiffness matrix
$[C]$	Viscous damping matrix
$[D]$	Structural (hysteretic) damping matrix
$[G]$	Skew-symmetric matrix due to Coriolis forces
$[K_S]$	Stress stiffening matrix due to centrifugal forces
$[S]$	Spin softening matrix
n	Number of modes
k	Number of bins in histogram
$\tilde{m}_x$	Data mean
$\tilde{D}_x$	Data variance
$\tilde{a}_x$	Third moment about the mean
$\tilde{e}_x$	Fourth moment about the mean
H_0	Null hypothesis
H_1	Alternative hypothesis

Greek symbols

$\phi_{n,s}^{\cos}$, $\phi_{n,s}^{\sin}$	Mode shapes of bladed disc expressed in polar coordinates
Ω	Rotation speed
λ	Eigenvalue
ψ	Eigenvector
ω	Frequency of excitation
γ	Coupling parameter
η	Damping loss factor
$\tilde{\sigma}_x$	Data standard deviation
χ_α	Chi-Square test statistic
λ_α	Kolmogorov-Smirnov test statistic

Other symbols and operators

$\{\ \}$	Vector
$[\ ]$	Matrix
$[\ ]^{-1}$	Matrix inversion
$[\ ]^{T}$	Matrix transpose
$\{\bar{\ }\}$	Complex conjugation

Abbreviations

HCF	High-cycle fatigue
LPM	Lumped parameter model
FE	Finite element
ROM	Reduced order model
EO	Engine order (excitation)
1F	First bending mode family
MC	Monte Carlo simulations
PDF	Probability density function
CDF	Cumulative distribution function
DOF(s)	Degree(s)-of-freedom
+C	with Coriolis forces
-C	without Coriolis forces
ND	Nodal diameter
BW	Backward travelling wave
FW	Forward travelling wave
LDV	Laser Doppler Velocimeter
SLDV	Scanning Laser Doppler Velocimeter
FFT	Fast Fourier Transform
FRF	Frequency response function
T	Vibration period
ref.	Reference mistuning pattern
T, SM, LM	Tuned, small mass, large mass
LM	Large mistuning

List of figures

List of tables

CHAPTER 1

Introduction

"Prevention is better than cure"

Desiderius Erasmus

1.1 The blade mistuning problem: historical perspective and facts

In the late 1960s, a new term "mistuning" was added to the vocabulary of turbomachinery practitioners. After more than four decades, it should be noted that the blade mistuning problem:

… persistently appears on more than 350 publications devoted to studies of dynamics and vibration of bladed discs, such as those in turbines, fans and compressors of aero engines;

… relentlessly causes a stir in the major worldwide annual technical congress and exposition (ASME TURBO EXPO) in the gas turbine community;

… has been one of the key topics of the National Turbine Engine High Cycle Fatigue (HCF) Science and Technology (S&T) Program during 1995-2005, an effort from the US government, industry and academia;

… defiantly opposes a 'solution' and continues to challenge researchers and engineers from the world-leading aero engine designers and manufacturers, such as Rolls-Royce, Pratt & Whitney and GE.

Mistuning is a term adopted to designate the small blade-to-blade variations in geometric and material properties, which are unavoidable in all practical bladed discs due to manufacturing and assembly tolerances and non-uniform wear during service. To shed some light on why, after so many years of research, mistuning is still on the agenda, it is necessary to establish its fundamental role in aero engine dynamics. A tremendous interest in the mistuning phenomenon can be attributed to its detrimental influence on bladed disc high-cycle fatigue (HCF) life and, consequently, to its negative impact on durability and reliability of the aero engine itself. HCF failures result from excessive blade vibration cycles, exacerbated by mistuning and aeromechanical sources, as thousands of cycles accumulate rapidly due to high rotation speeds of the engines. HCF has historically led to the premature failure of major aero engine components, and in rare cases has resulted in the loss of the engine and the entire aircraft. The National HCF S&T Program team estimates the cost of HCF at over $400 million per year[1].

"Suppression of vibratory fatigue"[2] is as much a design challenge today as it was when acknowledged in 1967 by Clarence Danforth, motivating researchers to obtain a better grasp of the phenomena leading to HCF and to seek new ways of preventing them.

1.2 Definition of the problem

The fundamental blade mistuning problem, illustrated in Fig. 1-1, stems from the fact that unavoidable (but generally small) blade-to-blade variations produce very large uncertainty in the forced response levels of bladed discs, which, in extreme cases, can lead to a catastrophic HCF failure.

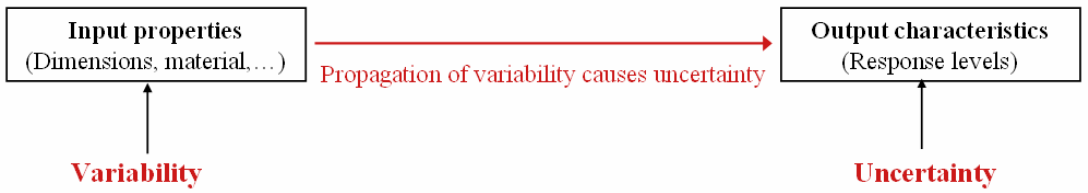

Fig. 1-1. Fundamental blade mistuning problem

[1] Garrison, B., 2000, "High-cycle fatigue (HCF) science and technology program 2000 Annual Report"
[2] Danforth, C.E., 1967, "Designing to Avoid Fatigue in Long Life Engines", *Society of Automotive Engineers Transactions*, Vol. 75, Sec. 2, New York, pp. 248-262

For this reason, the blade mistuning problem has been the focus of attention for many researchers for almost forty years, and indisputably, considerable progress has been made on the subject in that time. Numerous studies have contributed to encapsulate the physics of the mistuning phenomenon and its impact on the vibration characteristics of bladed discs. Diverse strategies have been suggested to circumvent the consequences of mistuning, yet the fundamental practical problem has not been resolved successfully. This paradox raised a suspicion that much of the past research effort might have been conducted in 'inappropriate' directions, leading to ever-improved understanding but *not* to solution of the problem. Moreover, a need was identified to establish the extent to which blade mistuning still poses a problem by contrasting the current academic endeavours and the industry requirements and efforts.

1.3 Philosophy and objectives of the research

The philosophy adopted in this research is to gain new insights into the blade mistuning problem by raising new questions seeking to address old mistuning problems from a new angle, as opposed to attempting to obtain 'correct' answers to the existing issues. With an emphasis on prevention of the mistuning problems, rather than curing the consequences, "critical outstanding mistuning questions" will be identified and addressed, which aim to merge the academic and industrial concerns and to identify their 'intersection plane'. This idea has fuelled the hope that realistic answers to the high-level questions will provide a useful contribution to a deeper understanding of how to deal efficiently with blade mistuning and to preclude its adverse effects, thereby reducing the occurrence of the HCF incidents in bladed discs, improving the reliability of the aero engine, and establishing the best strategies in practice, which are immensely beneficial for the engine industry designers.

With an ultimate aim of bringing new ideas and insights to regard the long-standing blade mistuning problem, the specific objectives of this study are:

- to establish the extent to which the blade mistuning still remains a problem in modern turbomachinery;
- to improve the fundamental bladed disc model used in analyses by including previously-neglected effects of Coriolis forces;

- to validate experimentally the predictions and to obtain an evidence of the importance of influence of the newly incorporated effects of Coriolis forces;
- to assess the mutual interaction of blade mistuning and Coriolis forces on vibration properties of bladed discs in order to determine, for the first time, whether contemporary mistuned bladed disc analyses should incorporate Coriolis forces so as to represent accurately all the significant factors that affect the forced response levels;
- to develop strategies for maximum forced response reduction and control based on the new "large mistuning" concept, and to assess their effectiveness;
- to discuss possibilities to generalise on blade mistuning problem from the specific cases addressed in this thesis.

1.4 Overview of the thesis

The chart shown in Fig. 1-2 summarises the contents of this thesis, which is an attempt to revisit the blade mistuning problem from a fresh perspective.

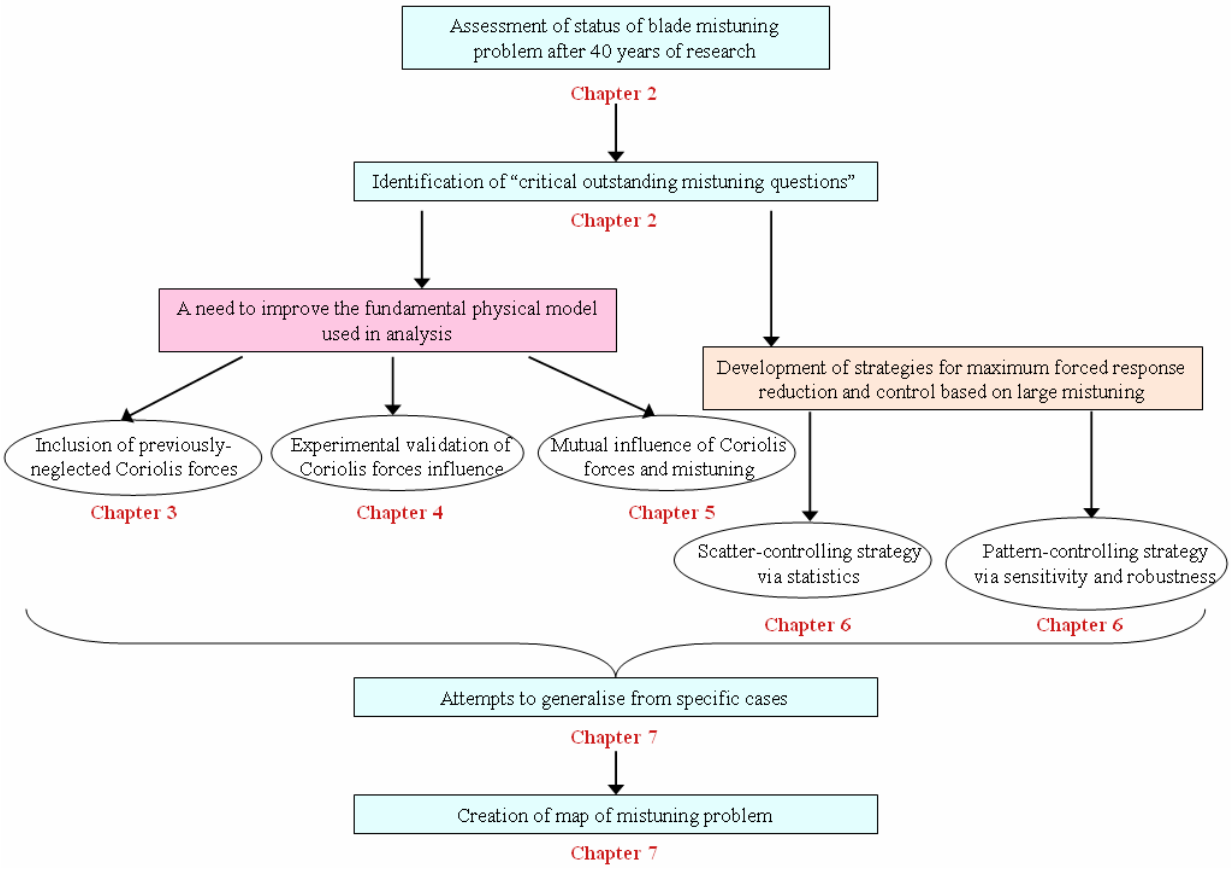

Fig. 1-2. Thesis contents

Chapter 2 presents a philosophical debate-style literature review with an aim to assess the extent to which blade mistuning still poses a problem. As a result, the current trends, prediction capabilities and controversial issues surrounding the blade mistuning phenomenon are unveiled to lead to the identification of so-called “critical outstanding mistuning questions”, some of which form the constituent parts of this thesis, in an attempt to prevent the mistuning-related problems, rather than to cure their consequences.

Motivated by a need to improve the fundamental physical model, Chapter 3 introduces the effects of Coriolis forces, in spite of their routine omission in traditional analyses of bladed discs. For the first time, the significance of incorporating these forces is demonstrated by presenting a theoretical account and several numerical examples of their influence on the vibration properties of tuned bladed discs. Subsequently, a need is identified for experimental validation of the effects of Coriolis forces, the successful implementation of which would increase confidence in the improved model and provide a base for further analysis. The impact of Coriolis forces with regard to current design trends and their critical interaction with blade mistuning is discussed.

In Chapter 4, the influence of Coriolis forces on nominally-tuned bladed disc vibration characteristics is validated experimentally using a carefully-designed testpiece. A state-of-the-art measurement technique and a non-conventional excitation system are employed to facilitate an unambiguous observation of the resulting non-trivial Coriolis forces effect. The implication of results and their influence on realistic bladed discs is established.

Chapter 5 is an ultimate attempt to determine whether current bladed disc analyses should include the Coriolis forces in order to represent accurately all the significant factors that affect the forced response levels. In the first part of the Chapter 5, a mathematical model of a bladed disc with a capability to simulate weak to strong Coriolis forces coupling is developed in order to assess the mutual influence of blade mistuning and Coriolis forces on forced response amplification factors. In the second part of Chapter 5, the results are presented from the experimental investigation of mutual interaction of Coriolis forces and deliberately introduced mistuning using a testpiece described in Chapter 4. Finally, some conclusions are drawn based on the evidence shown on the importance of considering the Coriolis forces in forced response analyses of mistuned bladed discs.

In an effort to prevent the HCF failure by controlling uncertainty of the vibration levels, a novel maximum forced response reduction strategy based on large mistuning concept is introduced in Chapter 6 with the application to an industrial fan bladed disc. The reliability of the random (or “scatter-controlling”) and the deterministic (or “pattern-controlling”) approaches, stemming from unconventionally large mistuning strengths, is assessed using two well-established tools for uncertainty analysis: (i) the statistics and (ii) the sensitivity and robustness. Feasibility and practical aspects of introduction of large mistuning as a means of maximum forced response control strategy are discussed.

In Chapter 7, an overview of the blade mistuning problem today is presented by summarising the lessons learned from specific cases studied in this thesis and from well-established mistuning facts. As a result, a “mistuning problem map” is created, which indicates the key factors that affect the maximum forced response amplification and their mutual interaction. Finally, some thoughts are dedicated to anticipation of future developments, trends and philosophy of the mistuned bladed disc vibration problems.

The thesis contributions, overall conclusions and recommendations for future research are succinctly outlined in Chapter 8. The details of publications of the thesis work are also given.

CHAPTER 2

Philosophical Debate On Mistuning And Literature Review

"…No single thing is to be found in it [philosophy] which is not subject of dispute, and in consequence which is not dubious…"
Rene Descartes
Discourse on the Method of Rightly Conducting the Reason and Seeking for Truth in the Sciences

2.1 Overview

This chapter endeavours to trace the roots of the long-standing blade mistuning problem by presenting a philosophical debate-style literature review on mistuning. With the aim to assess the extent to which mistuning still remains a problem after more than 40 years of research, carefully-selected studies will be classified and critically reviewed (i) to reveal current trends, prediction capabilities and controversial issues surrounding the blade mistuning problem, (ii) to 'map' the mistuning field, and (iii) to position this research within an appropriate context. The approach chosen in this study was to raise new questions to revisit old mistuning problems in a new, illuminating way. As a consequence, so-called "critical outstanding mistuning questions" will be postulated in an effort to bridge the gap between academic and industrial concerns, the solution to which might lead to a deeper understanding of the blade mistuning problem, and how to resolve it.

It should be noted that it is not intended here to summarize all existing mistuning publications (for this purpose, the reader is referred to several comprehensive surveys available in the published literature, such as [1]-[3]), but rather to support an argument, from which the constituent components of this study evolve logically in an attempt to provide new insights into effective ways of preventing the blade mistuning problem, rather than curing it.

2.2 Debate theme and structure

Blade mistuning has been extensively researched since Tobias and Arnold's [4], Whitehead's [5] and Ewins' [6] pioneering works in the 1960s, which shed light on the underlying physics of the problem. Since then, a considerable effort has been directed toward enriching the knowledge of the vibration characteristics of mistuned bladed discs and developing new perspectives and formulations to circumvent the mistuning problem, contributing to more than 350 publications over the past four decades. However, in spite of constant improvements and sophisticated methodologies used to address the problem, the ill-effects of blade mistuning have still not been successfully eliminated, and the turbomachinery blades nevertheless continue to vibrate and to fail, industry-wide. For this reason, the principal theme of debate can be formulated as:

Why, after so many years of research, has the blade mistuning problem still not been fully resolved? Is the present research effort being conducted in the 'appropriate' directions? Are we addressing the 'right' questions?

Of particular interest to the argument are the works carried out in the post-1990 period. However, a brief history of some fundamental studies performed in the 'early' years will be mentioned initially for the sake of completeness. The ultimate aim of the debate is to lead to identification of the "critical outstanding mistuning questions", several of which will be addressed in this thesis.

2.3 Status of mistuning after 40 years of research

2.3.1 Brief history of the 'early' mistuning studies (pre-1990)

The mistuning studies conducted prior to 1990 primarily served to provide a thorough analysis of the physics of the mistuning phenomenon, and they were generally divided into two distinctive groups. The first addressed the structural aspects, related to determination of the forced response characteristics of mistuned bladed discs, initiated after the publication by Tobias and Arnold [4] in 1957, which investigated the influence of dynamical imperfections on the vibration of rotating discs. Since then, it is possible to cite at least 60 significant research papers published prior to 1990, among which are [5]-[21]. The second group considered the aerodynamic aspects, attempting to understand the mechanism of flutter and its interaction with mistuning: [22]-[29]. The characteristic feature of the 'early' years

of mistuning prediction methods is attributed to the study of the mistuning phenomenon by the vast majority of researchers within a deterministic framework, via use of simple few degrees-of-freedom lumped parameter mass-spring models (LPMs). Statistical methods have been applied to the analysis of mistuned bladed discs in only few studies ([11], [16], [19], [30], [31]). In spite of the use of such restricted models to represent the bladed disc dynamics, and limited resources, many of the above-mentioned studies have established solid foundations for further developments of understanding of the mistuning phenomena, motivated by major computational advances in the post-1990 period.

2.3.2 Contemporary mistuning studies (post-1990)

2.3.2.1 'Literature tree' and current capabilities in relation to mistuning problem

Contemporary mistuning studies are represented in the form of a 'literature tree', illustrated in Figs. 2-1 and 2-2, which gives a comprehensive overview of the major areas of investigations and developments of the most significant researcher clusters since 1990. As for the 'early' mistuning studies, we observe a general classification into structural coupling methods for forced response predictions of mistuned bladed discs, incorporating deterministic and statistical approaches, and aerodynamic methods for turbomachinery applications. The evolution of a vast amount of studies is shown, among which there are papers concerned with (i) the exploration of general vibration characteristics of mistuned bladed discs, with a concentrated research effort toward producing the so-called "reduced order models" (ROMs), to allow extensive computations with realistic finite element (FE) bladed disc models; (ii) modelling and incorporating friction dampers in bladed discs, in order to reduce the maximum vibration levels experienced by blades; modelling the effects of (iii) cracks and (iv) shaft-bladed disc interaction; (vi) conducting experiments aimed mainly at validating the prediction codes, and (vii) the analysis of mistuned bladed discs with aerodynamic coupling and flutter assessment. The most noteworthy studies on mistuning are highlighted and grouped into 'families', according to their association with research centres.

A supplementary map of mistuning research areas is represented in Fig. 2-3.

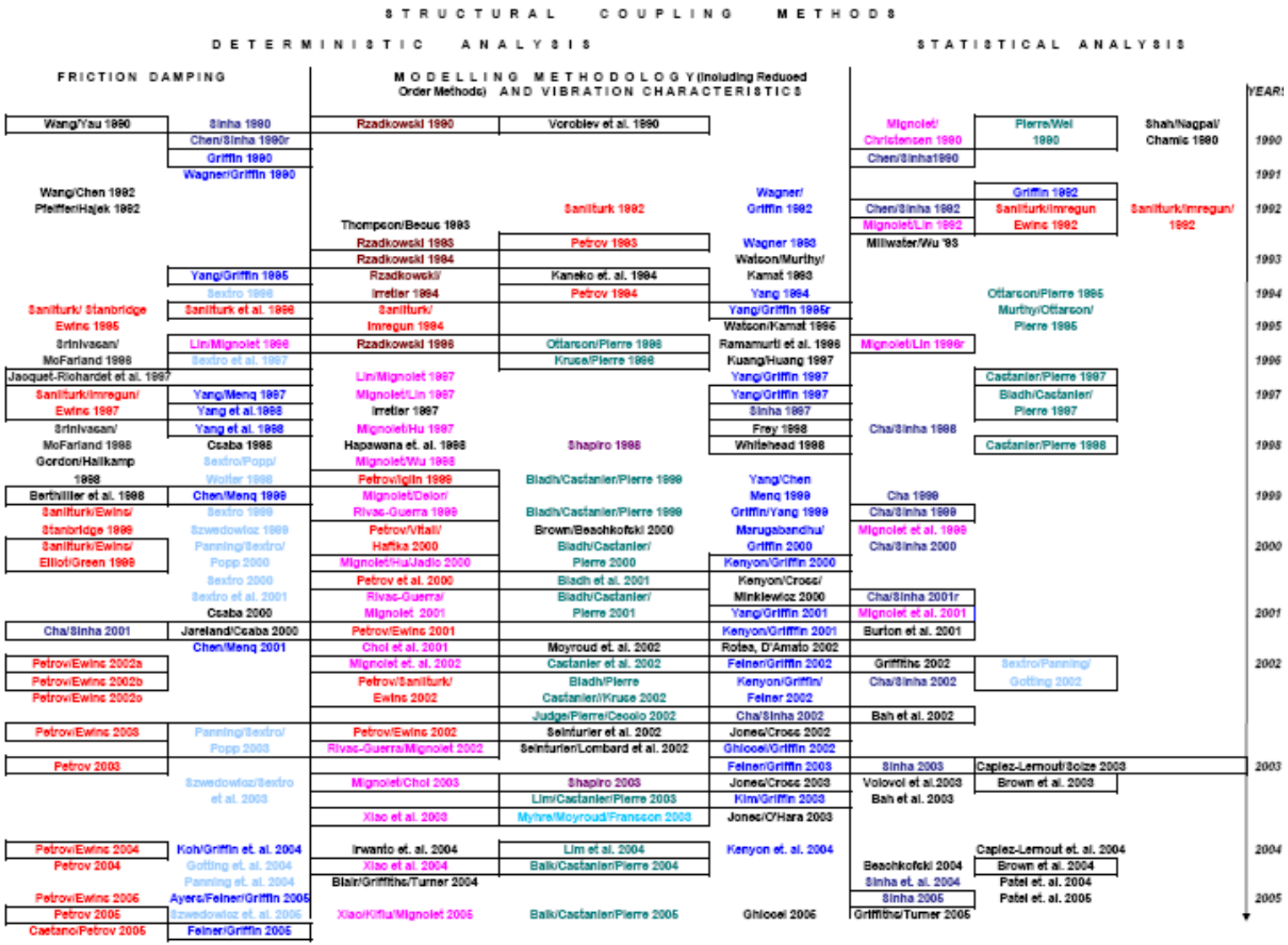

Fig. 2-1. Literature tree part 1

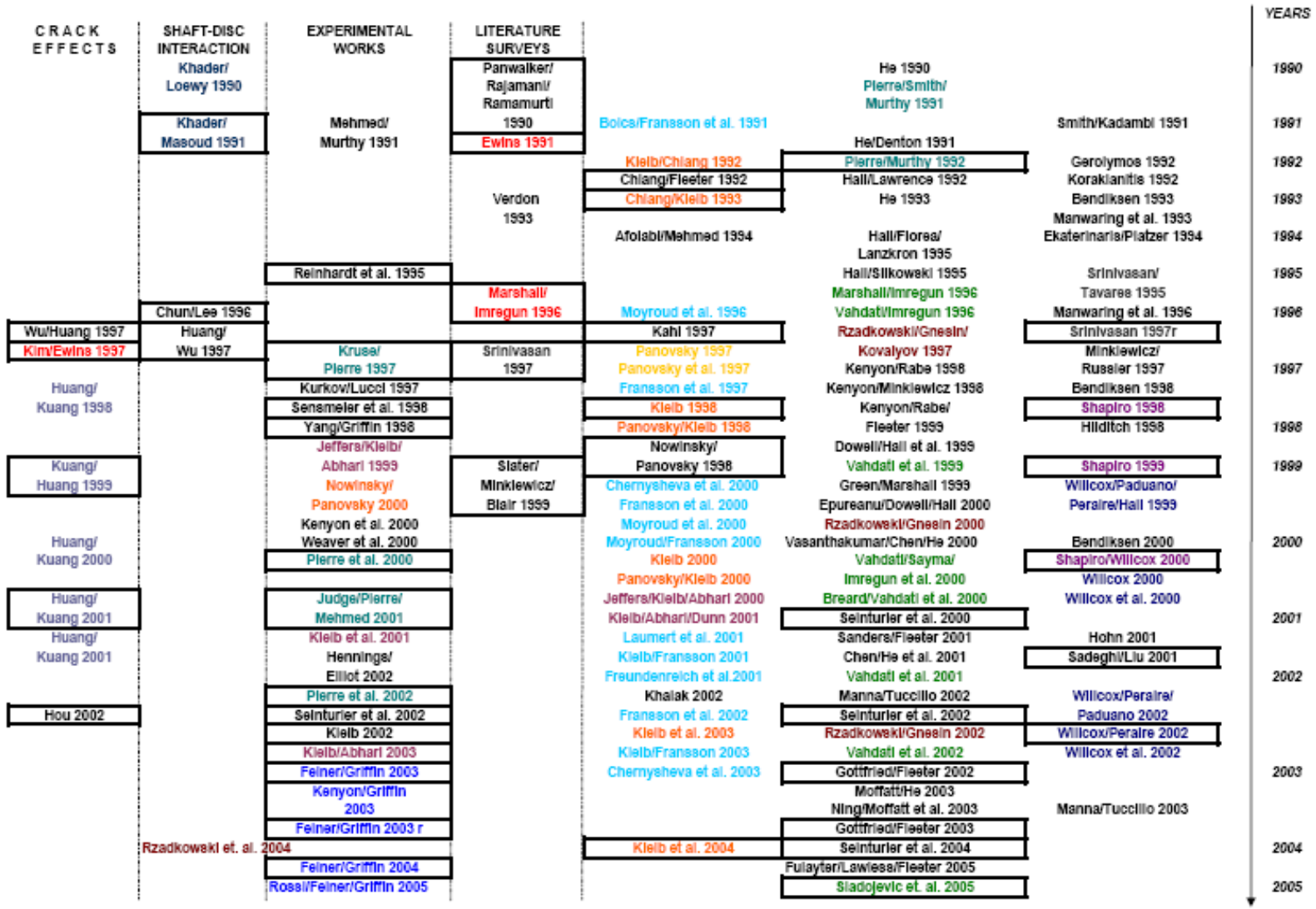

Fig. 2-2. Literature tree part 2

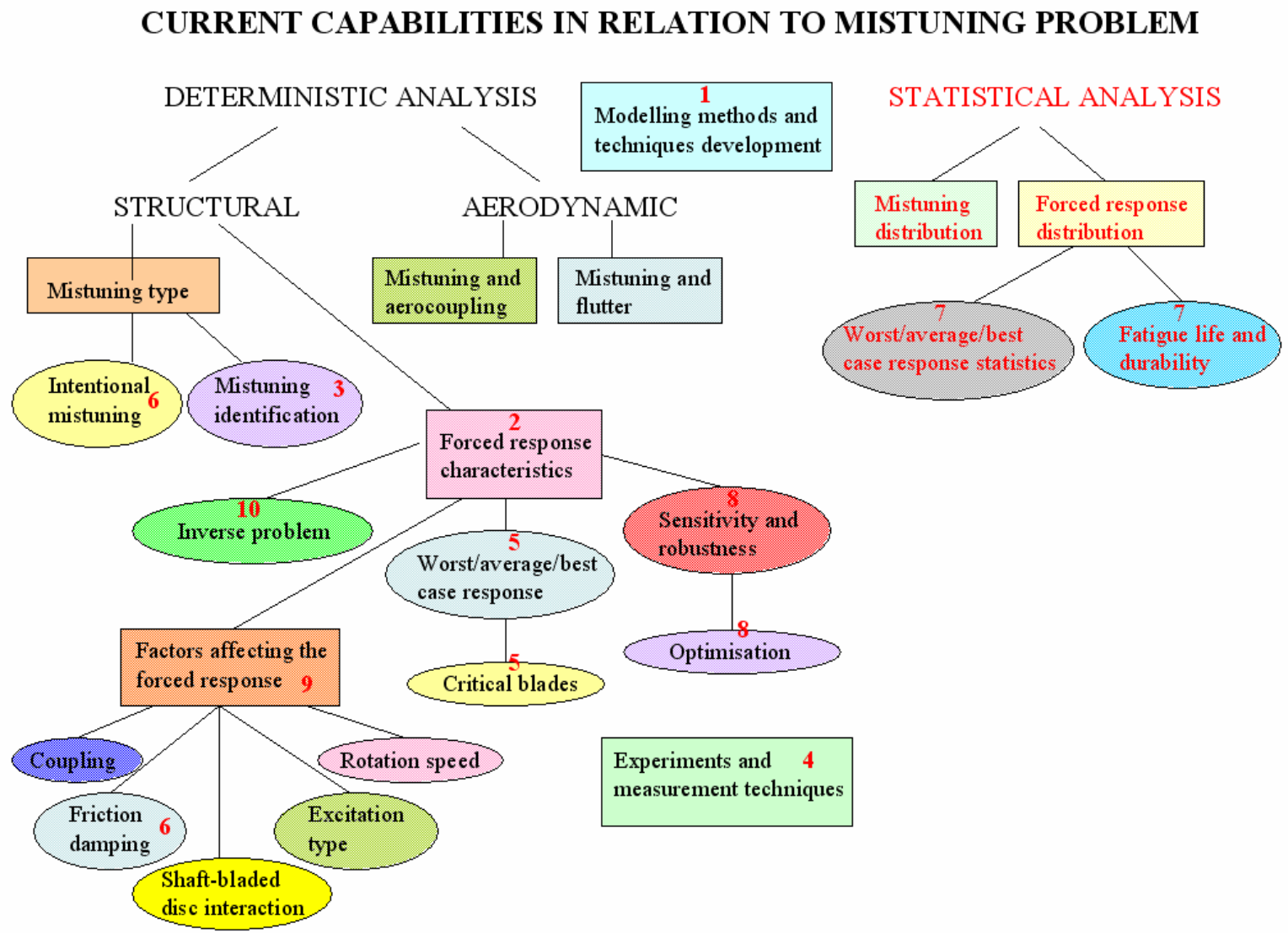

Fig. 2-3. Map of mistuning research areas

Although the mistuning studies mentioned in Figs. 2-1 and 2-2 differ significantly according to the topic and essence of work, some common current capabilities in relation to the blade mistuning problem can be summarised as:

1. An ability to model accurately mistuned bladed discs, and to compute their forced response characteristics efficiently via use of ROMs;
2. An ability to predict the uncertainty in forced response levels from a specified variability in blade properties and operating conditions;
3. An ability to infer the degree of mistuning from a given bladed disc assembly;
4. Guidance on how to perform experiments on bladed disc assemblies, to develop the measurement techniques and to interpret measured data;
5. An ability to predict the worst/average/best case response and to identify the critical blades in an assembly;
6. Guidance on how to develop strategies and implement design changes in order to reduce the maximum forced response levels;
7. An ability to obtain statistical characterisation of forced response, to predict the probabilities of extreme case scenarios and to estimate the fatigue life;
8. An ability to assess the sensitivity and robustness of the design to inevitable changes in blade properties due to wear and to guide the optimisation process;
9. An ability to predict the influence of various factors that have a non-trivial effect on the forced response characteristics;
10. Guidance on how to solve an inverse problem to define the manufacturing tolerances in order to achieve predefined ‘acceptable’ forced response levels;
11. Methods to establish the effects of aerodynamic coupling on mistuned bladed discs and to assess flutter.

The issues expressed in the above claims are by no means exhaustive, but are aimed to emphasize a remarkable progress made on the subject to date. Subsequent sections of this Chapter will elaborate on those issues directly related to the present thesis.

2.3.2.2 A need to include all physical phenomena into the fundamental model

(a) “A number of ways in which the theoretical predictions… fall short of their mission”

Throughout the last decade, FE methods have been employed to serve as numerical tools to model real mistuned bladed discs and to examine their

quantitative behaviour. The use of simple spring-mass models was understood to be infeasible for cases when large numbers of degrees-of-freedom are involved, even though many researchers agreed that a simple model was capable of capturing the essential features of the physical mechanisms associated with mistuning. The analysis of detailed FE structural models of bladed discs is computationally intensive and prohibitively expensive, and, hence, the need for model reduction tools emerged, which would reduce the computational models to manageable size, while retaining the model accuracy. It became a trend for researchers to develop ROMs, FE reductions for a single sector of a bladed disc, which differ from one research family to another in their efficiency and applicability to mistuned bladed discs. Several leading structural ROMs have been reported from Imperial College London – Petrov et al. [32] 2002, Carnegie Mellon University – Yang and Griffin [33] 2001 (SNM), Feiner and Griffin [34] 2002 (FMM); University of Michigan – Kruse and Pierre [35] 1996, Bladh et al. [36] 2001 (CB-CMS, NON-CMS and SMART); Royal Institute of Technology – Moyroud et al. [37] 2002 (CB substructuring and reduction method), as well as ROM aerodynamic counterparts from Massachusetts Institute of Technology – Shapiro and Willcox [38] 2000, and the latest Ghiocel [39] 2005 and Ayers et al. [40] 2005. However, despite the exploitation of refined and powerful state-of-the-art model reduction techniques, the resulting theoretical predictions are in certain ways limited. According to Ewins[1]:

"There are a number of ways in which the theoretical predictions…fall short of their mission. The first is that their numerical values are inaccurate, and can differ from reality by a margin which is unacceptable from the engineering viewpoint. The second is that they fail to predict all the events or phenomena which occur in practice. It is not satisfactory if those events which are predicted have an acceptable accuracy if others, which may be just as important, are overlooked. Third, they can only be as accurate as the input data used…"

[1] Ewins, D.J., "Exciting vibrations: A philosophical approach to resolving structural dynamics problems ", Structural dynamics @ 2000: current status and future directions, edited by D.J.Ewins and D.J.Inman, 2000

(b) Failure to predict all the phenomena which occur in practice

The second issue is of considerable importance to this thesis, and is a first milestone of the debate: notwithstanding the advancements in analysis techniques of mistuned assemblies, the acquired predictions are only as good as the initial bladed disc model provided. Thus, unless all physical phenomena affecting the behaviour of bladed discs are included accurately in the model, the forced response predictions may be doubtful and somewhat unreliable. The failure to include all the factors that have a non-trivial contribution to the vibration characteristics of bladed discs could provide an explanation for a recurrent mismatch being observed between theoretical predictions and experimental measurements. It has been established that several effects are either neglected or misrepresented in the published literature on mistuning. In particular, the effects of Coriolis forces, arising from the rotation of a bladed disc, have been conspicuously excluded from the analysis on the assumption that these forces usually alter natural frequencies, mode shapes and other dynamic properties of bladed discs by an insignificant amount when the analysis is aimed at modes of vibration with the numbers of nodal diameters greater than 1. This is in contrast to classical rotordynamics studies, in which the “gyroscopic effects”, being a direct result of forces of the Coriolis type, are known to be a significant effect and are traditionally incorporated in analysis (Khader and Loewy [41] 1990, Jacquet-Richardet et al. [42] 1996, Genta et al. [43] 1996, Chun and Lee [44] 1996). The deliberate disregard of the effects of Coriolis forces in the context of bladed disc dynamics without provision of sufficient justification or evidence to support the assumption is considered in this thesis to be inappropriate, and an attempt will be made to incorporate these effects into the analysis of mistuned bladed discs in order to assess their importance. Chapters 3 to 5 are devoted to a detailed analysis of this issue.

Another effect that has received attention by researchers in the 1970s and 1980s and only recently a revived interest among the contemporary studies is the influence of aerodynamic coupling on the uncertainty of forced response. The aerodynamic aspect is of passing interest to this thesis, but it is worth mentioning few recent works by Seinturier et al. [45] 2000, Kielb et al. [46] 2004 and Sladojevic et al. [47] 2005, which demonstrate the significance of including these effects due to non-trivial changes in the forced response scatter and flutter sensitivities.

An interesting study has been reported in Ayers et al. [40] 2005, which presented a method to predict the transient response of mistuned bladed discs to include previously unaccounted for transient effects of rapid engine accelerations. They showed that for some specific engine acceleration conditions, the transient effects play a role in mitigation of the HCF.

Only a few studies are devoted to modelling the flexible bladed disc on a flexible shaft system to assess the coupling effects, which, according to a study by Rzadkowski et al. [48] 2004, are important, as the addition of a shaft can change the spectrum of system's natural frequencies considerably.

Summarising the above, a trend is seen in recent years toward increasing awareness of the significance of including effects either previously absent or ignored from the mistuned blade disc analysis.

(c) Characterisation of blade mistuning in predictions

A third remark in the article by Ewins is related to the quality of input data provided to the analysis module. This is a very relevant issue in mistuning representation used in bladed disc predictions. Typically, blade mistuning has been characterised in terms of blade frequencies due to random variations in stiffness or mass, which is usually referred as "frequency mistuning". This is not a very precise definition of realistic mistuning parameters, since the frequencies are consequences of blade variations in physical properties, so that the consideration of all the factors which cause the blade responses to differ from one blade to another, including blade geometry tolerances, root fixing variability, crystal orientation and so forth, becomes an important concern. However, only a few studies in the mistuning literature, have considered changes in different mistuning parameters. Rzadkowski [49] 1993 examined a very general model of the vibration of bladed discs and showed that the stagger angle, the variable cross-sectional area and the twist angle of blades do not appreciably influence the distributions of blades' stresses around the disc, whereas these geometric parameters affect only the stress level and natural frequencies of the system. A motivating work has been reported by Lin and Mignolet [50] in 1996, where the effects of blade-to-blade variations in the damping coefficients on the forced response of a bladed disc have been investigated. It was found that such nonuniformities could lead to uncertainty in the blades' amplitudes, which are similar in magnitude to those obtained with stiffness mistuning, but are potentially

more dangerous due to the skewness of the distribution toward large amplitudes. A recent publication by Feiner and Griffin [51] 2003 also demonstrated that blade frequency deviations are not sufficient to characterise mistuning in a bladed disc. They proposed a more sophisticated measure of mistuning, a "sector frequency approach", which effectively uses a frequency quantity that describes the mistuning of an entire sector, rather than considering mistuning to be confined to the blades as in Judge et al. [52] 2002, thus providing a more accurate mistuning representation.

(d) Mistuning identification in bladed discs

Most of the mistuning analyses have assumed the blade properties to vary randomly, or in some specified fashion, thus, generally avoiding the characterisation of mistuning parameters from experimental data. However, in order to have a realistic mistuning representation, it is necessary to model the mistuning accurately. A precise identification of the degree of mistuning has become an important area of investigation, particularly in a practical implementation of forced response reduction strategies in bladed discs. The standard methods for discs with detachable blades consist of removing the individual blades for measurements of their natural frequency. This is not an accurate procedure, since it ignores the effects of blade attachment to the disc, and the problem is especially pronounced in integrally bladed rotors (blisks), where the blades and the disc form one integral piece. Therefore, in order to accurately identify mistuning in bladed discs, it is essential to develop methods that can produce measurements of the entire bladed disc assembly. Mignolet et al. [53] 1999 have first developed two distinct approaches from the measurements of the natural frequencies of the blades – random modal stiffnesses (RMS) and the maximum likelihood (ML) strategy – for an estimation of dynamic properties of the bladed disc to be used in accurate prediction of the forced response. A new method based on the ROM FMM has been generated by Feiner and Griffin [54] 2003, which relies on the measurements of the vibratory response of the system as a whole, and hence, is well suited for blisks. The approach is similar to the mistuning identification strategy of Judge et al. [52] 2002, which also manipulated the mistuned modes and frequencies to infer the mistuning, but is simpler and requires less input data. Recently, Lim et al. [55] 2004 have developed a new identification method, in which both free and forced response data can be used to gather blade mistuning data. With an emphasis on engine health monitoring and

crack detection, Feiner and Griffin's [56] 2005 effort to perform identification of not only blade mistuning, but also damping variations, is the latest development in the field.

In the light of the above-mentioned studies, a need is identified to account for all physical phenomena and to represent accurately all parameters that cause the uncertainty in forced response levels in order to improve the fundamental model to be used in the state-of-the-art prediction codes.

2.3.2.3 Confrontation of theory with experiment

Successful implementation of a previously-neglected effect, validation of theoretical predictions, or attempts to gain insights into the problem, are highly dependent on the availability of experimental evidence. Despite the advantages of conducting experiments, there have been very few experimental studies of mistuning. One of the first papers to study experimentally the mistuning effects on double modes using holographic interferometry and strain gauge measurements was Strange and MacBain [13] in 1981. Utilising a facility which provided an array of non-intrusive experimental techniques, Kruse and Pierre [57] 1997 and Pierre et al. [58] 2000 showed a high sensitivity of blisks to small mistuning, and corroborated the occurrence of mode localization phenomenon. Later, in Judge et al. [59] 2001, they conducted experiments to demonstrate the forced response magnification due to random mistuning, thus validating their ROM predictions, and explored the benefits of deliberately-introduced mistuning. Feiner and Griffin [51] 2003 developed an original experimental approach, FMM ID, which used measurements on the system as a whole (mode shapes and natural frequencies) and tuned system frequencies from FE analysis, to infer the mistuning in each bladed disc sector. Theory for prediction of the robust maximum forced response from a distortion of a structural mode was experimentally validated and reported in Kenyon and Griffin [60] 2003. A latest attempt has been made to experimentally validate a probabilistic model in Rossi et al. [61] 2005 using FMM and FMM ID codes, simulating a forced response of a 'fleet'.

Quoting Srinivasan [2] 1997: "…The principal gap in all the areas [of study of flutter and forced vibration characteristics of engine blades]…is a conspicuous lack of good test data. In addition to its intrinsic value, experimental data provide the needed stimulus toward more realistic modelling efforts…" A need for more

experimentally oriented mistuning studies is evident, as conducting experiments not only boosts confidence in developed prediction techniques, but also improves knowledge on phenomena and could provide foundations for resolving some of the controversies surrounding the blade mistuning problem. In this thesis, an attempt will be made to obtain experimental evidence of influence of effects of Coriolis forces on the vibration characteristics of bladed discs.

2.3.2.4 Predicting the maximum forced response

Having improved and validated a fundamental mistuning model, a major concern becomes the prediction of maximum attainable forced response levels. In traditional bladed disc analysis, the maximum amplification or magnification factor is defined as a ratio of the largest amplitude of mistuned bladed disc to the corresponding value of tuned response. Determination of the maximum forced response increase due to mistuning has been one of the most inconsistent and negotiable mistuning questions. A number of studies have attempted to provide a definitive answer, and as a result, the maximum amplification factors were announced ranging from about 1.2 to 5.3. The contradictory results are usually attributed to differences in mathematical models and operating conditions used in studies. As extreme vibration levels lead to considerably reduced blades' HCF lives, it is vital to predict reliably the largest amplification factor.

(a) First studies to address the maximum forced response

The first to address this issue was Whitehead [5] in 1966, who established a remarkably elegant upper limit of the effects of mistuning on vibration levels of blades, excited by wakes in the presence of mechanical and aerodynamic coupling, as $\frac{1}{2}\left(1+\sqrt{N}\right)$, where N is number of blades in the assembly, emphasising the crucial role of latter. Whitehead further investigated the conditions under which the maximum amplification factor could be obtained to reveal that damping had to be much less than the mistuning and coupling effects. Ewins [6] 1969 achieved the maximum blade stress level 20% higher than the equivalent tuned system for the case of an isolated 'double mode'. Further, in Ewins and Han [15] 1984, it was determined, using a simple mass-spring model of a 33-bladed disc, that the spread of mistuned forced responses varied from 66% to 120% of the tuned, depending on distribution of blades around the disc. Another notable 'early' study was performed

in Basu and Griffin [27] 1986, which examined the effects of changing the system parameters on amplitude scatter, to obtain the maximum amplification factor of 2.43.

(b) Contradictions in contemporary analyses of maximum forced response amplification

Significantly larger amplification factors were reported in the post-1990 period. Rzadkowski [49] 1993 found the maximum stress of a 36-bladed disc with 10% mistuning was 3.36 times that of the tuned system. Later, Petrov and Ewins [62] 2001, reported the amplitude magnification of response to reach 5.0, experienced for the first bending mode (1F) under 6 engine order (EO) excitation, which is near to the Whitehead's factor of 5.3 for 92-bladed disc. Among the other notable works is Kenyon et al. [63] 2002, which presented the maximum forced response from a distortion of a structural mode in an isolated family of modes in the presence of structural coupling. Concentrating on physics, the largest amplification was shown to occur when harmonic components of a distorted mode superimposed in a certain manner, causing localization of the mode and strong response in a particular blade. Damping variability was incorporated into the model, unlike in Whitehead [64] 1998, to demonstrate that with its inclusion, the maximum amplification factor was either lower or higher than Whitehead's, depending on the specific case. Interestingly, Kenyon et al. showed that the maximum amplification factor predicted by Whitehead could not be achieved with FE-based models currently employed by researchers. It is also appropriate to mention the work of Rivas-Guerra and Mignolet [65] 2001, who suggested that the maximum amplification due to mistuning occurs at very strong blade-to-blade coupling, and is associated with large mistuning levels. The comparison of the results with Whitehead's factor revealed good qualitative agreement in predictions, 2.69 vs. 2.95 for a 24-bladed disc. In a subsequent study, Rivas-Guerra and Mignolet [66] 2002, recovered Whitehead's upper bound for all EOs and numbers of blades, clarifying the conditions under which this limit was attained. Later in [67] 2004 with Xiao, they derived maximum amplification forced response due to mistuning in multi-degree-of-freedom models.

(c) How convincing are predictions of maximum forced response?

Examination of Whitehead's formula [5] suggests that the number of blades is a major factor governing the maximum forced response amplification, without providing any convincing explanations for the observed dependency. On the other

hand, numerous studies have argued plausibly that the maximum amplification factor is shaped by a range of factors, such as the amount of mistuning, coupling, damping, the specificity of operating conditions etc. For this reason, the conflicting results tend to be case-dependent and difficult to generalise, which implies over conservative bladed disc design to satisfy the safety requirements in the engine designer community. A better grasp of the interaction of important factors affecting the maximum forced response is needed, while there is a scope for academia to provide reliable design guidelines to ensure acceptable vibration levels and to improve fatigue life of blades.

2.3.2.5 Development of strategies for maximum forced response reduction

The worsening effects of mistuning have challenged researchers to seek means of forced response reduction and prevention of the worst case scenarios. Several strategies are used for this purpose, such as intentional or deliberately-introduced mistuning, installation of friction dampers, etc. The former has received a special attention in this thesis.

(a) A quest for deterministically-defined mistuning: from alternate to harmonic intentional mistuning patterns

Intentional mistuning refers to a systematic controlled introduction of variations in blade properties to obtain a desired level of forced response. The first to recognise the promising effects of “detuning” – deliberate and structured deviation from the symmetry of a tuned system – upon a forced response of a bladed disc, was a famous study by Ewins [6] in 1969. Further in 1980, Ewins [12] demonstrated the advantage of packeting configurations of blades as a possibility of minimising forced response levels for specific excitation orders. Another ‘early’ mistuning work by Griffin and Hoosac [16] 1984 incorporated “alternate” mistuning, by alternating high and low frequency blades, which resulted in some reduction in forced response. At the beginning of 1990s, Rzadkowski [49] 1993 searched for the optimal distributions of blades from a stress viewpoint, and found that n-periodic arrangement was most likely to minimise the maximum forced response. The first among the studies that used an intentional mistuning in design of mistuned bladed discs was research of Castanier and Pierre [68] in 1997. They demonstrated a feasibility of employing the intentional mistuning in sinusoidal patterns, by adopting the approach that utilised the cyclic nature of the system, to decrease considerably

the maximum forced response on a simple 12-bladed spring-mass model. A more practical "pseudo-harmonic" mistuning was introduced that exhibited a further reduction of the maximum forced response.

(b) Appreciation of sensitivity and robustness of intentional mistuning patterns

The findings of Castanier and Pierre [68] were extended by a subsequent work, Castanier and Pierre [69] 1998, to include the individual and combined effects of intentional and random mistuning on forced response of a ROM of a 29-bladed rotor obtained for two EO excitations. In general, it was observed that intentional mistuning reduced the amplification magnification from 1.9 to 1.4, and made the bladed disc design more robust with respect to small random mistuning, which was confirmed experimentally in the study of Pierre et al. [70] 2002. Robustness is a very desirable feature, as it ensures the forced response predictability, and, as a result, several studies established the robustness of the intentional mistuning as one of the key factors to be considered when developing such strategy. At the same time, Shapiro [71] 1998 concluded that intentional mistuning might improve both stability and forced response under manufacturing tolerance variability, thus acknowledging it as a viable technique for increasing safety and performance of bladed discs. Another study based on the concept of harmonic patterns was performed by Kenyon and Griffin [72] 2000 on a continuous ring model of a bladed disc, which showed that the use of intentional mistuning can reduce the magnification of the forced response. Further, their study with Feiner [63] in 2002, demonstrated that intentional mistuning could be used to mitigate the effects of small random mistuning inherent in bladed discs. Along the same lines, Mignolet et al. [73] 2000, examined harmonically mistuned bladed discs to find that the former exhibited many of the same characteristics as the randomly mistuned systems. A work by their colleagues, Choi et al. [74] 2001, focused on the optimisation of intentional mistuning of bladed discs to reduce their sensitivity to unintentional random mistuning. They determined that despite the response reduction by 20-30% in the absence of random mistuning, the situation changed when the random mistuning was factored in.

(c) Attempts to exploit other intentional mistuning patterns

Some of the research in the past few years considered a very different type of intentional mistuning and reached some contradicting conclusions compared to previous studies. Namely, Brown et al. [75] 2000 minimised the maximum forced

response with a descending pattern for certain EO excitation, while work by Jones and Cross [76] 2002 aimed at obtaining the mistuning pattern which would reduce the mistuned response below the tuned value. In particular, they showed that (i) linear intentional mistuning proved to be more effective than harmonic, (ii) the optimal mistuning pattern varies for different EOs, and (iii) the amount of random mistuning is a governing factor in successful implementation of intentional mistuning strategy.

(d) Influence of blade rearrangement on maximum forced response levels

Blade rearrangement around the disc has been a long-established strategy for potential maximum forced response drop. Ewins [6] 1969 first noted that by careful rearrangement of the same set of non-identical blades on rotor, it is possible to reduce the maximum forced response levels. In the 1990s, a series of investigations led by Petrov, [77] 1999, [78] 2000, used optimisation methods to search for the best and worst mistuning distributions. Petrov and Ewins [79] 2002 showed that the same set of 92 blades can be rearranged into a pattern, such that the maximum forced response could have a value less that 2 for the best arrangement and greater than 4 for the worst blade arrangement. This indicates a considerable potential for control of the forced response of mistuned bladed discs by simple reshuffling of the blade locations (but an equal disadvantage if blades' state of mistune might vary with time, or wear). The order of the mistuned blades around the disc, rather than the specific values of mistuning, has also been established in a study by Ayers et al. [80] 2005 as a viable strategy for minimising the vibratory response.

(e) A scope for new ideas in development of intentional mistuning strategy

Further inconsistencies in predictions with respect to type of intentional mistuning necessary for forced response reduction were observed in other studies. Instead of aiming to get the 'right' answer, it may be of advantage to seek new ideas for maximum forced response reduction and control. It has been noted that the surveyed works on use of intentional mistuning have never exploited large mistuning (large scatter in blade frequencies) as a means of incurring decreased bladed disc response amplitudes, focussing only on the variations in mistuning patterns for relatively small to moderate degree of mistuning, typically of the order ±0.5% to ±5%. Nevertheless, studies have shown that there is a threshold of small frequency mistuning up to which the forced response increases, but beyond which

the response levels off, or even drops, as the degree of mistuning is increased further (Ewins [6] 1969, Ottarson and Pierre [81] 1996, Castanier and Pierre [68] 1997 etc). The tendency of the amplitude magnification factor to decrease with blade mistuning after an initial rise suggests that there might be an advantage to exploit the effects of larger frequency mistuning ranges, perhaps of the order of ±15% to ±20%, which would introduce the possibility of relaxing the manufacturing tolerances as a way of producing reduced forced response levels of bladed discs. Chapter 6 of this thesis will assess the feasibility of introducing large mistuning as a viable design strategy.

As mentioned earlier, intentional mistuning is not the only feasible forced response reduction strategy. Use of friction dampers is widely spread in endeavouring to rectify the ill-effects of mistuning, and the amount of studies represented in the literature tree serves to justify its benefits. Studies on friction damping are of passing interest to this thesis, and hence, no review will be presented. An interested reader is referred to a survey by Griffin [82] 1990 for more information.

2.3.2.6 Assessing sensitivity and robustness

Independently of the selected forced response reduction strategy, the assessment of sensitivity and robustness of the design is vital, as blade properties are likely to change with time due to wear. Mistuning sensitivity is usually described as the dependence of forced response magnification of a bladed disc on the degree of mistuning. As mentioned earlier, blade amplitudes increase with mistuning strength up to a certain critical level, usually exhibiting a maximum response at a low degree of mistuning, beyond which a further increase in mistuning causes the forced response to drop and flatten out. This implies that the bladed disc system is highly sensitive to mistuning around the tuned condition, and that increasing the degree of mistuning may result in a decrease in the sensitivity of response.

(a) Sensitivity and robustness – an inherent part of recent investigations of forced response behaviour in presence of coupling

Sensitivity and robustness of forced response has been an inherent part of investigations in the past decade, since it secures the predictability of the response. The influence of coupling has been one of mostly studied factors of bladed disc sensitivity to mistuning. Kaneko et al. [83] 1994 explored mistuning effects on free standing and integral shroud blades to find that the weakly coupled systems with

low damping were very sensitive to mistuning. An interesting study was reported in Bladh et al. [84] 2001, who noted that the modified blade-disc modal interactions resulting from multistage coupling have significant impact on a design's sensitivity to blade mistuning. Their observations supported the hypothesis that mistuning sensitivity maxima are obtained for a delicate balance of blade and disc participation in the highest-responding eigenfrequency veering mode pair. The study indicated the possibility of alleviating the severity of unfavourable structural coupling by redesigning the discs and stage-to-stage connectivity. An attempt to study influence of rotation speed and coupling on the sensitivity to mistuning was carried out in Myhre et al. [85] 2003. Their results suggested that mistuning sensitivity of an unshrouded rotor was unaffected by rotation speed, due to insignificant changes in coupling strength, whereas the fan with shrouds manifested different behaviour at rest and under rotation. Concentrating on a single EO, they demonstrated that for both fan geometries, the maximum amplification factor was shifted toward higher degrees of mistuning due to rotation.

(b) Insights into physical mechanisms governing the sensitivity of mistuned bladed discs

Ottarson and Pierre [81] 1996 expressed sensitivity to mistuning using a 'sensitivity measure' intended for an efficient prediction of the mode localization factor. To gain insight into the physical mechanisms behind the sensitivity, Kenyon and Griffin [86] 2001 carried out a detailed study to observe that almost all sensitivity curves exhibited a steep slope near zero perturbation levels, confirming the inherent sensitivity of a nearly-tuned system. Other areas were located where the slope was small, showing the regions relatively insensitive to additional mistuning. It was also revealed that depending on damping, the sensitivity of the response of the split modes is dominated by a single-mode pair and by first-order terms in these modes. Subsequently, in Kenyon et al. [87] 2004, they considered the effects of frequency veerings on mode shapes in the context of the generalised forces exciting the system, and established some important implications for mistuning analysis using amplification factor as a metric of forced response increase. Recently, Baik et al. [88] 2004 approached the problem of assessing the sensitivity of system from an early design viewpoint: based on tuned free vibration characteristics, they predicted the effect of design changes on robustness of a system. Further, in Baik et al. [89]

2005, they included the effects of rotation and demonstrated the power flow analysis to predict the mistuning sensitivity of the structural system.

(c) The role of sensitivity and robustness analysis

It is important here to emphasise the role of sensitivity assessment in mistuned bladed disc analysis, which, in contrast to statistical studies on the subject, has not been fully appreciated until recently. Fundamentally, the sensitivity analysis contributes to the understanding of the factors and extent to which they affect the forced response of a particular design, thus providing some guidelines of how to improve the model in order to make it more robust. Statistics' role is to assess the severity and distribution of response with an ultimate aim to predict its HCF life. In this thesis, preference is given to sensitivity and robustness, which serve to establish the reliable bladed disc designs.

2.3.2.7 Statistical characterisation of the forced response

(a) Overview of statistical mistuning studies

Surveying the literature reveals that statistical mistuning studies employed the probabilistic approach that uses statistical characterisation of parameter uncertainties, since blade properties are stochastically defined quantities due to manufacturing variability and nonuniform wear. Various publications aimed at characterising the probability density function (PDF), cumulative distribution function (CDF) and the statistical moments of the distribution of the blades' response, in order to assess the forced response levels statistically and to estimate HCF lives. A myriad of 'exact' analytical and approximate methods were applied in the past for performing a statistical analysis of forced response of mistuned bladed discs, the most prominent of which will be mentioned below.

(b) Abundance of statistical methods developed to address the distribution of forced response

An enormous amount of statistical methods have been developed in the past to address the distribution of forced response. Most notable include: (i) first analytically-derived expressions for PDF and CDF of forced response reported in Sogliero and Srinivasan [11] in 1979, Griffin and Hoosac [16] 1984 and Singh and Ewins [30] 1988; (ii) first approximate perturbation technique using Taylor series to obtain worst case statistics reported in Sinha [19] 1986, and its further development

in Sinha and Chen [31] 1989; (iii) three probabilistic methods to generate the mean and variance of forced response, employed in Wei and Pierre [90] 1989; (iv) an original combined closed-form perturbation analysis for characterisation of PDF, demonstrated in Mignolet and Lin [91] 1992; (v) an approach for statistics computation based on Lyapunov equation and Taylor series summarised in Cha and Sinha [92] 1999; (vi) increasingly complex approach in Bah et al. [93] 2003, based on stochastic reduced basis vectors, developed for calculation of mean and variance of forced response for different mistuning, coupling and damping levels; (vii) a method of polynomial chaos as a means of computing the response statistics in Sinha [94] 2003; and most recent, (viii) Sinha [95] 2005, which uses neural networks for statistical characterisation of forced response as a function of input parameters. It would be very difficult to assess the relative merits of the above-mentioned works in providing accurate predictions of forced response statistics or to compare them, as their applications to bladed discs and operating conditions vary a great deal from study to study. It is sufficient to note, however, that statistical characterisation of forced response has been and still is an intensive and rendered as significant area of research, which has yielded a considerable amount of inconsistencies regarding the representation of distributions of blade amplitudes and resulting conclusions on worst case statistics and HCF life predictions.

(c) Inconsistencies in representation of the statistical distribution of forced response

Two statistical distributions, Weibull and Gaussian, were usually either assumed or shown to represent the best fit to the mistuned forced response characteristics. Among the first researchers to incorporate the Weibull distribution are Sogliero and Srinivasan [11] 1979, who used the Palmgren-Miner damage hypothesis to conclude influence of damping on the expected blades' HCF lives, and Griffin and Hoosac [16] 1984, who established that the mistuned maximum forced response was always greater and the fatigue life always shorter than that of a tuned disc. Later, Mignolet et al. [73] 2000 verified by performing the Monte Carlo simulations that the distribution of system's forced response also complied with the Weibull law. Jones and Cross [76] 2002 carried out a statistical analysis to determine the combination of mistuning strength and EO that was most likely to produce the greatest mistuning "attenuation", fitting the Weibull distribution to the response data. A major opposition to the modelling of forced response as a Weibull

distribution was Sinha [95] 2005, who claimed the corresponding statistical distribution to be accurately described as the Gaussian, as shown in Sinha [19] 1986 and Sinha [94] 2003. In response to the conflicting results on precise statistical distribution, Sanliturk et al. [96] 1992 undertook the task of clarification of the most controversial statements. They used a simple model to yield the PDF and CDF, and found that changes in the vibration characteristics due to random mistuning were dramatically affected by changes in EO excitation, with maximum response amplitudes occurring at intermediate EOs. Similarly, it was concluded that there was no unique distribution which could describe the blade amplitudes under every possible EO excitation. The results in this study were based on a simple model, so there is a scope for some further investigation using FE model of an industrial bladed disc, as will be shown in Chapter 6 of this thesis.

(d) Worst case statistics

The statistical papers concerned with the worst case response concentrated mainly (i) on obtaining the parameters of the assumed or computationally determined statistical distribution of the maximum response, and (ii) on identifying the highest responding blades in the assembly, such as Griffin and Hoosac [16] 1984 and Sanliturk et al. [96] 1992. Sinha [19] 1986 was a first study to develop an analytical expression for calculating the PDF of a blade exceeding some critical level. Later, Castanier and Pierre [68] 1997 employed extreme value theory to compute statistics of the worst case response by modelling it as a Weibull distribution.

(e) Statistical studies verdict

Statistical studies on mistuning demonstrate an abundance of methods used for characterisation of forced response, and conflicting results regarding its precise statistical distribution, which, as in the case of determination of the maximum amplification factor, is highly dependent on the assumed mistuned bladed disc design and analysed operating conditions. In the author's opinion, further qualitative studies alike Sinha [95] 2005 would be beneficial in establishing a correlation between the crucial bladed disc features and the statistical distribution of forced response, rather than developing increasingly complex statistical methods for the sake of obtaining more accurate statistical distribution for a particular bladed disc configuration. Also, statistical information had been rarely used in planning and

interpreting the blades' measurements, as in Griffin [97] 1992, or in thorough assessments of blades' HCF lives, as in Sogliero and Srinivasan [11] 1979, which are believed to be of importance to industry practitioners.

2.3.2.8 Identification of highest responding blades

Due to mistuning, nominally-identical blades vibrate with substantially different amplitudes, resulting in one or more blades possessing an excessively high forced response, which potentially leads to HCF. Thus, in the context of positioning the strain gauges (or any other response transducers) effectively to capture the worst response in blades' measurement process, it is crucial to predict which of the blades would suffer the highest response amplitudes, the so-called "rogue blades" (Afolabi [20] 1987), the identity of which has been another controversy issue. El-Bayoumi and Srinivasan [10] 1975, and afterwards Griffin and Hoosac [16] 1984, indicated that "the high response blades are neither the greatest nor the lowest frequency blades, but are those whose blade-alone frequencies are near the tuned system frequency". This is contrast to the findings of Ewins and Han [15] 1984 and Afolabi [20] 1987, who demonstrated that the highest response was always experienced by a blade of extreme mistune. The latter study also noted that the susceptibility of a blade to become highly responsive is a function of excitation pattern, in addition to mistuning and coupling strength. A promising recent study by Xiao et al. [98] 2003 aimed at predicting the critical blade identity by formulating and validating two different strategies for the experimental and computational statistical contexts. In the first, the authors proposed the maximum likelihood identification to select the highest, second and third highest responding blades as candidates to exhibit the largest forced responses. In the second, the forced response obtained by approximation algorithms with only two tuned modes and a partial mistuning model, provided a reliable basis for prediction of the worst blade, with an exponentially decreasing probability of mismatch.

2.3.2.9 Further practical aspects of bladed disc vibration

(a) Damage assessment: studies of effects of cracks on the vibration properties

Engine blade health monitoring and damage assessment is a routine procedure due to HCF failure risks. Cracks frequently appear in rotating machinery

components due to manufacturing flaws or HCF and these change the structural regularity of the system, causing the mode localization phenomenon, and consequently, altering the forced response characteristics. Several investigators have been working on modelling and vibration analyses of cracks in rotor systems since the early 1970s. Wu and Huang [99] 1997 found that the natural frequencies of the shaft-bladed disc system with a cracked blade were decreased due to the presence of the crack, while the blade vibration amplitudes were significantly different. Considering the effects of position and depth of the crack in the system, Kuang and Huang [100] 1999 reported drastic crack effect on mode localization in the vicinity of the cracked blade in rotating bladed discs. An important research was conducted by Kim and Ewins [101] 2000, where the effect of crack locations on the sensitivity of harmonics was examined, both theoretically and experimentally, with a view of developing a crack detection method.

(b) Specification of manufacturing tolerances

Current capabilities in relation to mistuning problem are in most cases limited to solving the so-called ‘forward’ problem. From a practical viewpoint, specification of precise manufacturing tolerances to ensure the ‘acceptable’ maximum forced response level is highly desirable. Nevertheless, there are only a handful of studies which undertook the challenge to formulate the ‘inverse’ problem in relation to blade mistuning. In Sanliturk and Imregun [102] 1994, a general inverse method was developed for obtaining some of the structural parameters of a model, when its response levels were specified under known excitation conditions. The conclusions drawn were that the identified solution might not have been unique and was difficult to generalise, so that a statistical approach was needed in most cases. Yet, an interesting result demonstrated that the relationship between the manufacturing tolerances and the forced response increase due to mistuning is almost linear up to 60% allowable response increase, and exponential thereafter. An original methodology based on the nonparametric approach was proposed almost a decade later in Capiez-Lernout and Soize [103] 2003, for solving the mistuning inverse problem based on Monte Carlo simulations. It allows specifying the manufacturing tolerances with respect to the confidence region of the magnification factor and probability level over a narrow frequency range. Their work was further extended in

Capiez-Lernout et al. [104] 2004 to validate the theory and to include results for an industrial bladed disc.

2.3.2.10 Controversy sources

To reach consensus about controversial predictions of the forced response characteristics of mistuned bladed discs, it is necessary to establish the factors which are the primary sources of conflicting issues. Clearly, the mistuning extent is an obvious such factor, and the reviewed studies have served to demonstrate its influence on vibration levels. However, mistuning is not the only forced response amplification cause: depending on the nature of mechanical and aerodynamic coupling, number of blades, damping, excitation conditions etc., the mistuned bladed disc predictions will change and contribute to significantly diverse conclusions and consequential strategies carried out in an attempt to circumvent the problem.

2.4 Bridging the gap between theoretical predictions and industrial concerns

2.4.1 Current industrial concerns

HCF is one of the leading causes of engine failure in aircraft, and the blade mistuning problem, which has been identified as one of major causes of HCF, has received considerable attention by engine industry practitioners in recent years. Inexpensive and rapid test methods that occasionally provide useful information about potential HCF problems are not readily available, and thus, many HCF problems are only discovered after completion of the engine design and development. Diagnosing and correcting these problems can be extremely expensive, often affecting the entire fleet and substantially reducing readiness of aircraft. For this reason, prevention rather than cure of mistuning-related problems is favoured, and the fundamental question that the industry practitioners face is how to remove blade mistuning from being a problem. The above-mentioned literature efforts demonstrate that no direct or simple answer can be offered to this apparently straightforward question, and that increased knowledge of the phenomenon cannot resolve the accumulated controversies. It therefore appears that the there is a need for current research to ‘evolve’ in order to address some of the practical issues experienced by the industry practitioners. Examples include the emphasis on

practically feasible strategies of maximum forced response reduction and control, the assistance in tests concerned with the problems of optimal blade selection for efficient measurements, accurate interpretation of the test data and correlation with theoretical models etc.

2.4.2 Defining the questions

As a result of this investigation, the essential philosophical questions underlying the mistuning issues, or the "critical outstanding mistuning questions", have been identified, in an effort to bridge the existing gap between the academic and industrial concerns. The approach chosen in this study is to raise challenging new questions to revisit longstanding mistuning problems from a new angle, rather than attempt to obtain the 'correct' answers to the existing issues. With an aim of prevention rather than cure for the mistuning issues, these high-level questions, given in Fig. 2-4, have been categorized according to the areas to which they correspond. The first four groups seek to improve the current theoretical aspects of mistuned bladed disc vibration which would contribute to a closer correlation between the theoretical studies and reality, while the last two attempt to address the issues directly encountered in practice in the processes of performing the screening and diagnosis tests. It is the intention in this thesis to address several issues identified in these first four groups. Specifically, in an effort to improve the fundamental model used in mistuning analysis, the previously-neglected effect of Coriolis forces will be included and experimentally validated, thus overturning the conventional belief of the bladed disc community. Subsequently, a novel strategy for the maximum forced response reduction will be introduced via large mistuning, where both statistical and sensitivity and robustness tools will be employed to assess the feasibility of the proposed strategy. Finally, an attempt to generalise from specific cases will be made about bladed disc vibration problems by discussing the lessons learned from specific cases studied and by anticipating future developments, trends and philosophy.

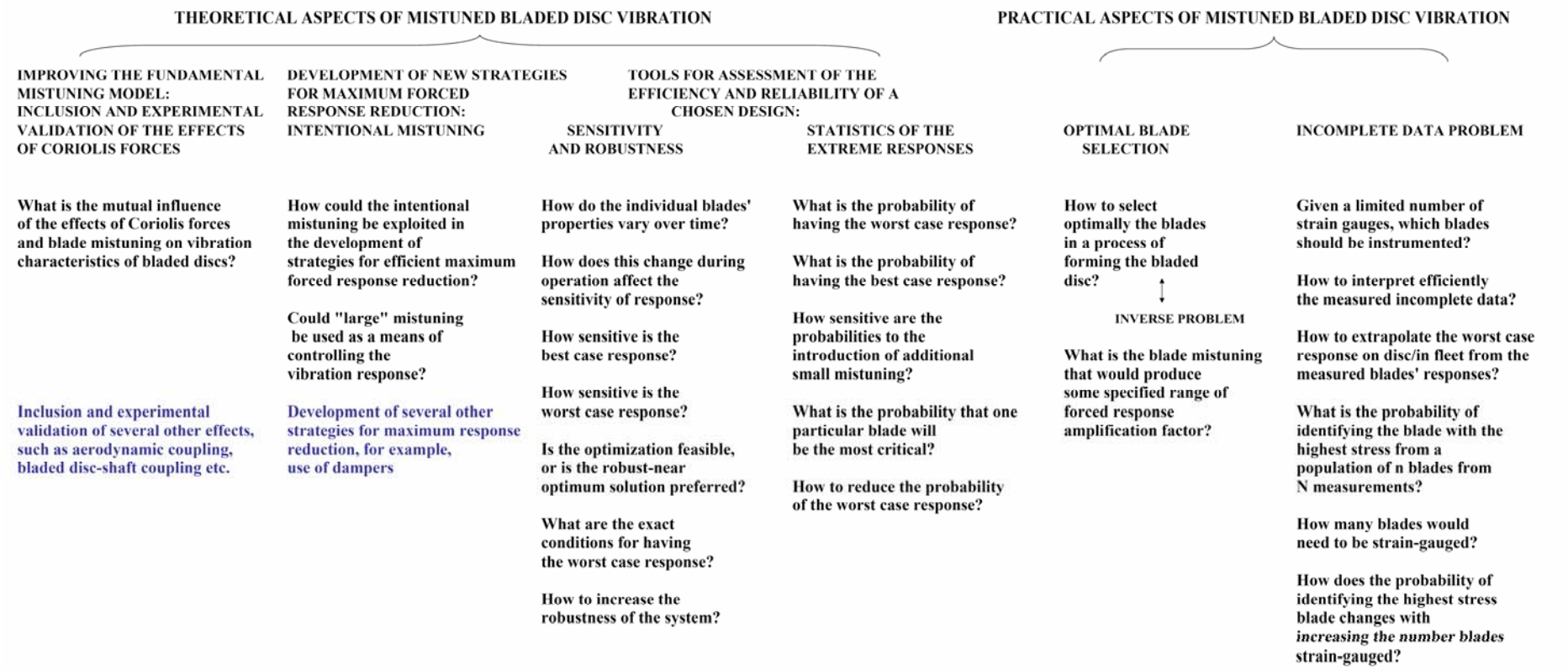

Fig. 2-4. “Critical outstanding mistuning questions”

2.5 Summary

In this Chapter, the status of mistuning after more than 40 years of research has been reviewed with an aim of assessing the extent to which it still poses a problem from the theoretical and industrial viewpoints. Current trends and prediction capabilities have been discussed by presenting the numerous publications related to (i) modelling of the mistuning phenomena and bladed disc features and (ii) assessment of the severity of its consequences on forced response characteristics. In particular, weaknesses of the myriad of studies have been exposed in relation to modelling of the non-trivial physical effects that have been conspicuously absent from the analysis. A lack of experimental validation has been identified as an important pitfall in theoretical attempts to gain confidence from the engine industry community. Efforts to predict and control the maximum forced response characteristics have been reviewed critically to reveal several controversial issues regarding the consequences of the blade mistuning problem. With an aim to reconcile the theoretical studies and industry practitioner needs, so-called “critical outstanding mistuning questions” have been identified, the solutions to which might provide new insights into seizing and apprehending the effects of blade mistuning problem, and its efficient prevention rather than cure.

CHAPTER 3

Improving The Model: Including The Effects Of Coriolis Forces Into Bladed Disc Analysis

3.1 Overview

In this Chapter, a conventional practice adopted in bladed disc analyses to exclude the effects of Coriolis forces is challenged in an attempt to represent accurately all the physical phenomena associated with bladed disc dynamics and to improve the fundamental model used in forced response predictions. The significance of incorporating the effects of Coriolis forces in bladed disc analysis is demonstrated by presenting a theoretical account of their influence on the vibration properties of tuned bladed discs. Several numerical examples serve to confirm the theoretical predictions and to establish an order-of-magnitude of the Coriolis forces intensity. Consequently, a need is identified for experimental validation of the effects of Coriolis forces, the successful implementation of which will increase confidence in the proposed improved model and provide a sounder basis for further analysis.

3.2 Rotation effects and definition of terminology

By definition, an inertial frame of reference is a coordinate system defined by the non-accelerated motion of particles with constant direction and velocity. A sufficient approximation of the inertial frame of reference, in which Newton's laws of motion are valid, is a system of coordinates fixed (or stationary) in the rotating Earth ([105]). A non-inertial frame of reference is a coordinate system which is accelerating: changing its direction and/or velocity. Many turbomachinery components, such as bladed discs, are exposed to effects of forces resulting from rotation and acting on the system in a rotating (non-inertial) frame of reference. An attempt is made below to characterise these forces, expressed from Newton's second law in the rotating reference frame.

Newton's second law with respect to an inertial frame of reference is expressed as:

$$\vec{F}_i = m\vec{a}_i \tag{3-1}$$

where $\vec{F}_i$ is the applied force acting on a particle of mass m, $\vec{a}_i$ is the particle's acceleration, and i refers to an inertial frame of reference.

In order to derive Newton's second law in a rotating frame of reference that rotates with angular velocity $\vec{\omega}$ relative to the inertial frame of reference, it is initially necessary to apply a coordinate transformation

$$\left(\frac{d}{dt}\right)_i = \left(\frac{d}{dt}\right)_r + \vec{\omega}\times \tag{3-2}$$

to the radius vector, $\vec{r}$, from the origin of the rotating frame of reference to the position of the particle:

$$\vec{v}_i = \vec{v}_r + \vec{\omega}\times\vec{r} \tag{3-3}$$

where $\vec{v}_i$ and $\vec{v}_r$ are the particle velocities relative to the inertial and rotating reference frames, respectively. Application of the coordinate transformation for the second time yields an expression for the acceleration vector, $\vec{a}_i$, in the rotating frame of reference:

$$\vec{a}_i = \vec{a}_r + 2\left(\vec{\omega}\times\vec{v}_r\right) + \vec{\omega}\times\left(\vec{\omega}\times\vec{r}\right) \tag{3-4}$$

Finally, substituting this expression into Newton's second law with respect to an inertial frame of reference and rearranging terms, we obtain:

$$\vec{F}_i - 2m\left(\vec{\omega}\times\vec{v}_r\right) - m\vec{\omega}\times\left(\vec{\omega}\times\vec{r}\right) = m\vec{a}_r \tag{3-5}$$

which is Newton's second law expressed in the rotating reference frame.

It is seen that two additional terms emerge in the equation of motion in the rotating frame of reference. The second of these, $m\vec{\omega}\times\left(\vec{\omega}\times\vec{r}\right)$, is commonly referred to as the *centrifugal force*, which is experienced by a particle moving in circular motion, and is directed radially outwards. Newton's first law states that a body will maintain a constant velocity unless a net force acts upon it. Thus, for a particle to be moving in a circle, a net force must exist to prevent it from travelling in a straight line. Hence, by Newton's third law of motion, centrifugal force is accompanied by an equal and opposite reaction force – the *centripetal force*, which is directed radially inwards, towards the axis of rotation. It is important to note that when the particle is stationary in the rotating system ($\vec{v}_r = 0$), centrifugal force is the only added term in (3-5). However, if the particle is not stationary, and moves relative to the rotating system ($\vec{v}_r \neq 0$), then the first term, $2m\left(\vec{\omega}\times\vec{v}_r\right)$, the *Coriolis force*, must also be taken into account. In his 1835 paper "Mémoire sur les équations du mouvement relatif des systèmes de corps"[1], the French mathematician Gaspard Gustave Coriolis (1792-1843) demonstrated that total inertial force is the sum of two inertial forces, the common centrifugal force and the "compound centrifugal force", subsequently known as the "Coriolis force". The latter is perpendicular to both the relative velocity, $\vec{v}_r$, and to the angular velocity, $\vec{\omega}$, and causes the particle velocity to change the direction, but not the magnitude, for which reason it is also known as a "deflecting force".

In this thesis, terms "*Coriolis forces"* and *"effects of Coriolis forces"* will be used to characterise consequences of the Coriolis-type accelerations on flexible bladed disc systems, unless stated otherwise. Furthermore, *"gyroscopic moments"* emerge as a result of Coriolis forces: when a moment is applied to a rotating body perpendicular to the body's axis of rotation, the body begins to rotate about a third axis mutually perpendicular to the other two. The induced rotation is known as *"gyroscopic precession"*, and can be accounted for by the principle of conservation of angular momentum. Gyroscopic moment depends on change of angular momentum of rotor, which in turn varies according to moment of inertia and rotational and precessional angular velocity, as $M = I\omega\omega_p$. On the other hand, the

[1] C.G. Coriolis, 1835, "Mémoire sur les équations du mouvement relatif des systèmes de corps", *J. Ecole Polytech.*, 15, pp 142-154

term "*gyroscopic effects*" will be employed in a rotordynamics whirling context, where – using bladed disc terminology – the emphasis is on 0 and 1 nodal diameter vibration modes of rigid bladed discs, which are coupled with shaft motion – bending and/or torsion.

3.3 Contrasting treatment of rotation effects

3.3.1 Rotation effects in classical rotordynamics

In the analysis of rotating turbomachinery components, two independent approaches have been traditionally adopted: namely, (i) the classical rotordynamics and (ii) the flexible bladed disc approach. The former considers a rigid disc and a flexible shaft (Fig. 3-1a), commonly classified as "rigid-disc flexible-shaft structure", whereas the latter's emphasis is on rigid-shaft flexible-disc model (Fig. 3-1b).

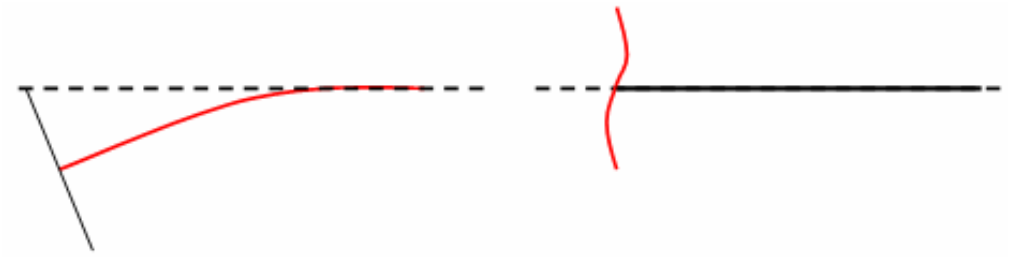

(a) (b)

Fig. 3-1. (a) Rigid disc – flexible shaft structure used in classical rotordynamics, and (b) Flexible disc – rigid shaft structure adopted in bladed disc analysis

In rotordynamics analysis, the modes of vibration associated with the 0 and 1 nodal diameter mode shapes are regarded as important because these modes are the only ones where a shaft motion can occur. The bladed disc modes with 0 nodal diameters (0ND) are characterised by a resulting axial force (and torsional moment) and interact with the longitudinal and torsional shaft deformation, while those described by the 1 nodal diameter (1ND) mode shape exert a net bending moment and a shearing force and, subsequently, interact with the shaft transverse bending motion [42]. Thus, in a typical rotordynamics study, both inertial and gyroscopic effects, which are a direct result of the Coriolis forces, are taken into account.

It is considered appropriate here to present a brief review of the rotordynamics publications addressing (i) gyroscopic effects[2] on the 1ND modes of tuned rotors,

[2] Throughout this brief review, the terminology used matches that adopted in the presented publications

and (ii) gyroscopic effects on 1ND modes and a form of blade mistuning, for which there are very few examples.

(i) Starting from the early 1980s, many rotordynamics studies were associated with assessment of (a) gyroscopic effects on 1ND modes of shaft-bladed disc systems and their natural frequency characteristics, and (b) gyroscopically-induced instabilities of rotors. Publications, such as [106], [107], and [41], established a splitting phenomenon of 1ND modes into a forward and backward pair sets, determining two possible resonance points on Campbell diagram for the first engine order (1EO) excitation. The 1ND natural frequency separation due to gyroscopic effect was validated experimentally in [108]. A significant investigation was carried out in [109], which stated a possibility of excitation of 1ND bladed disc mode and subsequent dramatic increase in peak forced response level up to ten times due to backward shaft whirl.

A publication reported in [110] presented a new approach for uncoupling of the equations of motion without neglecting the speed-dependent effects, and discussed the importance of their inclusion into full analysis of rotors.

(ii) A few attempts to incorporate both Coriolis effects and mistuning into shaft-bladed disc systems are reported in this sub-section. In 1996, [44] developed an analytical method for bladed disc assembly vibration with Coriolis and centrifugal forces accounted for, to find that the Coriolis and inertia forces and inertia torques induced by the 1ND modes vary depending upon stagger and pretwist angles, where the former was shown to have a dominant influence on system dynamics.

Two important studies were reported in 2001. The first of them, [111], employed a Galerkin method to derive mode localization equations of a mistuned system with consideration of the effects of Coriolis and centrifugal forces. Numerical results indicated that as the rotation speed was increased, the mode localization was enhanced and its patterns changed due to Coriolis effects. A subsequent paper, [112], analysed a rotating bladed disc with a cracked blade to show that Coriolis forces and coupling effects between longitudinal and bending vibrations could affect substantially the dynamic stability in a mistuned system, as the unstable zone could shift towards higher or lower frequency domains.

In summary, the above-mentioned rotordynamics studies show that the importance of including the effects of Coriolis forces is well understood in critical

speed analysis for the case of 1ND modes of tuned shaft-bladed disc systems. However, works that attempted to evaluate the influence of Coriolis forces and blade mistuning are rather limited, as they fail to describe the fundamental effect of Coriolis forces on *all* flexible bladed disc modes and to address the forced response considerations, typical for mistuned bladed disc analysis.

3.3.2 Rotation effects in bladed disc vibration

In contrast to the practice adopted in rotordynamics, the effects of Coriolis forces are usually excluded from the vibration analysis of bladed discs on the assumption that they are of negligible magnitude. The disregard of the effects of Coriolis forces in the context of bladed disc vibration is commonly attributed to the belief that Coriolis forces usually do not alter natural frequencies, mode shapes and other dynamic properties of bladed discs by a substantial amount when the analysis is aimed at modes of vibration with the number of nodal diameters greater than 1. It should be noted that for all mode shapes except those with dominant 0 or 1 nodal diameter components, all bending moments are balanced, so that there is no significant interaction energy transfer between the bladed disc and the supporting shaft, a feature which generally enables the analysis of the bladed disc vibration to be made in isolation from the supporting structure.

In this chapter, for the first time, effects of Coriolis forces will be demonstrated on tuned bladed discs to establish their significance in prediction of modal properties (natural frequencies and mode shapes for all nodal diameter modes).

3.4 Coriolis forces in blade vibration

Coriolis forces are associated with the components of bladed disc motion along axes which are perpendicular to the primary axis of rotation (or “spinning”) of the disc on which they are carried, while the component of motion parallel to the rotation axis does not contribute to Coriolis forces. Hence, in investigation of the Coriolis forces’ influence on vibration characteristics, we confine ourselves to study the in-plane radial and tangential blade vibrations only, as there is no coupling between out-of-plane and in-plane blade vibrations due to Coriolis forces. The effects of Coriolis forces arising from simultaneous rotation and in-plane tangential

or in-plane radial vibration of the bladed disc are illustrated in Fig. 3-2 for the case of a 3 nodal diameter (3ND) mode shape.

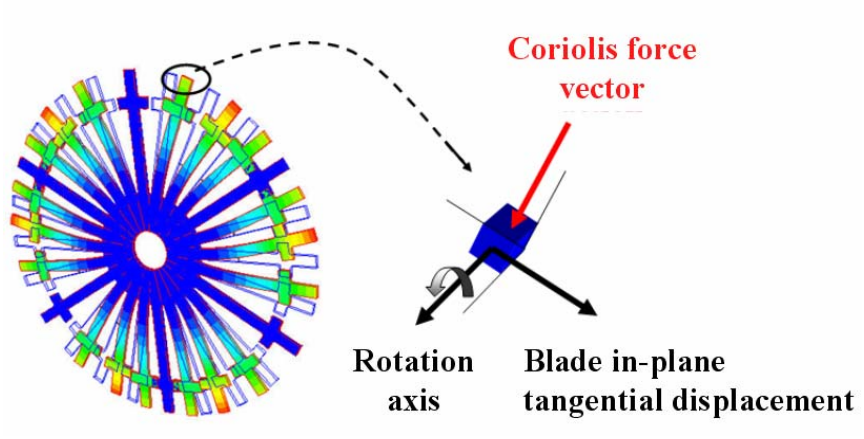

(a)

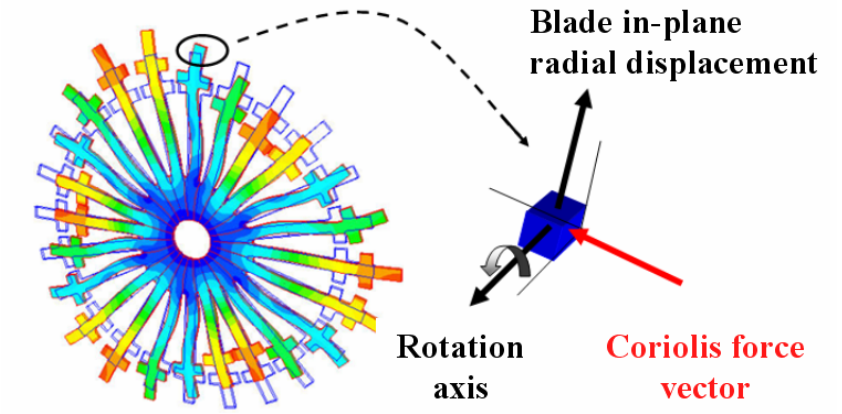

(b)

Fig. 3-2. The action of Coriolis forces: 3ND mode shapes of a bladed disc, (a) blade in-plane tangential vibration; (b) blade in-plane radial vibration

3.5 Tuned bladed disc vibration properties without Coriolis forces

In traditional analysis of perfectly tuned cyclically-periodic bladed discs, in which all blades are identical, the effects of Coriolis forces have usually been neglected. Such systems are characterised by pairs of "double" modes with identical natural frequencies and mode shapes which are orthogonal in spatial orientation ([6] and [8]).

Tuned bladed disc mode shapes can be expressed in polar coordinates as:

$$\phi_{n,s}^{\cos}(r,\theta) = R_{n,s}(r)\cos(n\theta), \quad \phi_{n,s}^{\sin}(r,\theta) = R_{n,s}(r)\sin(n\theta) \tag{3-6}$$

where r and θ are polar coordinates and n and s are the numbers of nodal diameters and nodal circles, respectively. Mode shapes of the two modes with identical natural frequencies differ only in the angular orientation of their nodal lines, and any combination of the two individual mode shapes is also a possible mode shape, including ones which rotate around the structure in a travelling wave motion. The concept of mode shape non-uniqueness in the case of tuned systems is further illustrated in Fig. 3-3, which shows a response of a bladed disc to a single point harmonic excitation adjusted to the natural frequency of the mode with two nodal diameters ([113]). For tuned bladed discs, the response is characterised by two nodal diameter lines symmetrically arranged about the excitation point (Fig. 3-3a). If the latter is relocated to another position along the bladed disc, the nodal diameter lines also "move to follow" the excitation point, as indicated in Fig. 3-3b.

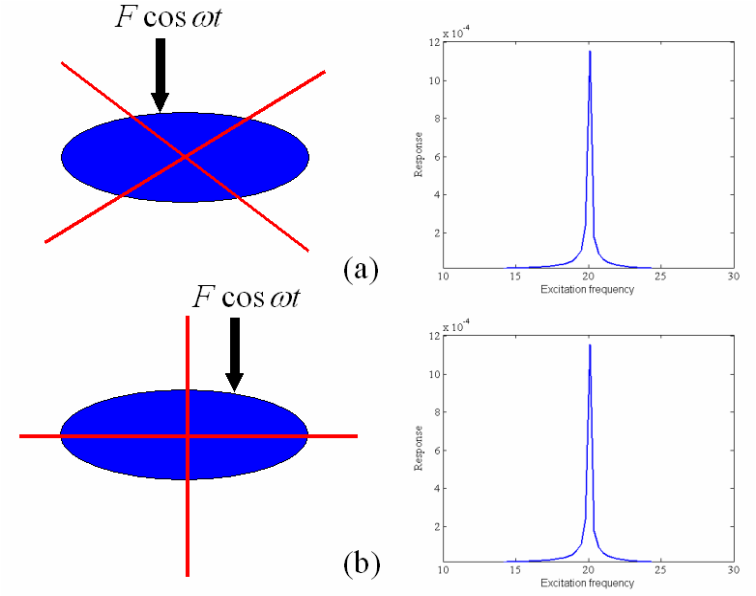

Fig. 3-3. Tuned bladed disc response in 2 nodal diameter modes

In the next few sections, an attempt will be made to characterise the effects of Coriolis forces on tuned bladed disc vibration properties.

3.6 Effects of Coriolis forces on tuned bladed disc behaviour

3.6.1 Rotating bladed disc system with the effects of Coriolis forces

Mathematical models for structures with rotating components possess features distinctively different from their stationary counterparts. While the latter are characterised by symmetric system matrices, and thus mathematically referred to as

"self-adjoint" systems, the equations of motion for systems that include rotation are prone to (i) loss of symmetry in the velocity- and/or displacement-dependent matrices, (ii) generation of complex eigenvalues and/or eigenvectors resulting from asymmetry in the velocity- and/or displacement-dependent matrices, respectively, and (iii) inclusion of time-dependent coefficients in system matrices ([114]).

For rotating tuned bladed discs, the general equation of motion for forced vibration in the time-domain is known to be "non-self-adjoint" [114], [115] and is presented in a rotating frame of reference as:

$$[M]\{\ddot{q}(t)\}+\left[G(\Omega)+[C]\right]\{\dot{q}(t)\}+\left([K]+\left[K_S(\Omega)\right]-[S(\Omega)]\right)\{q(t)\}=\{f(t)\} \quad (3\text{-}7)$$

where $\{q\}$ is the response of the system; $\{f\}$ is the vector of applied external forces; Ω is rotation speed; $[M]$, $[K]$ and $[C]$ are mass, stiffness and viscous damping matrices respectively; $\left[G(\Omega)\right]$ is a speed-dependent skew-symmetric matrix due to Coriolis forces; $\left[K_S(\Omega)\right]$ is a speed-dependent stress stiffening matrix due to centrifugal forces; $[S(\Omega)]$ is a speed-dependent spin softening matrix that accounts for changes in the centrifugal force that result from the structural deformations when a rotating bladed disc is vibrating. It is very important to note here that in formation of the stress-stiffening matrix, $\left[K_S(\Omega)\right]$, both strains and rotations are assumed to be small or infinitesimal, and thus, the matrix does not take into account geometry changing effects. In the latter situation, large or finite strain arise, and often, a non-linear analysis is performed to satisfy this condition. The inability of the $\left[K_S(\Omega)\right]$ matrix to include the geometry changing effect as well as the stress stiffening, will play a major role in the following chapter, where a special attention will be devoted to this issue.

In contrast to "self-adjoint" models for non-rotating structures, whose system matrices are symmetric, [115], the inclusion of Coriolis terms, which increase in magnitude with rotation speed, gives rise to asymmetric equations of motion and asymmetric system matrices, so that:

$$[M]=[M]^T,\left[K^*\right]=\left[K^*\right]^T,[G]=-[G]^T \quad (3\text{-}8)$$

where $\left[K^*\right]=[K]+\left[K_S(\Omega)\right]-\left[S(\Omega)\right]$.

The equation for undamped free vibration is obtained from (3-7) by dropping matrices of viscous damping and excitation forces:

$$[M]\{\ddot{q}(t)\}+[G(\Omega)]\{\dot{q}(t)\}+[K^*]\{q(t)\}=\{0\} \tag{3-9}$$

We shall seek the free response solution of (3-9) in the form [116]:

$$q(t)=\psi e^{\lambda t}\text{, where } q(t),\psi,\lambda\in\mathbb{R}^N \tag{3-10}$$

Substituting (3-10) into (3-9), we define the eigenproblem, the solution to which yields the natural frequencies and mode shapes:

$$(\lambda^2[M]+\lambda\Omega[G]+[K^*])\psi=0 \tag{3-11}$$

The solution to (3-11) yields the eigenvalues, λ , and the associated two different kinds of eigenvectors due to asymmetry of the velocity-dependent matrix: "right" and "left" eigenvectors, both of which are complex [113]. A right-hand eigenvector, ψ_r , satisfies $\chi(\lambda_r)\psi_r=0$, while the left-hand eigenvector, ψ_l , complies with $\psi_l^T\chi(\lambda_r)=0$. While the former vector is generally known as the "mode shape", the latter is a second set of eigenvectors which contains information regarding the ability of excitation forces to produce a vibration corresponding to a specific mode when applied to the structure, or the "normal excitation shape" [113]. Real and imaginary parts of complex eigenvalues can be interpreted as indicative of decay and oscillatory components in the natural frequencies. A complex mode is characterised as one in which each part of the structure has both the amplitude and phase of vibration. As a consequence, each part of a rotating structure will reach its maximum deflection at a different instant in the vibration cycle compared with its neighbours, which all vibrate with different phases [113].

It is known that the eigenvalues of (3-11) consist of *N* complex conjugate pairs and, correspondingly, the eigenvectors also occur in complex conjugate pairs, [116]. Thus, it is possible to express the eigenvector as $\psi_r=y+iz$, where *y* is the real part and *z* is the imaginary part of the eigenvector, ψ_r . Hence, by pre-multiplying equation (3-11) by $\overline{\psi_r}^T$, we obtain:

$$\left\{\overline{\psi}\right\}^T\left(\lambda^2[M]+\lambda\Omega[G]+[K*]\right)\{\psi\}=0$$

$$(y-iz)^T\left(\lambda^2[M]+\lambda\Omega[G]+[K*]\right)(y+iz)=0 \tag{3-12}$$

Using symmetry properties, it can be shown that (3-12) leads to:

$$\lambda^2 m+2i\lambda\Omega g+k=0 \tag{3-13}$$

where $m = y^T[M]y + z^T[M]z$, $k = y^T[K^*]y + z^T[K^*]z$, $g = z^T[G]y$.

Solving equation (3-13) yields the eigenvalues as complex conjugate pairs, given $m > 0,\ k > 0,\ g \in \mathbb{R}^N$:

$$\lambda = \frac{-i\Omega g \pm \sqrt{\Omega^2 g^2 + mk}}{m} \tag{3-14}$$

Finally, after substituting the standard $\omega_n^2 = k/m$ and $\mu = g/m$, the expression for λ becomes:

$$\lambda = -i\Omega\mu \pm \sqrt{(\Omega\mu)^2 + \omega_n^2} \tag{3-15}$$

which demonstrates the crucial result of the *split* in the natural frequencies of the "double modes" of the tuned bladed disc system due to effects of Coriolis forces.

3.6.2 Effects of Coriolis forces on a simple tuned bladed disc

In the previous section it has been established theoretically that inclusion of Coriolis forces into the analysis of tuned bladed discs introduces specific qualitative changes in their free vibration characteristics and, consequently, forced response predictions, predominantly by *Coriolis-splitting* of the natural frequencies into pairs of distinct modes. Furthermore, in this section the influence of Coriolis forces on a simple tuned bladed disc is demonstrated by presenting theoretical predictions acquired using a FE software package SAMCEF, which permits modal analysis of rotating bladed discs with the Coriolis and centrifugal forces included. The eigenvalue solver implemented in this software is based on a pseudo-modal method that uses the Lanczos algorithm [117].

A simple 24-bladed disc, depicted in Fig. 3-4, was selected for analysis, FE sector model of which comprises 45,756 degrees-of-freedom. A distinguishing feature of the considered bladed disc constitutes blade leaning with respect to axial direction by 15 degrees to create a pronounced modern three-dimensional shape of the structure, which is motivated by latest bladed disc developments in the engine industry, such as the highly three-dimensional fan blades in the Trent 1000 from Rolls-Royce, shown in Fig. 3-5.

The tuned bladed disc model was assumed to be fully fixed at centre. The natural frequencies, shown in Figs. 3-6 and 3-7, were calculated at rest and 2500rev/min for all the nodal diameter modes for the first two mode families.

Further, Fig. 3-8 illustrates the first mode family natural frequency and split dependency upon rotation speed.

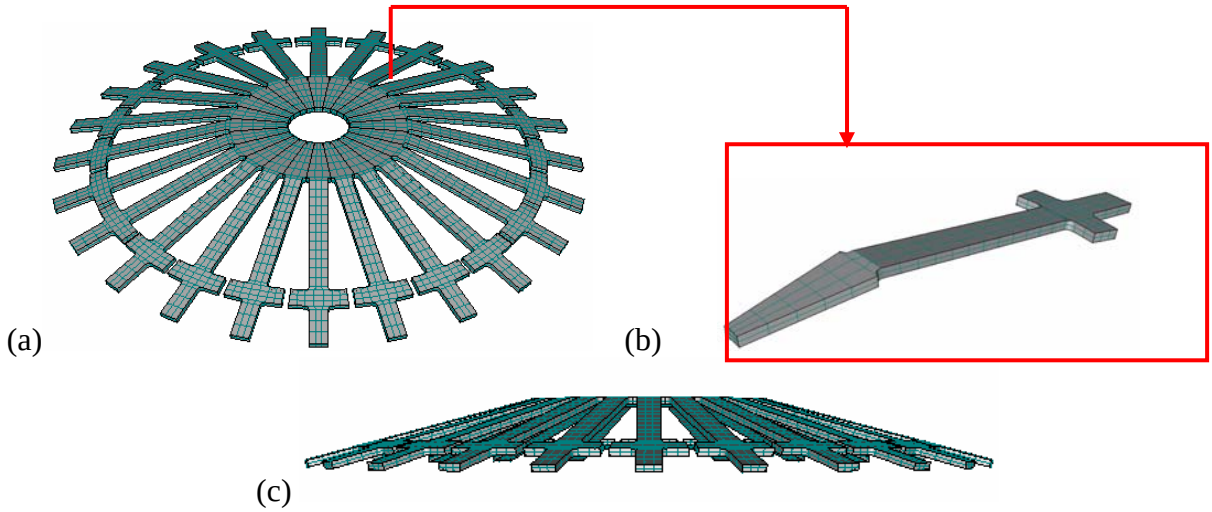

Fig. 3-4. Simple bladed disc: (a) full model (isometric view), (b) its cyclic sector, and (c) full model (left view)

Fig. 3-5. Trent 1000 fan ran for the first time on 14th February 2006

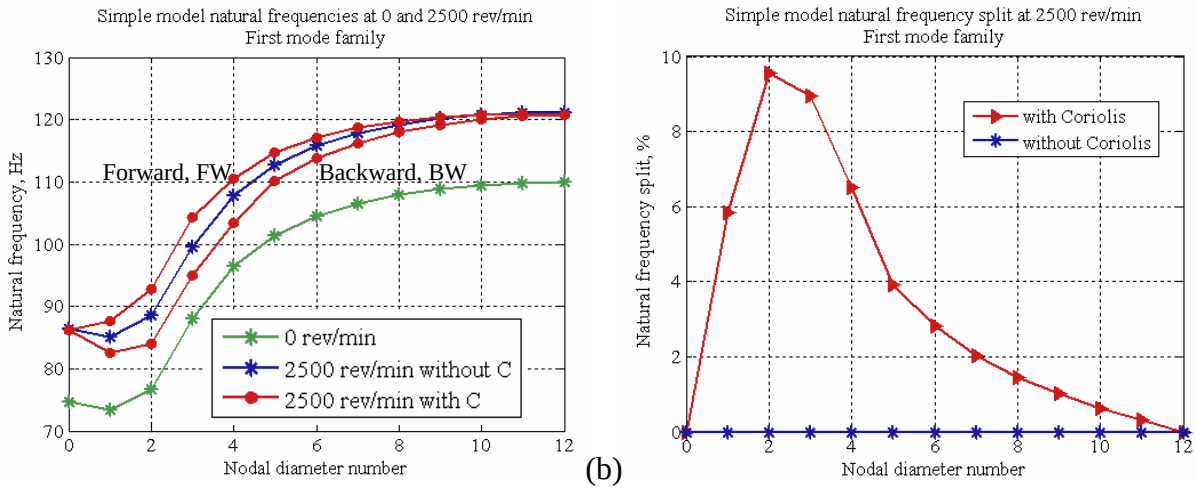

Fig. 3-6. Simple model natural frequencies (a) and split (b) of the first mode family due to Coriolis forces

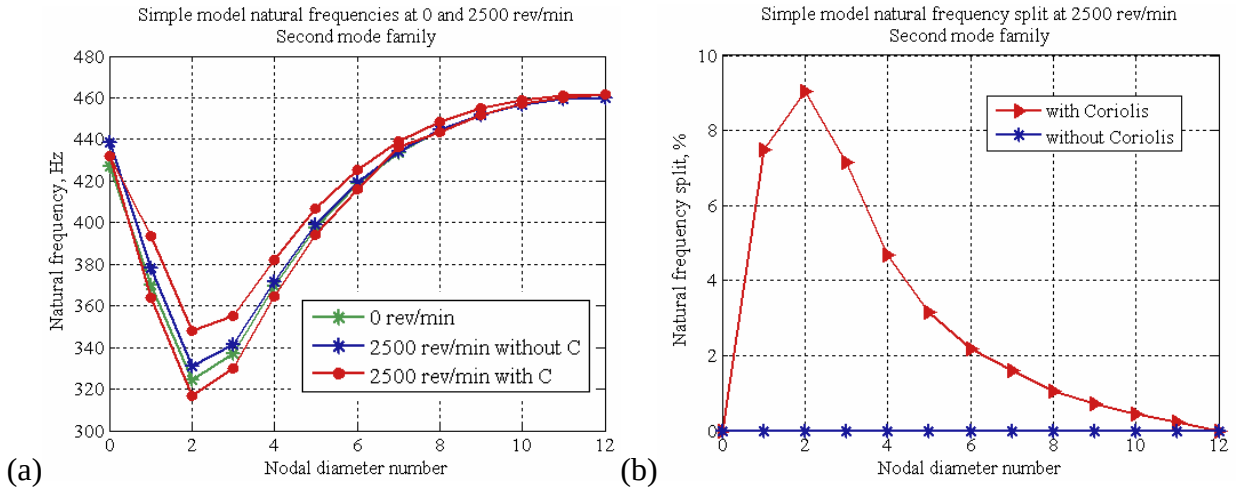

Fig. 3-7. Simple model natural frequencies (a) and split (b) of the second mode family due to Coriolis forces

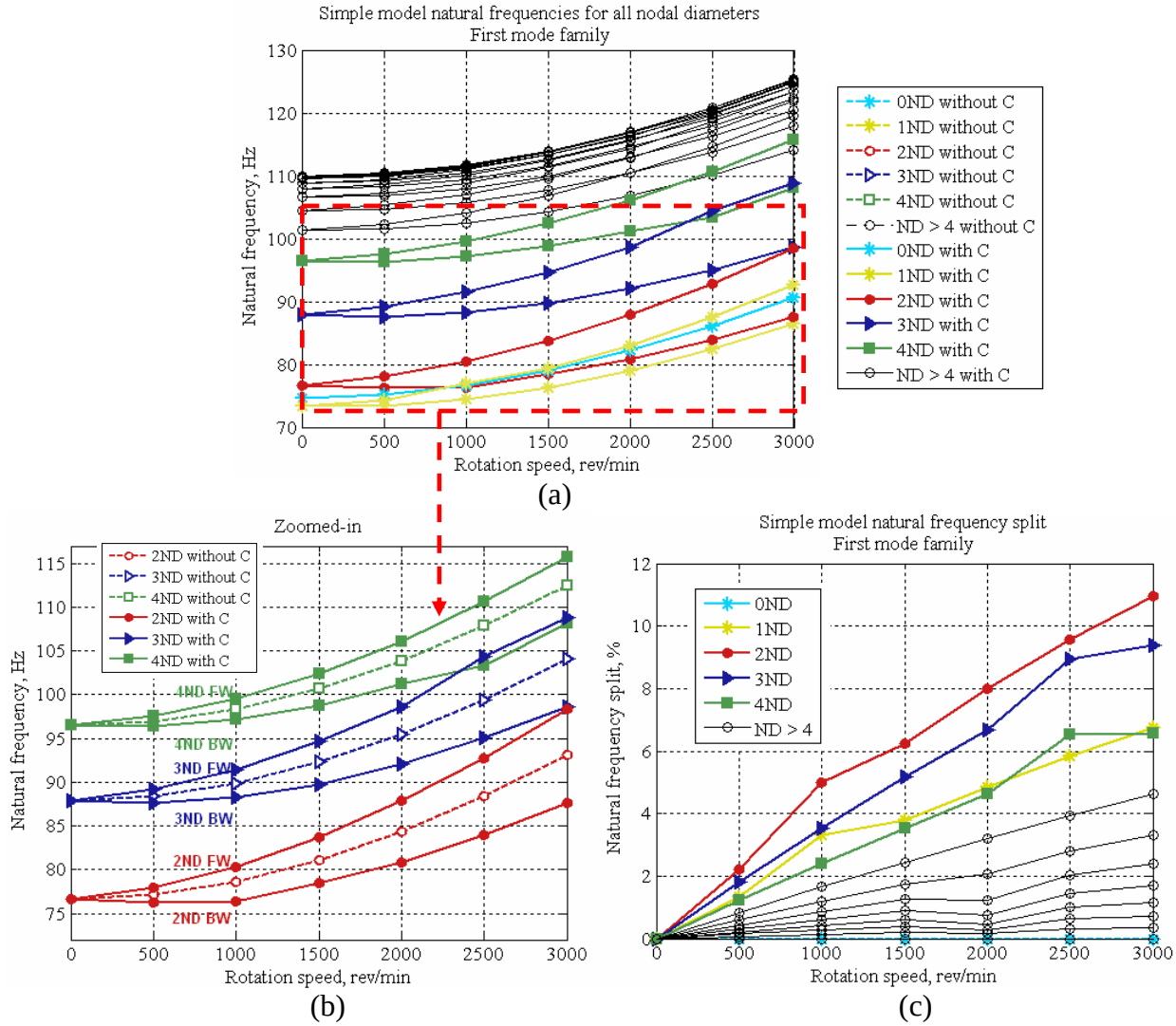

Fig. 3-8. Simple model natural frequency (a, b) and split (c) dependency upon rotation speed

The difference between the results obtained with and without Coriolis forces is apparent. When analysed in the absence of Coriolis forces, as demonstrated in Figs. 3-6 and 3-7 at 0rev/min and 2500rev/min with centrifugal forces included only, a perfectly-tuned cyclically-symmetric bladed disc is characterised by double modes with identical natural frequencies for each number of nodal diameters, except for those with nodal indexes equivalent to 0 and $\frac{N}{2}$, where N is a number of blades. When Coriolis forces are taken into account, these double modes split into pairs of single modes with different natural frequencies and with mode shapes corresponding to a forward or backward travelling wave mode for each nodal diameter number. A forward travelling wave, defined with respect to the rotating frame of reference, is a wave that travels in the same direction as the rotation of a bladed disc, while a backward travelling wave moves in the opposite direction to the bladed disc rotation. It is also observed from Figs. 3-6 and 3-7 that for both analysed mode families, the Coriolis-generated natural frequency split is largest for lower numbers of nodal diameters, characterised by high coupling between the blades and disc. As expected, the influence of Coriolis forces increases significantly with the rotation speed for all nodal diameter modes. Tables 3-1 and 3-2 show the order-of-magnitude of Coriolis-induced natural frequency splits predicted using SAMCEF software for the first two mode families of a simple tuned bladed disc.

Simple tuned bladed disc - First mode family													
	0ND	**1ND**	**2ND**	**3ND**	**4ND**	**5ND**	**6ND**	**7ND**	**8ND**	**9ND**	**10ND**	**11ND**	**12ND**
0 rev/min													
Frequency	74.72	73.36	76.64	87.96	96.47	101.45	104.53	106.56	107.93	108.86	109.47	109.81	109.92
(Hz)	-	73.36	76.64	87.96	96.47	101.45	104.53	106.56	107.93	108.86	109.47	109.81	-
Split (%)	-	**0.0%**	**0.0%**	**0.0%**	**0.0%**	**0.0%**	**0.0%**	**0.0%**	**0.0%**	**0.0%**	**0.0%**	**0.0%**	-
2500 rev/min (Centrifugal forces only)													
Frequency	86.31	85.12	88.48	99.47	107.85	112.79	115.84	117.85	119.20	120.12	120.72	121.06	121.17
(Hz)	-	85.12	88.48	99.47	107.85	112.79	115.84	117.85	119.20	120.12	120.72	121.06	-
Split (%)	-	**0.0%**	**0.0%**	**0.0%**	**0.0%**	**0.0%**	**0.0%**	**0.0%**	**0.0%**	**0.0%**	**0.0%**	**0.0%**	-
2500 rev/min (Coriolis and centrifugal forces)													
Frequency	86.15	82.44	83.92	95.02	103.38	110.15	113.81	116.25	117.95	119.14	119.96	120.50	120.80
(Hz)	-	87.56	92.79	104.38	110.60	114.65	117.09	118.66	119.69	120.35	120.73	120.87	-
Split (%)	-	**5.9%**	**9.6%**	**9.0%**	**6.5%**	**3.9%**	**2.8%**	**2.0%**	**1.5%**	**1.0%**	**0.6%**	**0.3%**	-

Table 3-1. Simple model natural frequencies and splits due to Coriolis forces of the first mode family

The largest natural frequency split of almost 10% at maximum rotation speed of 2500rev/min was obtained for 2ND mode of the first mode family. More importantly, it is seen that in addition to Coriolis-induced split in the 1ND modes, which is anticipated by classical rotordynamics, all other nodal diameter modes are

also split by a non-negligible amount. A similar trend is observed in natural frequencies belonging to the second mode family.

Simple tuned bladed disc - Second mode family													
	0ND	1ND	2ND	3ND	4ND	5ND	6ND	7ND	8ND	9ND	10ND	11ND	12ND
0 rev/min													
Frequency	426.91	370.11	324.62	337.09	369.33	397.61	418.69	433.85	444.53	451.85	456.58	459.22	460.07
(Hz)	-	370.11	324.62	337.09	369.33	397.61	418.69	433.85	444.53	451.85	456.58	459.22	-
Split (%)	-	0.0%	0.0%	0.0%	0.0%	0.0%	0.0%	0.0%	0.0%	0.0%	0.0%	0.0%	-
2500 rev/min (Centrifugal forces only)													
Frequency	438.62	378.33	331.15	341.31	371.67	398.84	419.31	434.14	444.65	451.88	456.57	459.19	460.04
(Hz)	-	378.33	331.15	341.31	371.67	398.84	419.31	434.14	444.65	451.88	456.57	459.19	-
Split (%)	-	0.0%	0.0%	0.0%	0.0%	0.0%	0.0%	0.0%	0.0%	0.0%	0.0%	0.0%	-
2500 rev/min (Coriolis and centrifugal forces)													
Frequency	432.25	364.03	313.50	329.98	364.30	393.87	416.16	436.24	443.70	451.67	456.96	460.11	461.45
(Hz)	-	393.41	347.99	355.40	382.24	406.77	425.41	438.93	448.47	454.95	459.02	461.11	-
Split (%)	-	7.5%	9.1%	7.2%	4.7%	3.2%	2.2%	1.6%	1.1%	0.7%	0.5%	0.2%	-

Table 3-2. Simple model natural frequencies and splits due to Coriolis forces of the second mode family

It was demonstrated that the order of magnitude of the anticipated natural frequency splits due to effects of Coriolis forces can be quite large for several of the lower numbers of nodal diameters. A consequence of this is to shift resonance positions on the Campbell diagram from those of a tuned system, thereby introducing a potentially significant effect on an important design feature, as indicated in Fig. 3-9. Furthermore, this may provide an explanation for surprising and unexpected occasional failures of bladed discs due to unpredicted resonance conditions, reported for lower nodal diameter modes.

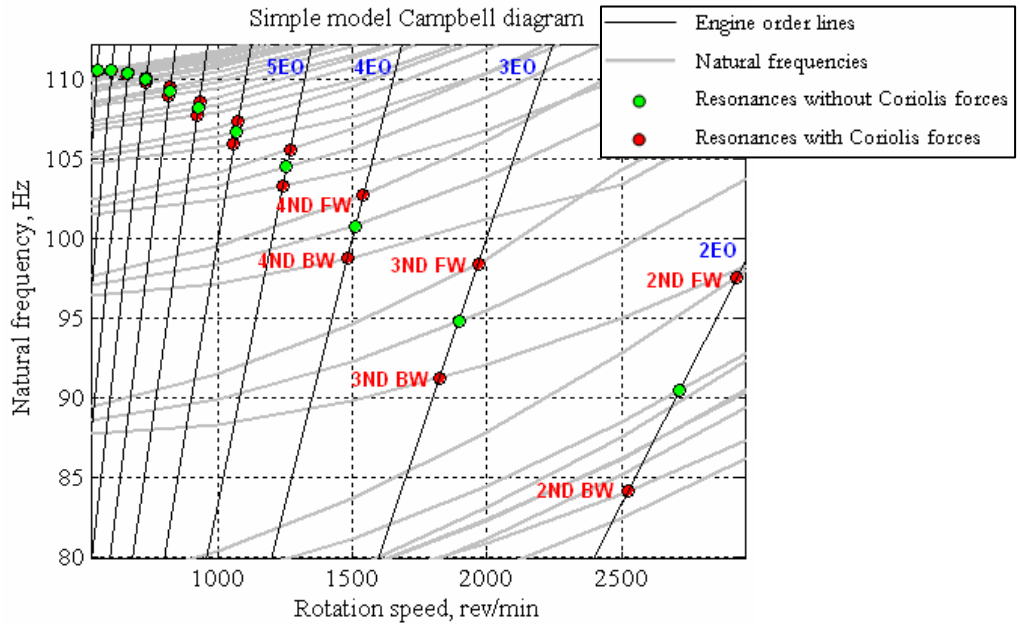

Fig. 3-9. Simple model Campbell diagram with and without Coriolis forces

So far, attention has been drawn in this thesis to the effects of Coriolis forces on natural frequencies of a tuned structure. As mentioned briefly above, the mode shapes of a system with Coriolis forces are complex and are believed to comprise forward and backward travelling waves in a rotating frame of reference. Fig. 3-10 exhibits 2ND mode shapes of the first two mode families of a simple bladed disc at 2500rev/min. It should be noted here that even though SAMCEF software is assumed at this stage to provide correct natural frequencies, its mode shape representation poses some difficulties. In particular, it is known that the mode shapes are not mass-normalised, and hence cannot be used in forced response calculations. Secondly, it is not entirely clear whether predictions of mode shapes are accurate. Nevertheless, at this moment, graphical demonstration of mode shapes is useful in indicating the general characteristics of the first two mode families, which may be classified as blade out-of-plane vibration for the first mode family, and blade in-plane tangential vibration for the second mode family.

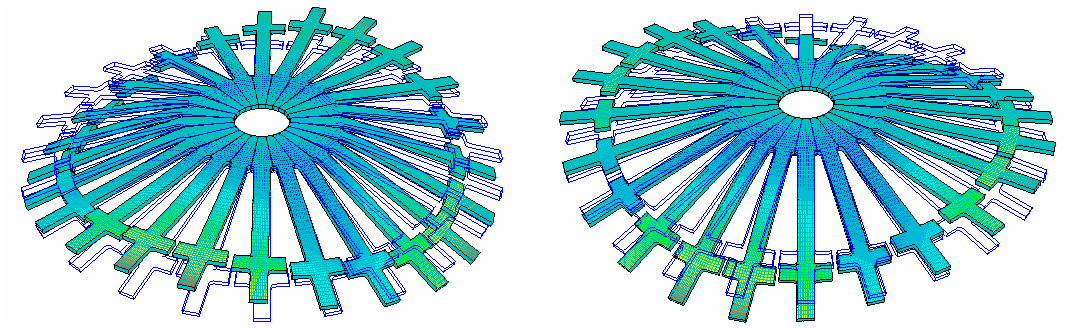

(a) 83.92 Hz (b) 92.79 Hz

(c) 313.50 Hz (d) 347.99 Hz

Fig. 3-10. Simple model 2ND forward and backward mode shapes at 2500rev/min of the first (a,b) and second (c,d) mode family

3.6.3 Effects of Coriolis forces on a realistic tuned bladed disc

An example of a simple tuned bladed disc served to confirm theoretically predicted influence of Coriolis forces on free vibration properties. In this part of the chapter, results obtained with a more realistic bladed disc are presented with an aim

to provide some indication of the order-of-magnitude of Coriolis-generated splits in tuned natural frequencies that might be expected in practice. The bladed disc chosen in the following study, further referred to as "Blisk1" and described in detail in [118], was designed as a part of an EU project "Aeromechanical Design of Turbine Blades II" (ADTurB II). The model of Blisk1 turbine bladed disc shown in Fig. 3-11, consisting of 24 blades staggered by 30degrees and 21,555 degrees-of-freedom per sector, was analysed using SAMCEF software.

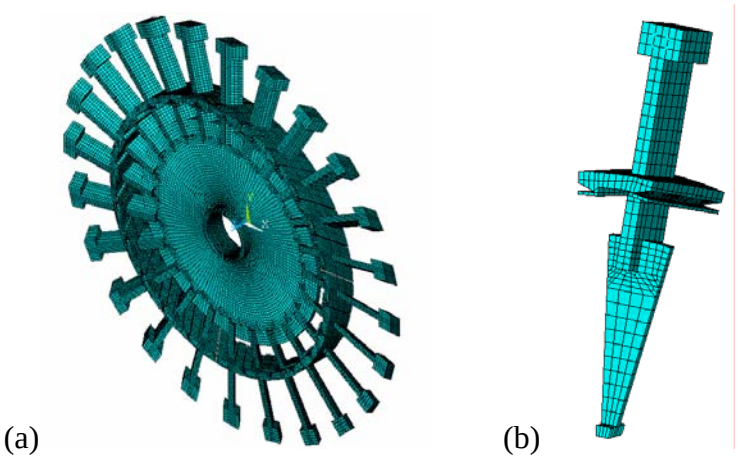

(a) (b)

Fig. 3-11. Blisk1: (a) full model, and (b) its cyclic sector

Blisk1 natural frequencies obtained at 0rev/min and 4000rev/min with and without Coriolis forces are presented in Fig. 3-12a and Table 3-3. As for the simpler bladed disc reported earlier, larger natural frequency splits due to Coriolis forces were calculated for lower numbers of nodal diameters, as shown in Fig. 3-12b. In particular, a significant split of approx. 0.5% at 4000rev/min was obtained for 2ND mode.

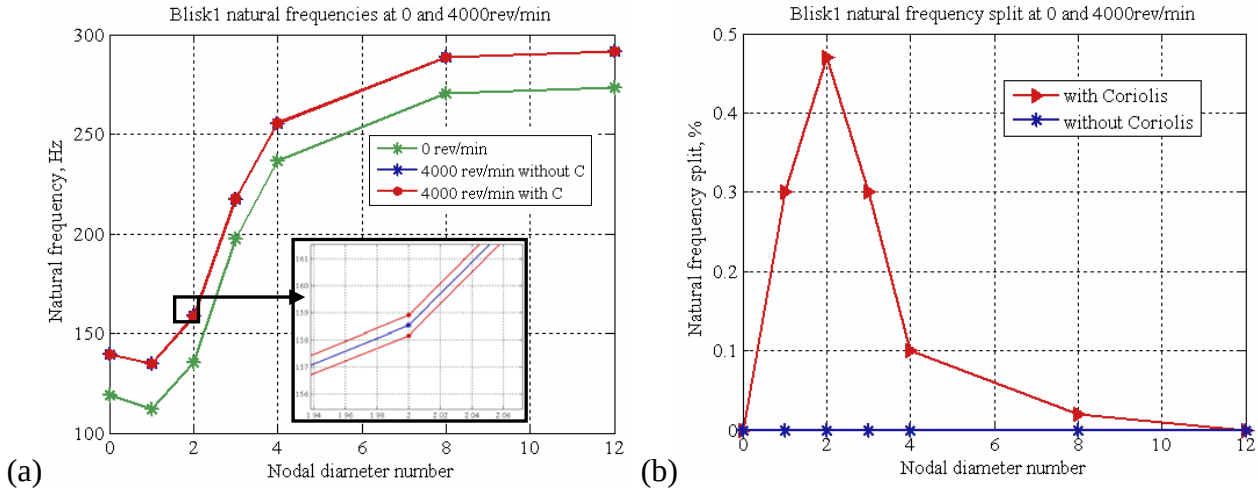

(a) (b)

Fig. 3-12. Blisk1 natural frequencies (a) and split (b) due to Coriolis forces

Bliskl tuned bladed disc							
	0ND	1ND	2ND	3ND	4ND	8ND	12ND
0rpm							
Frequency	119.05	112.25	135.20	197.48	236.75	270.24	273.57
(Hz)	-	112.25	135.20	197.48	236.75	270.24	-
Split (%)	-	0.00%	0.00%	0.00%	0.00%	0.00%	-
4000rpm	(Centrifugal forces only)						
Frequency	139.40	134.87	158.55	217.29	255.48	288.43	291.66
(Hz)	-	134.87	158.55	217.29	255.48	288.43	-
Split (%)	-	0.00%	0.00%	0.00%	0.00%	0.00%	-
4000rpm	(Coriolis and centrifugal forces)						
Frequency	139.40	134.66	158.17	216.97	255.35	288.40	291.66
(Hz)	-	135.07	158.92	217.61	255.62	288.46	-
Split (%)	-	0.30%	0.47%	0.30%	0.10%	0.02%	-

Table 3-3. Blisk1 natural frequencies and splits due to Coriolis forces

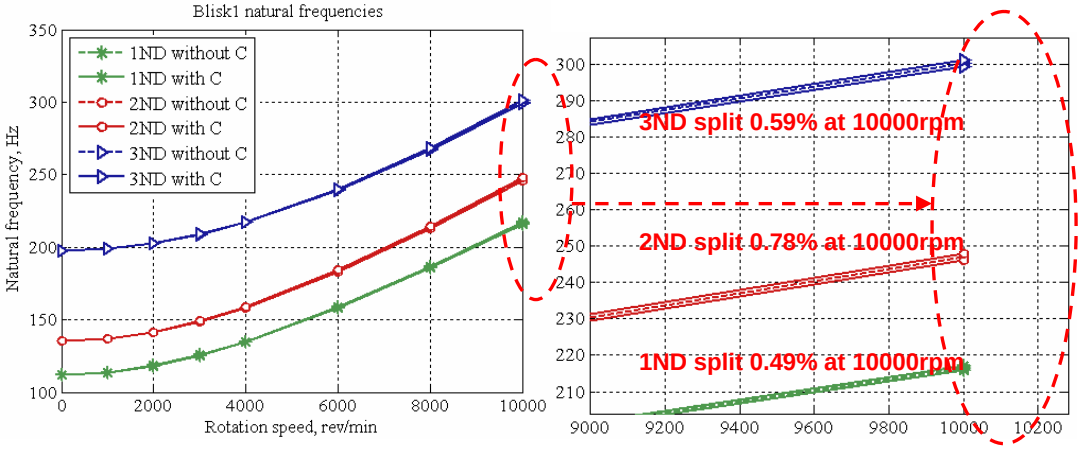

Fig. 3-13. Evolution of Blisk1 natural frequencies with rotation speed

Fig. 3-13 further demonstrates evolution of Blisk1 natural frequencies with rotation speed up to 10000rev/min. A steady increase in all lower nodal diameter natural frequency splits is observed with rotation speed, whereas the split in the 2ND modes reaches 0.8% at 10,000rev/min.

Mode shapes calculated for first 2ND mode at 4000rev/min are presented in Fig. 3-14. They correspond to first blade out-of-plane (bending) mode shapes.

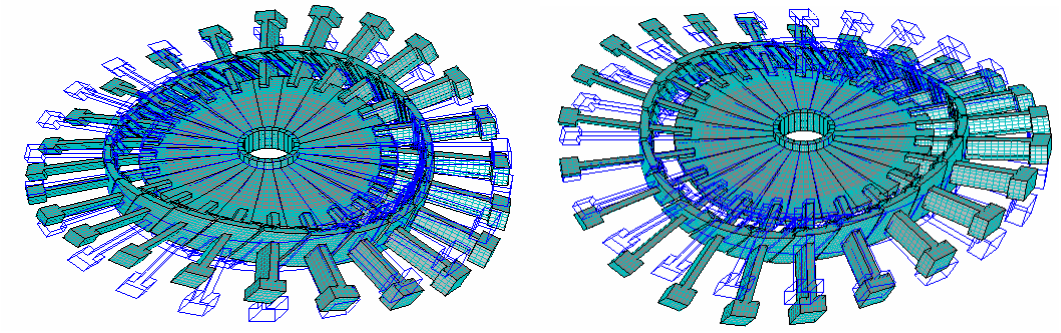

(a) 158.17 Hz (b) 158.92 Hz

Fig. 3-14. Blisk1 mode shapes of the first 2ND mode at 4000rev/min

3.6.4 On the availability of codes capable of including the effects of Coriolis forces in bladed disc vibration analysis

A FE software package, SAMCEF from SAMTECH S.A., has been used for analysis of both cyclically-symmetric and whole bladed disc structures with the effects of Coriolis forces included, as it has been the only code readily available throughout the course of this work. As mentioned above, the drawback with this code lies in its provision of non-mass-normalised mode shapes, which does not permit forced response analysis. The latest version from ANSYS, version 10.0, which was released on the market in July 2005, offers similar capability in relation to Coriolis forces. The disadvantages of this software compared with SAMCEF are (i) the necessity to analyse the whole structure as opposed to a cyclically-symmetric sector model, (ii) restrictions on element types used in the analysis with Coriolis forces included, and (iii) problems with non-mass-normalisation of mode shapes. Accordingly, a few ANSYS results will be presented in Chapter 4 of this thesis in order to verify numerically SAMCEF natural frequency predictions. Finally, a third rotordynamics software package from INSA, Lyon – CORIODYN – has been identified as a possible candidate for analysis of bladed discs with Coriolis effects. The author does not have any experience with this code. However, there are indications ([119]) that it could provide reliable natural frequency results.

3.7 Significance of effects of Coriolis forces

3.7.1 General considerations

Current commercial aircraft design trends lean towards lighter and faster engines, which result in increased flexibility of structure and a gradual stretch of design limits to higher operational speeds, as indicated in Fig. 3-15. Consequently, the lower nodal diameter modes are more likely to be brought into the operating region, and accurate prediction of their resonances becomes critical at high rotation speeds. The influence of Coriolis forces rises with rotation speed and increased amount of coupling, which is particularly relevant in the case of low nodal diameter modes. The several examples above serve to demonstrate large splits in natural frequencies occurring for these modes, and resulting dramatic resonance condition changes on Campbell diagrams. Thus, at design stage, it is important to establish the precise effects of Coriolis forces on operating characteristics of a given bladed disc in order to avoid failures.

Moreover, the conspicuous absence of Coriolis forces from bladed disc analyses in the past may be a responsible factor for recurring inconsistency between theoretical predictions and experimental data and rare unanticipated failures.

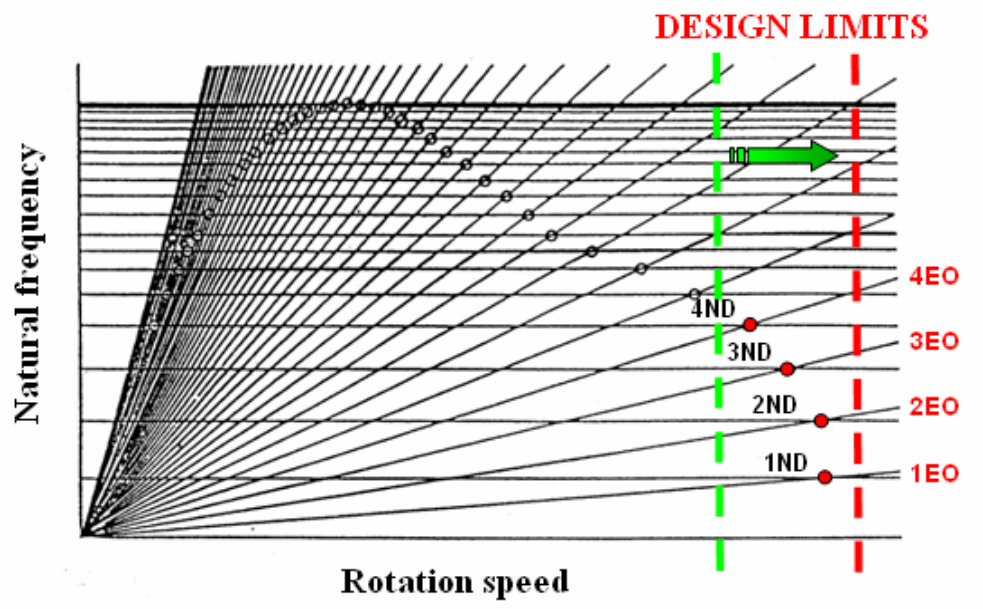

Fig. 3-15. In pursuit of lighter and faster engines, design limits stretch towards higher rotation speeds, thus exposing vulnerable low nodal diameter modes

3.7.2 Interaction with mistuning

Until now, analysis of bladed discs in this thesis has been confined to tuned assemblies, in which all sectors possess identical properties and, thus, permit analysis using a single cyclically-symmetric sector model. In practice, however, such an idealised tuned state never exists, as bladed disc properties are random variables and differ from sector to sector. This phenomenon is commonly referred to as mistuning, and has been a major investigation issue among bladed disc researchers for many years. In contrast to tuned bladed disc characteristics, mistuning causes doubles modes to split into two distinct natural frequency modes, and nodal lines to become fixed uniquely in their orientation on the bladed disc ([113]). Furthermore, the responses of two mistuned modes do not constitute a pure travelling wave only, but include an additional standing, or body-fixed, wave component as well. In traditional mistuned bladed disc analysis, similarly to the analysis of tuned structures, the effects of Coriolis forces have hitherto been considered to be negligible ([32], [34], [36]). To the best of author's knowledge, there are no investigations available in the published literature on the effects of

mutual influence of Coriolis forces and typical blade mistuning. Nevertheless, as has been shown in this Chapter, the order of magnitude of Coriolis-generated natural frequency splits is comparable to splits typically resulting from the loss of symmetry of the structure caused by mistuning, as illustrated in Fig. 3-16. This strongly suggests that the analysis of bladed discs should include all important physical phenomena to ensure accurate prediction of forced response characteristics. A study of mutual influence of Coriolis forces and mistuning will be presented in Chapter 5 of this thesis.

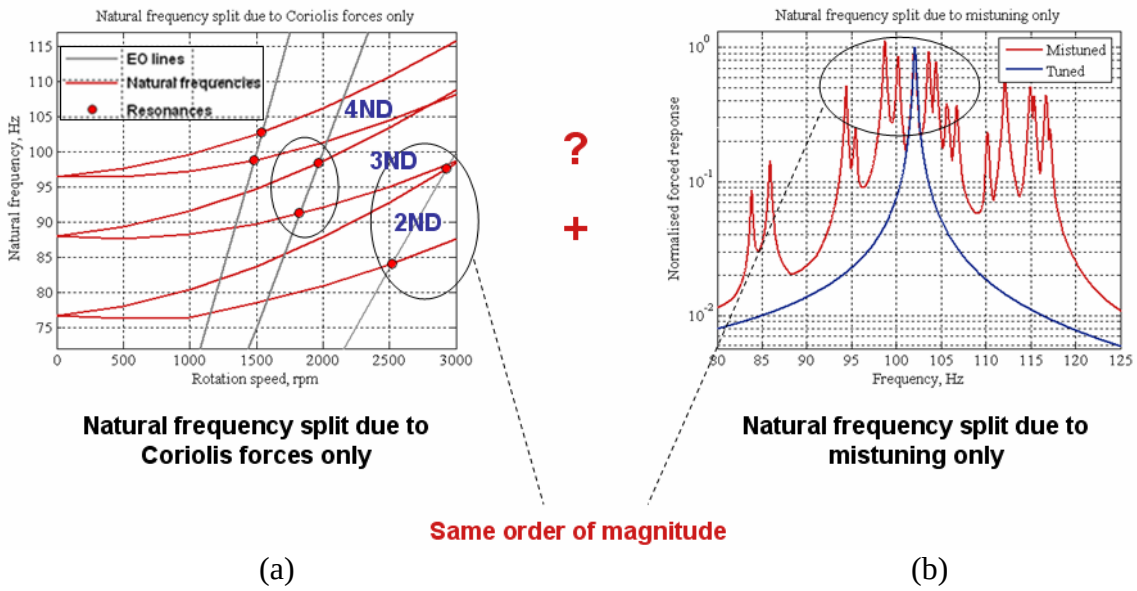

(a) (b)

Fig. 3-16. Natural frequency split due to Coriolis forces (a) and typical blade mistuning (b)

3.8 A need for experimental validation of effects of Coriolis forces

Numerical results obtained in this Chapter using a simple model and realistic bladed discs indicate that the influence of Coriolis forces is non-trivial due to significant changes that these forces impose on vibration characteristics of bladed discs. However, the effects of Coriolis forces on bladed discs have never been validated experimentally, the process of which is believed to add credibility to model under consideration. For this reason, and before proceeding with further predictions of behaviour of bladed disc systems incorporating Coriolis forces and typical blade mistuning, the need for validation is identified, which will provide indisputable evidence of the influence of Coriolis forces. Experimental validation is subject of the following Chapter.

3.9 Summary

In contrast to traditional bladed disc analysis, this Chapter has provided an assessment of previously-neglected rotation effects of Coriolis forces on free vibration characteristics of tuned bladed discs. By presenting theoretical analysis and a few typical numerical examples, the significance of Coriolis forces has been established with regard to current design trends and the critical interaction with mistuning identified. Consequently, the need for experimental validation has been identified in order to provide sound evidence of the influence of Coriolis forces and to boost confidence in the improved model of bladed discs.

CHAPTER 4

Experimental Validation Of The Effects Of Coriolis Forces

"Argument is conclusive, but it does not remove doubt, so that the mind may rest in the sure knowledge of the truth, unless it finds it by the method of experiment"
Roger Bacon

4.1 Overview

The influence of Coriolis forces on bladed disc vibration characteristics is validated experimentally in this Chapter using a carefully-designed testpiece, the principal feature of which emphasises the action of Coriolis forces. A non-intrusive state-of-the-art measurement technique is employed using an SLDV (Scanning Laser Doppler Velocimeter) with blade point-tracking method under both rotating and stationary conditions. A special in bladed disc experiments excitation system using a fixed AC magnet is exploited to facilitate the measurements of both the backward and forward travelling waves for mode shapes with predominantly lower number of nodal diameters. Theoretical predictions including Coriolis forces are compared with measured data and factors stimulating these forces intensity are discussed. The significance of the results achieved and their impact on realistic bladed discs is established.

4.2 Aim and significance of experimental validation

A need for experimental validation or empirical justification of the effects of Coriolis forces on bladed discs has been identified in Chapter 3. The primary aim of this process is to provide quantitative confidence assessment of the improved theoretical model reliability and accuracy of representation of bladed disc dynamics.

In addition to experimental validation, which is usually believed to consolidate theoretical academic capabilities with practical industry needs, numerical verification is a complementary procedure often used for complete assessment of the prediction competence. While experimental validation refers to "the process of determining the degree to which a model is an accurate representation of the real world", model verification is "the process of determining that a model representation accurately represents the developer's conceptual description and solution of the model"[1], as shown in Fig. 4-1. The emphasis of this Chapter is on experimental validation. However, a brief numerical verification of SAMCEF code will also be presented.

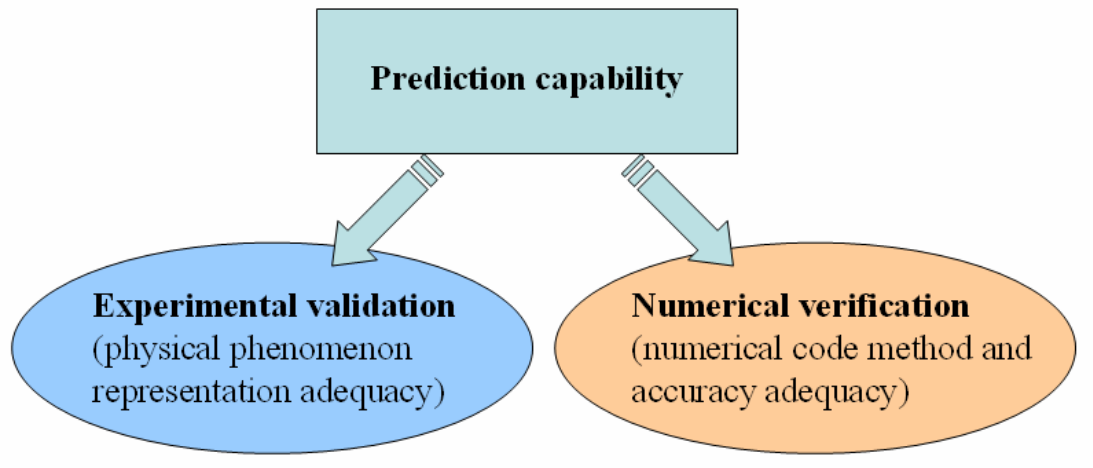

Fig. 4-1. Experimental validation and numerical verification of prediction capability

It should be noted that experimental validation of the effects of Coriolis forces on free vibration properties of nominally-tuned bladed discs is performed for the first time and significance of these forces in bladed disc vibration characteristics is established conclusively.

[1] Oberkampf, W.L., Trucano, T.G. and Hirsch, C., 2002, "Verification, Validation And Predictive Capability In Computational Engineering and Physics", Presentation for Foundations for Verification and Validation in the 21st Century Workshop, Maryland

4.3 Testpiece design

4.3.1 Design requirements

The aim of the testpiece design is to provide experimental validation of the predictions made for natural frequency splits of tuned bladed discs resulting from the effects of Coriolis forces, as reported in Chapter 3. Therefore, the following design specifications have been identified:

- The bladed disc design should be simple with a capability to demonstrate clearly and unambiguously the effect of Coriolis forces on first bending mode family within the operating rotation speed range of the rig (preferably, less than 2500rev/min);
- The bladed disc should be as tuned as possible to avoid any unintentional mistuning-generated natural frequency splits;
- Since the emphasis is on the lower nodal diameter modes for which relatively large natural frequency splits were anticipated, the relevant testpiece modes should be reasonably well separated.

4.3.2 Discussion of features stimulating a prominent effect of Coriolis forces and testpiece design

In order to design a testpiece to exhibit a strong Coriolis forces effect, it is necessary to establish the crucial characteristics of design and test conditions that contribute to the enforced action of Coriolis forces. As discussed in Chapter 3, there are several factors governing the intensity of Coriolis forces. Firstly, Coriolis is a speed-dependent effect and so the testpiece measurements should be carried out under rotating conditions at appropriate rotation speeds. Secondly, it has been established that Coriolis forces are generated when there is bladed disc rotation and significant radial and tangential components in blade vibratory displacements. Coriolis forces produce coupling between these displacements, and the higher the coupling, the more prominent the effect of Coriolis forces is on the natural frequencies. A strong coupling can be achieved in several ways. One way to increase the coupling is by introducing ‘swept’ blades, i.e. blades which lean in the axial direction. The higher the angle by which the blades lean or, as will be referred in this thesis, the higher the ‘sweep’ angle, the greater the influence of Coriolis forces, as there is a strong in-plane vibration coupling. In particular, in a swept blade configuration, there is a prominent radial component of vibration, compared with

'straight' or unswept bladed structure. Thus, it was decided to study the effects of Coriolis forces on "two" testpieces instead of one, by conducting experiments initially on a 'straight' bladed disc, and, subsequently, by bending the testpiece blades to a chosen angle in order to obtain a 'swept' bladed disc. The two configurations of these testpieces, practically emerging from the same bladed disc, will be further referred to as "Flat Blisk" and "Swept Blisk". The selection of a swept testpiece is justified by recent trends towards increasingly complex three-dimensional blade designs in gas-turbine engines.

The angle of inclination of the blades with respect to the axial direction, or the 'sweep' angle, is a very important feature of the design affecting the Coriolis forces effect. The exact amount of sweep of the blades was dictated by predictions and existing test rig limitations and needs to detect unambiguously the effect of Coriolis forces. Furthermore, experimental confirmation of the increased Coriolis forces intensity due to an increase of the sweep angle was desired. In the light of this, it was decided to sweep the Flat Blisk blades initially by 10degrees (10deg), subsequently increased to 15degrees (15deg).

A rather flexible bladed disc was chosen with a "blade" thickness of 1.89mm, contributing to a blade length-to-thickness ratio of 90:1, and with an overall diameter of 525mm. A FE model of the Flat Blisk created in PATRAN using Hex20 (20-node hexahedron 3D solid) element type is illustrated in Fig. 4-2. The full bladed disc model consists of 261,072 nodes and 49,680 elements, comprising 783,216 DOFs. All models were considered fully fixed at the disc inner radius to represent a reasonable approximation to the practical situation encountered in the test rig.

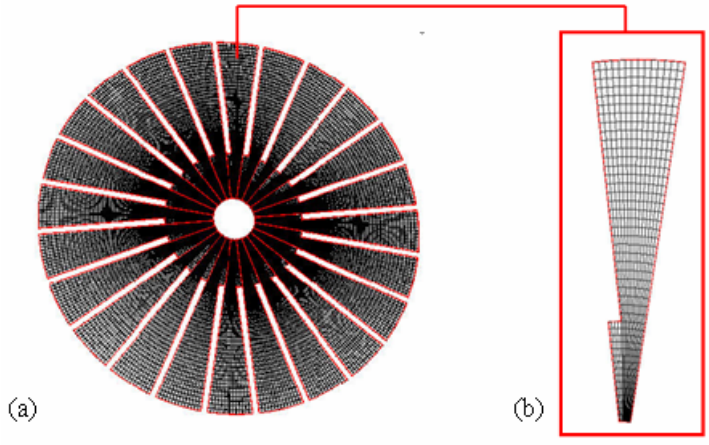

Fig. 4-2. FE full model of a Flat Blisk (a) and its cyclic sector (b)

Fig. 4-3. Flat Blisk (before bending)

Photographs of the testpiece before and after bending processes are given in Figs 4-3 to 4-5. The Blisk was accurately manufactured using a laser cutting technique from a hot-rolled mild steel sheet.

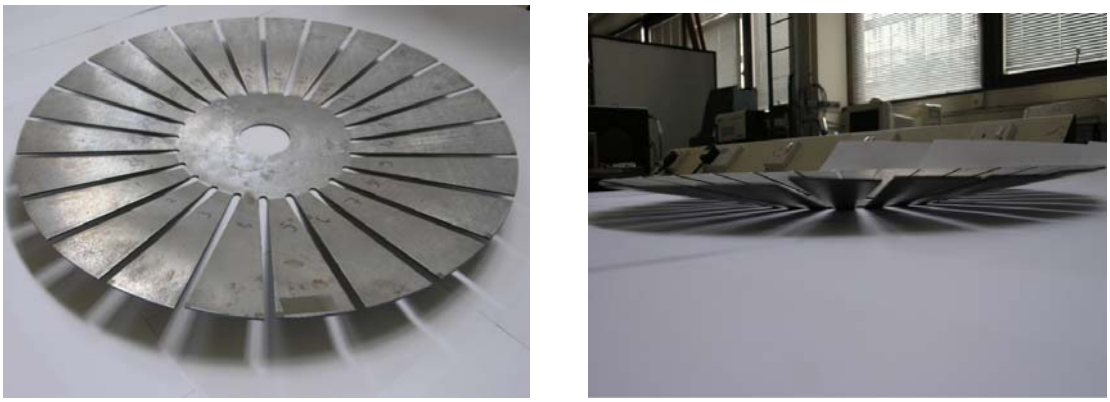

Fig. 4-4. Swept Blisk 10deg (after first bending)

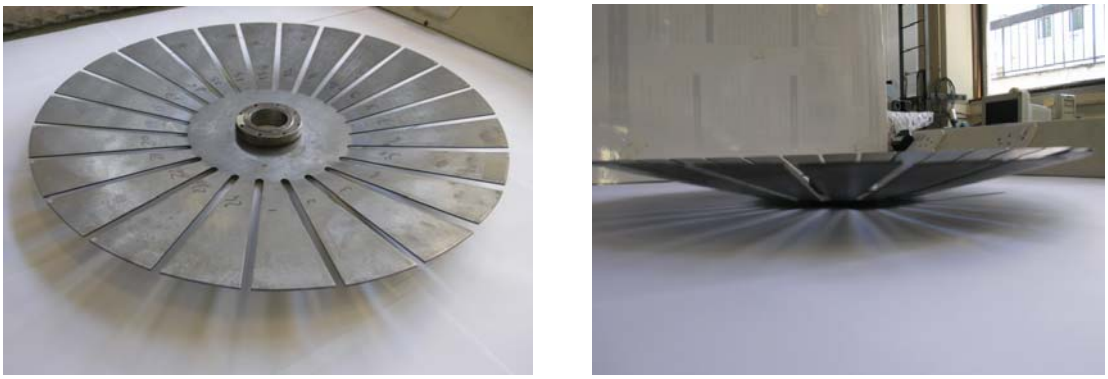

Fig. 4-5. Swept Blisk 15deg (after second bending)

Campbell diagrams shown in Figs. 4-6 and 4-7 were constructed for the Swept Blisk 10deg and Swept Blisk 15deg designs, respectively, using natural frequency data obtained with the SAMCEF FE software package.

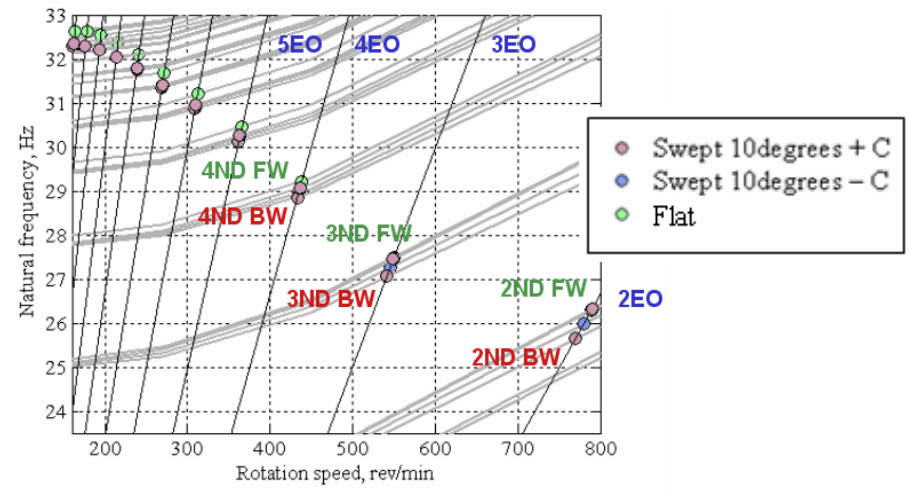

Fig. 4-6. Flat Blisk and Swept Blisk 10deg Campbell diagram*

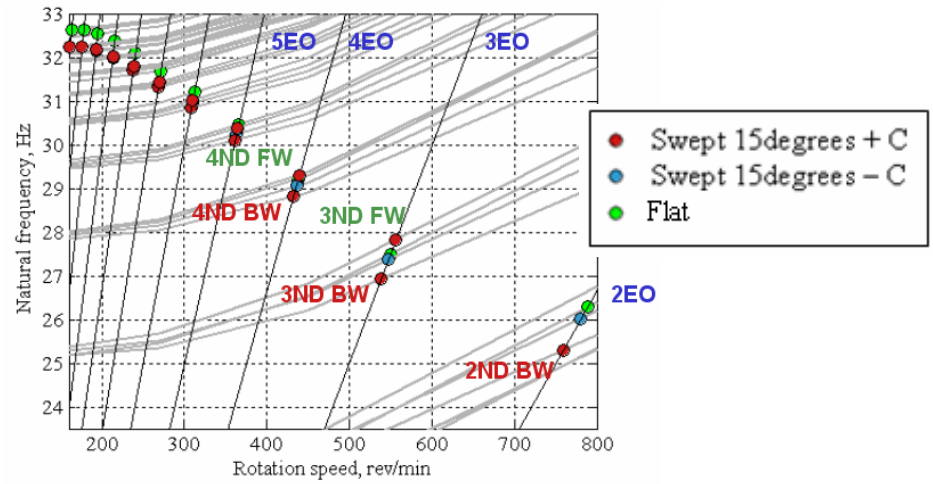

Fig. 4-7. Flat Blisk and Swept Blisk 15deg Campbell diagram

The resonances corresponding to the first bending (1F) family of modes are illustrated. For both blisks with swept blades, the natural frequencies predicted with and without the influence of Coriolis forces are clearly different: double natural frequencies calculated in the absence of Coriolis forces at each rotation speed are replaced with two distinct natural frequencies corresponding to backward and forward travelling waves when Coriolis forces are included in the analysis. The consequence of this as seen on the Campbell diagrams is to shift the resonance positions of different speeds. In practice, the conventional (stationary) engine order

* "+C" means "with Coriolis forces", "–C" – without Coriolis forces

excitation excites the backward travelling wave only. By considering a bladed disc rotating clockwise, shown schematically in Fig. 4-8(a), a stationary force will be always experienced by a rotating bladed disc in an opposite direction, or anti-clockwise. Thus, a typical stationary ($\omega = 0$) engine order excitation would excite a backward travelling wave, as viewed in stationary frame of reference, Fig. 4-8(b). In order to capture the forward travelling wave resonance, the engine order excitation is insufficient and an alternative, variable frequency excitation system is required, the details of which and a comprehensive mathematical account are given below in section 4.4.2 of this chapter.

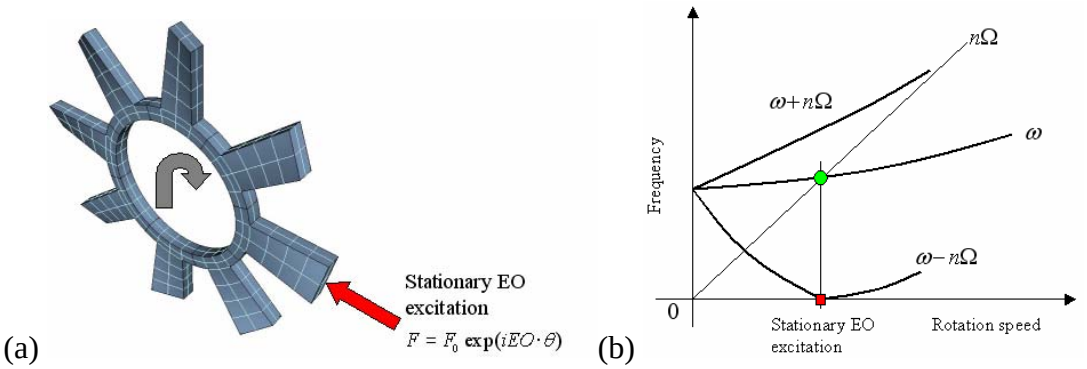

Fig. 4-8. Engine order excitation

Detailed results will be given in the subsequent sections, while here it is sufficient to note that the natural frequency split due to Coriolis forces predicted by SAMCEF at the maximum speed of 2500rev/min is 3.5% for the first 2ND mode pair for the Swept Blisk 10deg and, correspondingly, 8.1% in the case of Swept Blisk 15deg obtained for the same mode pair. The latter pair of 1F bending mode shapes is illustrated in Fig. 4-9.

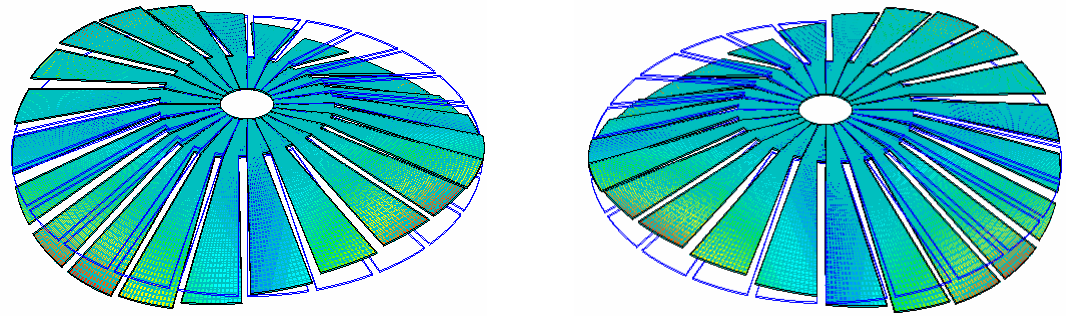

Fig. 4-9. Swept Blisk 15deg first 2ND mode pair

A smaller predicted natural frequency split is observed for Swept Blisk 15deg compared to the Simple bladed disc design with the same sweep angle analysed in Chapter 3 (8.1% versus 9.6% for first 2ND mode pair at 2500rev/min). This is due to differences in the moments of inertia of two structures: the Simple bladed disc has a ratio of blade length-to-thickness of 36:1, while significantly more flexible Swept Blisk 15deg - 90:1. It is to be noted from Chapter 3 that gyroscopic moment depends on change of angular momentum of rotor, which in turn varies according to moment of inertia and rotational and precessional angular velocity, as $M = I\omega\omega_p$. Thus, if rotation speed is kept constant, a structure with larger moment of inertia (alike Simple bladed disc from Chapter 3) will be more prone to the effects of Coriolis forces. This demonstrates that not only the sweep angle governs the Coriolis forces sensitivity, but also the overall geometry of a bladed disc.

For the Flat Blisk, as expected, the effects of Coriolis forces do not change the natural frequencies and do not introduce any split at all. Nevertheless, originally Flat Blisk results will be used as a reference case and a valuable means of comparison with the swept blisks. Since the predictions using blisks with swept blades indicated that the natural frequencies of the first family of modes are split to a greater extent compared to those belonging to the second mode family, the experimental validation study will focus on first bending family of modes in both blisk cases.

4.4 Test rig

4.4.1 Hardware of the test rig

The test rig used in the experiments is depicted in Fig. 4-10. It consists of a support structure enclosing the rig, test chamber with a clear polycarbonate cover and a rear panel housing various other parts, including the electromagnetic exciter. A detailed description of the test rig can be found in [118].

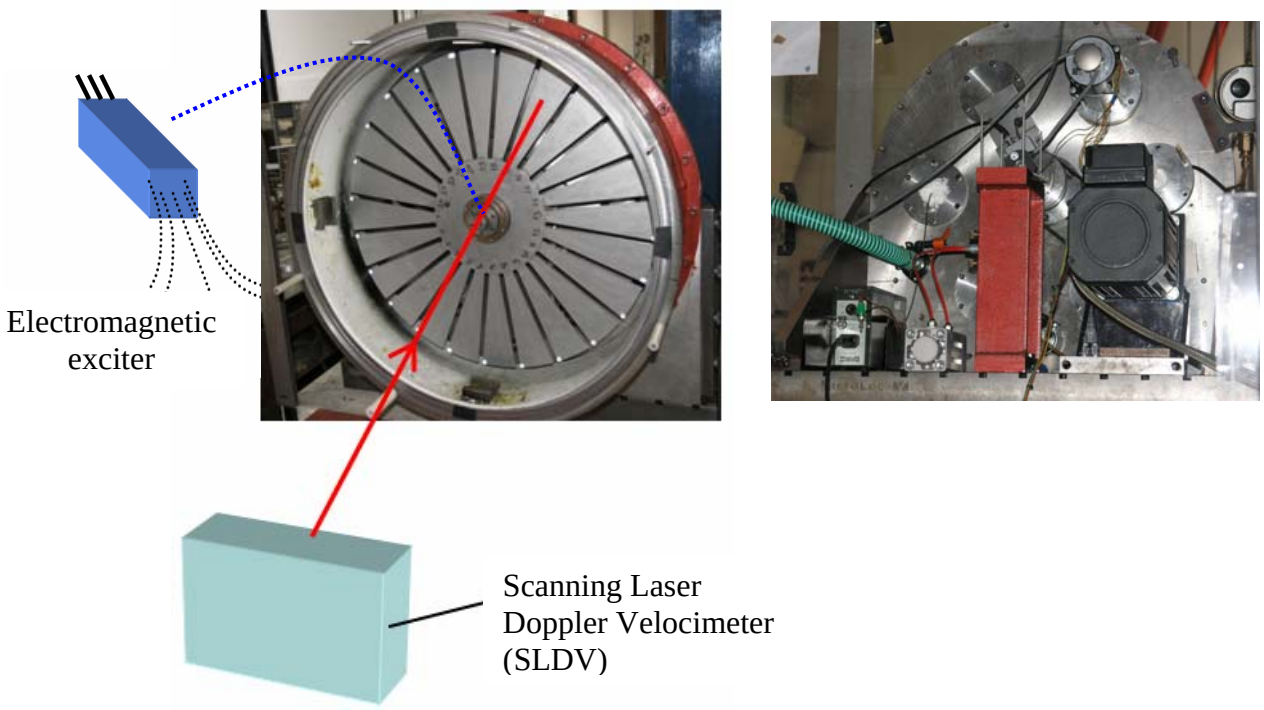

Fig. 4-10. Test rig

4.4.2 Electromagnetic excitation system

Bladed discs in turbomachinery are usually subjected to engine order excitation, angular variation in axial (static) pressure which is experienced by rotating blades as a set of periodic forces exerted on every blade, but with a phase lag between the action on adjacent blades. A detailed explanation of the nature of this type of excitation is given in Appendix A4-1. It is well known that such an excitation, which in testing practice is often achieved by employing permanent DC magnets, excites backward travelling waves only, and this is not sufficient to demonstrate the phenomenon of a split in natural frequencies into forward and backward travelling waves due to effects of Coriolis forces. To avoid this limitation, a non-contacting AC electromagnetic excitation is proposed instead, which allows both backward and forward travelling waves to be excited at any rotation speed.

For a bladed disc rotating at speed Ω, the coordinate of a point in fixed frame of reference, θ_0, is related to the coordinate of the point in a rotating frame of reference, θ, by:

$$\theta_0 = \theta - \Omega t \tag{4-1}$$

Assuming a harmonic stationary single point force applied in a fixed frame of reference of the form:

$$f(t) = F_0 \cos \omega t \text{ , where } \omega \text{ is the excitation frequency,} \tag{4-2}$$

the force acting on a bladed disc system can be expressed as:

$$F(\theta, t) = (F_0 \cos \omega t)\delta(\theta - \Omega t) \tag{4-3}$$

where δ, the Kronecker delta, satisfies:

$$\begin{aligned} &\delta(\theta - \Omega t) = 0 \quad \text{for} \quad \theta - \Omega t \neq 0 \\ &\int_{-\infty}^{+\infty} \delta(\theta - \Omega t) d\theta = 1 \end{aligned} \tag{4-4}$$

Assuming the pair of *n-th* nodal diameter (ND) bladed disc modes to have a standard form of mode shapes: $\phi_{1s}(\theta) = \sin n\theta$ and $\phi_{1c}(\theta) = \cos n\theta$, the generalised forces for the assumed modes become:

$$\begin{aligned} Q_{1n} &= \int_0^{2\pi} F(\theta, t)\phi_{1s}(\theta) d\theta \\ Q_{2n} &= \int_0^{2\pi} F(\theta, t)\phi_{1c}(\theta) d\theta \end{aligned} \tag{4-5}$$

which, after integration, are transformed into:

$$\begin{aligned} Q_{1n} &= f(t) \sin n\Omega t \\ Q_{2n} &= f(t) \cos n\Omega t \end{aligned} \tag{4-6}$$

Finally, using the standard trigonometric functions transformations, the two generalised forces acting in rotating frame of reference can be expressed as:

$$\begin{aligned} Q_{1n} &= F_0 \cos \omega t \sin n\Omega t = \frac{F_0}{2} \sin(\omega - n\Omega)t + \frac{F_0}{2} \sin(\omega + n\Omega)t \\ Q_{2n} &= F_0 \cos \omega t \cos n\Omega t = \frac{F_0}{2} \cos(\omega - n\Omega)t + \frac{F_0}{2} \cos(\omega + n\Omega)t \end{aligned} \tag{4-7}$$

It has been shown that the stationary single point force will generate a series of excitations experienced by the bladed disc in a rotating frame of reference at two distinct frequencies, $(\omega \pm n\Omega)$, for each *n*ND mode. In the case of engine order excitation (the static force, $\omega = 0$), the excitation is experienced at a frequency of $n\Omega$ for each *n*ND mode. The *n*ND response of a bladed disc consists of a summation of orthogonal modes and can be expressed in the form [120]:

$$\begin{aligned} \mathrm{X}_n(\theta,t) &= \mathrm{X}_{1n}(\theta,t) + \mathrm{X}_{2n}(\theta,t) \\ \mathrm{X}_n(\theta,t) &= -\Xi_1 \sin[(\omega + n\Omega)t + \xi]\sin n\theta + \Xi_2 \sin[(\omega - n\Omega)t - \xi]\sin n\theta \\ &\quad + \left\{-\Xi_3 \cos[(\omega + n\Omega)t + \xi]\cos n\theta + \Xi_4 \cos[(\omega - n\Omega)t - \xi]\cos n\theta\right\} \end{aligned} \tag{4-8}$$

where Ξ_1, Ξ_2, Ξ_3 *and* Ξ_4 are the response amplitudes of the orthogonal components and ξ is a response phase angle.

Hence, the electromagnetic excitation alternating at frequency ω^+ gives a response at frequency $R^+ = \omega^+ - n\Omega$, whereas the excitation frequency ω^- yields the response frequency of $R^- = \omega^- + n\Omega$, thus allowing both backward travelling and forward travelling waves to be excited experimentally. Further information on this kind of excitation of rotating bladed discs can be found in references [121] and [122].

4.4.3 Vibration measurement system

Vibration measurements of testpiece were achieved using a non-intrusive state-of-the-art SLDV (Scanning Laser Doppler Velocimeter). Fundamentally, the LDV transducer is a device which performs velocity measurement of the surface of a structure by directing a laser beam at the desired point and by measuring the Doppler shift between the incident light and scattered light returning from the target structure. A typical advantage of LDV lies in its ability to measure successively response at a large number of points without introducing any structural modification to the vibrating structure. On the other hand, the main limitations of this type of response transducer are due to “line of sight” requirements and the problems associated with speckle noise, an optical phenomenon which results in occasional “drop-outs” or “null measurements” that need to be eliminated from the data set [113]. A scanning velocimeter, SLDV, provides an extension of the LDV capabilities by incorporating a scanning device which relocates the laser beam from one measurement site to the next in a controlled way. A technique used in this work was that of tracking a specific point on a blade and performing scanned measurements on rotating (in addition to vibrating) testpiece. A detailed analysis of SLDV theory and measuring techniques can be found in [113].

4.5 Comparison of predicted and measured† results

4.5.1 A note on comparison procedure

A typical modal analysis validation process of theoretical predictions against experiment involves several stages from a direct comparison of specific dynamic properties and correlation to identification of sources of discrepancies and adjustments or updating of the theoretical model to reconcile it with behaviour observed in practice [113]. Usually, both sets of modal properties (natural frequencies and mode shapes) are featured in the comparison process. In this Chapter, the above-mentioned procedure will be followed in the case of natural frequency data only, since, as noted in Chapter 3, section 3.6.4, the predicted mode shape data are not readily available and suitable for comparison due to the format obtained from SAMCEF code.

4.5.2 Results after first bending process

As mentioned in section 4.3.2, it was decided to sweep the Flat Blisk blades initially by 10deg, subsequently increased to 15deg, in order to obtain the experimental confirmation of the increased Coriolis forces' intensity due to an increase of the sweep angle. The full set of results for the Swept Blisk 10deg (after first bending process) under stationary and rotating conditions is given in Appendices A4-2 and A4-3. However, for the sake of clarity, only the selected results for the Swept Blisk 15deg (after second bending process) will be presented here.

4.5.3 Results after second bending process

4.5.3.1 Swept Blisk 15deg stationary conditions results

Measurements of natural frequencies of the first bending family of modes were initially acquired under non-rotating conditions in vacuum in order (i) to assess the degree of correlation between the measured results and FE model predictions, and (ii) to identify the level of blade tuning (or, strictly, mistune). Natural frequencies of the Blisk testpiece before and after the bending processes were measured by impact testing, so that the impact was applied at a point on a disc and the response measured at different blades using the SLDV. The FFT resolution was

† The author gratefully acknowledges a contribution from Mr. Dario Di Maio in providing the measured results in this Chapter

such that the natural frequencies in the region of 0-50Hz could be identified to within 0.01Hz.

Detailed experimental and predicted* results at 0rev/min obtained for the Swept Blisk 15deg testpiece (after the second bending process) are presented in Tables A4-6 and A4-7 in the Appendix A4-4. Swept Blisk 10deg results are included for comparison purposes. Table A4-6 reveals that additional blade sweep does not introduce any additional mistuning for most of the modes. In particular, while the 2ND mode remains mistuned by approximately 0.36%, the 3ND mode does not appear to be influenced by inherent mistuning of the testpiece, which makes it adequate for further measurements under rotating conditions.

The predicted natural frequencies for Swept Blisk 15deg at 0rev/min, illustrated in Fig. 4-11, compare well with those measured, with the average difference less than 1.4%.

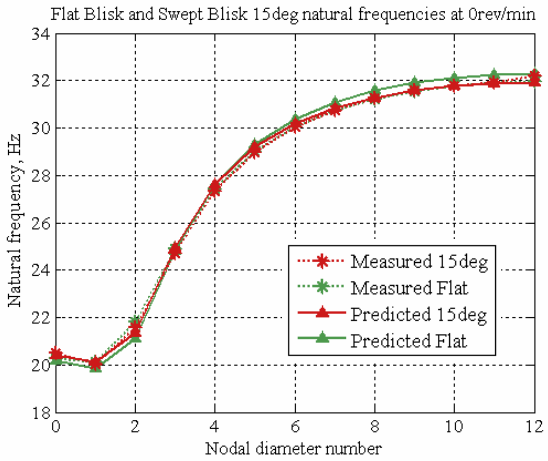

Fig. 4-11. Flat Blisk and Swept Blisk 15deg natural frequencies at rest

4.5.3.2 Swept Blisk 15deg rotating conditions results

Experimental and predicted natural frequencies have been obtained for Flat Blisk and Swept Blisk 15deg in the case of first 1, 2 and 3ND mode pairs under rotating conditions. Classical rotordynamics 1ND results are presented as means of comparison with higher nodal diameter modes. Tables A4-8 to A4-10 in the Appendix A4-4 show detailed results for the first 2 and 3ND mode pairs, while Table 4-1 summarises the most important results for all considered mode pairs.

The first 1ND mode pair (rotating conditions) results are illustrated in Fig. 4-12. As expected, predictions for the Swept Blisk 15deg indicate a steady rise in the natural frequency split of the first 1ND mode pair. With the aim of brief numerical

* "Predicted" refers to SAMCEF code predicted data

code verification, in addition to the SAMCEF predictions, ANSYS results for the Swept Blisk 15deg including both Coriolis and centrifugal forces were acquired at 450rev/min. The difference between the SAMCEF and ANSYS predicted natural frequency splits is 0.01%, which shows that two codes based on the same theory, predict very close natural frequency separations due to Coriolis forces. A disadvantage of using the ANSYS code compared to SAMCEF is the necessity of analysing a whole bladed disc model (in ANSYS) as opposed to a single cyclic sector (in SAMCEF), which dramatically increases the computation time.

		1ND		2ND			3ND	
	Speed, rev/min	Measured Split, %	Predicted Split, %	Measured Split, %	Predicted Split, %	Speed, Rev/min	Measured Split, %	Predicted Split, %
Flat	0	0.00%	0.00%	0.50%	0.00%	0	0.00%	0.00%
Blisk	450	-	0.00%	0.42%	0.00%	450	0.08%	0.00%
	900	-	0.00%	0.49%	0.00%	700	0.10%	0.00%
	-	-	-	-	-	1000	0.22%	0.00%
Swept	0	0.00%	0.00%	0.36%	0.00%	0	0.00%	0.00%
Blisk	450	-	1.58%	1.70%	2.61%	450	1.67%	2.20%
15deg	600	-	2.01%	1.78%	3.34%	540	1.81%	2.58%
	900	-	2.73%	0.95%	4.54%	900	1.64%	3.96%

Table 4-1. Selected Flat Blisk and Swept Blisk 15deg results

Interpreting the measured data for 1ND under rotating conditions was difficult due to significant interaction between the bladed disc and shaft for this mode, which resulted in noisy and unclear data.

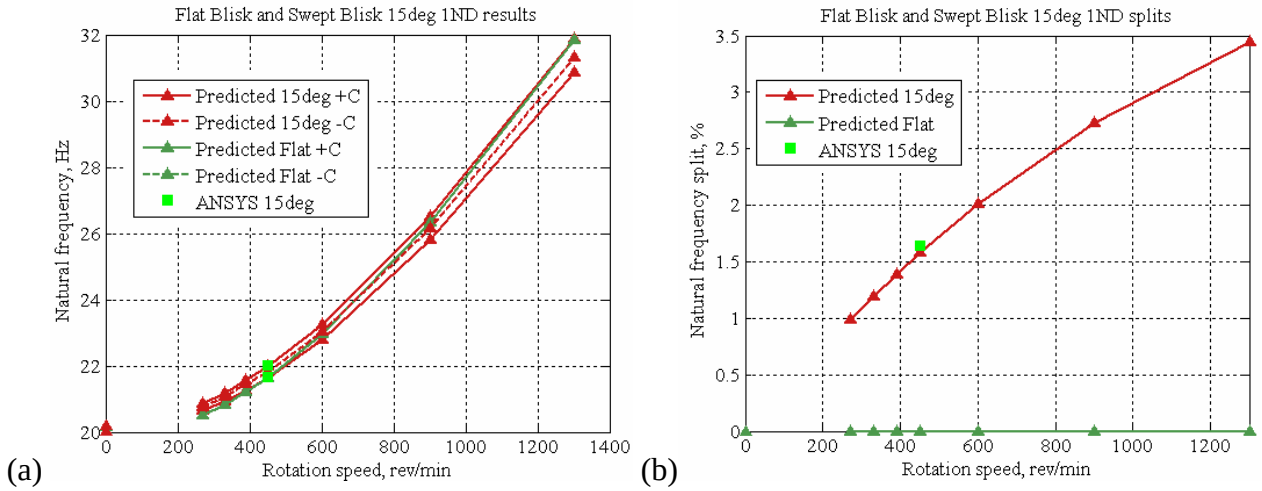

(a) (b)

Fig. 4-12. Flat Blisk and Swept Blisk 15deg first 1ND mode pair rotating conditions results: natural frequencies (a) and their splits (b)

Fig. 4-13 illustrates the first 2ND mode pair results for the Swept Blisk 15deg under rotating conditions. A comparison of all results with the Swept Blisk 10deg is given in Figs. 4-14 and 4-15.

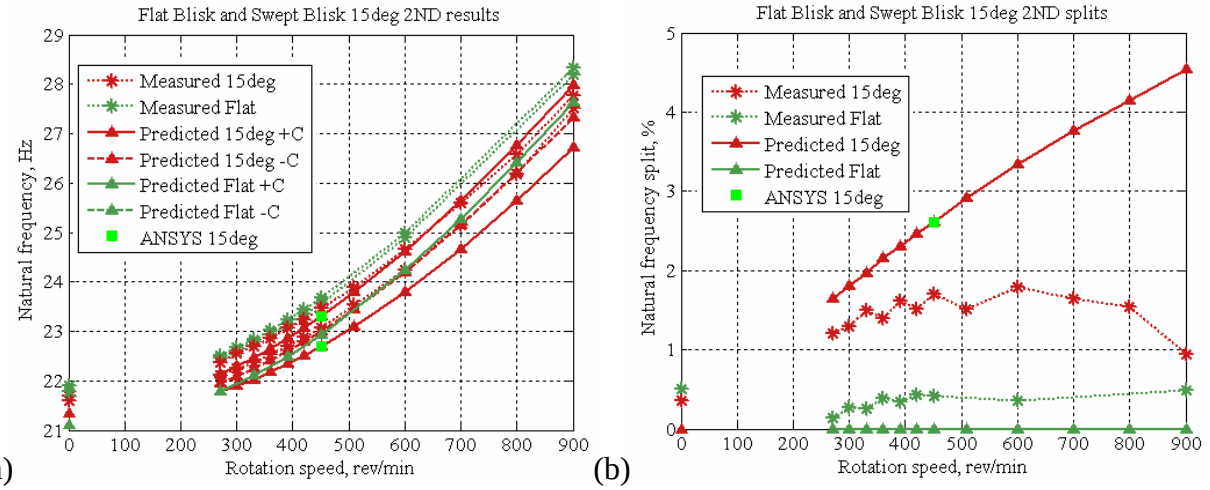

Fig. 4-13. Flat Blisk and Swept Blisk 15deg first 2ND mode pair rotating conditions results: natural frequencies (a) and their splits (b)

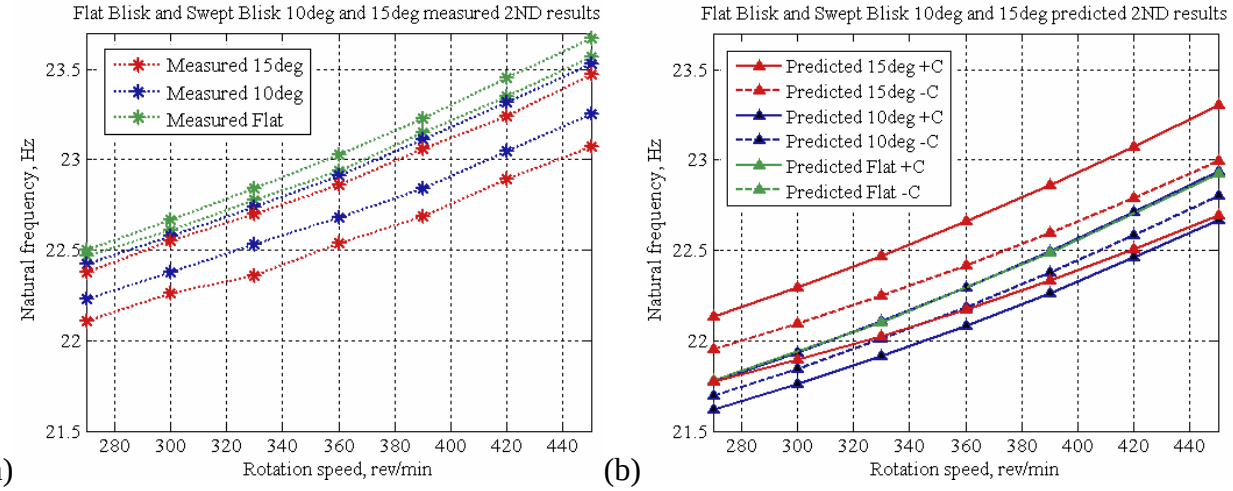

Fig. 4-14. Flat Blisk and Swept Blisk 10deg and 15deg first 2ND mode pair rotating conditions natural frequency results: measured (a) and predicted (b)

From Figs. 4-14 and 4-15 it is evident that the measured natural frequency split for Swept Blisk 15deg has increased by approximately 40% compared to the split measured for the Swept 10deg. Moreover, the experimentally-established split for Swept Blisk 15deg increases from 0.36% at 0rev/min (due to mistuning only) to 1.78% at 600rev/min (which is almost 5 times the split at 0rev/min), but then gradually decreases. Such a substantial increase in the natural frequency split is not likely to be due to mistuning, and suggests strongly that Coriolis-splitting is a genuine phenomenon. Predictions which include the effects of Coriolis and centrifugal forces, on the other hand, indicate a nearly linear increase in the natural frequency split, and thus poor correlation at higher frequencies. Further explanations

for the reasons of the mismatch between the measured and predicted results for Swept Blisk 15deg will follow in the next section of this Chapter.

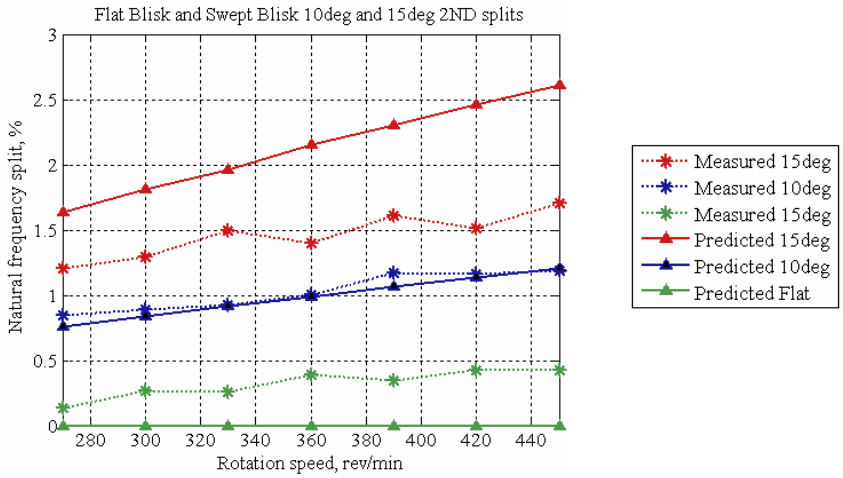

Fig. 4-15. Flat Blisk and Swept Blisk 10deg and 15deg first 2ND mode pair rotating conditions natural frequency splits

Corresponding natural frequency results were also obtained for the first 3ND mode pair. Measured natural frequency split for Swept Blisk 15deg illustrated in Fig. 4-16 increases from 0% up to 1.81% at approximately 540rev/min and then diminishes as the rotation speed is increased further. It is important to note here that the 3ND mode is not affected significantly by inherent mistuning and the observed natural frequency split is almost entirely due to the effects of Coriolis forces.

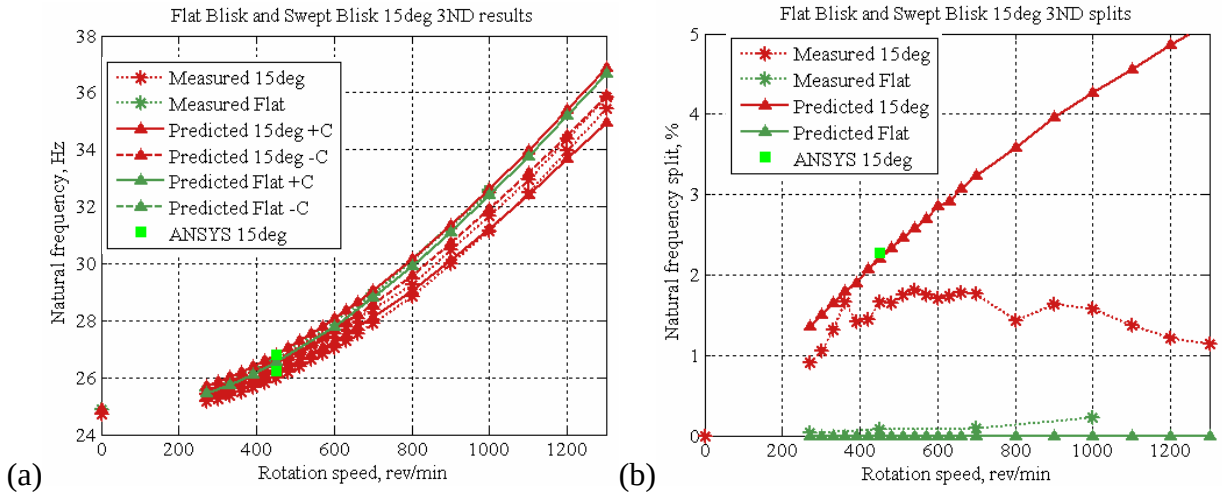

Fig. 4-16. Flat Blisk and Swept Blisk 15deg first3ND mode pair rotating conditions results: natural frequencies (a) and their splits (b)

As for the 2ND case, the predicted results are close to the 3ND experimental data up to a certain speed, beyond which the predicted natural frequency split increases almost linearly, while the measured values remain constant, even falling at

higher speeds. The ANSYS-predicted splits for the first 2 and 3ND mode pairs at 450rev/min are consistently close to SAMCEF-generated results, with a maximum absolute difference of less than 0.01%.

4.5.4 Effects of centrifugal forces on geometry of the testpiece

The measured results have provided evidence of the essential phenomenon of a steady increase of the natural frequency split up to a certain rotation speed and then a gradual decline of the split as the rotation speed is increased further. The reason for the observed 'convex' shape of the measured split curve and for the encountered mismatch between measurements and predictions at high rotation speeds is found to be due to an effect not included in the analysis – the significant static deflections resulting from centrifugal forces. Both prediction codes, the SAMCEF and ANSYS, fail to incorporate the appropriate geometry change arising from centrifugal forces due to extremely flexible nature of the testpiece, the influence of which, as seen from measurements, is to reduce gradually the blade sweep angle as the rotation speed is increased. The reduction of the sweep angle causes a diminished influence of Coriolis forces and, thus, a resulting decrease in the measured split magnitudes after an initial rise.

The data presented in this Chapter confirm that the influence of the Coriolis forces is directly dependent upon a precise magnitude of the sweep angle: the higher the sweep angle, the more intense the Coriolis forces action on a blade becomes, and vice versa. Thus, a decrease in the sweep angle will be accompanied by a diminished effect of the Coriolis forces, which supports the evidence of a drop in the generated measured natural frequency splits.

The effect of static deflections due to centrifugal forces on the blades is illustrated experimentally in Fig. 4-17. Here, the blade tip static deflections have been captured at 450, 700, 1000 and 1300rev/min and their values interpreted to indicate the change in the sweep angle as a function of rotation speed. Further plots in Fig. 4-18 and 4-19 and Table 4-2 summarise the measured and predicted results for this effect.

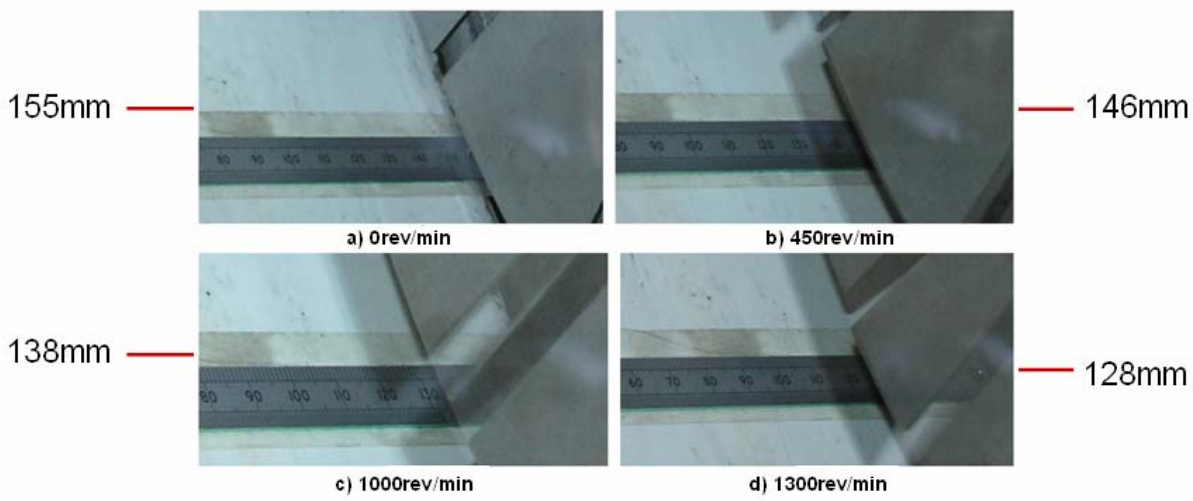

Fig. 4-17. Swept Blisk 15deg measured static deflections due to centrifugal forces

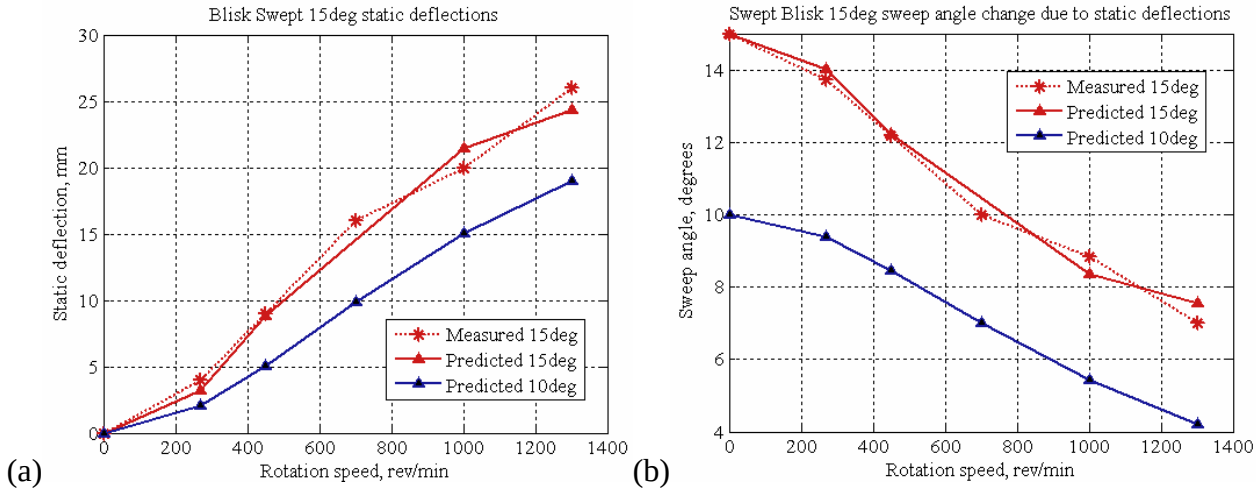

Fig. 4-18. Swept Blisk 15deg static deflections due to centrifugal forces, (a), and sweep angle change due to static deflections (b)

	Measurements		Predictions	
Speed (rev/min)	Static defl. (mm)	Sweep angle (deg)	Static defl. (mm)	Sweep angle (deg)
0	0.00	15.00	0.00	15.00
270	4.00	13.74	3.19	14.01
450	9.00	12.17	8.85	12.22
700	16.00	10.01	-	-
1000	20.00	8.85	21.42	8.37
1300	26.00	7.00	24.38	7.54

Table 4-2. Swept Blisk 15deg measured and predicted static deflections and sweep angle changes due to centrifugal forces

It is undoubtedly evident that the action of centrifugal forces is particularly prominent at higher rotation speeds, as the testpiece is a highly flexible bladed disc. For the Swept Blisk 15deg testpiece, the sweep angle almost halves from 15deg to

8deg between 0 and 1300rev/min, an effect which explains the decreased magnitude of the measured natural frequency splits after approximately 540rev/min, observed in Figs. 4-13(b) and 4-16(b).

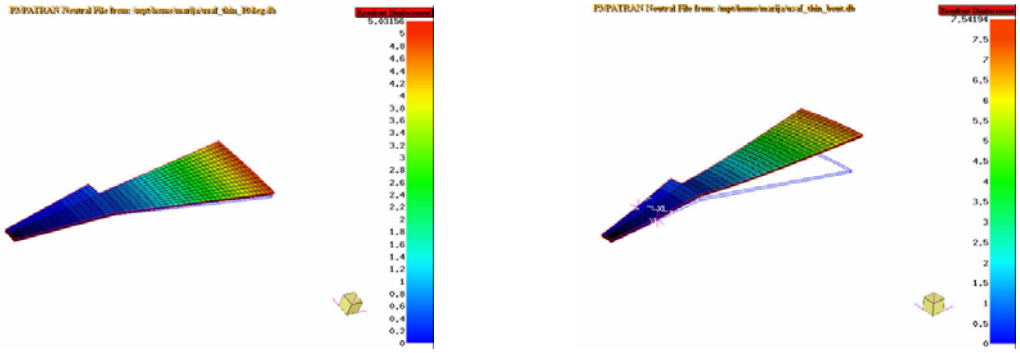

(a) Swept Blisk 10deg – 450rev/min (b) Swept Blisk 15deg – 450rev/min

Fig. 4-19. Swept Blisk 10deg (a) and Swept Blisk 15deg (b) static deflections due to centrifugal forces

4.5.5 Rotating conditions results revisited: effects of variation of geometric shape due to centrifugal forces

Figs. 4-13 and 4-16 show that the predicted natural frequency splits are close to the experimental values in the lower speed ranges, but that they are distinctly different at higher rotation speeds. The reason for such a discrepancy is attributed to the omission of geometry change of the model used in predictions due to the effects of centrifugal forces, which are essentially to decrease the sweep angle of the testpiece with increase in rotation speed (i.e. to straighten out the disc blades). Thus, in order to reconcile the predictions with the measurements, the FE analysis of first 2 and 3ND mode pairs was repeated with the appropriate manual sweep angle change due to centrifugal forces effects at relevant rotation speeds, as demonstrated in Fig. 4-20(a). The final comparison of the two sets of results is given in Table 4-3 and Fig. 4-20 (b,c), from which significantly better agreement is observed.

Speed, rev/min	2ND		% diff.	3ND		% diff.
	Measured Split, %	Predicted Split, %	Meas. vs. Predicted	Measured Split, %	Predicted Split, %	Meas. vs. Predicted
300	1.29%	1.81%	+28.73	1.05%	1.51%	+30.46
330	1.50%	1.96%	+23.47	1.32%	1.65%	+20.00
510	1.51%	1.78%	+15.17	1.78%	1.51%	-15.17
700	1.65%	1.67%	+1.20	1.76%	1.44%	-18.18
900	0.95%	1.70%	+44.12	1.64%	1.49%	-9.15

Table 4-3. Measured and predicted (with geometry change included) natural frequency splits

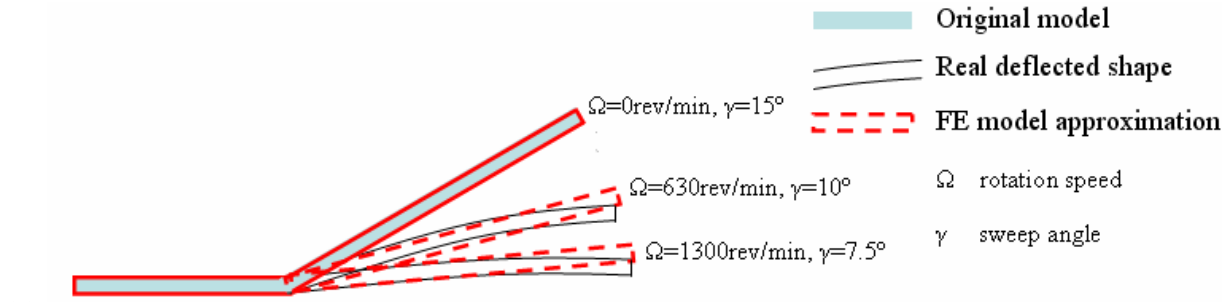

(a)

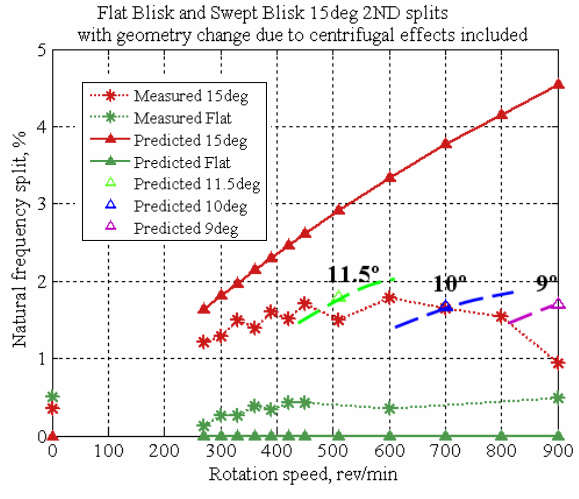

(b)

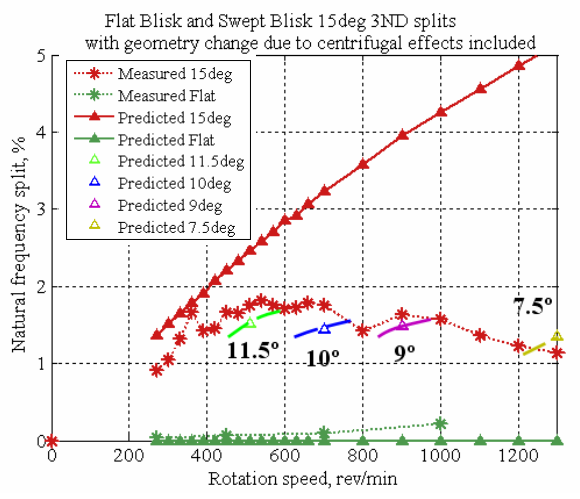

(c)

Fig. 4-20. Swept Blisk approximate geometry change due to centrifugal forces (a), first 2ND (b) and 3ND (c) mode pairs results with the geometry change due to centrifugal forces included

It should be noted that the experimental effort described in this Chapter has resulted in an *approximate experimental validation* of the SAMCEF predictions, as the static geometry change effect is not fully accounted for in the prediction code and had to be compensated manually, in which case the sweep angle magnitude at various rotation speeds is only an approximation to the real deflected shape of the testpiece resulting from the action of centrifugal forces.

4.5.6 Some further characteristics of the measured 3ND mode pair

Fig. 4-21 demonstrates the 3ND frequency response functions (FRFs) obtained at 540rev/min with a single peak for Flat Blisk and two unambiguous split peaks for the Swept Blisk 15deg, thus clearly demonstrating influence of Coriolis forces on this mode.

Schematic representation of the measured mode shapes for the first 3ND mode pair at 540rev/min, where the largest natural frequency split was obtained, is given in Fig. 4-22. It shows displacements of each of a number of blades, which were measured at the blade tips over vibration period T.

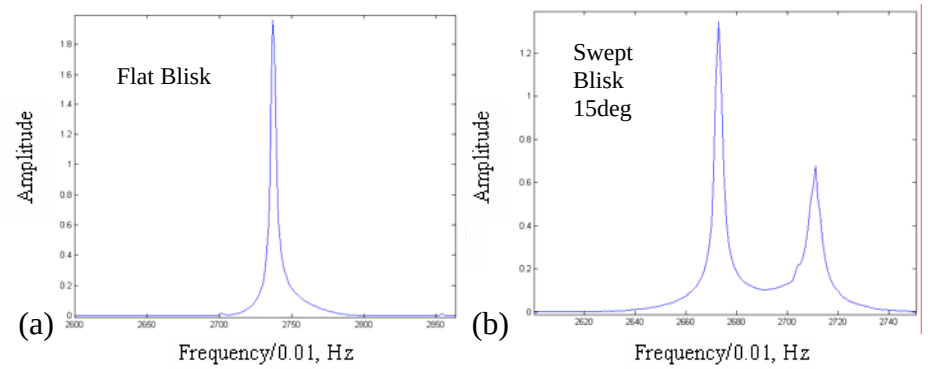

Fig. 4-21. Flat Blisk (a) and Swept Blisk 15deg (b) FRFs at 540rev/min for the first 3ND mode pair

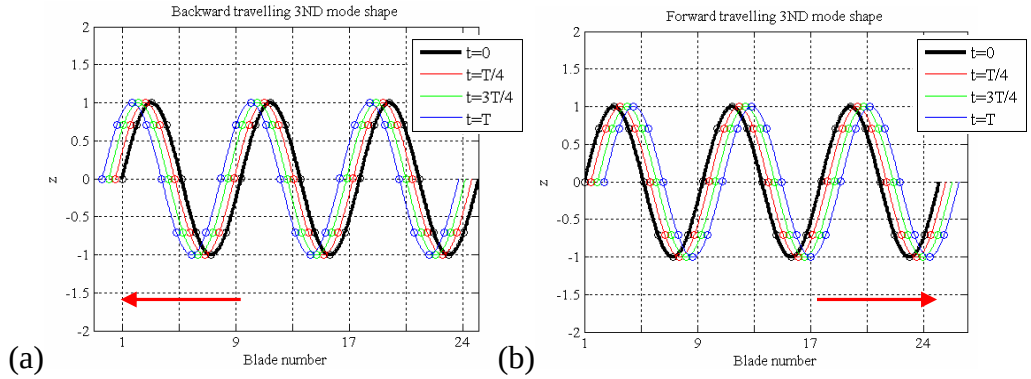

Fig. 4-22. Schematic representation of the measured mode shapes for 3ND at 540rev/min: backward travelling wave mode (a) and forward travelling wave mode (b)

From an animation of the two measured mode shapes, it is clear that they constitute, respectively, a backward wave (travelling in the opposite direction to the rotation of the disc) and a forward wave (travelling in the same direction as the disc rotation).

4.5.7 Sources of discrepancies between the predictions and experimentally-acquired data

Some of the sources of discrepancies observed between the predicted and measured data are identified and discussed below.

a) Model parameter errors. As mentioned in Appendix A4-3, a very simple model updating procedure including modification of material properties was carried out in an attempt to bring the predicted and measured natural frequencies closer together. Still, the measured natural frequencies are slightly higher than those predicted in all considered cases. Further rectification of this inconsistency was regarded as unimportant, as the primary aim of this work was to validate natural frequency splits, the magnitude of which is independent of exact range of pairs of natural frequencies.

b) Every FE model used to represent a continuous structure bears small discretization errors, although a large enough number of nodes and elements was selected.

c) Model structural errors, "which result when features in the actual structure are omitted from the idealization that is created for the mathematical model" [113]. Two types of inherent mistuning of the testpiece belong to this category: (i) small random imperfections in dimensions and material properties due to manufacturing tolerances, and (ii) small random blade-to-blade variations in the sweep angle due to subsequent bending of the blades introduced by tolerances of the press tool. While the real testpiece contains mentioned inherent mistuning, the model used in the predictions was considered to be perfectly symmetric.

d) In section 4.5.4, the influence of centrifugal forces on testpiece geometry was established and an attempt made to reconcile measured and predicted results by accounting for sweep angle changes at higher speeds. This process also carries small errors, as it was difficult to estimate exact change of sweep angle due to centrifugal forces.

e) Another source of results inconsistency stems from fixation boundary conditions, which changed every time the testpiece was removed from and re-installed on the shaft. This is particularly important, as the exact influence of Coriolis forces was found to vary according to precise boundary conditions. The following shows a brief summary of natural frequency splits dependency upon model centre boundary fixation conditions.

Swept Blisk 15deg **Influence of boundary conditions on the natural frequency splits**							
Case	**Fixation conditions at model centre**						
	1dof	2dof	3dof	1-2dof	1-2-3dof	Fully fixed	Split diff,%*
1ND, 900rpm							
without C	22.455	NA	NA	25.899	26.152	27.145	
with C	21.957	NA	NA	25.527	25.793	26.825	
	22.965	NA	NA	26.278	26.516	27.468	
split, %	**4.39%**	**NA**	**NA**	**2.86%**	**2.73%**	**2.34%**	**38% less**
2ND, 900rpm							
without C	25.940	26.101	25.799	27.164	27.340	28.155	
with C	25.213	25.391	25.070	26.524	26.710	27.589	
	26.689	26.831	26.548	27.819	27.980	28.733	
split, %	**5.53%**	**5.37%**	**5.57%**	**4.65%**	**4.54%**	**3.98%**	**18% less**
3ND, 1300rpm							
without C	35.769	35.832	35.873	35.879	35.910	36.121	
with C	34.803	34.876	34.921	34.936	34.970	35.223	
	36.762	36.814	36.852	36.847	36.870	37.041	
split, %	**5.33%**	**5.26%**	**5.24%**	**5.19%**	**5.15%**	**4.91%**	**3.5% less**

* Split difference between fully fixed and 1dof

1dof - Radial DOF, 2dof - Tangential DOF, 3dof - Axial DOF

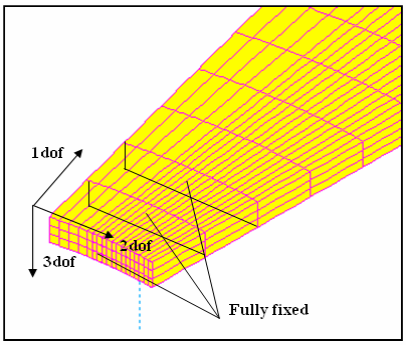

Table 4-4. Natural frequency split dependency upon boundary conditions

It is seen from Table 4-4 that as the flexibility of bladed disc centre decreases, the magnitude of the natural frequency splits due to the influence of Coriolis forces reduces. The effect of changing the boundary conditions is particularly pronounced on splits of the 1ND mode pair, as there are movements of bladed disc centre due to unbalanced inertial forces in this case. Thus, the difference in natural frequency splits for this mode pair can be as much as 38%, depending on the precise boundary conditions. On the other hand, for numbers of nodal diameters higher than 1, the net inertial forces are perfectly balanced, and the effect of varying centre fixation conditions has a lesser effect (18% and 3.5% for 2 and 3ND mode pairs, respectively).

f) Measurement errors. SLDV measurements were made during synchronous scanning of a particular point on the spinning testpiece blade. A possible source of error could be due to the difficulty of scanning exactly the same spot on a blade and aligning the laser light beam perpendicular to the direction of motion, consequently detecting different vibration velocity. Also, several measurements provided noisy data, which made the interpretation of acquired data difficult in those cases.

4.5.8 Coriolis forces chart – factors influencing their intensity

Fig. 4-23 summarises main factors established throughout Chapters 3 and 4 which influence the intensity of Coriolis forces on bladed disc natural frequency splits.

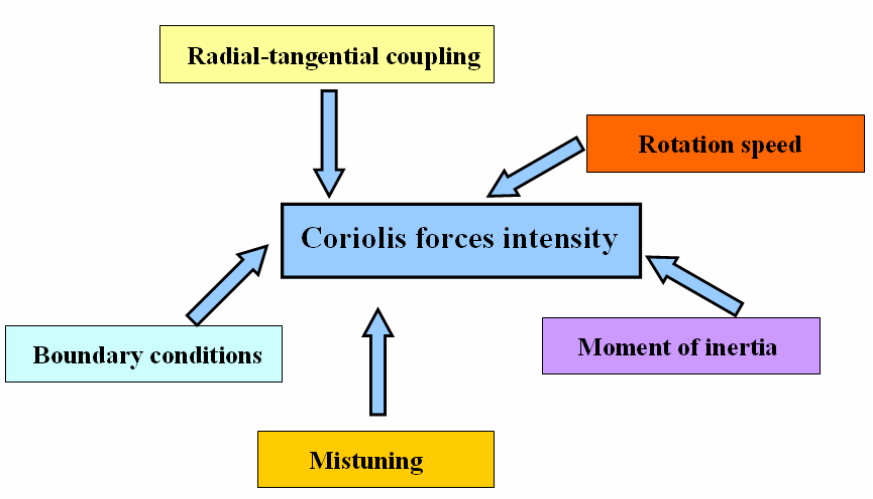

Fig. 4-23. Factors influencing the intensity of Coriolis forces on natural frequency splits

4.6 Importance of results obtained

For the first time, the non-trivial influence of the effects of Coriolis forces on all nodal diameter mode pairs of a nominally-tuned bladed disc has been approximately validated, bearing in mind that the static geometry change effect is not fully integrated in the prediction code, which resulted in explained inconsistency between experimental and predicted data at higher rotation speeds. An immediate implication of this is that the theoretical model including these forces is now suitable for further analysis incorporating typical blade mistuning, which will establish their importance in the characterisation of forced response and resulting bladed disc fatigue life. Moreover, the effects of Coriolis forces could be a missing link in contemporary bladed disc analysis and a plausible reason for repeatedly-experienced mismatch between theoretical predictions and real measured data.

4.7 Summary

The phenomenon of the natural frequency split into backward and forward travelling wave modes for all numbers of nodal diameters of a tuned bladed disc due to effects of Coriolis forces has been convincingly approximately validated in this Chapter. The experimental validation employed a testpiece with a prominent radial flexibility, which allowed observation of the resulting significant Coriolis forces effect. The results obtained had demonstrated a dominant sensitivity of the action of Coriolis forces to the amount of radial-tangential coupling of the structure. Moreover, due to the flexible nature of the testpiece used, a ‘convex’ shape of the natural frequency split plot was observed, which is a consequence of mutual influence of Coriolis and centrifugal forces. Contrary to current practice adopted in most bladed disc analyses, the evidence obtained in this Chapter suggests that there might be designs of realistic bladed discs which are particularly prone to the effects of Coriolis forces and thus require a careful re-examination.

CHAPTER 5

Mutual Influence Of Coriolis Forces And Blade Mistuning

"Everything should be made as simple as possible, but not simpler"

Albert Einstein

5.1 Overview

Indisputable evidence of influence of Coriolis forces on modal properties of bladed discs, demonstrated in Chapter 4, has increased confidence in the theoretical model including these forces and served to identify a crucial design feature stimulating their prominent intensity. This Chapter presents a new study of the mutual interaction of the effects of Coriolis forces and blade mistuning on the vibration characteristics of bladed discs. In the first part of the Chapter, the influence of different degrees of mistuning on forced response and amplification factors is examined in the presence of Coriolis forces and then compared with their non-Coriolis counterparts using a computationally inexpensive, yet representative, simplified model of a bladed disc assembly. A second part of the Chapter presents results from an experimental investigation of the mutual influence of Coriolis forces and deliberately introduced mistuning using the testpiece described previously in Chapter 4. The primary objective of the study addressed in this Chapter is to establish whether current mistuned bladed disc analyses should incorporate Coriolis effects in order to represent accurately all the significant factors that affect the forced response levels.

5.2 Numerical study of mutual influence of Coriolis forces and blade mistuning on forced response characteristics

5.2.1 Aims of the study

One of the main problems in turbomachinery bladed disc vibration is related to scatter in the blades' forced response amplitudes, as this can lead to excessive vibration levels confined to few blades and, subsequently, to premature high-cycle fatigue failures in those blades. Mistuning, or a random variability in the blades' properties, is known to be a factor playing a major role in the amplification of forced response levels, introducing significant uncertainty in the vibration characteristics by splitting double mode natural frequencies and fixing their orientation uniquely in the bladed disc. As mentioned in Chapter 3 (section 3.7.2), Coriolis forces generate similar order-of-magnitude effects on bladed disc vibration properties, and it is this which imposes a compelling reason for their inclusion in mistuned bladed disc analyses.

In traditional mistuned bladed disc analysis, the effects of Coriolis forces have previously been considered to be negligible. To the best of the author's knowledge, there are no investigations reported in the published literature on the effects of Coriolis forces and mistuning on the forced response characteristics of bladed disc vibration levels. The main goals of the study reported here are (i) to determine the mutual influence of the effects of Coriolis forces and blade mistuning on vibration properties of bladed discs, and (ii) to establish whether Coriolis forces should be included as a missing link in the analyses of mistuned bladed discs. The impact of different mistuning degrees on forced response and amplification factors will be investigated for several bladed disc designs incorporating varying strengths of Coriolis forces.

5.2.2 Mathematical model description

In view of the lack of finite element codes capable of forced response analysis of rotating bladed discs with Coriolis forces and blade mistuning included[1], a simple lumped parameter mass model was chosen to study the mutual influence of Coriolis

[1] SAMCEF software has been used throughout this thesis to compute the natural frequencies and mode shapes of bladed disc systems including the effects of Coriolis forces. However, due to the fact that the mode shapes provided are not mass-normalised, this code cannot be used for forced response analysis, which is the reason behind creation of a simple lumped parameter mass model

forces and blade mistuning. It is believed that a simple system will serve as a useful tool to explore the underlying physics of the combined complex effects of the two phenomena. Since there is no coupling between out-of-plane and in-plane blade vibrations due to Coriolis forces, the model includes in-plane radial and tangential vibration only. Thus, a suitable lumped parameter model of bladed disc dynamics must comprise four degrees-of-freedom per sector with two degrees-of-freedom per mass. The bladed disc chosen for this study contains 24 sectors. The model, depicted in Fig. 5-1, contains a pair of masses representing each blade and disc segment and a series of springs in the x and y directions representing radial and tangential connections (vibrations). It is assumed that the springs' stiffnesses in the radial direction are much greater than those in the tangential direction. The values for the lumped parameter mass model used in the numerical study are listed in Table 5-1. It should be noted that these values are not intended to represent any particular bladed disc, but are chosen with the aim of demonstrating the appropriate physics. Therefore, no units are connected with these values, simply the assurance that they are consistent.

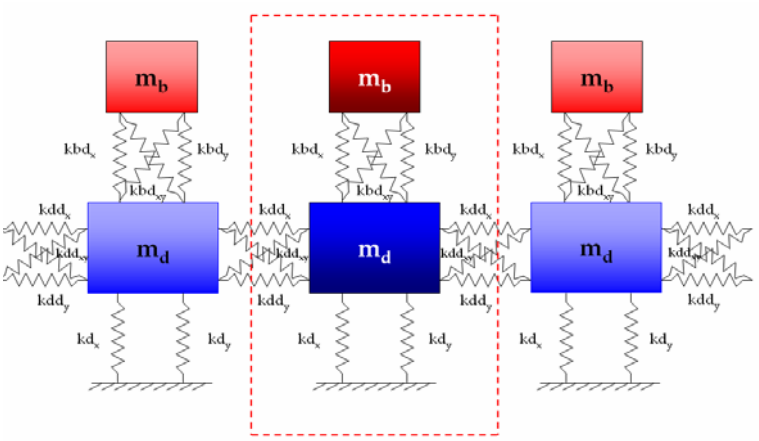

Fig. 5-1. Lumped parameter mass model

Parameter	Value
m_d	8
m_b	3
kdd_x	$5.8x10^6$
kbd_x	$15.4\ x10^5$
kd_x	$0.9x10^6$
kdd_y	$kdd_x x100$
kbd_y	$kbd_x x100$
kd_y	$kd_x x100$
kdd_{xy}	$5.0x10^3$
kbd_{xy}	$5.0x10^4$

Table 5-1. Lumped parameter mass model properties

The most important feature of this model is related to the added disc-to-disc cross-coupling stiffness terms, which simulate the strength of in-plane tangential and radial coupling. A detailed description of the basis of the lumped parameter model stiffness matrix is given in Appendix A5-1, whereas here it is important to note that the disc-to-disc stiffness matrix, which connects *nth* disc mass to the *(n-1)th* disc mass, can be expressed as:

$$\begin{Bmatrix} F_1 \\ F_2 \end{Bmatrix} = \begin{bmatrix} k_{11} & k_{12} \\ k_{21} & k_{22} \end{bmatrix} \begin{Bmatrix} q_1 \\ q_2 \end{Bmatrix} = \begin{bmatrix} k_{11} & k_{11}R^T \\ Rk_{11} & Rk_{11}R^T \end{bmatrix} \begin{Bmatrix} q_1 \\ q_2 \end{Bmatrix} \tag{5-1}$$

where

$$k_{11} = \begin{bmatrix} kdd_x & kdd_{xy} \\ kdd_{yx} & kdd_y \end{bmatrix} \tag{5-2}$$

(k_{11} is a symmetric positive matrix, $kdd_{yx} = kdd_{xy}$)
$_{(2\times2)}$

$$R = -\begin{bmatrix} \cos\gamma & -\sin\gamma \\ \sin\gamma & \cos\gamma \end{bmatrix} \tag{5-3}$$

$$q_{1,2} = \begin{Bmatrix} x \\ y \end{Bmatrix}_{1,2} \text{ and } F_{1,2} = \begin{Bmatrix} F_x \\ F_y \end{Bmatrix}_{1,2} \tag{5-4}$$

Blade-to-disc cross-coupling stiffness terms are expressed in a similar way.

The choice of the form of stiffness matrix in (5-2) is not unique and is just one of the ways of representing the degree of coupling. A parameter for the radial-tangential coupling, which will subsequently be referred to as the "coupling parameter", γ, is used as a control parameter to regulate the Coriolis forces' strength: the higher the value of γ, the stronger the effect of Coriolis forces.

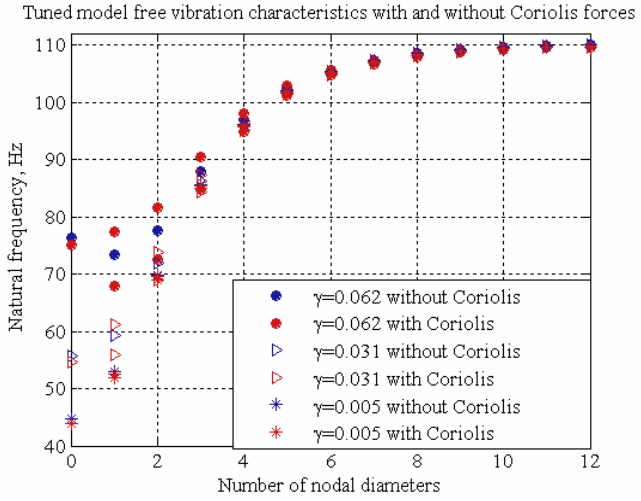

Fig. 5-2. Tuned model free vibration properties dependence on coupling parameter γ

For the case when γ=0, there is no radial-tangential coupling and, as a result, no Coriolis forces effect. This is demonstrated in Figs. 5-2 and 5-3 and Table 5-2 below.

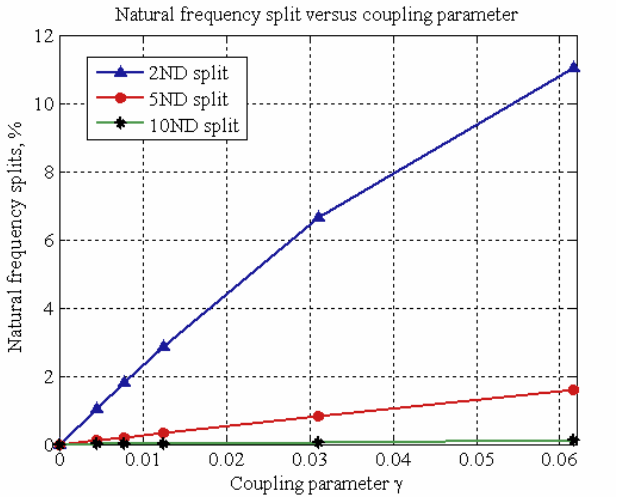

Fig. 5-3. Tuned model natural frequency split as a function of coupling parameter γ

Coupling Parameter γ	2ND split,%	5ND split,%	10ND split,%
0.000	0.00	0.00	0.00
0.005	1.04	0.12	0.01
0.008	1.81	0.21	0.01
0.013	2.86	0.34	0.02
0.031	6.65	0.83	0.06
0.062	11.03	1.61	0.11

Table 5-2. Tuned model dependence on coupling parameter

The choice of coupling parameter value was determined by the desired shape of the natural frequency versus number of nodal diameters plot. As the coupling parameter is increased from 0.005 to 0.062, the split of the otherwise-identical double natural frequencies due to Coriolis forces only in the 2ND mode pair has increased from 1% to 11%. While a corresponding increase in the split of natural frequencies is also observed for the 5ND and 10ND mode pairs, the actual split magnitudes are much smaller than that corresponding to the 2ND mode pair. The reason for such a result is due to the fact that the amount of blade-to-blade coupling through the disc decreases with the number of nodal diameters, which in turns reduces the effects of Coriolis forces.

5.2.3 Forced response considerations

In this section, the main forced response characteristics of the combined system, including the effects of Coriolis forces and mistuning, are presented. The coupling parameter γ was initially set to 0.005, so that the influence of Coriolis forces only on tuned natural frequencies was relatively small (the 2ND mode pair split being approximately 1%). A random mistuning pattern, depicted in red in Fig. 5-4, was chosen as a reference pattern and was generated within a frequency mistuning range of ±5%, which is typical for bladed discs. Subsequently, several other frequency mistuning patterns were created in order to study the effect of increasing mistuning ranges on the forced response of a system with Coriolis forces. These patterns were based on the same reference pattern, but spanned different mistuning ranges. The secondary patterns were obtained by multiplying the individual blade mistuning values in the reference pattern by an identical multiplier for all blades. The following values of this multiplier were considered: 0.25, 0.5, 2.0, 3.0, and 4.0, which cover wide but practically attainable mistuning ranges. Relatively large blade mistuning of 17% is represented for the mistuning pattern resulting from the multiplier 4.0, and while not very common, it is not implausible in practice for bladed fan discs, where large differences may exist from blade to blade ([123]).

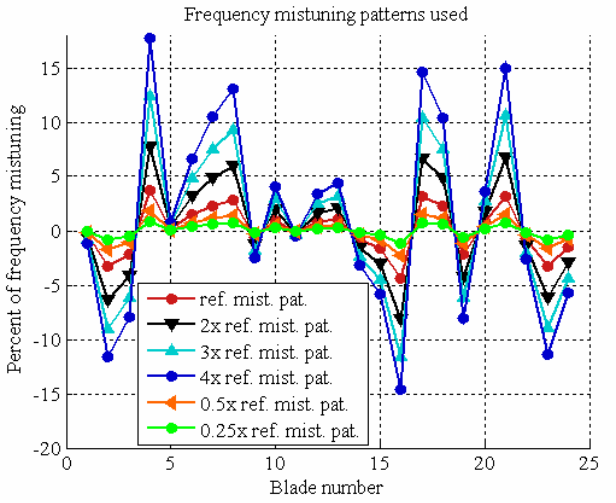

Fig. 5-4. Frequency mistuning patterns used

The damping loss factor was set to 0.003, which is typical for bladed discs. A simple engine order forcing field was applied of the form:

$$F(\theta,t) = F_0 e^{iEO(\Omega t \pm \theta)} \tag{5-5}$$

where F_0 is the force amplitude, *EO* is the engine order, Ω is the rotation speed, *t* is time and θ is the circumferential position around the disc. A forward (response backward) travelling wave was obtained by applying a positive imaginary term in (5-5).

Forced response levels were calculated from the following equation:

$$\{Q\} = \left([K] - \omega^2 \left([M] + [\Delta M] \right) + i[D] + i\omega[G] \right)^{-1} \{F\} \tag{5-6}$$

where $\{Q\}$ is the forced response, $[K]$ is the system stiffness matrix, $[M]+[\Delta M]$ represents mass-mistuned system, $[D]=\eta[K]$ is the structural (hysteretic) damping matrix, η is the damping loss factor, $[G]$ is the Coriolis matrix and $\{F\}$ is the applied force.

Tuned bladed disc backward (EO=+2) and forward (EO=–2) forced responses[2], with (+C) and without (-C) Coriolis forces, are shown in Fig. 5-5. The so-called "forward" travelling wave response does not have immediate practical interest, but is physically possible under certain circumstances. As expected, in the case of a tuned system without Coriolis forces, the responses to the backward and forward waves are identical, whereas the presence of Coriolis forces generates these forced responses at distinct frequencies.

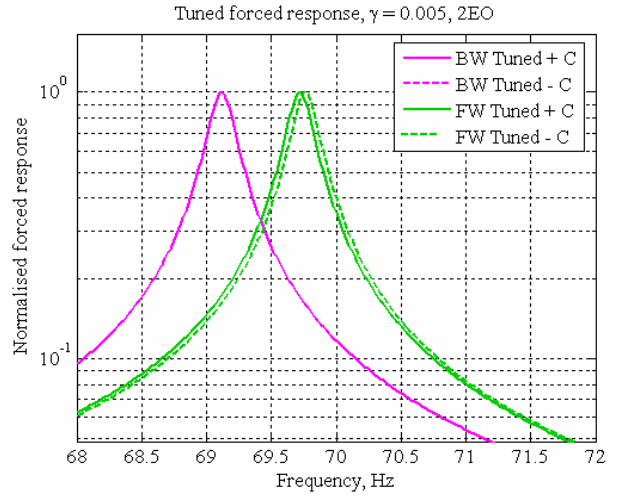

Fig. 5-5. Tuned forced responses, coupling parameter γ = 0.005, 2EO[3]

Normalised mistuned forced responses and their envelopes, with and without Coriolis forces taken into account, are illustrated in Fig. 5-6, response normalisation

[2] "Forward" and "backward" forced responses are defined with respect to rotating frame of reference
[3] For a system without Coriolis forces, the backward and forward travelling wave responses are identical, so only three curves are visible in Fig. 5-5

being made with respect to the maximum tuned response levels in the frequency range of interest. It can be observed from Fig. 5-6 that the backward and forward mistuned travelling wave responses obtained for 2EO with Coriolis forces are 'nearly' mirror images of each other. A lower amplitude peak in each mistuned FRF with Coriolis forces can be considered as a small contribution of a travelling wave component to the main stationary component. Mistuned responses without Coriolis forces are also not identical due to the blade mistuning which has been introduced and to the coupling between tangential and radial vibrations (see (5-2)). If the model had no tangential-radial coupling, then mistuned forward and backward forced responses would have been identical to each other. Moreover, envelopes of the maximum forced responses are clearly dissimilar for the cases of calculations with and without Coriolis forces included. Also, it is worth noting that since 2EO and low coupling case have been portrayed in these plots, one can see only two peaks in the envelope of the mistuned forced response. Subsequent plots for 5EO are noticeably different and appear to have a commonly observed envelope shape.

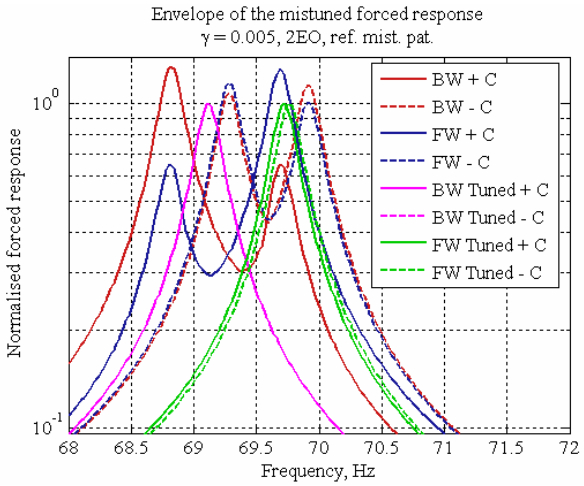

Fig. 5-6. Envelope of the mistuned forced responses, coupling parameter $\gamma = 0.005$, 2EO

The results in Fig. 5-7 demonstrate that the individual (specifically, blade no.10, which is representative of the others) frequency response functions are different when the Coriolis forces are present compared to the non-Coriolis counterparts, which could provide an explanation for a mismatch observed sometimes between theoretical predictions and experimental data for bladed discs.

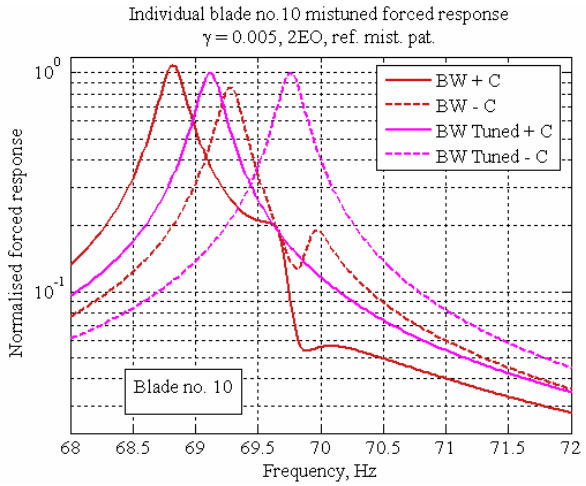

Fig. 5-7. Individual blade no. 10 mistuned forced responses, coupling parameter $\gamma = 0.005$, 2EO

The amplitude spread as a function of blade number, depicted in Fig. 5-8, shows that the maximum blade amplitude can be higher by 14% when the Coriolis forces are included in the analysis compared to that for a mistuned-only system.

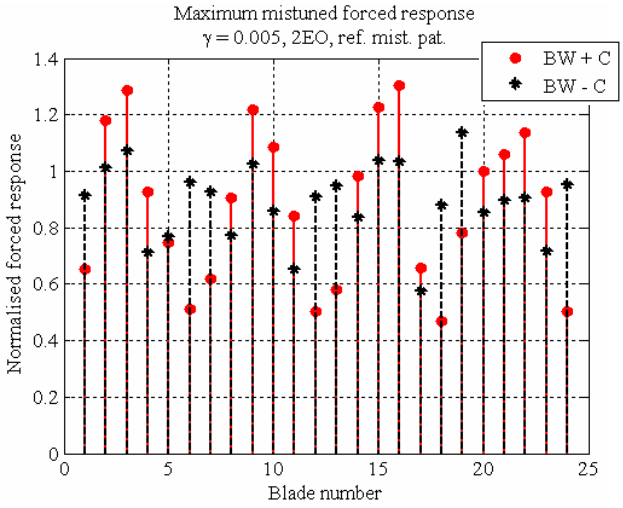

Fig. 5-8. Maximum blade amplitudes with and without Coriolis forces, coupling parameter $\gamma = 0.005$, 2EO

5.2.4 Influence of mistuning ranges on forced response with and without Coriolis forces

5.2.4.1 Weak influence of Coriolis forces, coupling parameter $\gamma = 0.005$

In the following sections, for each coupling parameter value manifesting the strength of Coriolis forces, the backward forced response will be shown for different frequency mistuning ranges spanning from ±1% to ±20%, based on a reference mistuning pattern, as shown in Fig. 5-4.

Envelopes of the mistuned forced responses for different blade frequency mistuning degrees under 2, 5 and 10EO are given in Fig. 5-9. They show shapes of envelopes of the FRFs under different EOs and their gradual peak separation from a nearly-tuned to a heavily mistuned system. In the case of 5 and 10EO, the envelopes of the forced response functions with and without Coriolis forces are very similar and, thus, overlapping in Fig. 5-9 (b,c).

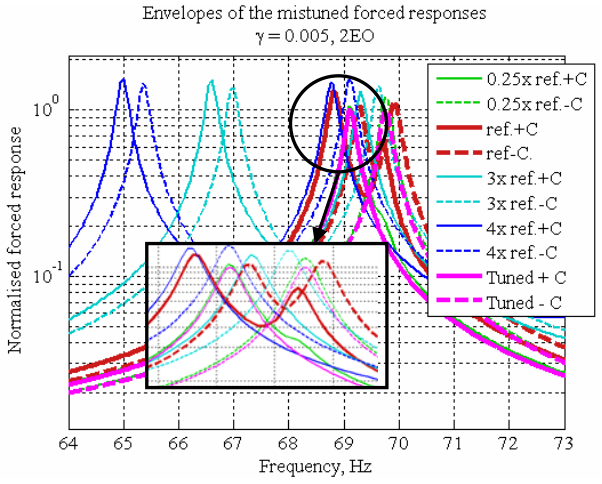

(a)

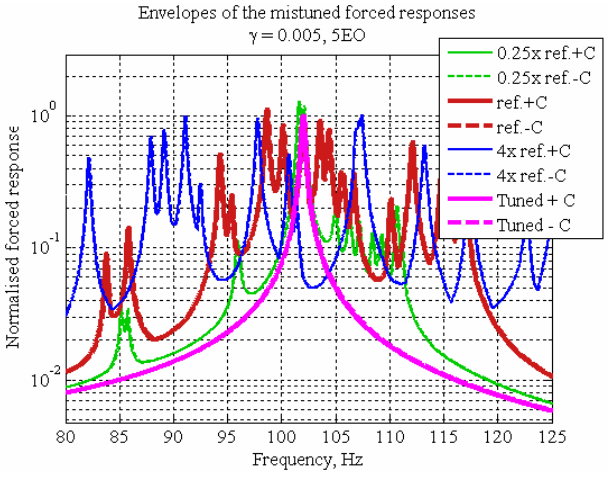

(b)

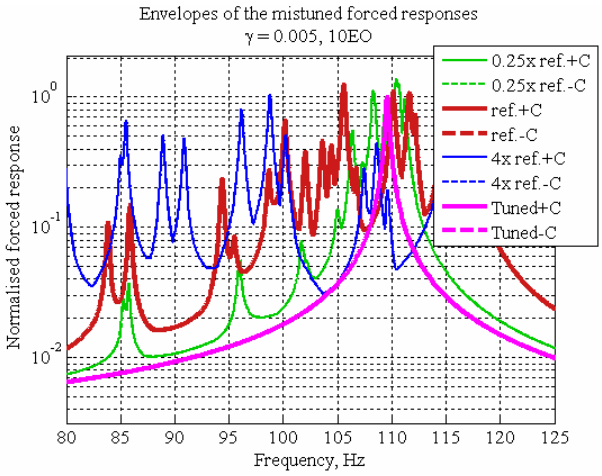

(c)

Fig. 5-9. Envelopes of mistuned forced responses for different blade frequency mistuning ranges, coupling parameter γ = 0.005, (a) 2EO, (b) 5EO, (c) 10EO

Maximum forced responses for coupling parameter γ = 0.005 with Coriolis forces included are compared with their non-Coriolis counterparts for different mistuning degrees and EOs in Fig. 5-10.

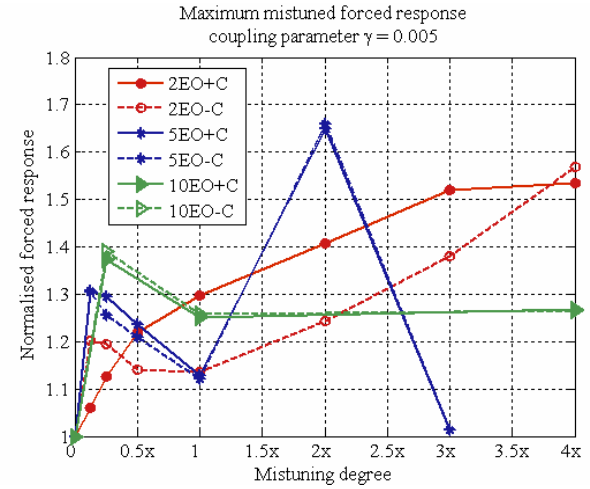

Fig. 5-10. Maximum mistuned forced responses with and without Coriolis forces, coupling parameter γ = 0.005

It is seen from Fig. 5-10 that in the case of 2EO, for relatively small frequency mistuning, the forced response without Coriolis forces is higher, whereas for most of other mistuning degrees, the forced responses including Coriolis forces are above those for mistuned-only system by approximately 15%. For 5EO and 10EO, there is almost no difference in maximum forced responses.

5.2.4.2 Strong influence of Coriolis forces, coupling parameter γ = 0.062

Fig. 5-11 demonstrates a rather different envelope of the mistuned forced response for different blade frequency mistuning degrees for 2EO and similar features for 5 and 10EO, obtained for a system with coupling parameter γ = 0.062, simulating a strong influence of Coriolis forces.

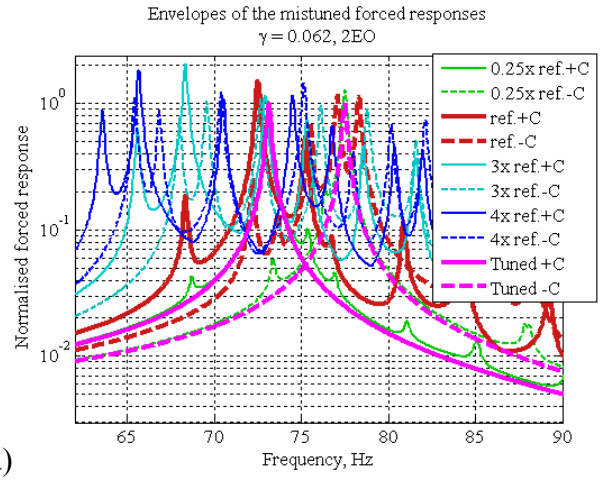

(a)

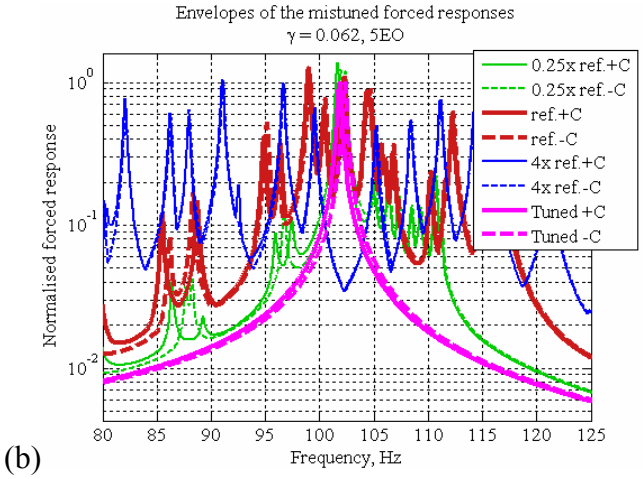

(b)

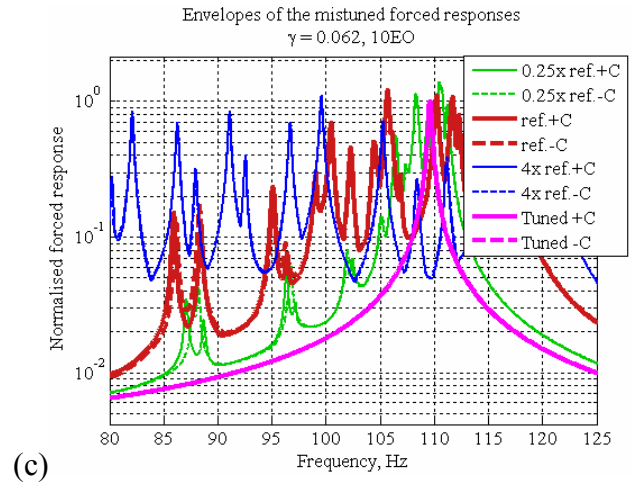

(c)

Fig. 5-11. Envelopes of mistuned forced responses for different blade frequency mistuning ranges, coupling parameter γ = 0.062, (a) 2EO, (b) 5EO, (c) 10EO

The maximum forced responses obtained for strong Coriolis forces influence case are presented in Fig. 5-12. The response with Coriolis forces included for 2EO is much higher than that corresponding to mistuned-only system, reaching levels which are 75% greater at mistuning equal to 3 times the original mistuning pattern. The responses with and without Coriolis forces are much more similar to each other for 5EO and 10EO.

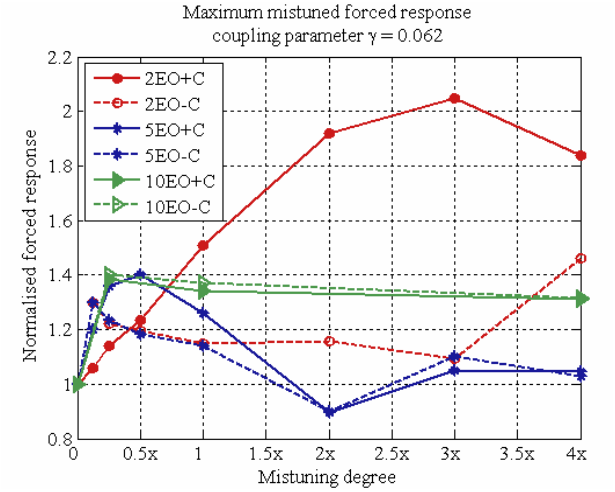

Fig. 5-12. Maximum mistuned forced responses with and without Coriolis forces, coupling parameter γ = 0.062

5.2.5 Statistical characterisation of forced response

Figs. 5-13 to 5-17 represent selected statistical results for forced responses obtained from Monte Carlo simulations of 500 randomly generated mistuning patterns, with and without the effects of Coriolis forces. Blade frequency mistuning was assumed to lie in the typical range for bladed discs of ±5% of the nominal first blade-alone frequency. The maximum forced responses calculated for each blade and for all mistuning patterns generated are plotted in Figs. 5-13 to 5-15 for all considered EO excitations.

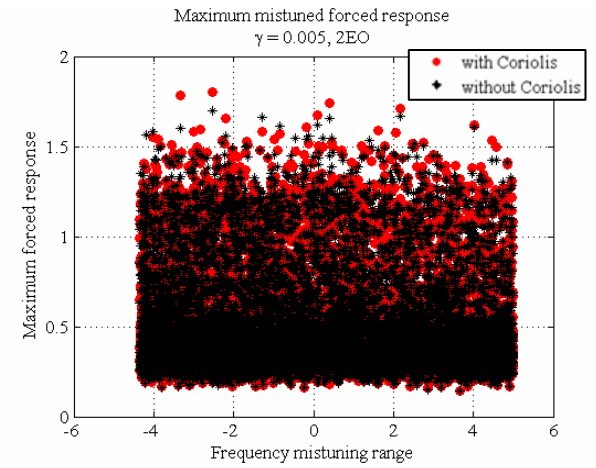

(a) γ=0.005 (weak coupl.)

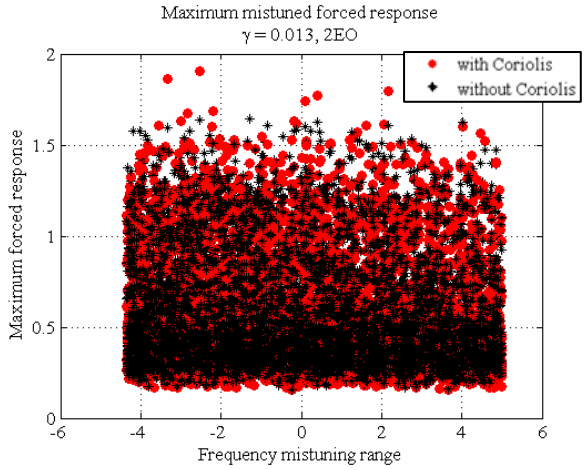

(b) γ=0.013 (moderate coupl.)

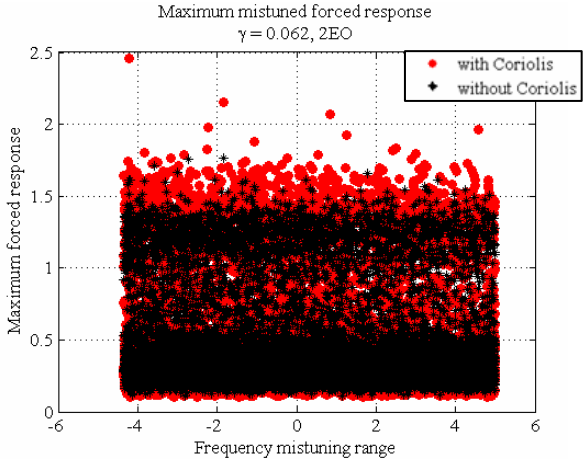

(c) γ=0.062 (strong coupl.)

Fig. 5-13. Statistical 2EO results for the maximum mistuned forced response for each blade for (a) γ=0.005, (b) γ=0.013, (c) γ=0.062

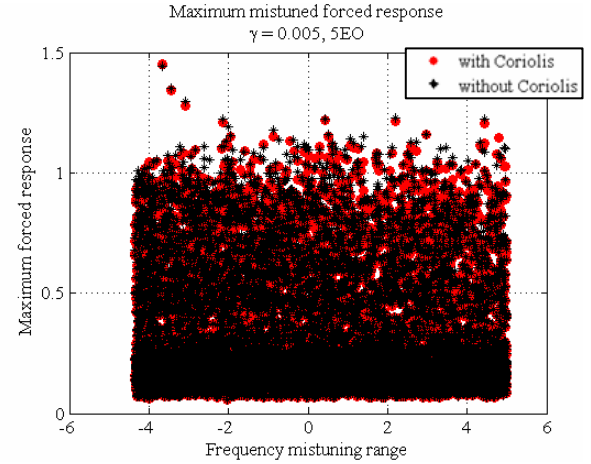

(a) γ=0.005 (weak coupl.)

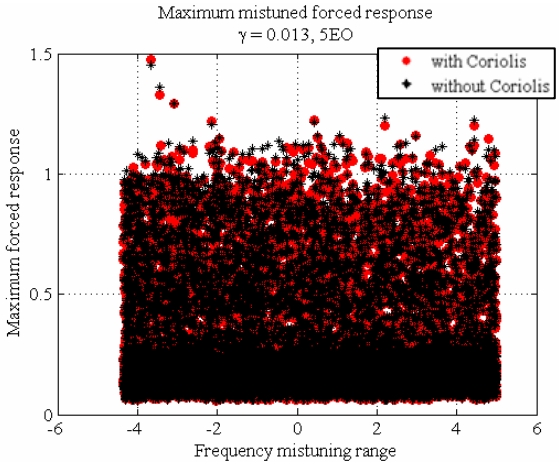

(b) γ=0.013 (moderate coupl.)

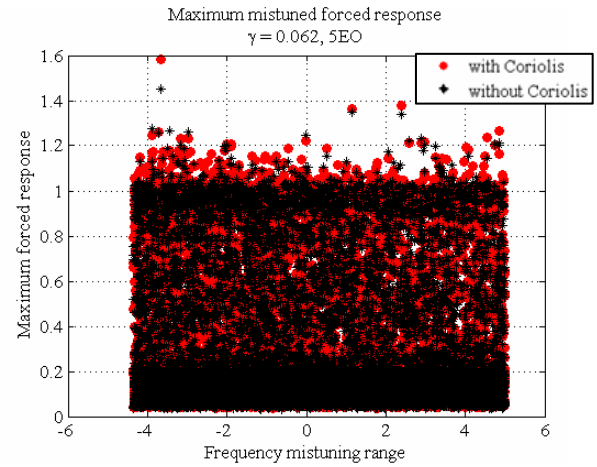

(c) γ=0.062 (strong coupl.)

Fig. 5-14. Statistical 5EO results for the maximum mistuned forced response for each blade for (a) γ=0.005, (b) γ=0.013, (c) γ=0.062

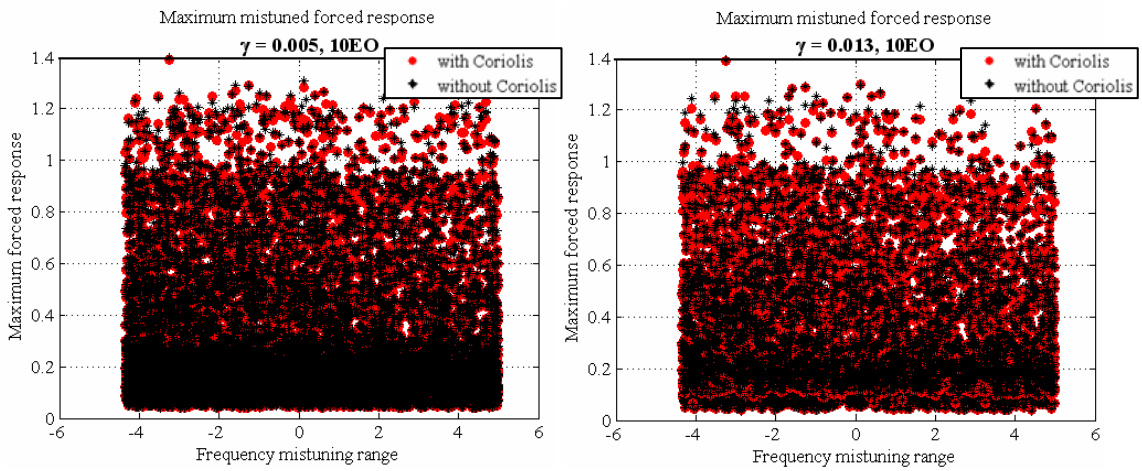

(a) γ=0.005 (weak coupl.) (b) γ=0.013 (moderate coupl.)

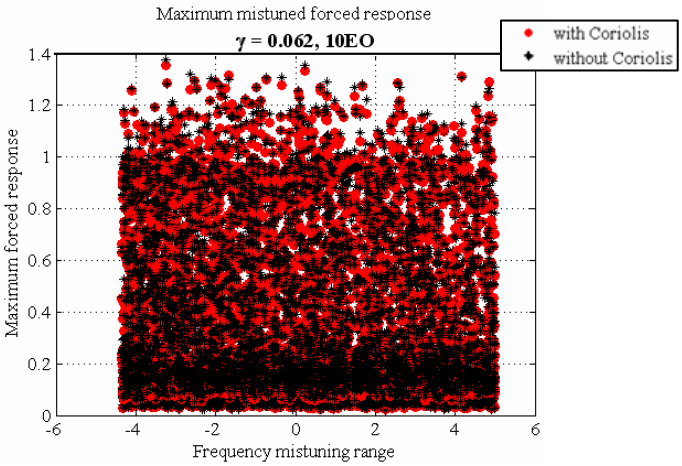

(c) γ=0.062 (strong coupl.)

Fig. 5-15. Statistical 10EO results for the maximum mistuned forced response for each blade for (a) γ=0.005, (b) γ=0.013, (c) γ=0.062

For the case of 2EO excitation, one can see significant differences in blade amplitudes determined with and without Coriolis forces included. As the coupling parameter, γ, increases from 0.005 to 0.062, the effects of the Coriolis forces on blade amplitudes rise. Hence, for the same degree of mistuning, the maximum forced response with Coriolis forces included obtained in Fig. 5-16 over all 500 mistuning patterns is higher by approximately 40% than that corresponding to the mistuned-only system. For 5EO and 10EO, the maximum forced response levels with and without Coriolis forces calculated over 500 mistuning patterns are similar to each other.

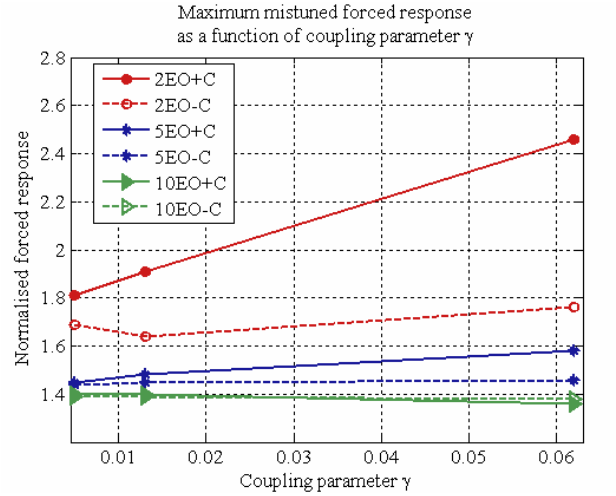

Fig. 5-16. Maximum mistuned forced response over all 500 mistuning patterns

Histograms in Figs. 5-17 show the statistical distributions of maximum mistuned forced responses with and without Coriolis forces. In the case of 2EO, the statistical distributions are significantly different for strong coupling case with γ=0.062. For 5 and 10EO, the difference between the histograms of maximum forced responses is minimal for both weak and strong coupling cases.

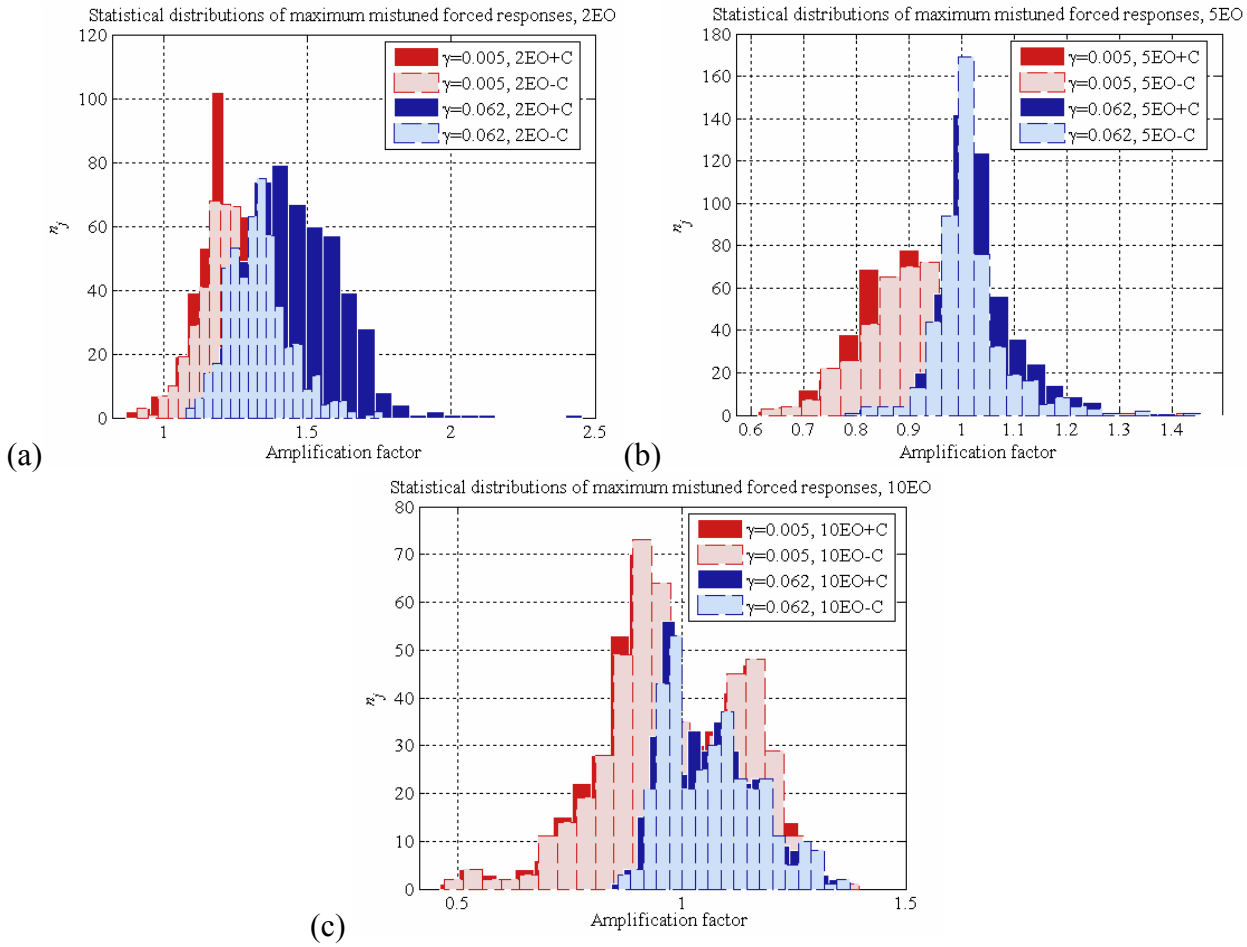

Fig. 5-17. Histograms of maximum mistuned forced responses with and without Coriolis forces for γ=0.005 and γ=0.062 for (a) 2EO, (b) 5EO, (c) 10EO

5.2.6 Discussion and significance of results

For the first time, an assessment of the mutual influence of Coriolis forces and blade mistuning on forced response characteristics has been obtained using a simple lumped parameter mass model which gives insight into the physics of this complex interaction. No attempt is made at such an early stage to generalise with regard to realistic bladed disc geometries, although this is a future goal. Further work should be carried out to achieve this, while the emphasis of this study has been on a fundamental demonstration of the combined effects of Coriolis forces and blade mistuning. Nonetheless, several interesting and thought-provoking results have been obtained. In the previous section, it was demonstrated that for the lower nodal diameter modes the maximum forced response level of the combined Coriolis-mistuned system varies with the amount of coupling between tangential and radial component of displacements, represented in the simple lumped parameter mass-spring model by the coupling parameter, γ. The stronger the coupling, the more pronounced the effects of Coriolis forces, which, in turn, produce higher maximum forced response levels compared with their non-Coriolis counterparts. In practice, the above-mentioned coupling could be characterised by the amount of radial flexibility inherently present in a bladed disc. For example, a non-staggered[†] flat bladed disc does not include a prominent radial component, and, thus, its vibration properties would not be affected notably by Coriolis forces. Conversely, contemporary, increasingly complex three-dimensional designs of bladed discs incorporate a more significant radial flexibility, for which the inclusion of Coriolis forces into mistuned analysis may be important, as the same physical principles demonstrated on a simple model would apply, but at realistic speeds and operating conditions.

The results obtained in this study indicate that in some of the cases considered the additional effects of Coriolis forces could be considered as “minor” in comparison with the typical blade mistuning influence on maximum amplification factors attainable in bladed discs. However, there are particular designs of bladed discs with a prominent radial flexibility where the Coriolis forces effects could not be neglected and which require careful examination. Such systems were found to have maximum forced response levels with the Coriolis effects included which were

[†] Stagger angle is the angle between the chord line and the bladed disc axial direction. In a non-staggered configuration, the stagger angle is zero

significantly higher (approximately 40% in the case of frequency mistuning within a ±5% range) and their statistical distributions significantly different from those corresponding to mistuned-only system. Moreover, the variation between the maximum forced responses with and without Coriolis forces was seen to depend on the specific degree of mistuning.

In this study, the individual blade frequency response functions were found to be different when the Coriolis forces are present compared to their non-Coriolis counterparts. This could provide an explanation for a recurrent mismatch between theoretical predictions and experimental measurements for bladed discs.

The precise amount of forced response amplification also depends on the damping included, which in this study was assumed to be 0.003 (Q≈300). Chapter 7 of this thesis includes an investigation of the effect of different damping levels on forced response amplification with and without Coriolis forces.

Results presented in Chapter 4 showed the dependency of Coriolis forces influence on vibration properties of bladed discs on boundary fixation conditions, which, in a simple model, is exhibited though the stiffness parameter, kd_y. The exact value of this parameter could also affect the influence of Coriolis forces and, more importantly, its mutual interaction with blade mistuning.

5.3 Experimental investigation of mutual influence of Coriolis forces and blade mistuning

5.3.1 Aims of the experimental investigation

The numerical study reported in the first part of this Chapter indicated that for certain designs of bladed discs the influence of Coriolis forces is more prominent than that of typical blade mistuning. The following study seeks to investigate experimentally the mutual effects of Coriolis forces and deliberately introduced blade mistuning on the free vibration properties of Swept Blisk 15deg testpiece, described in Chapter 4. Results acquired for the nominally-tuned system will be compared with results obtained for a deliberately-mistuned testpiece with the aim of identifying how addition of blade mistuning affects the vibration characteristics in presence of Coriolis forces.

5.3.2 Introduction of deliberate mistuning of the Swept Blisk 15deg testpiece

As established in Chapter 4, the 3ND mode pair does not appear to be significantly affected by inherent mistuning of the Swept Blisk 15deg testpiece. Thus, an opportunity was seen in attempting to mistune this particular mode pair in a regulated and controlled fashion. From fundamental mistuning theory, it is well known that a harmonic $\sin 6\theta$ mistuning pattern will predominantly split the 3ND mode pairs, as the Fourier analysis performed on this pattern would yield 0^{th}, 6^{th}, 12^{th}, 18^{th} and 24^{th} significant harmonics, which would cause the 0, 3, 6, 9 and 12ND mode pairs to split [124]. Being single modes, the 0 and 12ND modes do not split and, thus, only those with 3, 6 or 9ND would split. For a 24-bladed disc, harmonic $\sin 6\theta$ mistuning contains 3 different blade types: tuned (T), small mass (SM) and large mass (LM), illustrated in Fig. 5-18.

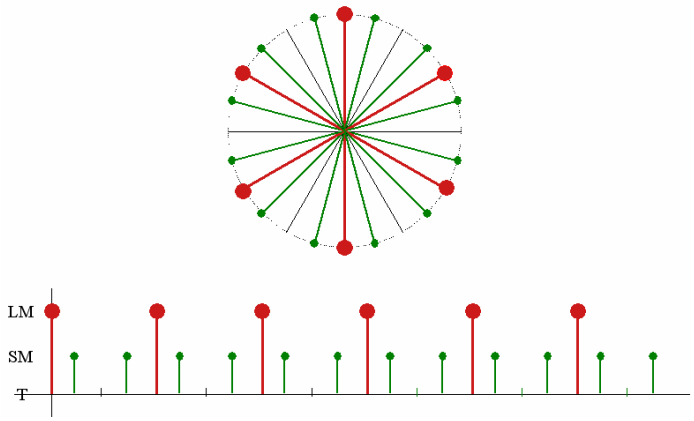

Fig. 5-18. Harmonic $\sin 6\theta$ mistuning

In an attempt to model physically attached mistuning as accurately as possible, a simple relationship was established between the testpiece and model mass, as shown in Fig. 5-19.

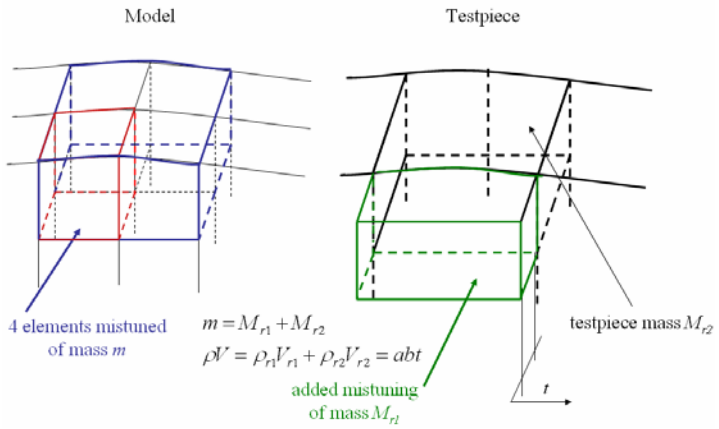

Fig. 5-19. Relationship between model and testpiece mistuning mass

As indicated in Figs. 5-19 and 5-20(a), 4 elements (2 elements across the width and 2 elements in the thickness direction) were mistuned, simulating attached masses at the blade tips, M_{r1}, of volume *abt* or 15.16mm x 10.78mm x relevant thickness, corresponding to the mass attached. The model density of the relevant sectors was modified to simulate the introduced deliberate mistuning, thus matching the addition of blade masses. Several combinations of candidate masses were considered. The main criteria in their selection were (i) the maximum permissible mass that could be glued to the Swept Blisk 15deg and run safely at rotation speeds of interest, and (ii) the difference between the corresponding natural frequency split due to mistuning at rest and the combined split due to both mistuning and Coriolis forces under rotating conditions. A summary of combinations considered for "large mass, LM" and "small mass, SM" is given in Table 5-3.

Combination of LM and SM	0rev/min			270rev/min			% split diff.
	3ND frequencies		3ND split*	3ND frequencies		3ND split	
	BW	FW		BW	FW		
10gr/5gr	23.02	24.20	4.89%	NA†	NA	-	-
5gr/3gr	23.88	24.51	2.55%	24.44	25.15	2.82%	11.0%
4gr/2gr	24.14	24.66	2.12%	24.67	25.30	2.48%	14.5%
3gr/1gr	24.40	24.81	1.65%	24.92	25.46	2.12%	28.5%
2gr/1gr	24.54	24.81	1.09%	25.03	25.48	1.76%	61.5%
1gr/0.5gr	24.74	24.88	0.55%	25.20	25.59	1.51%	174.6%

* Note: indicated split is due to deliberate mistuning only

† "NA" indicates "not available"

Table 5-3. Predicted 3ND natural frequency splits for considered combination of LM and SM

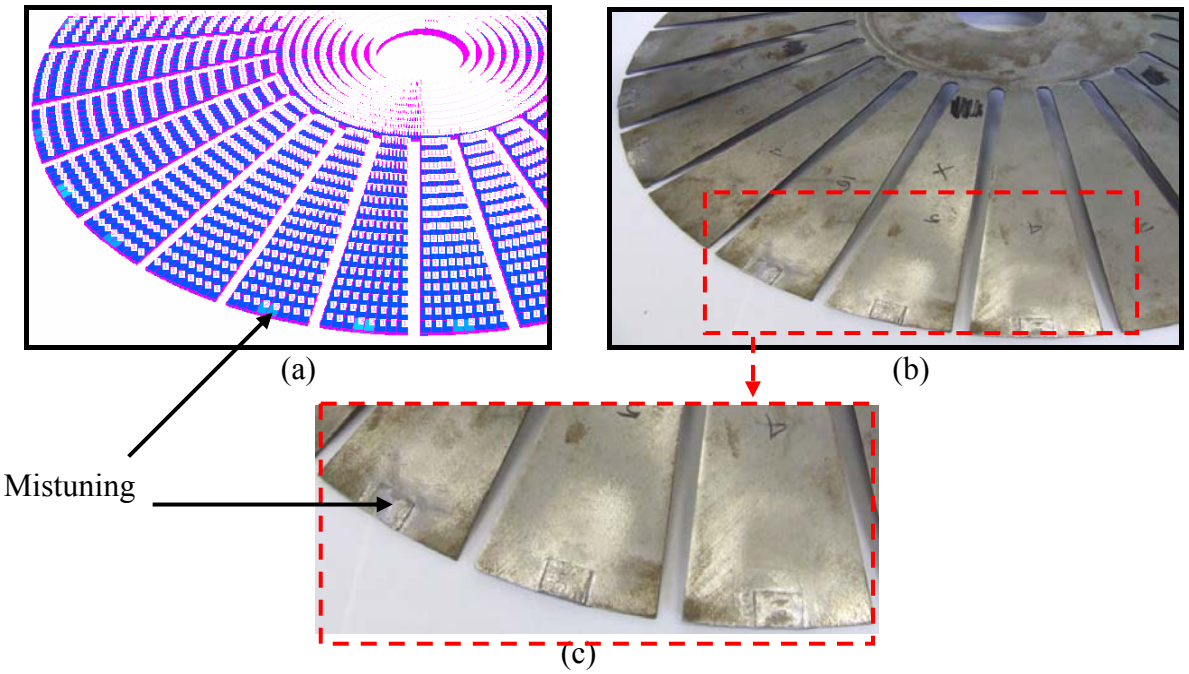

Fig. 5-20. Swept Blisk 15deg with deliberate mistuning: model (a), testpiece (b,c)

A combination of 2gr/1gr masses shows a natural frequency split at rest due to mistuning of 1.09% and its increase to 1.73% split at 270rev/min, thus a corresponding growth of 61.5% due to the combined effect of deliberate mistuning and Coriolis forces. Other mass combinations either yield a considerable split due to mistuning only and a small increase under rotating conditions (as for 5gr/3gr case), or a rather small split due to deliberate mistuning at rest (as in 1gr/0.5gr case). For this reason, the 2gr/1gr combination for deliberate mistuning was chosen and is shown glued to the Swept Blisk 15deg testpiece in Fig. 5-20(b,c).

5.3.3 Results for deliberately-mistuned testpiece

5.3.3.1 Results for deliberately-mistuned 2gr/1gr Swept Blisk 15deg

Experimentally measured[†] natural frequency results were acquired for the deliberately-mistuned 2gr/1gr Swept Blisk 15deg testpiece both at rest and under rotating conditions for both the first 2ND and 3ND mode pairs. Although the emphasis is placed on experimental investigation, the SAMCEF predicted results are also indicated. It should be noted that the SAMCEF results still do not include the correct testpiece sweep angle change due to centrifugal forces, as described in Chapter 4, and, thus, do not provide reliable predictions at higher rotation speeds.

Table 5-4 shows detailed measured and predicted results for first 3ND mode pair, whereas the corresponding results for the first 2ND mode pair are given in Appendix A5-2. Results obtained for the 2ND mode pair were more difficult to examine because the 2ND mode pair is split by inherent mistuning of the Blisk, but not by the harmonic $\sin 6\theta$ deliberate mistuning. Moreover, problems were experienced with measuring the 2ND natural frequencies beyond 390rev/min.

Measured and predicted natural frequency results for the deliberately-mistuned 3ND mode pair are further illustrated in Figs. 5-21. Results acquired previously for nominally-tuned system are indicated for comparison purposes.

[†] The author gratefully acknowledges a contribution from Mr. Dario Di Maio in providing measured results in this part of the Chapter

3ND results				Mistuning + Coriolis			Mistuning only		
Speed (rev/min)	Measured Freq. (Hz) BW	Measured Freq. (Hz) FW	Measured Split, %	Predicted Freq. (Hz) BW	Predicted Freq. (Hz) FW	Predicted Split, %	Predicted Freq. (Hz) w/o C	Predicted Freq. (Hz) w/o C	Predicted Split, % w/o C
0	24.36	24.62	1.08%	24.54	24.81	1.09%	24.54	24.81	1.09%
60	24.37	24.65	1.16%	24.56	24.84	1.14%	24.56	24.84	1.09%
120	24.44	24.74	1.21%	24.63	24.95	1.26%	24.65	24.92	1.09%
180	24.57	24.90	1.33%	24.75	25.11	1.44%	24.80	25.07	1.07%
270	24.87	25.23	1.45%	25.03	25.48	1.76%	25.12	25.39	1.05%
360	25.27	25.67	1.56%	25.42	25.98	2.13%	25.57	25.83	1.01%
450	25.79	26.22	1.64%	25.93	26.59	2.49%	26.13	26.39	0.97%
480	25.99	26.43	1.66%	26.12	26.82	2.62%	26.34	26.60	0.96%
510	26.22	26.66	1.65%						
540	26.43	26.89	1.71%	26.54	27.32	2.86%	26.80	27.05	0.93%
570	26.67	27.13	1.70%						
600	26.91	27.37	1.68%	27.00	27.86	3.10%	27.30	27.55	0.90%
630	27.16	27.63	1.70%						
660	27.43	27.90	1.68%	27.50	28.44	3.33%	27.84	28.09	0.86%
690	27.70	28.17	1.67%						
720	27.99	28.46	1.65%	28.04	29.07	3.55%	28.43	28.67	0.83%
780	28.59	29.06	1.62%	28.61	29.73	3.77%	29.05	29.28	0.80%
840	29.22	29.69	1.58%	29.22	30.43	3.98%	29.70	29.93	0.77%

Table 5-4. Deliberately-mistuned 2gr/1gr Swept Blisk 15deg measured and predicted 3ND natural frequency splits

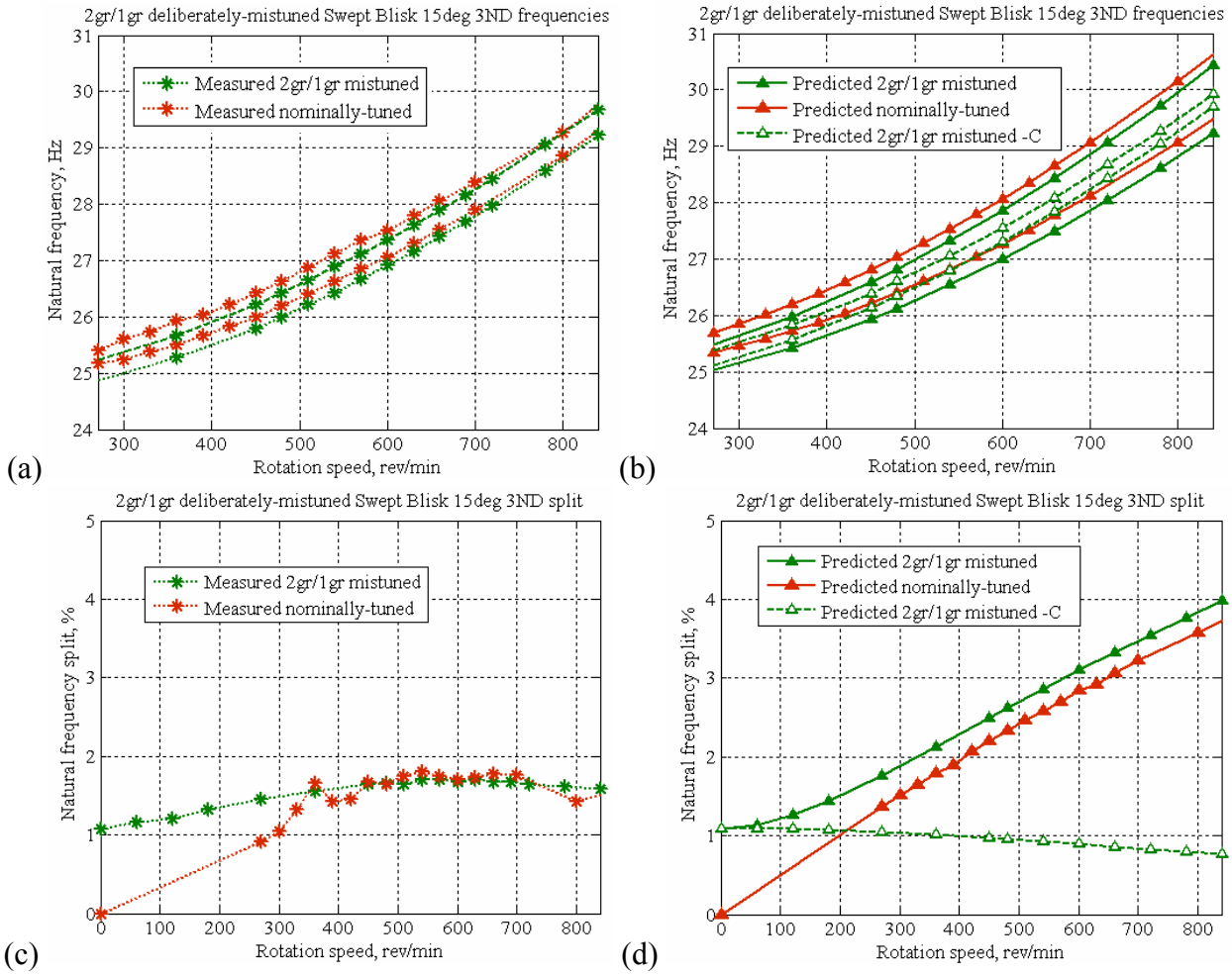

Fig. 5-21. Deliberately-mistuned 2gr/1gr Swept Blisk 15deg rotating conditions natural frequencies (a,b) and their splits (c,d) for first 3ND mode pair

By examining the measured results for the nominally-tuned and deliberately-mistuned 3ND mode pairs in Figs. 5-21 (a,c), several observations can be made. Natural frequency splits obtained for the deliberately-mistuned system are much smoother and more regular than those for the nominally-tuned Blisk (reported earlier) due to the fact that the excitation system (and, correspondingly, the measured response) had been improved by introducing an AC magnet synchronously rotating with the Blisk, as opposed to fixed AC magnet used in measurements described in Chapter 4. As expected, the effect of adding mistuning masses is to lower all the natural frequencies of the Blisk, as demonstrated in Fig. 5-21(a). Comparing the two measured natural frequency split curves in Fig. 5-21(c), it can be seen that these are very close for rotation speeds above about 350rev/min. The difference at rest is 1%, as the nominally-tuned 3ND mode pair is not affected by Blisk inherent mistuning and the introduction of deliberate mistuning causes this mode pair to split by 1% at 0rev/min. The split difference gradually decreases as the rotation speed is increased, while both split curves demonstrate a 'convex' shape due to significant static deflections stemming from the influence of centrifugal forces. An important implication of the closeness of the two measured sets of results is that the addition of mistuning, which splits the 3ND mode pair natural frequencies at rest by approximately 1%, does not contribute to any significant split change under higher rotation speeds. This could mean that for certain designs of bladed discs with prominent radial flexibility, the commonly-observed natural frequency split under rotating conditions, customarily accounted for in previous studies as a purely mistuning-generated effect, could be in fact due to mainly Coriolis forces. This inevitably may lead to the conclusion that for the particular degree of deliberate mistuning considered, the effect of Coriolis forces on natural frequency split can be predominant at higher rotation speeds. Further experiments on the modified Swept Blisk 15deg testpiece with increased mistuning strength are presented below in order to observe the change in measured natural frequency split under rotating conditions.

As in the case of the nominally-tuned system 3ND mode pair, predictions obtained for the deliberately-mistuned system indicate a steady increase of calculated natural frequency split from 1% at 0rev/min to almost 4% at 840rev/min. A possible reason for the discrepancy between the above-mentioned trend in the measured data and the predictions following a relatively close agreement up to almost 200rev/min is not unexpected and is mainly due to the inability of the

prediction code to incorporate a relevant change in geometry of the testpiece, which occurs as the rotation speed increases, due to noticeable static deflections resulting from centrifugal loads, as was explained in Chapter 4.

Comparing the 3ND mode pair predicted data with and without deliberate mistuning, it can be seen that, similarly to the trend in measured natural frequency splits, the effect of adding mistuning of 2gr/1gr intensity does not contribute significantly to increase in split acquired at higher rotation speeds.

5.3.3.2 Results for deliberately-mistuned 4gr/2gr Swept Blisk 15deg

In an attempt to observe the effect of increasing the degree of mistuning on natural frequency split under rotating conditions, the deliberate mistuning of Swept Blisk 15deg was doubled to obtain the harmonic $\sin 6\theta$ 4gr/2gr configuration. Table 5-5 and Figs. 5-22 show measured and predicted results obtained for the 3ND mode pair.

3ND results				Mistuning + Coriolis			Mistuning only		
Speed (rev/min)	Measured Freq. (Hz) BW	Measured Freq. (Hz) FW	Measured Split, %	Predicted Freq. (Hz) BW	Predicted Freq. (Hz) FW	Predicted Split, %	Predicted Freq. (Hz) w/o C	Predicted Freq. (Hz) w/o C	Predicted Split, % w/o C
0	23.90	24.45	2.25%	24.14	24.66	2.12%	24.14	24.66	2.12%
60	23.93	24.48	2.25%	24.16	24.69	2.14%	24.17	24.69	2.12%
120	24.01	24.57	2.28%	24.24	24.79	2.19%	24.26	24.78	2.12%
180	24.15	24.72	2.31%	24.38	24.95	2.29%	24.40	24.92	2.07%
240	24.35	24.92	2.29%	-	-	-	-	-	-
270	-	-	-	24.68	25.30	2.48%	24.73	25.24	2.03%
300	24.59	25.18	2.34%	-	-	-	-	-	-
360	24.89	25.49	2.35%	25.09	25.79	2.71%	25.18	25.69	1.96%
420	25.23	25.84	2.36%	-	-	-	-	-	-
450	-	-	-	25.61	26.39	2.96%	25.75	26.25	1.88%
480	25.63	26.24	2.32%	25.81	26.62	3.04%	25.97	26.46	1.84%
540	26.07	26.68	2.29%	26.23	27.12	3.28%	26.43	26.91	1.78%
600	26.55	27.17	2.28%	26.70	27.66	3.47%	26.94	27.41	1.71%
660	27.08	27.69	2.20%	27.21	28.24	3.65%	27.49	27.96	1.68%
720	27.65	28.26	2.16%	27.76	28.86	3.82%	28.08	28.54	1.60%
780	28.26	28.87	2.11%	28.34	29.53	4.03%	28.71	29.15	1.51%
840	28.90	29.50	2.03%	28.96	30.22	4.19%	29.37	29.80	1.47%

Table 5-5. Deliberately-mistuned 4gr/2gr Swept Blisk 15deg measured and predicted 3ND natural frequency splits

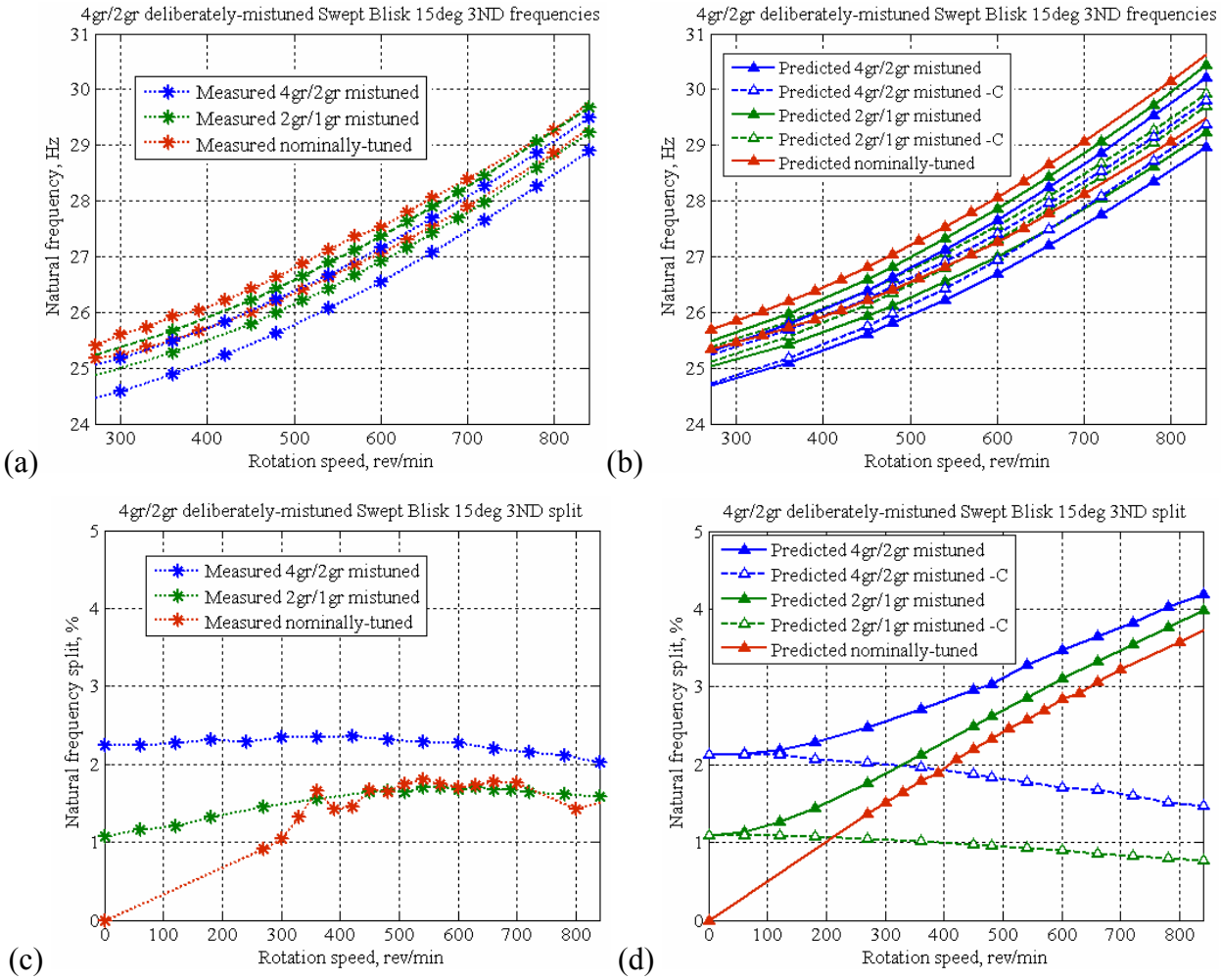

Fig. 5-22. Deliberately-mistuned 4gr/2gr Swept Blisk 15deg rotating conditions natural frequencies (a,b) and their splits (c,d) for first 3ND mode pair

As expected, addition of further blade mistuning lowers the measured natural frequencies of the first 3ND mode pair, as illustrated in Fig. 5-22(a). The measured natural frequency split for the 4gr/2gr mistuning combination, shown in Fig. 5-22(c), still possesses a 'convex shape', albeit of a less protruding nature. Namely, while the measured split for 2gr/1gr configuration increases by approximately 60% from 0rev/min to 540rev/min, the corresponding rise in the 4gr/2gr mistuning combination is only 5% for the same range of rotation speeds. Hence, the difference between the two measured curves for mistuned Swept Blisk 15deg decreases as the rotation speed is increased from 108% at 0rev/min to 33% at 540rev/min. This shows evidence of mistuning-generated effect of 4gr/2gr combination 'overtaking' that of Coriolis forces at lower rotation speeds. Addition of mistuning masses certainly has an effect on Coriolis forces' intensity, as these forces are proportional to the mass of the blades, however, the added mass is not sufficient to stimulate

significantly higher Coriolis-generated splits. At the same time, the addition of the 4gr/2gr mass combination contributes to 2.25% split in the measured natural frequencies due to mistuning at rest, which subsequently marginally increases with rotation speed due to combined effect with Coriolis forces and then diminishes after approximately 400rev/min, as a result of centrifugal forces' action that subsequently reduces the Coriolis forces influence. Furthermore, an interesting feature of the measured deliberately-mistuned split curve is that it appears to lean asymptotically towards the split of the nominally-tuned system at high rotation speeds, suggesting a dominant influence of Coriolis forces on natural frequency split at high rotation speeds. The measured results demonstrate the variability of the mutual effects of Coriolis forces and blade mistuning on natural frequency split depending on precise combination of geometric features and degree of mistuning in a bladed disc.

Fig. 5-22(d) demonstrates a similar trend of decreasing difference in the predicted natural frequency splits calculated for the two mistuned harmonic configurations.

5.3.4 Main conclusion from the experimental investigation study

The experimental investigation study presented in this Chapter contributed to a fundamental understanding of the mutual interaction of Coriolis forces and blade mistuning on natural frequency splits in bladed discs. It was found that for a certain design exhibiting a prominent influence of Coriolis forces, there is a limit of rotation speed up to which addition of blade mistuning contributes significantly to the generated natural frequency split, but beyond which an increase in mistuning degree has no considerable influence, as the split is caused predominantly by the Coriolis forces.

5.4 Summary

The mutual influence of the effects of Coriolis forces and blade mistuning on forced response characteristics of bladed discs has been studied in this Chapter for the first time. A simple, yet representative, lumped parameter model has been developed to demonstrate the effects of Coriolis forces for varying strengths of in-plane radial-tangential coupling, which was established to be the most important

feature that affects the maximum forced response amplification factors of the combined Coriolis-mistuned system. In this study, it was found that despite the fact that in some of the cases considered, the effects of Coriolis forces could be considered as small compared with typical mistuning, their influence certainly cannot be neglected for bladed disc designs with prominent radial flexibility. Moreover, for such bladed discs, depending on the precise degree of blade mistuning present, the maximum forced response levels with Coriolis forces can be significantly higher then their mistuned-only counterparts.

Experimental investigation of mutual influence of Coriolis forces and deliberately introduced mistuning on natural frequency splits of the Swept Blisk 15deg testpiece provided some further insights into physics of this complex interaction. It was demonstrated that Coriolis forces have a dominant impact on the observed splits for higher rotation speeds, while the blade mistuning is the major cause of the splits at lower rotation speed ranges.

The evidence presented in this Chapter strongly suggests that effects of Coriolis forced should be customarily included into contemporary mistuned bladed disc analysis in order to characterise accurately the maximum forced response levels and to assess the associated fatigue life.

CHAPTER 6

Development Of Strategies For Maximum Forced Response Reduction Based On Large Mistuning Concept

"Uncertainty is the only certainty there is, and knowing how to live with insecurity is the only security"

John Allen Paulos

6.1 Overview

The first part of this thesis developed and validated an improved bladed disc model including previously-neglected Coriolis forces effects. From the theoretical viewpoint, once an appropriate model is established, the biggest challenge in turbomachinery design is to assess the uncertainty of predicted forced response levels and to develop ways for their effective control. Thus, in the second part of this thesis, a new maximum forced response reduction strategy is introduced based on "large mistuning", including both (i) random (or "scatter-controlling") and (ii) deterministic (or "pattern-controlling") approaches. An industrial bladed fan disc serves as an application example for the reliability assessment of the aforementioned methods using two well-established tools for uncertainty analysis: (i) statistics and (ii) sensitivity and robustness. The feasibility and other practical aspects of introducing large mistuning as a means of maximum forced response control strategy are discussed.

6.2 Introduction and aims of the study

Since the major problem surrounding mistuned bladed discs is related to uncertainty in the blades' forced response amplitudes, which might lead to excessive vibration levels confined to one or more blades, one of the key issues that current industry practitioners face remains the development of efficient ways of mitigating the hazardous forced response levels and preventing the worst case scenarios. As indicated in Chapter 2, various strategies have been generated during the past 40 years to address this problem, some of which seek to establish the most favourable mistuning patterns from the forced response perspective. They involve the introduction of deliberate, systematically controlled variations in blade properties to obtain the desired response characteristics, commonly referred to as "intentional mistuning". A literature review of the most significant intentional mistuning studies is presented in Chapter 2, section 2.3.2.5. Different types of intentional mistuning patterns have been adopted in the past, such as (i) "alternate" mistuning, by alternating high and low frequency blades [16]; (ii) symmetric, n-periodic mistuning [24], [49], (iii) harmonic mistuning [68], [72], [73], and, most recently, (iv) linear mistuning [75], [76]. The advantage of implementing an intentional mistuning lies in the ability to predict and control the vibration levels at a design stage. However, as blade properties change with time, a chosen mistuning pattern strategy might be appropriate in a short timescale only. For this reason, most of the above-mentioned studies identified the robustness of a selected pattern as one of the crucial factors to be considered when developing an intentional mistuning strategy, and this resulted in the assessment of sensitivity of the selected intentional mistuning to the additional "unintentional" random mistuning. From the papers surveyed, it can be concluded that in the past researchers have only exploited the effects of intentional mistuning for relatively small blade frequency mistuning ranges, from approximately ±0.5% to ±5%. Nevertheless, studies have shown that there is a threshold at small frequency mistuning up to which the forced response increases, but beyond which the response levels off as the degree of mistuning is increased further, as depicted in Fig. 6-1.

From Fig. 6-1 it is evident that there are two possible intentional mistuning strategies for reducing the forced response amplification factor. The first one is to introduce a very small amount of mistuning and, subsequently, endeavour to maintain a nearly-tuned system, which is an expensive procedure in terms of

manufacturing costs and may not be successful due to blade properties changes with time, so that the initial system may depart significantly from the nearly-tuned state. On the other hand, the tendency of the forced response amplification factor to decrease with blade mistuning after the initial rise suggests that there might be an advantage to exploit the effects of larger frequency mistuning ranges, approximately above ±10/±15%, which would introduce a possibility of relaxing the manufacturing tolerances as a means of producing reduced forced response levels of bladed discs. This novel intentional mistuning idea will be subsequently referred to as "large mistuning" (LM), implying large frequency mistuning scatter.

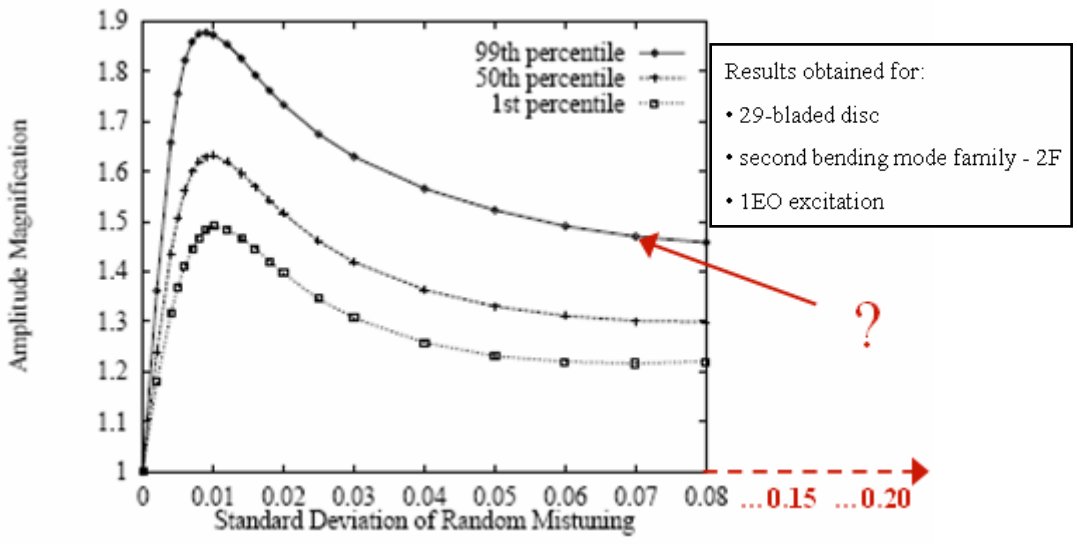

Fig. 6-1. Statistics of the amplitude magnification factor versus random mistuning strength for engine order 1EO excitation, adopted from [68]

The aims of the LM study are (i) to assess effectiveness and reliability of a novel technique for minimising consequences of blade mistuning on forced response of bladed discs and (ii) to establish whether current trends to relax manufacturing tolerances that might have apparent financial incentives and advantages could be used to control the vibration levels. This work will endeavour to obtain the answers to the following questions:

- Could a substantial increase in frequency mistuning range contribute to a reduction of maximum forced response levels?
- How could the maximum forced response be controlled efficiently?

6.3 Chapter outline

This Chapter consists of two parts: (i) an assessment of random or so-called "scatter-controlling" LM strategy, and (ii) utilization of the LM concept in a regulated (deterministic or "pattern-controlling") manner, involving commonly accepted intentional mistuning patterns of unconventionally large strength of mistuning. Both parts include the forced response results of an industrial 26-bladed disc obtained with a high-fidelity in-house prediction tool.

(i) The first part of this Chapter focuses on a statistical approach using the fact that the blade mistuning phenomenon possesses random nature, as all the processes from blade manufacture to their assembly on the disc are random, complicated additionally by the evolutionary changes in blade properties due to effects of ageing and wear under operating conditions and exposure to an aggressive environment. Statistical characterisation of forced response is obtained numerically via extensive Monte Carlo (MC) simulations, which have been widely used in blade mistuning literature. The forced response results from MC simulations of bladed disc frequency mistuning patterns drawn randomly from a uniform distribution are presented for different blade frequency mistuning ranges (spanning small to large mistuning ranges) under several engine order excitations. The maximum, mean and minimum forced responses are assessed as functions of blade frequency mistuning ranges. Subsequently, a statistical analysis is carried out to obtain the probability density and cumulative density functions of the forced response for maximum, mean and minimum values. Goodness-of-fit tests based on the Kolmogorov-Smirnov and the Chi-Square (Pearson's) criteria are performed to identify the theoretical distribution functions that represent the best match to the empirical distributions of forced responses obtained from the MC simulations. As a result of this investigation, a scatter-controlling LM strategy is tested and its usefulness assessed from a practical viewpoint.

(ii) In the second part of the Chapter, the effectiveness of several deterministic intentional mistuning patterns based on LM, including the alternate, harmonic, linear mistuning and best and worst mistuning patterns obtained in part (i), is examined and their sensitivity and robustness to small changes in blade properties are tested in an attempt to determine the most beneficial and successful LM intentional mistuning patterns. Moreover, the effect of random blade rearrangements of some of the

above-mentioned patterns is assessed. A discussion of advantages and drawbacks of the two considered uncertainty estimation tools, the statistical analysis and the sensitivity and robustness, in relation to the blade mistuning problem is presented in order to establish the most useful analysis technique.

Finally, the scatter-controlling and pattern-controlling LM intentional mistuning strategies are compared in terms of their practicality and overall success.

6.4 Random or "scatter-controlling" large mistuning (LM) intentional mistuning strategy

6.4.1 Model description

A realistic bladed fan disc illustrated in Fig. 6-2 has been used in this analysis. Its finite element model contains 26 blades and consists of over 120,000 DOFs per sector, contributing to more than 3,000,000 DOFs of a full structure. The model consists of flexible blades mounted on a relatively stiff disc, and its blades are weakly coupled and vibrate more-or-less independently of each other. Free tuned vibration characteristics shown in Fig. 6-3 reveal that the bladed disc assembly has modes of vibration with rather close natural frequencies for most of the mode families.

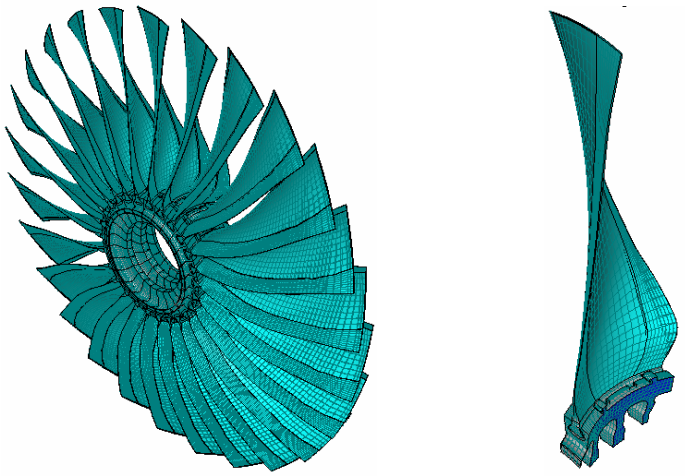

(a) (b)

Fig. 6-2. Bladed fan disc: (a) full model, and (b) its cyclic sector

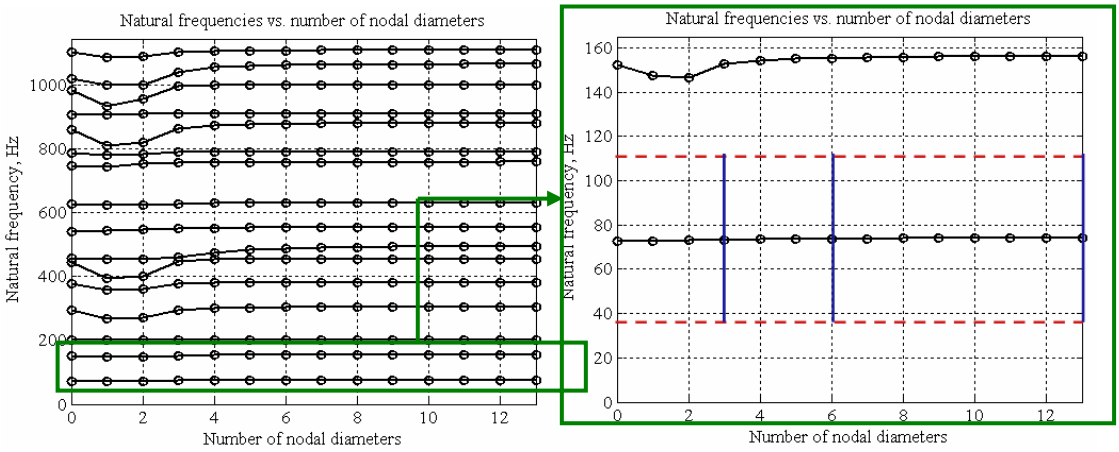

(a) (b)

Fig. 6-3. Natural frequencies of a tuned bladed fan disc, the excitation frequency range (rectangular area between two red dashed horizontal lines) and analysed excitation engine orders (blue vertical lines)

6.4.2 Mistuning type

Mistuning expressed in terms of blade frequency deviations from the nominal values, which are the consequence of mass and stiffness variations, was chosen for the study. Moreover, the random blade frequency values used were generated from a finite uniform distribution, representing a predetermined frequency mistuning range, as depicted in Fig. 6-4.

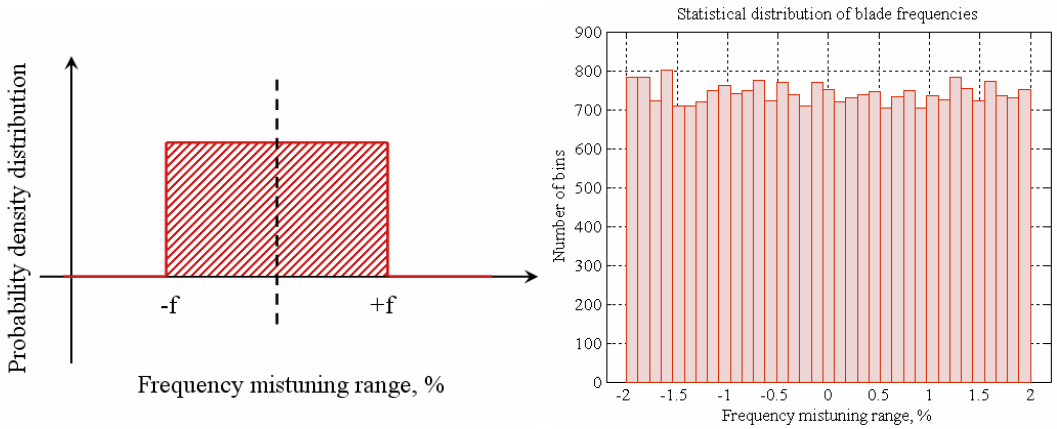

(a) (b)

Fig. 6-4. A uniform probability density function of frequency mistuning range

The specific frequency mistuning ranges considered were (i) ±20, 30, 40% representing large mistuning, (ii) ±5, 10, 15%, and (iii) ±0.5, 1, 1.5, 2% accounting for “moderate” and “small” frequency mistuning ranges respectively, included in this study for the sake of comparison with the large mistuning results.

In this work, the MC simulations of bladed disc frequency mistuning values were generated. The MC method or “synthetic or empirical sampling” consists of

"building" many systems by computer calculations and evaluating the performance of the resulting "synthesized" systems. A flow chart of the MC simulation method is given in Fig. 6-5. The biggest drawback of the MC approach is generally attributed to the computational expense due to the very large number of mistuning simulations required to obtain an accurate and reliable PDF of the forced response. A compromise was achieved in this study by considering an optimum number of MC simulations sufficient to accurately capture the forced response features, which has been established as 1,000 [96].

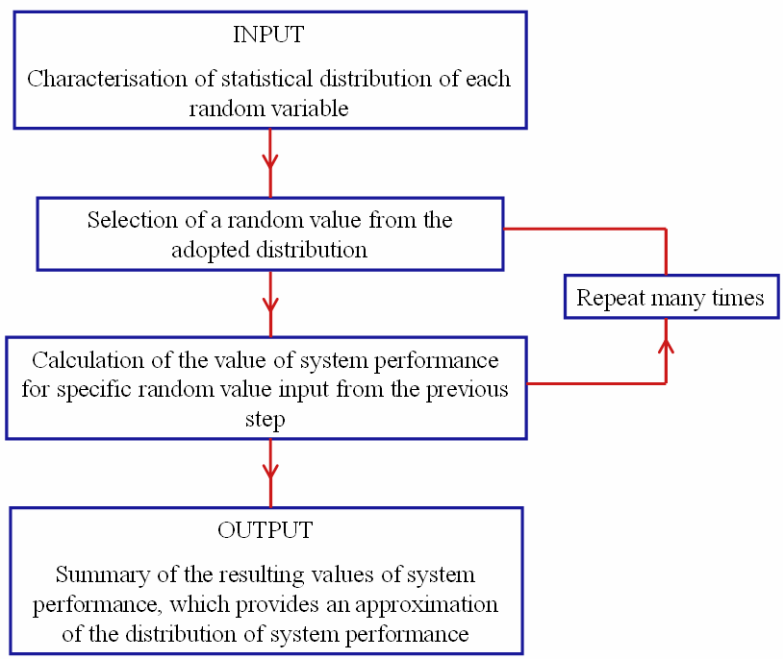

Fig. 6-5. Flow chart of MC simulation method

6.4.3 Forced response considerations

Forced response[1] calculations for different frequency mistuning ranges were performed using MISTRES in-house prediction code based on a new method for dynamic analysis of mistuned bladed disks developed in [32]. The method is based on an exact relationship between tuned and mistuned systems, which allows use of large FE models, since only one sector is needed to represent the tuned and mistuned systems, while the computational cost is independent of the size of the original single blade segment. Since the program permits computation of the forced response at selected, so-called "active" DOFs only, the amplitudes of forced response were

[1] "Forced response" will be used in this Chapter to refer to the maximum forced response calculated by the MISTRES code over all nodes of all bladed disc sectors

obtained for all bladed disc sectors at 4 chosen nodes where the maximum displacements were anticipated. The "active" nodes where the forced response amplitudes were calculated, and condensed mass mistuning elements were applied, are shown as red circles in Fig. 6-6. Green circles indicate the "passive" nodes subjected to the uniformly-applied loads.

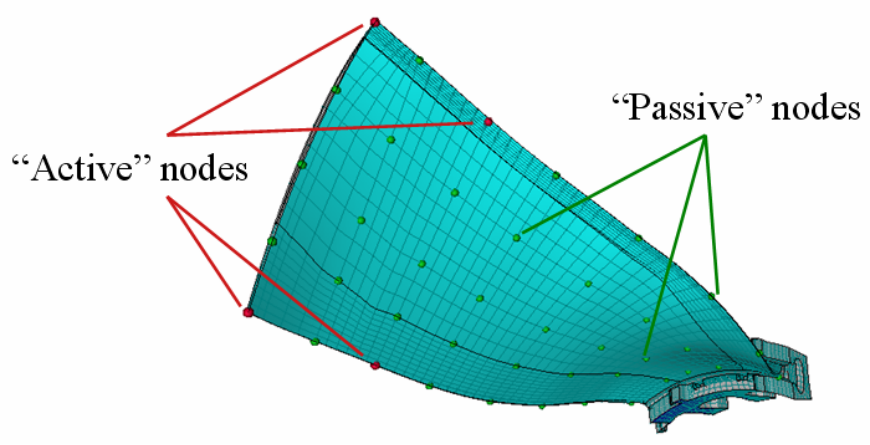

Fig. 6-6. "Active" and "passive" nodes

A conventional engine order excitation was assumed. The specific orders of excitations chosen were (i) 3EO, at the lower end of the natural frequency versus number of nodal diameters plot shown by blue vertical lines in Fig. 6-3(b), (ii) 6EO, at the middle of the plot, and (iii) 13EO, at the end of the plot. The engine orders were considered in the analysis over an excitation frequency range corresponding to the predominantly first flapwise vibration mode (1F), as shown in Fig. 6-3(b) by a rectangular area constrained between the two red dashed horizontal lines.

Forced response amplitudes of the mistuned system were normalised with respect to maximum amplitudes of the tuned bladed disc under the same excitation conditions. The damping loss factor was set to 0.003.

6.4.4 Dependency of forced response on frequency mistuning range

As mentioned above, the MC simulations for 1,000 random bladed disc frequency mistuning configurations generated from the uniform distribution yielded normalised forced response amplitudes for all blades for different frequency mistuning ranges and three distinct EO excitations. The complete set of plots is available in Appendix A6-1: here, only selected results are presented and discussed.

Figs. 6-7 to 6-9 show the results obtained from 1,000 MC simulations for ±40, 15 and 0.5% frequency mistuning ranges under 3, 6 and 13EO excitation.

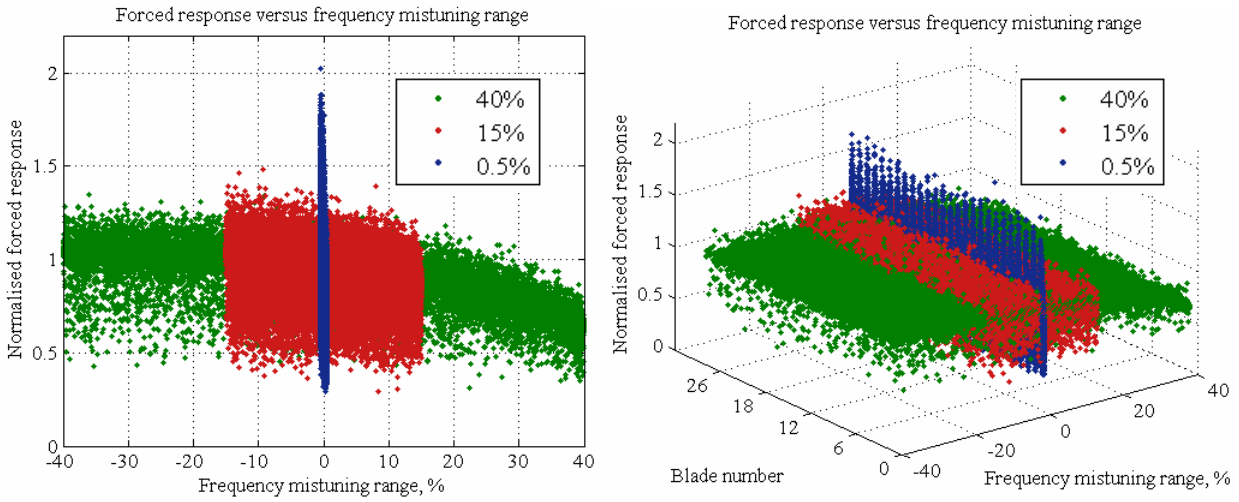

Fig. 6-7. Forced response results for ±40, 15 and 0.5% frequency mistuning ranges obtained for 3EO

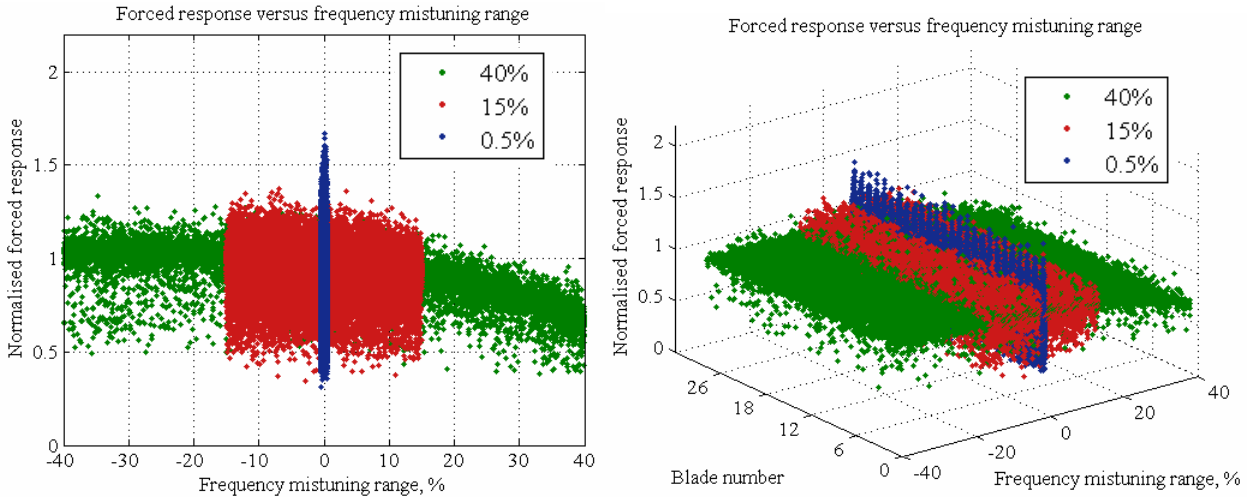

Fig. 6-8. Forced response results for ±40, 15 and 0.5% frequency mistuning ranges obtained for 6EO

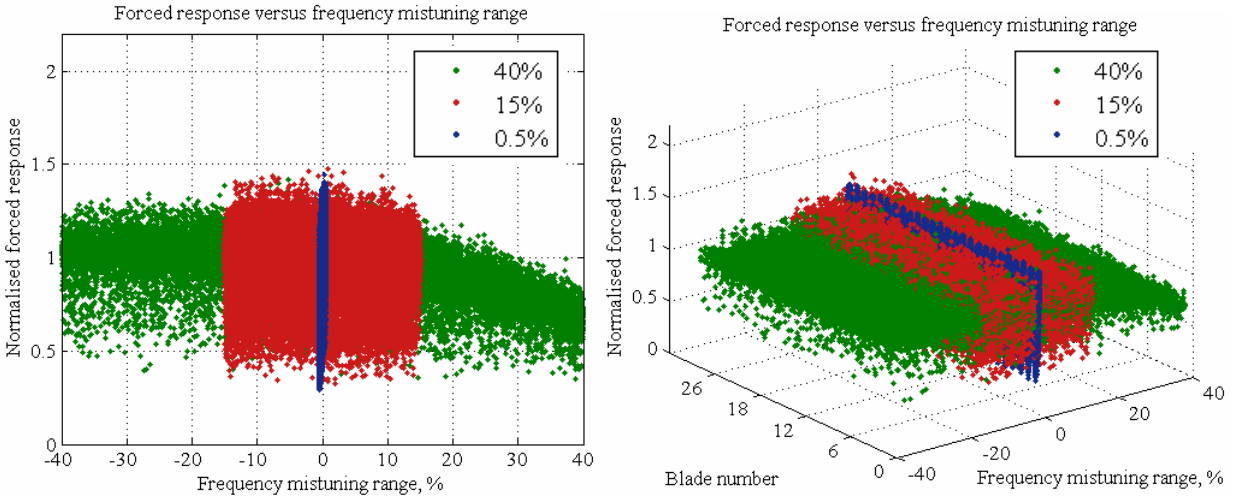

Fig. 6-9. Forced response results for ±40, 15 and 0.5% frequency mistuning ranges obtained for 13EO

From the results presented in Figs. 6-7 to 6-9 it is evident that the normalised forced response (i) decreases as the frequency mistuning range is increased, and (ii) varies depending on the engine order of excitation. Furthermore, Figs. 6-10 to 6-12 demonstrate that (iii) the spread of forced response decreases as the frequency mistuning range is increased, and that (iv) there is no clear indication about the natural frequency characteristics of the highest responding blades.

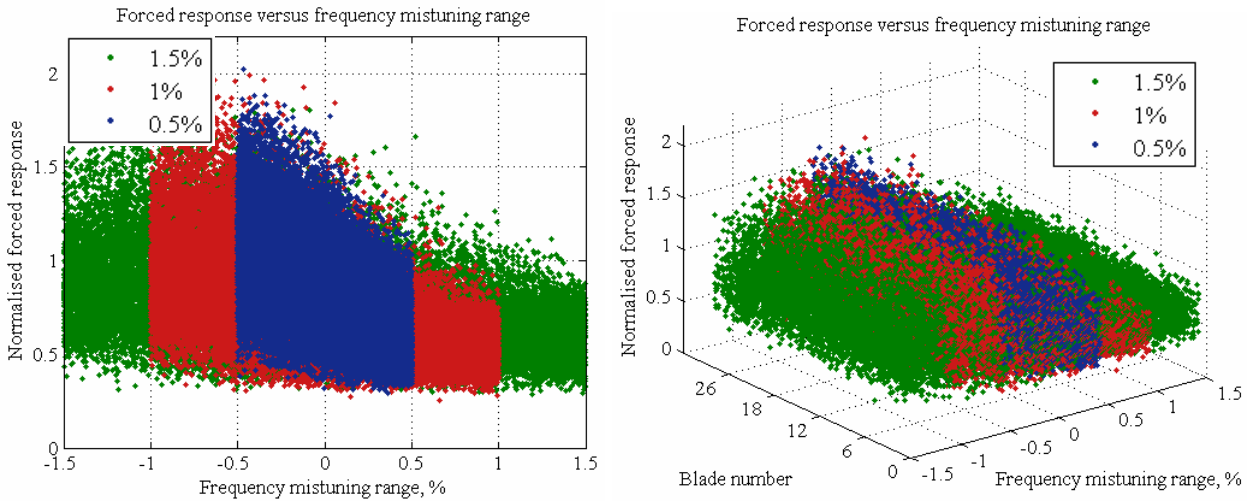

Fig. 6-10. Forced response results for ±1.5, 1 and 0.5% frequency mistuning ranges obtained for 3EO

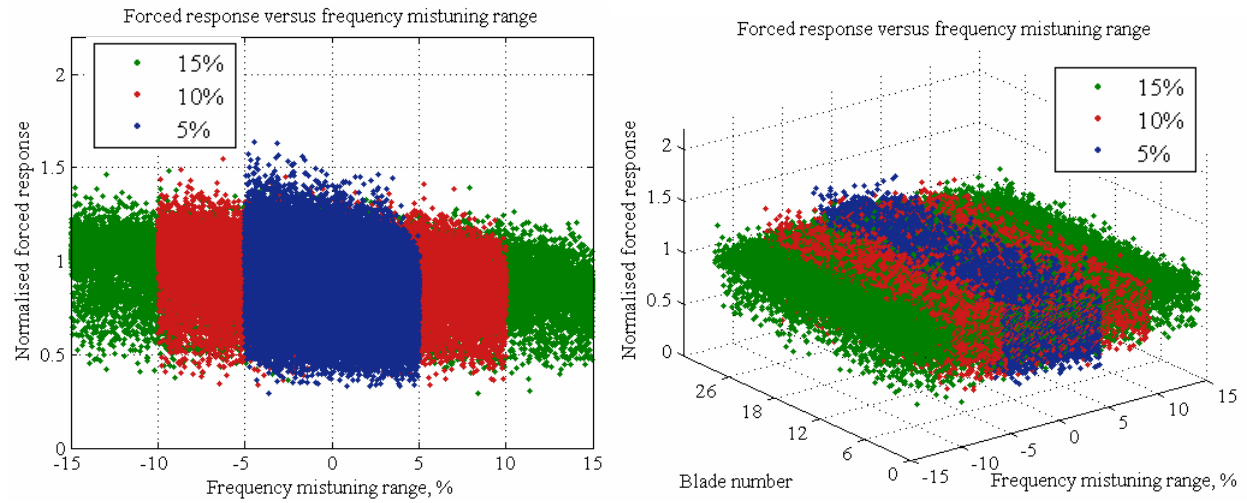

Fig. 6-11. Forced response results for ±15, 10 and 5% frequency mistuning ranges obtained for 3EO

The maximum, mean and minimum forced response amplitudes for each of the analysed random mistuning patterns are shown in Figs. 6-13 for the cases of ±0.5 and 40% frequency mistuning ranges. The spread of maximum forced response reduces with the frequency range, while that of minimum forced response increases under same conditions.

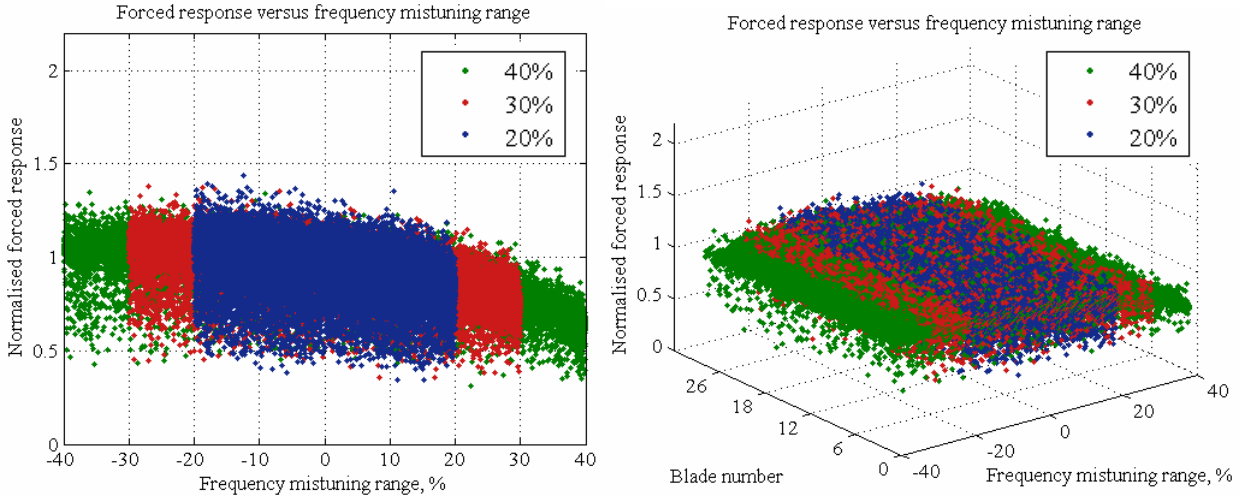

Fig. 6-12. Forced response results for ±40, 30 and 20% frequency mistuning ranges obtained for 3EO

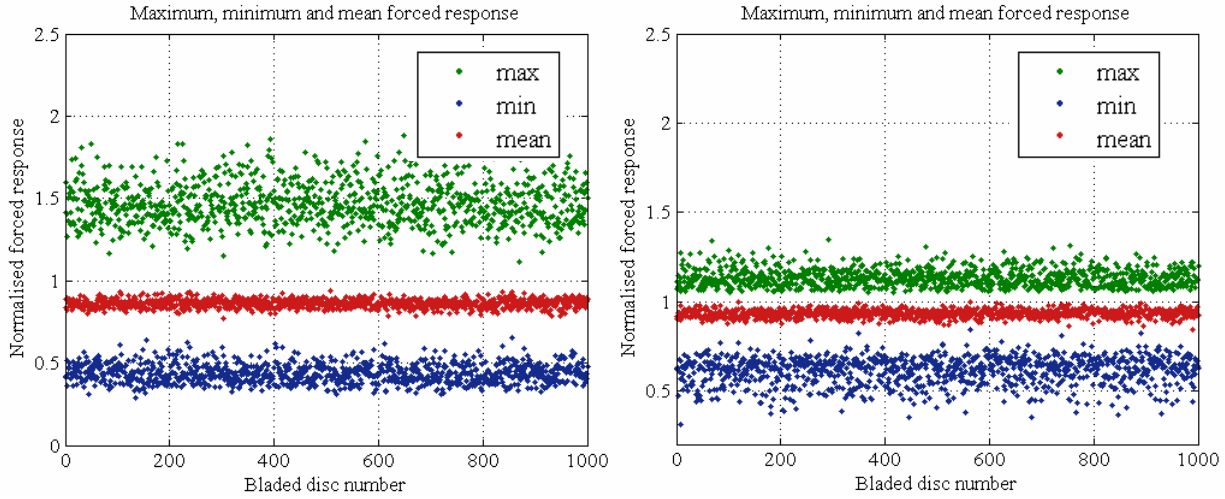

(a) (b)

Fig. 6-13. Maximum, minimum and mean forced response results for ±0.5% (a) and ±40% (b) frequency mistuning ranges obtained for 3EO

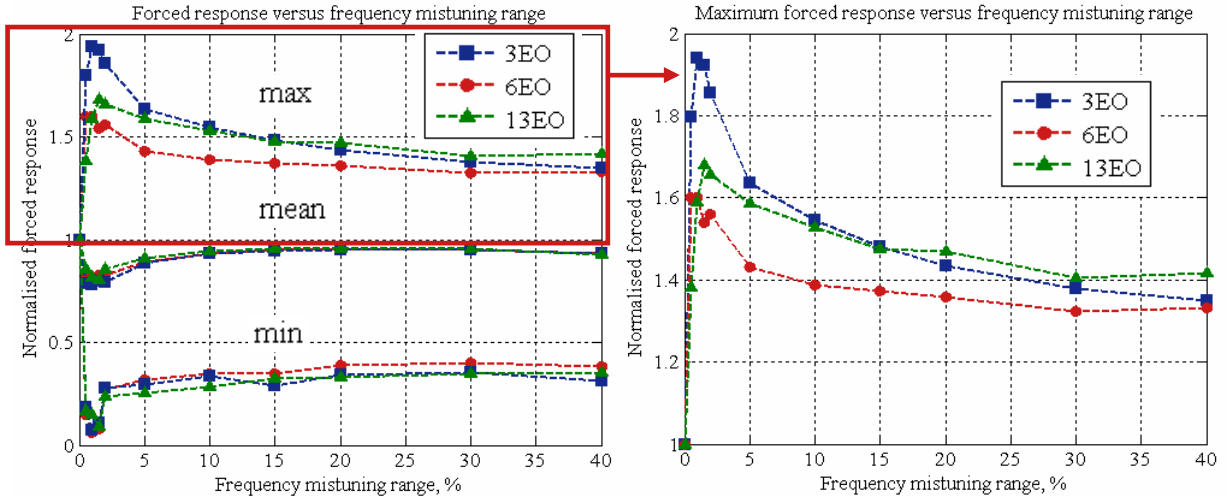

(a) (b)

Fig. 6-14. Maximum, minimum and mean forced response results for 3, 6 and 13EO

Results obtained from this statistical study are finally summarised in Fig. 6-14 and Table 6-1, which depict the forced response dependency upon frequency mistuning range for maximum, mean and minimum values under 3, 6 and 13EO excitations.

Frequency mistuning range	3EO			6EO			13EO		
	Max	Min	Mean	**Max**	Min	Mean	**Max**	Min	Mean
±0.5%	**2.02**	0.29	0.86	**1.67**	0.31	0.85	**1.44**	0.30	0.88
±1%	**1.99**	0.25	0.76	**1.70**	0.29	0.81	**1.62**	0.24	0.85
±1.5%	**1.94**	0.28	0.77	**1.61**	0.29	0.81	**1.68**	0.24	0.85
±2%	**1.92**	0.28	0.80	**1.56**	0.27	0.83	**1.66**	0.24	0.86
±5%	**1.64**	0.29	0.88	**1.43**	0.32	0.89	**1.59**	0.25	0.91
±10%	**1.55**	0.34	0.93	**1.39**	0.35	0.94	**1.53**	0.28	0.94
±15%	**1.48**	0.29	0.95	**1.37**	0.35	0.95	**1.47**	0.33	0.95
±20%	**1.44**	0.34	0.95	**1.36**	0.39	0.96	**1.47**	0.33	0.96
±30%	**1.38**	0.36	0.95	**1.33**	0.40	0.95	**1.42**	0.35	0.96
±40%	**1.35**	0.31	0.93	**1.32**	0.38	0.94	**1.41**	0.35	0.93
% reduction	**33.25%**			**22.12%**			**16.30%**		
(from ±0.5% to ±40%)				(from ±1% to ±40%)			(from ±1.5% to ±40%)		

Table 6-1. Maximum, minimum and mean forced response results for 3, 6 and 13EO

The results obtained indicate a reduction in the maximum forced response of approximately 33% from 2.02 at ±0.5% frequency mistuning range to 1.35 at ±40% frequency mistuning range for 3EO excitation. The maximum forced response decreases for 6EO and 13EO are 22% and 16%, respectively. It is evident that the precise amount of maximum forced response reduction is dependent upon the engine order excitation considered, however, there is a clear trend of a consistent response reduction with the increase of frequency mistuning range after the initial rise. The observed tendency of the maximum forced response to decrease could be explained as follows. Figs. 6-15 demonstrate the FRFs calculated for all blades for very small (±0.1%), small (±2%) and large (±20%) frequency mistuning ranges. It can be seen that there is very little interaction between the blades for very small and large frequency mistuning ranges, and subsequently, low energy transfer between the blades, whereas the opposite is true for ±2% (small frequency mistuning) case. The amount of interaction between the blades and the energy transfer between them could be associated with the maximum forced response amplification levels, which are high in the latter ±2% frequency mistuning case as this leads to a localised response of one blade that is contributed by the accumulated responses of all the other blades. The maximum forced response levels are substantially lower in the

nearly-tuned and heavily mistuned systems as low energy transfer between the blades does not contribute substantially to formation of the localised response.

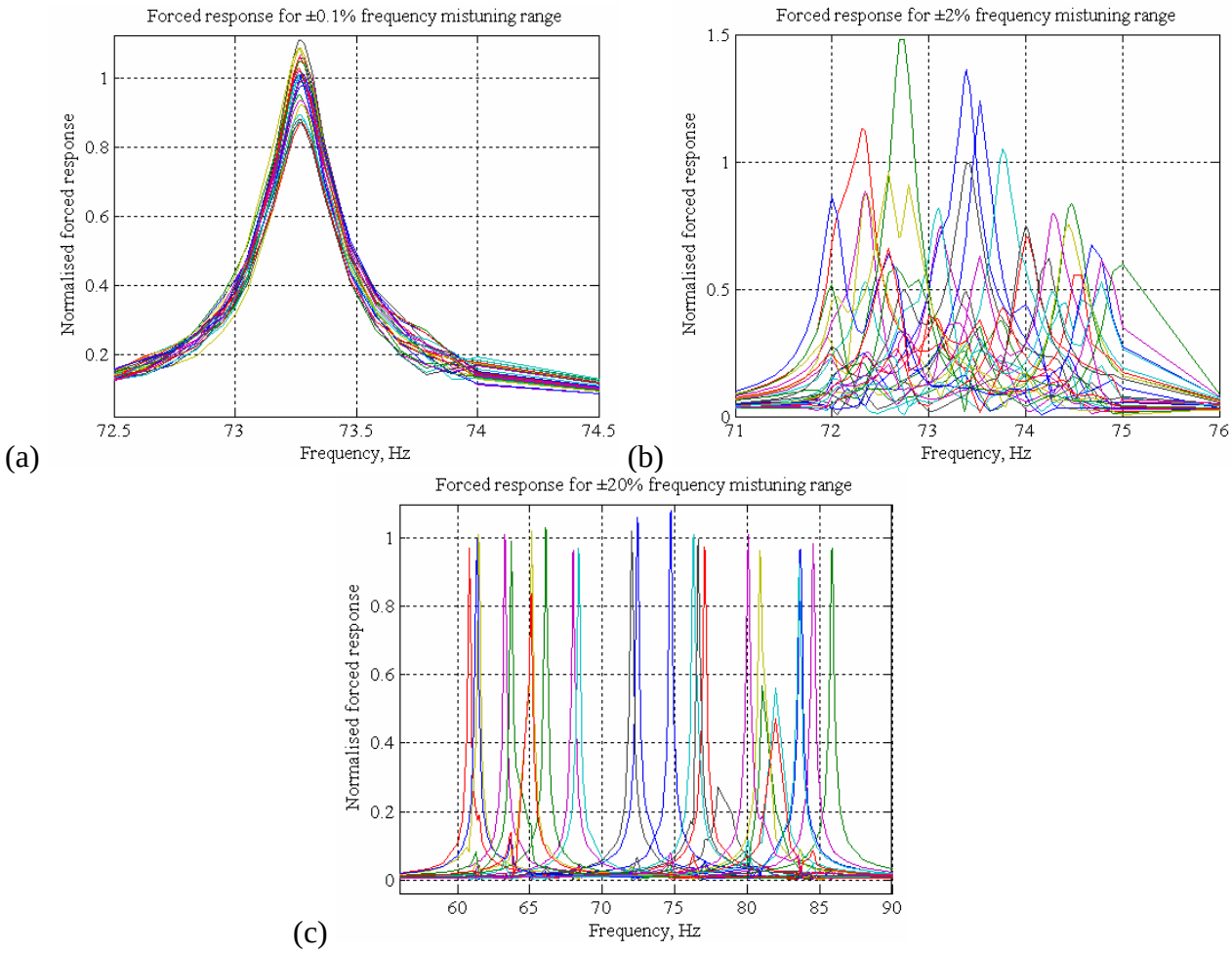

Fig. 6-15. Frequency response functions (FRFs) for all blades under 3EO excitation for ±0.1% (a), ±2% (b) and ±20% (c) frequency mistuning ranges

In this study, the maximum forced response encountered was 2.02 at ±0.5% frequency mistuning range. This is a lower value than Whitehead's upper limit of the maximum amplification factor, which in the present case of 26 blades becomes 3.05. Since Whitehead's formula provides a very general estimate, and does not account for the specific bladed disc design and operating conditions, the factor of 3.05 may not be achievable with the chosen bladed fan disc.

The evidence presented in this section suggests that random or scatter-controlling large mistuning (LM) is a promising approach that, if practically feasible, could be employed as a potentially-beneficial deliberate forced response diminution strategy.

6.4.5 Practical issues of LM implementation

Large mistuning levels for few blades in the assembly are not uncommon in bladed disc practice. Examples include (i) single-crystal turbine blades known for their unmatched resistance to high-temperature creep and fatigue and (ii) damaged blades, which can reach ±34% deviation in the first natural frequency compared with the corresponding value of the tuned blade [123]. Practically, if the implementation of LM blade types in the bladed disc assembly does not introduce any adverse effects, then the advantage is seen in extending design acceptance limits as a way to reduce the manufacturing costs. Moreover, a study of forced response characteristics of few blades with uncommonly large natural frequency discrepancies provides a means of assessment of the damage tolerance of the assembly, which is of importance in the engine industry.

6.4.6 Statistical characterisation of forced response

6.4.6.1 Outline of the statistical analysis

Statistical methods are widely employed in all branches of scientific endeavour as a useful tool of uncertainty assessment. The use of statistical techniques is essential in the construction of an appropriate statistical model and estimation of its parameters in order to make predictions about the model's future performance and, most importantly, its life expectancy and risks of failure. Statistical characterization is inherently appropriate for the analysis of mistuned bladed discs due to uncertainty of the forced response levels imposed by individual blade variability with time under fluctuating operating conditions.

The aim of statistical analysis presented in this Chapter is to characterise the statistical distributions of forced response levels obtained in section 6.4.4 and ultimately to gain some insight into the bladed disc worst case response likelihood. Initially, two histogram-based methods are applied in order to yield an estimate of the empirical distribution function of the normalised forced response population. Descriptive measures, or the "first four moments" of the distribution, are then determined, including the expected value or mean, variance, skewness and kurtosis. Subsequently, the confidence intervals for the general parameters are calculated using the obtained empirical distribution parameters. Theoretical distributions, including Gaussian, uniform, Rayleigh, Beta, Gamma, Weibull and Type I extreme

value distributions, are fitted to the empirical distribution, where their parameters are estimated using the method of moments and the principle of maximum likelihood. By performing two of the standard hypothesis tests, namely, the Kolmogorov-Smirnov and the Chi-square (Pearson's), the "degree of fit" of the theoretical distributions with the empirical is assessed at a given significance level. Some conclusions are made about the statistical distributions of maximum, mean and minimum values of forced responses and bladed disc life.

6.4.6.2 Statistical analysis of forced response levels

(a) Construction of an empirical distribution of forced response

A histogram of the obtained blade forced response amplitudes is introduced initially as a graphical way of summarising the accumulated data. The histogram visually conveys how an empirical data set is distributed and provides information about relative frequencies of observations. In calculation of the histogram, two parameters which define the mesh over which it is constructed must be chosen: (i) an origin for the bins, and (ii) a bin width or the "smoothing parameter", as this determines the smoothness of the histogram. In this work, two different selection procedures for the bin width were considered: (i) the often-presented Sturges' rule, which estimates the number of bins in the histogram, k, as a function of the number of observed data, n:

$$k = 1 + 3.3 \log_{10} n \tag{6-1}$$

and (ii) the number of bins obtained as the closest whole number to $\sqrt{n}$. Common sense indicates that the number of bins should be as large as possible, while, on the other hand, as many of the data points should fall into these bins. The compromise is reached by having a number of bins characterised by Sturges' rule. Figs. 6-16 illustrate the two histograms obtained using the aforementioned procedures for the case of blade forced response amplitudes calculated for ±2% frequency mistuning range under 6EO excitation.

(b) Characterisation of the first four moments of an empirical distribution

Having constructed an empirical distribution of forced response amplitudes, it is appropriate to describe its spread, symmetry and peakedness characteristics, which can be summarised adequately by the first four moments of the distribution.

The data mean, or the expected value, denoted by $\tilde{m}_x$, is the best known measure of central tendency and is calculated as:

$$\tilde{m}_x = \frac{1}{n}\sum_{i=1}^{n} x_i \tag{6-2}$$

where x_i, $i = 1, 2, ..., n$, are the values for the n data points.

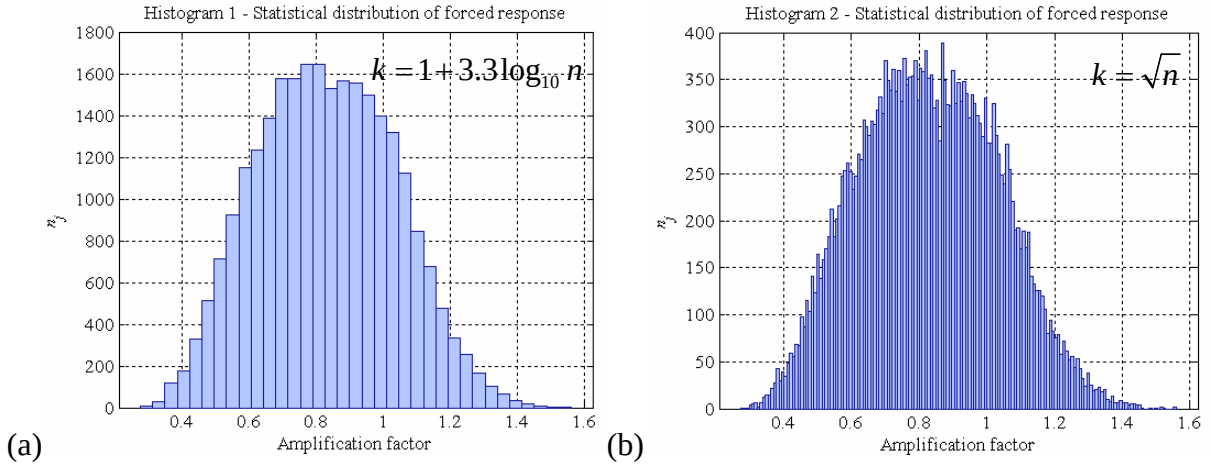

(a) (b)

Fig. 6-16. Histograms of forced response obtained using Sturges' rule ($k = 1 + 3.3\log_{10} n$) (a) and $k = \sqrt{n}$ method (b)

The second moment about the mean is a measure of dispersion. This is known as the variance and is defined as:

$$\tilde{D}_x = \frac{1}{n-1}\sum_{i=1}^{n}\left(x_i - \tilde{m}_x\right)^2 \tag{6-3}$$

The square root of the variance is known as the standard deviation:

$$\tilde{\sigma}_x = \sqrt{\tilde{D}_x} \tag{6-4}$$

The third moment about the mean is related to the asymmetry or skewness of a distribution and is given by:

$$\tilde{a}_x = \frac{1}{(n-1)\tilde{\sigma}_x^{\,3}}\sum_{i=1}^{n}\left(x_i - \tilde{m}_x\right)^3 \tag{6-5}$$

Finally, the fourth moment about mean is related to the peakedness – also called kurtosis – of the distribution and is defined as:

$$\tilde{e}_x = \frac{1}{(n-1)\tilde{\sigma}_x^{\,4}}\sum_{i=1}^{n}\left(x_i - \tilde{m}_x\right)^4 - 3 \tag{6-6}$$

In reality, it is unlikely that the moment estimates obtained from a limited random sample will match precisely the true values of the population parameters. Thus, it might be more beneficial to specify the relevant confidence intervals that we expect will contain values of the parameters, [125]. A confidence interval is used to

express the uncertainty in a quantity being evaluated and it gives an estimated range of values that is likely to include an unknown population parameter, the estimated range being calculated from a given set of sample data. If independent samples are taken repeatedly from the same population, and a confidence interval calculated for each sample, then a certain percentage (the confidence level) of the intervals will include the unknown population parameter. Usually, the confidence intervals are 90, 95, 99 and 99.9%, which signifies that 90, 95, 99 and 99.9% of such intervals will contain the true parameters, respectively.

The confidence interval for the precision of the estimate of the mean value is calculated as:

$$\tilde{m}_x - \frac{\tilde{\sigma}_x t_{1-\frac{p}{2}}(f)}{\sqrt{n}} \le m_x \le \tilde{m}_x + \frac{\tilde{\sigma}_x t_{1-\frac{p}{2}}(f)}{\sqrt{n}} \tag{6-7}$$

where $\tilde{m}_x$ and $\tilde{\sigma}_x$ are the estimated mean and standard deviation; $t_p(f)$ is the Student's t-distribution quantile, obtained from tables, corresponding to p – the statistical significance level – from which the confidence interval is given as $(1-p)$.

The corresponding confidence interval for the variance is found from:

$$\frac{f\tilde{D}_x}{\chi^2_{1-\frac{p}{2}}(f)} \le D_x \le \frac{f\tilde{D}_x}{\chi^2_{\frac{p}{2}}(f)} \tag{6-8}$$

where $\tilde{D}_x$ is the estimated variance; $\chi^2_p(f)$ is the Pearson's χ^2-distribution quantile corresponding to p (obtained from tables); f is the number of degrees-of-freedom.

Similarly, the confidence intervals for the skewness and kurtosis are obtained using the Tchebyshev inequality as:

$$\tilde{a}_x - \sqrt{\frac{D_a}{p}} \le a_x \le \tilde{a}_x + \sqrt{\frac{D_a}{p}} \tag{6-9}$$

$$\tilde{e}_x - \sqrt{\frac{D_e}{p}} \le e_x \le \tilde{e}_x + \sqrt{\frac{D_e}{p}} \tag{6-10}$$

where D_a and D_e are the variances of the estimated skewness and kurtosis:

$$D_a = \frac{6(n-1)}{(n+1)(n+3)} \tag{6-11}$$

$$D_e = \frac{24n(n-2)(n-3)}{(n+1)^2(n+3)(n+5)} \tag{6-12}$$

It should be noted that the calculation of confidence intervals in (6-7) and (6-8) is based on the assumption that the random variables, i.e. the blade forced

response amplitudes, are normally distributed in the population. Nevertheless, these formulae are often used for any kind of distributions; in such cases, the results obtained are approximate, rather than exact. In contrast, equations (6-9) and (6-10) are valid for any distribution type, [126]. This situation should not present a problem as long as the sample size is sufficiently large, as in this study: 1,000 frequency mistuning patterns have been generated from a uniform distribution, which yield 26,000 blade forced response amplitudes. In the present case, the distribution of the latter is still unknown and will be discussed further in the next sections.

(c) Selection of theoretical distributions and estimation of their parameters

The next phase of the statistical characterisation of forced response involved (i) the choice of the theoretical probability density (PDF) and cumulative density (CDF) functions to describe the empirical data, and (ii) the estimation of their parameters: the location, scale and shape of the distribution. For predictive and controlling purposes, it is often desirable to calculate accurately the attributes of an underlying distribution of population. To determine this distribution, it is common to fit hypothetical theoretical distributions to an empirical distribution and, subsequently, to assess the degree of correlation between the two. The fitting of distributions to data has a long history, and many different procedures have been advocated. The choice of theoretical distribution to represent a physical system or collected empirical data is generally motivated by understanding the nature of underlying phenomenon or assumed by examining the empirical distribution characteristics. In this study, several different statistical distributions have been considered as potential candidates to represent adequately the computed blade amplitudes and the selection of their maximum, minimum and mean values: (i) normal or Gaussian distribution, (ii) Rayleigh distribution, closely related to the Gaussian, (iii) Gamma and Beta distributions, which are more versatile than the Gaussian, (iv) uniform distribution, as a special case of the Beta distribution, (v) Weibull and Type I extreme value distributions. A brief account of the aforementioned distributions is given in the Appendix A6-2.

The parameters of the above-mentioned theoretical distributions were estimated using (i) the method of moments and (ii) the principle of maximum likelihood. A simpler method of moments sets the distribution moments equal to the empirical distribution moments, and solves to obtain estimates for the distribution

parameters. The principle of maximum likelihood is a general and more reliable method of estimating parameters of a population by values that maximize the likelihood of a sample. The likelihood L of a sample of n observations $x_1, x_2, ..., x_n$ is the joint probability function $p(x_1, x_2, ..., x_n)$.

(d) Statistical hypothesis test analysis

The final stage of the statistical analysis included "hypothesis testing", or assessment of the "goodness-of-fit" of the chosen theoretical distributions with empirical data. Hypothesis testing is a method of inferential statistics, which is used to draw conclusions about a population and to measure the reliability of these conclusions using the information obtained from a random sample. The first step of the hypothesis testing is to specify the null hypothesis, H_0, which represents the hypothesis we wish to test. There is also an alternative hypothesis such that we would decide in favour of one or the other, which is commonly denoted as H_1. In this study, the null hypothesis, H_0, states that there is a correlation between the selected theoretical distribution and empirical forced response data. If we reject H_0, then this leads to the acceptance of H_1. Having established the null and the alternative hypothesis, the so-called "test statistic" is calculated based on the sample data, which provides the information on the null hypothesis that is used in a decision-making process: if the value of the test statistic is consistent with the null hypothesis, then the null hypothesis is accepted. There are two types of errors that can occur in testing of a statistical hypothesis: (i) a "Type I error", which arises when we reject the H_0 when it is genuinely true, and (ii) a "Type II error", if we fail to detect that H_0 is actually false. The maximum probability of making a Type I error that will be tolerated is denoted by α and is frequently called the "significance level" of the test or the criterion used for rejecting the null hypothesis. The significance level is employed as follows. The difference between results of the theoretical distribution and empirical data is determined. Then, assuming the null hypothesis to be true, the probability of difference is computed, which is subsequently compared to the significance level. If the probability is less than or equal to the significance level, then the null hypothesis is rejected and the outcome is said to be "statistically significant". Traditionally, the significance levels used are

0.01, 0.05 and 0.1; however, their choice is largely subjective, [127]. In general, the likelihood of committing the Type II error is inversely related to the likelihood of committing a Type I error. In other words, as the likelihood of committing one type of error decreases, the likelihood of committing the other type of error increases. Thus, with respect to the alternative hypothesis one employs, there is a higher likelihood of committing a Type II error when the significant level is 0.01 than when it is set equal to 0.05. Conversely, the larger the significance level, the higher the likelihood of committing a Type I error, [128].

There are many statistical hypothesis tests available, such as Chi-square or Pearson's, Kolmogorov-Smirnov, Cramer-von Mises, Anderson-Darling, to mention a few. Of all the goodness-of-fit tests, the oldest is the Chi-square test proposed by Pearson in 1900. The idea of the test is to divide the range of distribution into bins and to compare the observed number in each bin to the number that would be expected if the assumed distribution were true. A test statistic approximately follows a chi-square distribution with $(k-c)$ degree-of-freedom, where k is the number of non-empty bins and c is the number of estimated parameters for the distribution plus 1 (e.g. for a 3-parameter Weibull distribution, $c=4$) [125]. The hypothesis that the data are from a population with the specified distribution is rejected if the following relationship for the chi-square test holds:

$$\sum_{j=1}^{k}\frac{\left(n_j-np_j\right)^2}{np_j}\le {\chi_\alpha}^2\left(k-c\right) \tag{6-13}$$

where n_j is the empirical observed number in each bin, np_j is the theoretical observed number in each bin, $p_j=F_t\left(b_j\right)-F_t\left(a_j\right)$, $F_t\left(x\right)$ is the theoretical cumulative density function, a_j and b_j are the lower and upper bin limits, ${\chi_\alpha}^2\left(k-c\right)$ is the chi-square test statistic at a significance level α (obtained from Tables), j is the jth bin.

The major advantage of the Chi-square test is its versatility, as it can be applied to any distributional assumption without having the knowledge of values of the distribution parameters. On the other hand, the biggest drawbacks of this test are (i) the lack of sensitivity in detecting inadequate models when few observations are available, and (ii) the need to arrange the data into arbitrary bins, which could affect the outcome of the test.

Another powerful test employed to draw conclusions related to the association of the sample to the particular distribution is the Kolmogorov-Smirnov goodness-of-fit test. The test is based on the largest difference in absolute value between the empirical distribution function and its hypothesised counterpart:

$$D = \max_x \left| F_x(x) - \tilde{F}_x(x) \right| \tag{6-14}$$

where $F_x(x)$ is the theoretical cumulative distribution, $\tilde{F}_x(x)$ is the empirical distribution.

Using D, the certain $\lambda = D\sqrt{n}$ is evaluated, which is subsequently compared to the Kolmogorov-Smirnov test statistic, λ_α, obtained from tables: if $\lambda \le \lambda_\alpha$, then the null hypothesis can be accepted at a given significance level; if $\lambda > \lambda_\alpha$, the theoretical distribution hypothesised is rejected.

Attractive advantages of the Kolmogorov-Smirnov test include: (i) the fact that distribution of the test statistic does not depend on the underlying cumulative density function being tested, and (ii) the Kolmogorov-Smirnov is the exact test (while the Chi-square depends on an adequate sample size for the approximations to be valid). However, the limitations of this test are related to (i) its applicability to continuous distributions only, (ii) increased sensitivity near the centre of the distribution compared to its tails, and (iii) the parameters of the theoretical distribution tested must be fully specified, [128].

6.4.6.3 Statistical analysis of forced response results obtained for all blades over 1,000 bladed discs

The statistical results for forced response for all 26 blades over 1,000 bladed discs were obtained for all frequency mistuning ranges under three engine order excitations. Figs 6-17 to 6-19 demonstrate selected results for ±0.5, 15 and 40% frequency mistuning ranges representing small, moderate and large ranges respectively, which include: (a) the calculated empirical distribution functions for a sample size of 26,000; (b) the comparison between the empirical and the theoretical (hypothetical) probability density functions (PDFs); (c) the comparison between the empirical and the theoretical cumulative density functions (CDFs); and (d) the best-fit theoretical CDF and the greatest vertical distance between the two CDFs used in the Kolmogorov-Smirnov hypothesis test.

Fig. 6-17 displays the statistical results for forced response obtained for ±0.5% frequency mistuning range under 3, 6 and 13EO excitations. It can be seen that the forced response empirical distribution characteristics are dependent upon the engine order excitation, as shown also in Table 6-2. While the first two moments of the distributions are reasonably close in all three cases, the third and the fourth moments, the skewness and the kurtosis, describing the asymmetry and the peakedness properties, are dissimilar, accounting for the observable differences in the histogram shapes.

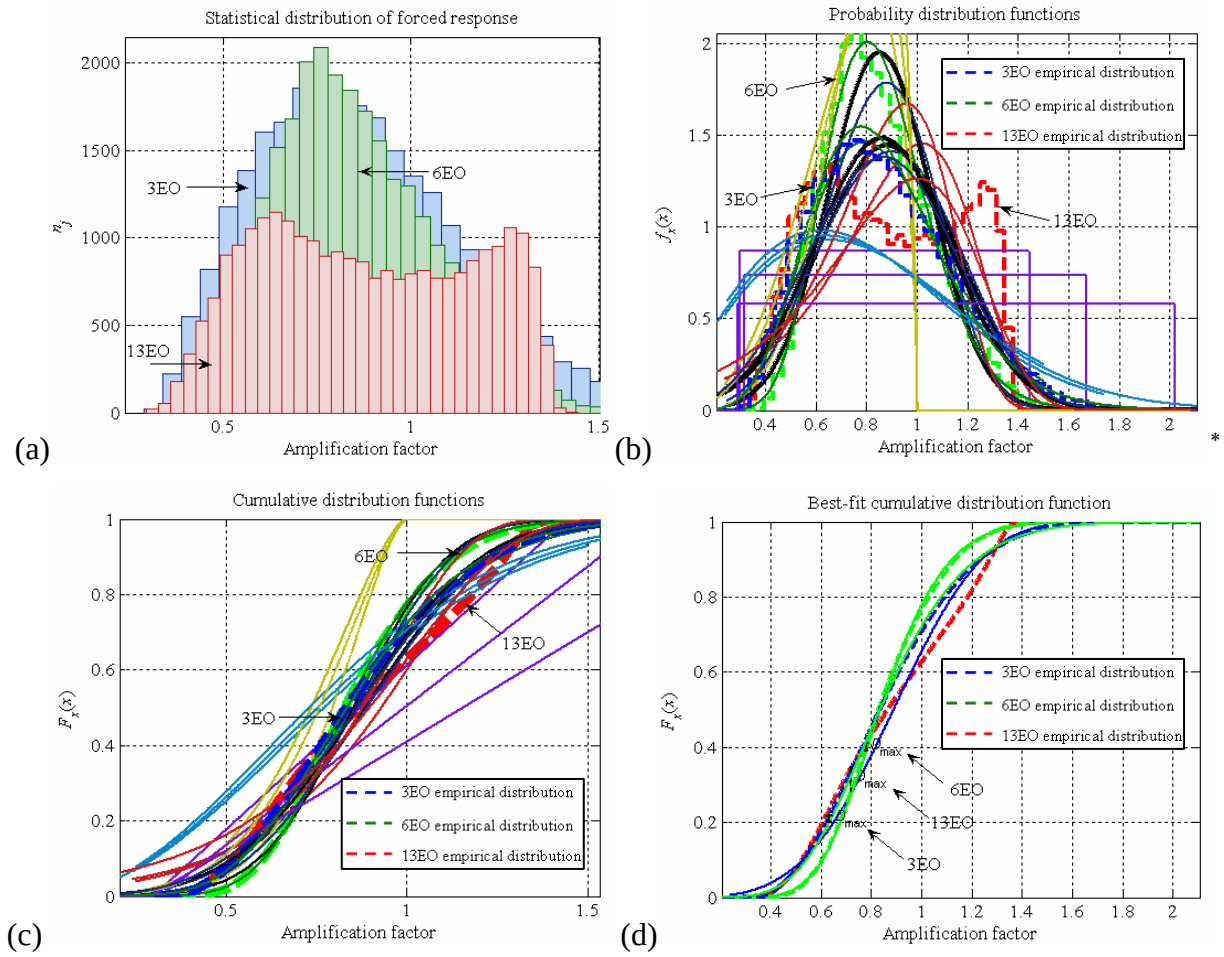

Fig. 6-17. Forced response statistical results for ±0.5% frequency mistuning range

	$x_{\min}$	$x_{\max}$	$\tilde{m}_x$	$\tilde{\sigma}_x$	$\tilde{D}_x$	$\tilde{a}_x$	$\tilde{e}_x$
3EO	0.29	2.02	0.86	0.27	0.07	0.50	-0.15
6EO	0.32	1.67	0.85	0.21	0.04	0.47	-0.14
13EO	0.30	1.45	0.88	0.28	0.08	0.07	-1.22

Table 6-2. Forced response empirical data characteristics for ±0.5% frequency mistuning range

* Different solid-line colours denote the theoretical hypothetical distribution functions

Subsequently, the theoretical closest fit distribution functions are different: the Gamma CDF is found to be the most suitable in representing the empirical data in the case of 3EO and 6EO, while the Weibull CDF is the best-fit theoretical approximation to the MC simulation (empirical) results for 13EO (for details refer to Table 6-5). It is noted here that the theoretical distribution parameters were obtained using the principle of maximum likelihood with 95% confidence intervals and were tested according to the Kolmogorov-Smirnov and the Chi-square hypothesis tests under a 0.01 (or 1%) significance level.

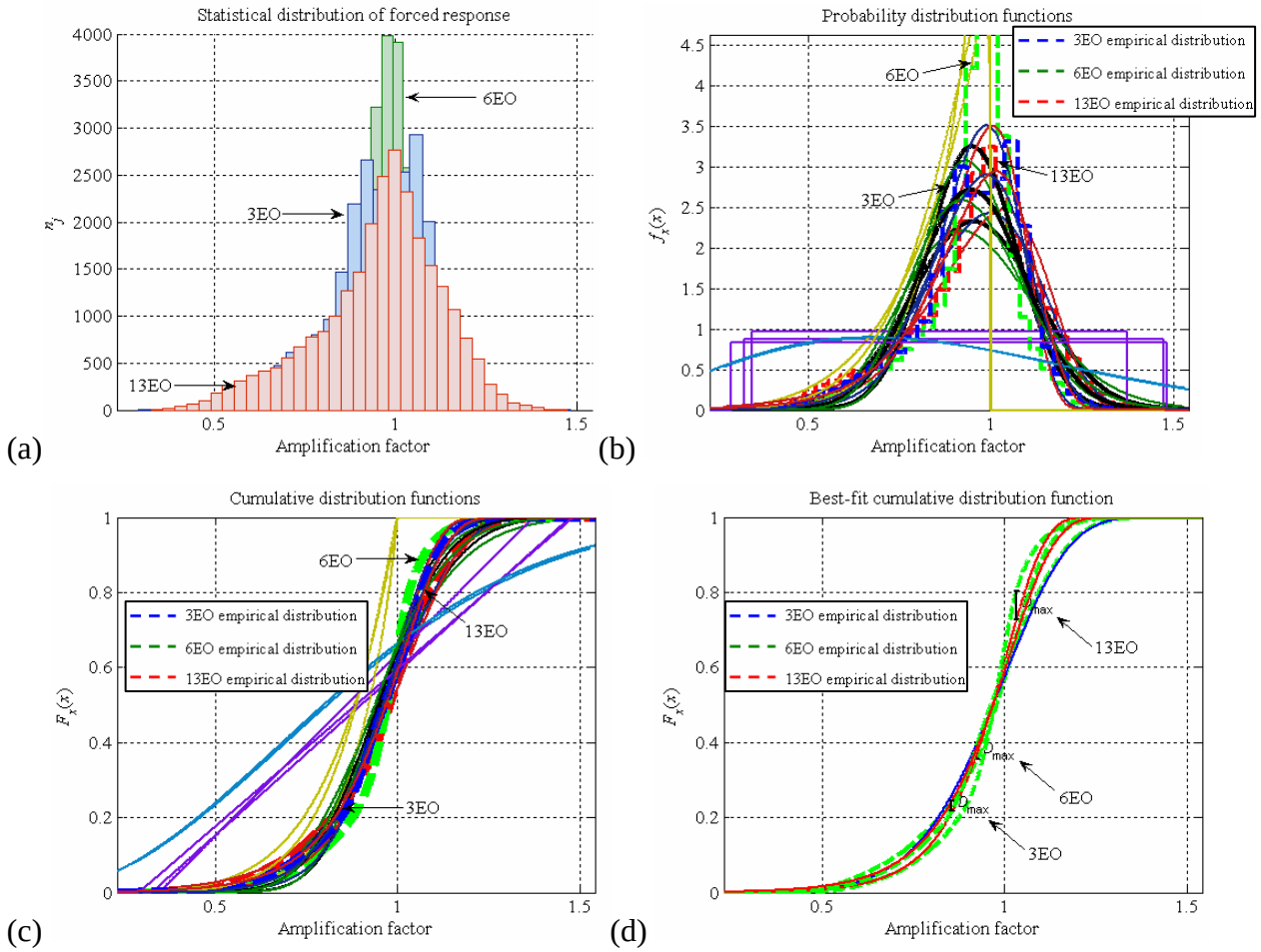

Fig. 6-18. Forced response statistical results for ±15% frequency mistuning range

The empirical distribution descriptive measures for ±15% frequency mistuning range are presented in Table 6-3 and Fig. 6-18.

	$x_{\min}$	$x_{\max}$	$\tilde{m}_x$	$\tilde{\sigma}_x$	$\tilde{D}_x$	$\tilde{a}_x$	$\tilde{e}_x$
3EO	0.29	1.48	0.95	0.15	0.02	-0.73	0.64
6EO	0.35	1.37	0.95	0.12	0.02	-0.99	1.73
13EO	0.33	1.47	0.96	0.17	0.03	-0.60	0.30

Table 6-3. Forced response empirical data characteristics for ±15% frequency mistuning range

As for the ±0.5% range, the skewness and the kurtosis of the distributions vary for different EOs for the ±15 frequency mistuning range. The best-fit CDF for 3EO and 6EO is the extreme value distribution, whereas that corresponding to 6EO is the Weibull distribution, as shown in Fig. 6-18(d).

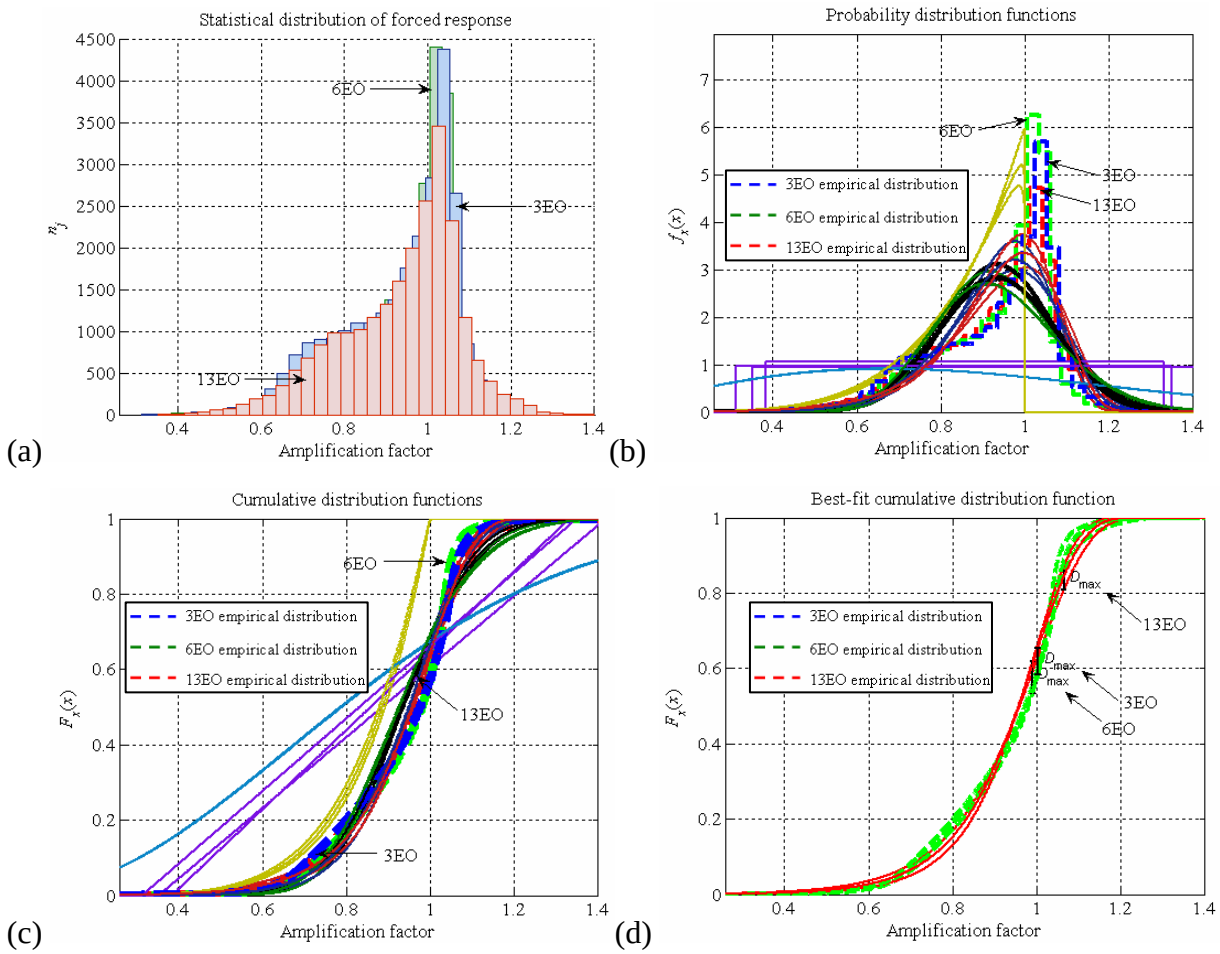

Fig. 6-19. Forced response statistical results for ±40% frequency mistuning range

Table 6-4 summarises the moments of the obtained distributions for ±40% frequency mistuning range.

	$x_{\min}$	$x_{\max}$	$\tilde{m}_x$	$\tilde{\sigma}_x$	$\tilde{D}_x$	$\tilde{a}_x$	$\tilde{e}_x$
3EO	0.31	1.35	0.93	0.14	0.02	-0.81	0.08
6EO	0.38	1.33	0.94	0.13	0.02	-0.94	0.45
13EO	0.35	1.42	0.94	0.14	0.02	-0.68	0.26

Table 6-4. Forced response empirical data characteristics for ±40% frequency mistuning range

From the Table 6-4, it can be seen that the third and fourth moments of the distributions are distinct, but to a lesser degree than for the ±0.5% and ±15% frequency mistuning ranges. As a consequence, the CDF that is the best-fit to all

empirical distributions is the extreme value distribution, as shown in Fig. 6-19 and Table 6-5.

Table in the Appendix A6-3 summarises the statistical hypothesis testing results obtained for all of the frequency mistuning ranges considered, while here only the selected results are shown in Table 6-5. The significance level for the Kolmogorov-Smirnov and the Chi-square tests adopted was 0.01, unless stated otherwise. As mentioned previously, the significance level indicates how likely a result is due to chance and comprises a fixed probability of wrongly rejecting the null hypothesis when it is in fact true. In this study, a 0.01 (or 1%) significance level means that there is a 99% chance that the selected theoretical distribution is a genuine statistical distribution of the response data, but also that there is a 1% chance that the difference between the theoretical and the empirical distributions is true.

Forced response results obtained for all blades over 1,000 bladed discs

Frequency mistuning range and EO	Goodness-of-fit test analysis, 26,000 samples				
	Best-fit distribution	Test statistic	Cutoff	Conclusion	Goodness-of-fit test
±0.5%, 3EO	Gamma	2.62	1.63	NA*	Kolmogorov-Smirnov
	"	399.00	53.40	NA	Chi-square
±0.5%, 6EO	Gamma	3.12	1.63	NA	Kolmogorov-Smirnov
	"	301.30	42.60	NA	Chi-square
±0.5%, 13EO	Weibull	10.90	1.63	NA	Kolmogorov-Smirnov
	"	6060.00	53.50	NA	Chi-square
±15.0%, 3EO	Extreme	4.37	1.63	NA	Kolmogorov-Smirnov
	"	1580.00	46.90	NA	Chi-square
±15.0%, 6EO	Extreme	12.50	1.63	NA	Kolmogorov-Smirnov
	"	5370.00	48.30	NA	Chi-square
±15.0%, 13EO	Weibull	6.97	1.63	NA	Kolmogorov-Smirnov
	"	1060.00	52.20	NA	Chi-square
±40.0%, 3EO	Extreme	11.40	1.63	NA	Kolmogorov-Smirnov
	"	4650.00	49.60	NA	Chi-square
±40.0%, 6EO	Extreme	13.80	1.63	NA	Kolmogorov-Smirnov
	"	5730.00	48.30	NA	Chi-square
±40.0%, 13EO	Extreme	7.94	1.63	NA	Kolmogorov-Smirnov
	"	2990.00	46.90	NA	Chi-square

Table 6-5. Statistical hypothesis tests results for forced response characteristics obtained for all blades over 1,000 bladed discs*

The results from the Table 6-5 suggest the closest theoretical CDFs fit to the empirical distributions. However, for all of the frequency mistuning ranges results considered, the indicated hypotheses were not accepted at the significance level adopted. This could signify that none of the tested theoretical distributions model the

* "NA" means that the null hypothesis is not accepted under a given significance level

empirical data accurately enough. On the other hand, the statistical studies indicate that there is an effect of the sample size on the result of a goodness-of-fit test: “if one employs a large enough sample size, almost any goodness-of-fit test will result in rejection of the null hypothesis”, [128]. In order to conclude on the basis of a goodness-of-fit test that data conforms to a specific distribution, the data should be reasonably close to the specifications of the distribution. Thus, in some cases, when a large sample size is involved, such as 26,000 forced responses considered here, the null hypothesis may be rejected. Yet in spite of the latter, if the sample data are reasonably close to the hypothesized distribution, one can operate on the assumption that the sample data provide an adequate fit for the hypothesised distribution. Table 6-6 demonstrates an effect of sample size on statistical hypothesis tests results, from which one can see that reduction of the sample size from 26,000 to 1,000 results in the acceptance (A) of the hypothesised theoretical distribution.

Forced response results obtained for all blades over 1,000 bladed discs

Frequency mistuning range and EO	Sample size	Goodness-of-fit test analysis				
		Best-fit distribution	Test statistic	Cutoff	Conclusion	Goodness-of-fit test
±0.5%, 3EO	26,000	Gamma	2.62	1.63	NA	Kolmogorov-Smirnov
	"	"	399.00	53.40	NA	Chi-square
±0.5%, 3EO	13,000	Gamma	1.89	1.63	NA	Kolmogorov-Smirnov
	"	"	215.60	49.58	NA	Chi-square
±0.5%, 3EO	6,500	Gamma	1.49	1.63	A	Kolmogorov-Smirnov
	"	"	136.70	46.96	NA	Chi-square
±0.5%, 3EO	1,000	Gamma	1.06	1.63	A	Kolmogorov-Smirnov
	"	"	46.10	36.20	NA	Chi-square
±0.5%, 6EO	26,000	Gamma	3.12	1.63	NA	Kolmogorov-Smirnov
		"	301.30	42.60	NA	Chi-square
±0.5%, 6EO	6,500	Gamma	1.84	1.63	NA	Kolmogorov-Smirnov
	"	"	93.70	46.90	NA	Chi-square
±0.5%, 6EO	1,000	Gamma	0.65	1.63	A	Kolmogorov-Smirnov
	"	"	26.90	37.60	A	Chi-square

Table 6-6. Effect of sample size on statistical hypothesis tests results

From the mistuning literature, it was found that the forced response data for all blades have been represented in the past using the Weibull or the extreme value distributions, which is in agreement with the results obtained in this study for the frequency mistuning ranges in the excess of ±5%. Studies reported in [68] and [129] employed the extreme value theory to compute the statistics of the resonant response, by modelling it as a Weibull distribution, and demonstrated that using such a distribution could provide savings in the computational cost of the MC simulations. Along a same line, [85] and [76] illustrated similar characteristics and benefits of the extreme value statistical model. The study in [96] showed that there

was no unique statistical distribution that could describe the forced response under every possible engine order excitation, which is in agreement with findings of this thesis.

Several conclusions were drawn from the statistical analysis of the forced response results for all blades:

(i) The forced response empirical distribution characteristics are dependent upon the engine order excitation for all frequency mistuning ranges: in particular, the third and the fourth moments of the distributions, the skewness and the kurtosis, describing the asymmetry and the peakedness properties, are dissimilar, accounting for the observable differences in the histogram shapes. As the frequency mistuning range increases, the PDFs of the resonant response become narrower and shift towards the lower values, which indicates benefits of the LM.

(ii) The hypothesis tests suggest that the best-fit theoretical CDFs are the Weibull and the extreme value distributions for the frequency mistuning ranges above ±5%, whereas the closest statistical models to describe the empirical data obtained for small frequency mistuning ranges are the Gamma or the Gaussian CDF, depending on the engine order excitation. Thus, it seems that the empirical distributions most significant changes occur around ±5% frequency mistuning range.

6.4.6.4 Statistical analysis of maximum forced response results

Similar statistical results are presented for the maximum forced response data obtained from each of 1,000 bladed discs simulated. Since the maximum forced response was extracted for each bladed disc, Figs. 6-20 to 6-22 show (a) the empirical distributions constructed from a sample size of 1,000 and (b) their best-fit CDFs for three different engine orders.

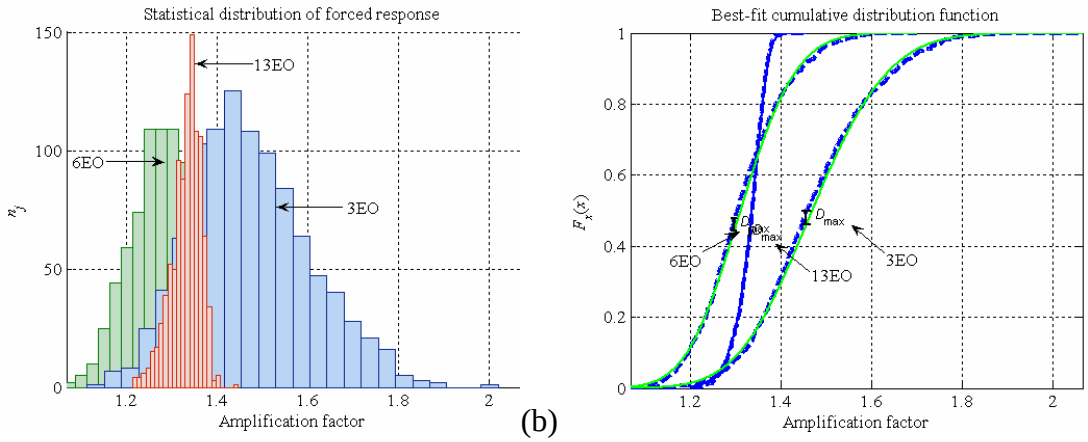

(a) (b)

Fig. 6-20. Maximum forced response statistical results for ±0.5% frequency mistuning range

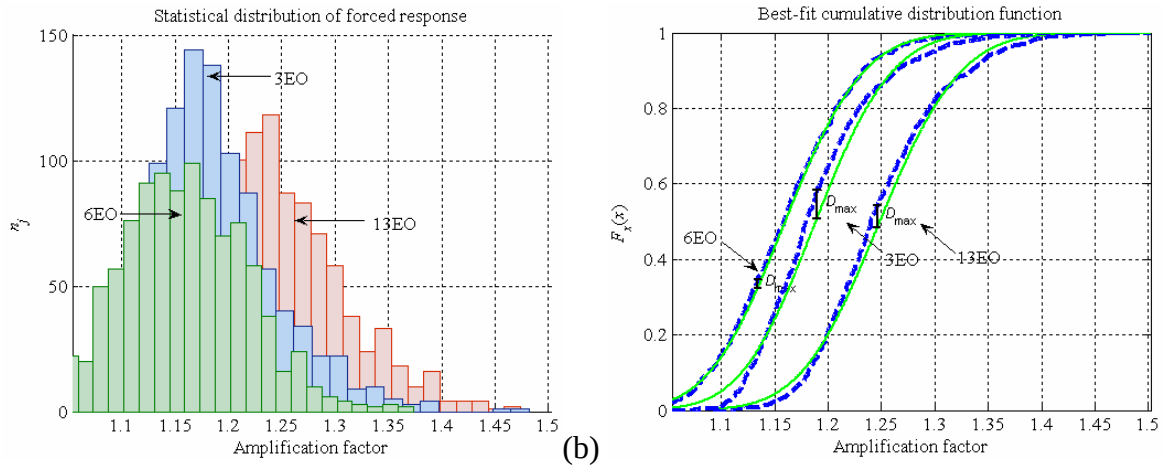

(a) (b)

Fig. 6-21. Maximum forced response statistical results for ±15% frequency mistuning range

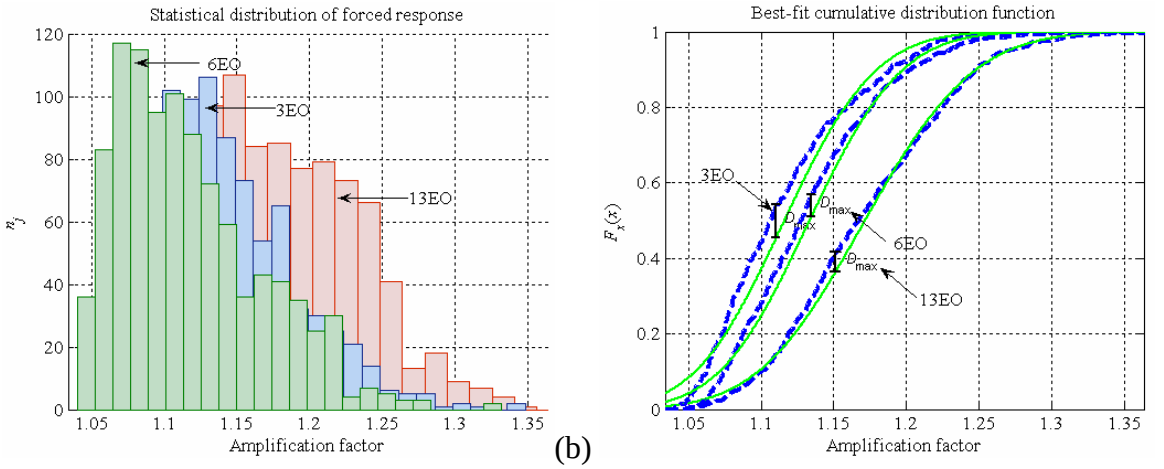

(a) (b)

Fig. 6-22. Maximum forced response statistical results for ±40% frequency mistuning range

Table 6-7 demonstrates selected results from the hypothesis tests applied to the above-mentioned empirical distributions of the maximum forced responses found on each bladed disc. Full statistical results for all frequency mistuning ranges can be found in Appendix A6-4.

For all frequency mistuning ranges considered, the theoretical distribution that provides the best match to the maximum forced response empirical data is the Gamma distribution.

Maximum forced response results obtained over 1,000 bladed discs

Frequency mistuning range and EO	Goodness-of-fit test analysis, 1,000 samples				
	Best-fit distribution	Test statistic	Cutoff	Conclusion	Goodness-of-fit test
±0.5%, 3EO	Gamma	1.16	1.63	A	Kolmogorov-Smirnov
	"	21.48	32.00	A	Chi-square
±0.5%, 6EO	Gamma	1.10	1.63	A	Kolmogorov-Smirnov
	"	29.33	34.81	A	Chi-square
±0.5%, 13EO	Gamma	0.67	1.63	A	Kolmogorov-Smirnov
	"	22.23	30.58	A	Chi-square
±15.0%, 3EO	Gamma	2.43	1.63	NA	Kolmogorov-Smirnov
	"	127.02	27.69	NA	Chi-square
±15.0%, 6EO	Gamma	0.76	1.63	A	Kolmogorov-Smirnov
	"	33.42	33.41	NA	Chi-square
±15.0%, 13EO	Gamma	1.88	1.63	NA	Kolmogorov-Smirnov
	"	72.77	33.41	NA	Chi-square
±40.0%, 3EO	Gamma	1.87	1.63	NA	Kolmogorov-Smirnov
	"	124.67	30.58	NA	Chi-square
±40.0%, 6EO	Gamma	2.72	1.63	NA	Kolmogorov-Smirnov
	"	183.70	29.14	NA	Chi-square
±40.0%, 13EO	Gamma	1.66	1.63	NA	Kolmogorov-Smirnov
	"	45.74	32.00	NA	Chi-square

Table 6-7. Statistical hypothesis tests results for maximum forced response characteristics obtained for each bladed disc

6.4.6.5 Statistical analysis of mean forced response results

The empirical distributions of the mean forced responses for selected representatives of small, moderate and large frequency mistuning ranges are depicted for 3, 6 and 13EO in Figs. 6-23 for a sample size of 1,000.

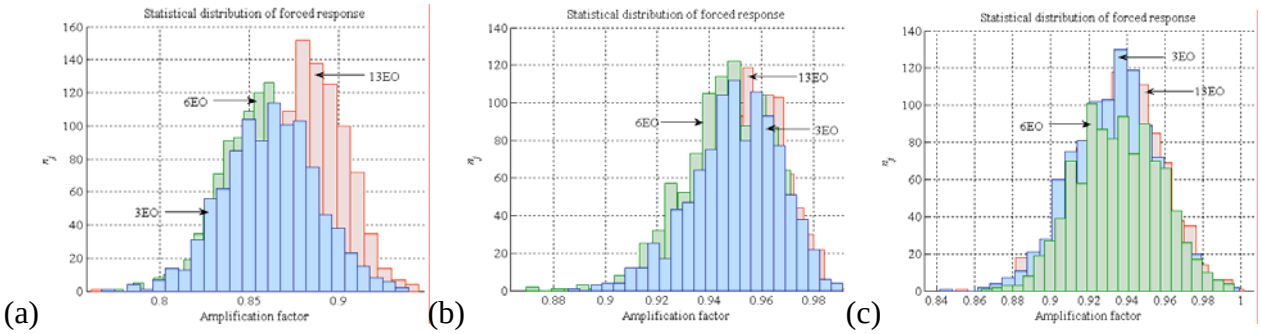

(a) (b) (c)

Fig. 6-23. Mean forced response empirical distributions for ±0.5% (a), ±15% (b) and ±40% (c) frequency mistuning range

The selected statistical results obtained for the mean forced responses under all three engine order excitations are shown in Table 6-8. Full statistical results for all frequency mistuning ranges can be found in Appendix A6-5. It can be noticed that for small frequency mistuning ranges, the empirical distribution of mean forced response depends highly on engine order excitation; for moderate ranges, the Beta

distribution models the mean forced response; and for large frequency mistuning ranges, the Gaussian distribution is in best agreement with the empirical results.

Mean forced response results obtained over 1,000 bladed discs

Frequency mistuning range and EO	Goodness-of-fit test analysis, 1,000 samples				
	Best-fit distribution	Test statistic	Cutoff	Conclusion	Goodness-of-fit test
±0.5%, 3EO	Gamma	0.62	1.63	A	Kolmogorov-Smirnov
	"	11.44	33.41	A	Chi-square
±0.5%, 6EO	Beta	0.85	1.63	A	Kolmogorov-Smirnov
	"	27.93	32.00	A	Chi-square
±0.5%, 13EO	Beta	0.64	1.63	A	Kolmogorov-Smirnov
	"	10.87	27.69	A	Chi-square
±15.0%, 3EO	Beta	0.87	1.63	A	Kolmogorov-Smirnov
	"	18.93	30.58	A	Chi-square
±15.0%, 6EO	Beta	1.04	1.63	A	Kolmogorov-Smirnov
	"	23.09	33.41	A	Chi-square
±15.0%, 13EO	Beta	0.86	1.63	A	Kolmogorov-Smirnov
	"	22.86	32.00	A	Chi-square
±40.0%, 3EO	Gaussian	1.02	1.63	A	Kolmogorov-Smirnov
	"	16.28	30.58	A	Chi-square
±40.0%, 6EO	Gaussian	0.87	1.63	A	Kolmogorov-Smirnov
	"	26.23	36.19	A	Chi-square
±40.0%, 13EO	Gaussian	0.98	1.63	A	Kolmogorov-Smirnov
	"	22.07	32.00	A	Chi-square

Table 6-8. Statistical hypothesis tests results for mean forced response characteristics obtained for each bladed disc

6.4.6.6 Statistical analysis of minimum forced response results

Finally, the minimum forced responses obtained for each bladed disc were analysed statistically. All the results for minimum forced response can be found in Appendix A6-6. Figs. 6-24 demonstrate the empirical distributions for ±0.5, 15 and 40% frequency mistuning ranges constructed from a sample size of 1,000.

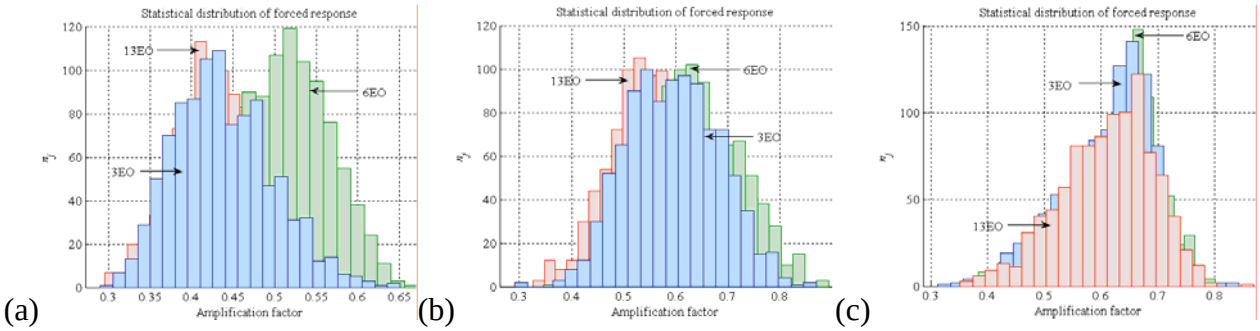

(a) (b) (c)

Fig. 6-24. Minimum forced response empirical distributions for ±0.5% (a), ±15% (b) and ±40% (c) frequency mistuning range

Table 6-9 summarises the statistical tests results for minimum forced response. The minimum forced response distribution type changes as the frequency mistuning

range is increased and is dependent upon the engine order considered. Hence, there is no single distribution that can express uniquely the minimum forced response for all cases studied.

Minimum forced response results obtained over 1,000 bladed discs

Frequency mistuning range and EO	Goodness-of-fit test analysis, 1,000 samples				
	Best-fit distribution	Test statistic	Cutoff	Conclusion	Goodness-of-fit test
±0.5%, 3EO	Gamma	0.89	1.63	A	Kolmogorov-Smirnov
	"	27.86	34.81	A	Chi-square
±0.5%, 6EO	Beta	0.57	1.63	A	Kolmogorov-Smirnov
	"	8.98	30.58	A	Chi-square
±0.5%, 13EO	Gamma	0.49	1.63	A	Kolmogorov-Smirnov
	"	18.45	33.41	A	Chi-square
±15.0%, 3EO	Gamma	0.88	1.63	A	Kolmogorov-Smirnov
	"	25.49	32.00	A	Chi-square
±15.0%, 6EO	Gaussian	0.84	1.63	A	Kolmogorov-Smirnov
	"	26.12	34.81	A	Chi-square
±15.0%, 13EO	Gamma	0.56	1.63	A	Kolmogorov-Smirnov
	"	21.04	34.81	A	Chi-square
±40.0%, 3EO	Extreme	0.99	1.63	A	Kolmogorov-Smirnov
	"	46.24	33.41	NA	Chi-square
±40.0%, 6EO	Extreme	1.19	1.63	A	Kolmogorov-Smirnov
	"	67.02	36.19	NA	Chi-square
±40.0%, 13EO	Weibull	0.53	1.63	A	Kolmogorov-Smirnov
	"	19.28	33.41	A	Chi-square

Table 6-9. Statistical hypothesis tests results for minimum forced response characteristics obtained for each bladed disc

6.4.7 Discussion of random or “scatter-controlling” large mistuning (LM) intentional mistuning strategy

The hypothetical LM random or “scatter-controlling” forced response reduction strategy was verified in the case of an industrial bladed fan disc. Although increasing the frequency mistuning range decreases the maximum forced response, the exact amount of this reduction varies depending on the engine order excitation considered. The largest forced response reduction obtained was approximately 33% (from 2.02 at ±0.5% frequency mistuning range to 1.35 at ±40% frequency mistuning range) for 3EO excitation. The forced response decreases for 6 and 13EO were 22% and 27%, respectively.

The forced response statistical hypothesis analysis based on the Kolmogorov-Smirnov and the Chi-square (Pearson’s) goodness-of-fit tests indicate that the closest theoretical distribution function fit to the empirical data obtained from a sample of 26,000 values are the Weibull and the extreme value distributions for the

frequency mistuning ranges higher than the ±5%, which is in consensus with the past mistuning literature studies; for smaller frequency mistuning ranges, the theoretical distributions (in particular, the Gamma, the Gaussian and the Weibull) that model the forced response are dependent on the specific engine order excitation. The theoretical distribution that provides the best match to the maximum forced response empirical results based on a sample of 1,000 bladed discs is the Gamma distribution, while that of the mean forced response could be modelled as the Beta distribution (for moderate frequency mistuning ranges) and the Gaussian (for large mistuning ranges). The empirical data of the minimum forced response conform to different theoretical distributions under distinct engine order excitations and frequency mistuning ranges and, thus, would be difficult to generalise.

The knowledge of accurate statistical distributions of the forced response is important, as it gives the probability that the maximum blade amplitudes will be less than a specified critical value, which also could be used to predict durability and reliability of bladed disc assemblies. The latter is out of scope of this thesis, where the emphasis is placed on rigorous statistical characterisation of the forced response distributions as a result of increasing the frequency mistuning range.

6.5 Deterministic or “pattern-controlling” large mistuning (LM) intentional mistuning strategy

6.5.1 Deterministic intentional mistuning patterns based on LM

The first part of this Chapter introduced the concept of LM and determined its effectiveness by controlling the mistuning scatter as a means of alleviating the severity of the maximum forced response. In this section, several deterministic intentional mistuning patterns based on LM, including alternate, harmonic and linear mistuning etc, are exploited and their sensitivity and robustness to small unavoidable random mistuning due to manufacturing tolerances and wear is assessed.

6.5.1.1 Alternate mistuning patterns

The simplest form of intentional mistuning from the practical viewpoint – alternate mistuning – is investigated initially using an industrial bladed fan disc introduced in 6.4.1. The alternate mistuning patterns incorporate combinations of mistuning degrees, such as 0.5% / -0.5%, 20% / -20% etc, shown in Figs. 6-25 and

Table 6-10 along with the estimated forced response amplification factors. Compared with the 'reference' random mistuning cases reported in 6.4.4, Table 6-1, it can be seen that introduction of regulated mistuning decreases appreciably the maximum amplification factors. Moreover, it can be observed that an increase in the intensity of mistuning decreases the maximum forced response levels by a small amount.

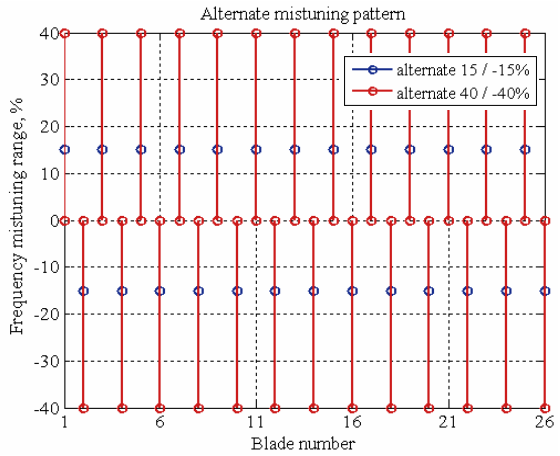

(a)

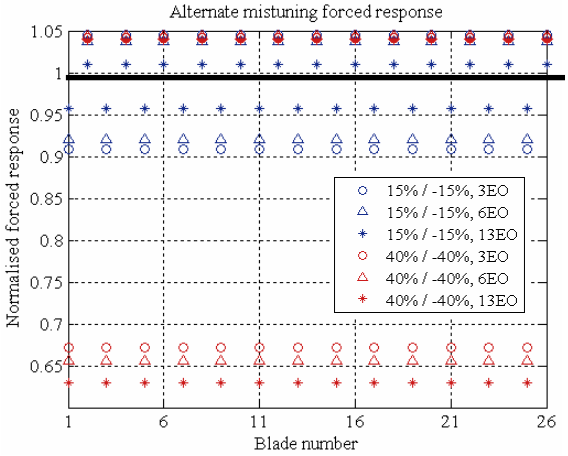

(b)

Fig. 6-25. Selected alternate mistuning patterns (a) and their forced responses (b)*

Alternate mistuning pattern	Normalised forced response			Alternate mistuning pattern	Normalised forced response		
	3EO	6EO	13EO		3EO	6EO	13EO
0.5% / -0.5%	1.204	1.042	1.179	**15% / -15%**	1.045	1.037	1.011
5% / -5%	1.054	1.015	1.068	**20% / -20%**	1.046	1.042	1.024
10% / -10%	1.039	1.020	1.013	**40% / -40%**	1.042	1.044	1.038

Table 6-10. Alternate mistuning forced response

6.5.1.2 Harmonic mistuning patterns

Several researchers in the past considered harmonically mistuned systems, claiming that such systems exhibited many of the same qualities as their randomly mistuned counterparts. Moreover, harmonic mistuning is significant as the periodicity of the bladed disc requires that any pattern of perturbations in system properties be decomposable into Fourier components [86].

Figs. 6-26 and 6-27 and Table 6-11 demonstrate the maximum attainable forced response levels for harmonics 1-4 based on LM. It can be seen that depending on the engine order excitation, an increase in frequency mistuning scatter range may result in either an increase or a decrease of the maximum forced response.

* A black horizontal line indicates a tuned system datum

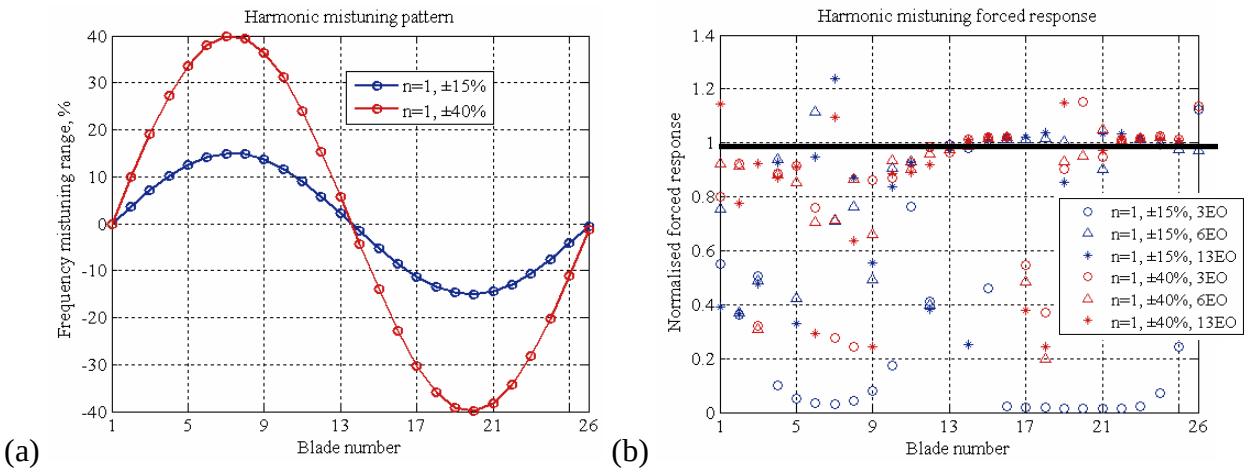

(a) (b)

Fig. 6-26. Selected harmonic n=1 mistuning patterns (a) and their forced responses (b)

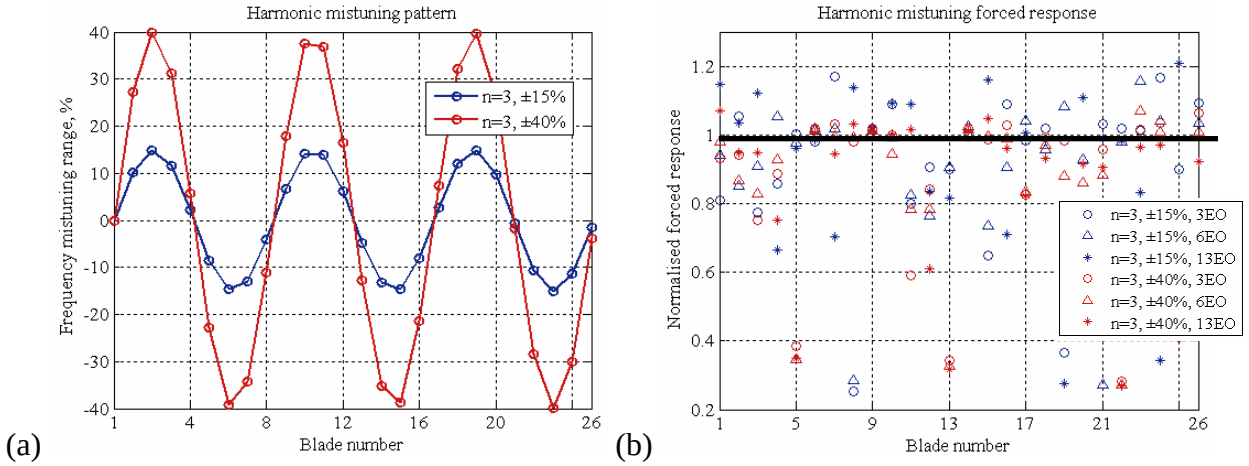

(a) (b)

Fig. 6-27. Selected harmonic n=3 mistuning patterns (a) and their forced responses (b)

Harmonic mistuning pattern	Normalised forced response			Harmonic mistuning pattern	Normalised forced response		
	3EO	6EO	13EO		3EO	6EO	13EO
n=1, ±0.5%	1.020	1.230	1.140	n=3, ±0.5%	1.220	1.298	1.343
n=1, ±5%	1.080	1.290	1.280	n=3, ±15%	1.170	1.160	1.210
n=1, ±15%	1.130	1.120	1.240	n=3, ±40%	1.070	1.070	1.070
n=1, ±20%	1.170	1.050	1.210	n=4, ±0.5%	1.108	1.269	1.350
n=1, ±40%	1.150	1.050	1.150	n=4, ±15%	1.158	1.120	1.185
n=2, ±0.5%	1.070	1.370	1.296	n=4, ±40%	1.120	1.130	1.100
n=2, ±15%	1.160	1.150	1.180				
n=2, ±40%	1.146	1.160	1.200				

Table 6-11. Harmonic mistuning forced response

6.5.1.3 Linear mistuning patterns

Following a trend introduced by [76], which aimed at reducing the maximum forced response below the tuned level, “linear” mistuning patterns, including linearly increasing frequency mistuning values, were investigated. Selected results are illustrated in Figs. 6-28 and Table 6-12, from which one can observe an

occasional small adverse influence of increasing the frequency mistuning range on maximum forced response levels for some engine order excitations.

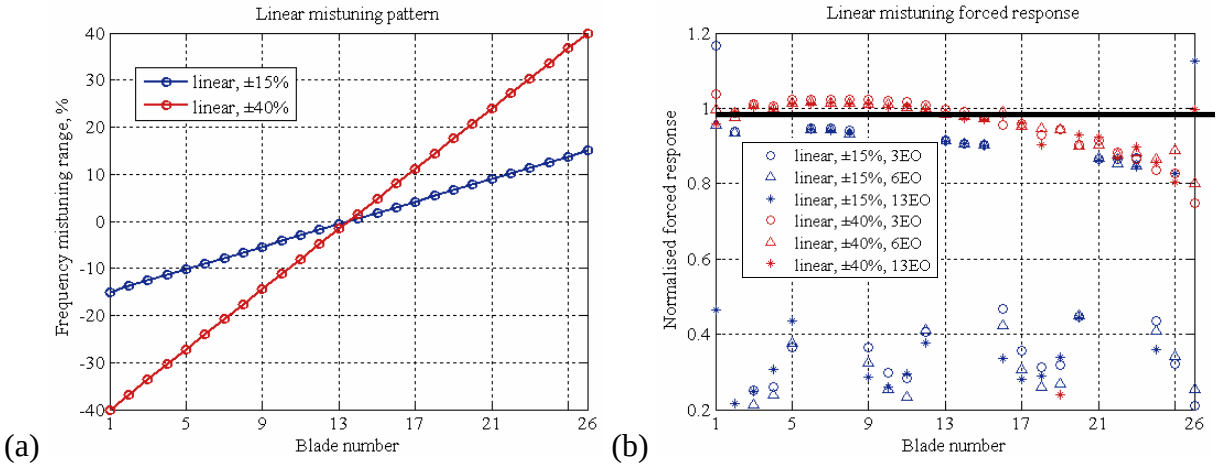

(a) (b)

Fig. 6-28. Selected linear mistuning patterns (a) and their forced responses (b)

Linear mistuning pattern	Normalised forced response			Linear mistuning pattern	Normalised forced response		
	3EO	6EO	13EO		3EO	6EO	13EO
±0.5%	1.250	1.110	1.210	**±20%**	1.130	0.990	0.980
±5%	0.920	0.980	1.180	±30%	1.080	1.010	1.000
±15%	1.170	0.960	1.130	**±40%**	1.040	1.020	1.010

Table 6-12. Linear mistuning forced response

6.5.1.4 Simulation of damaged blades in the assembly

In order to determine the influence of a few blades with LM, which will be subsequently referred to as the "damaged" blades, the forced response characteristics have been calculated for a chosen 'randomly' selected mistuned pattern from ±5% frequency mistuning range with 1, 2 or 3 damaged blades.

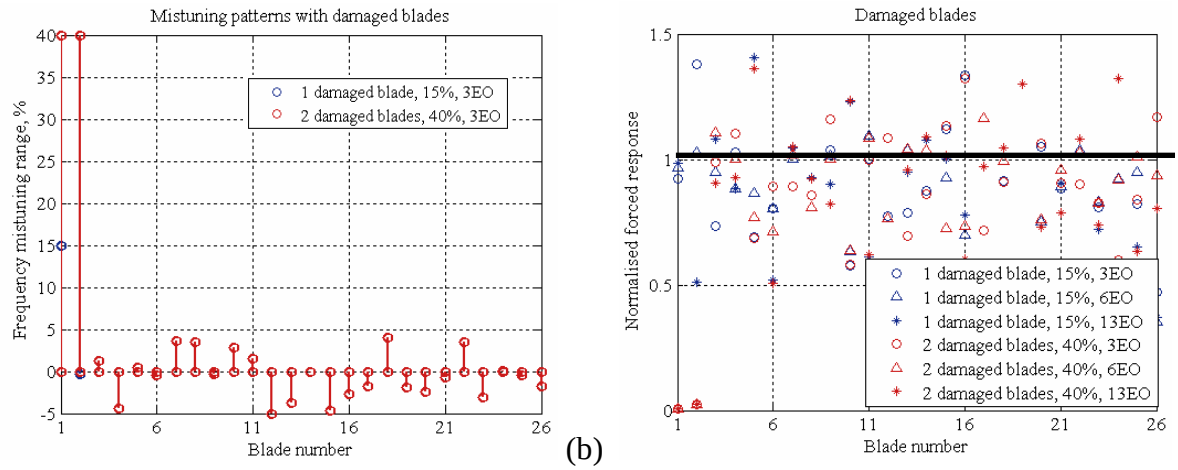

(a) (b)

Fig. 6-29. Selected mistuning patterns with damaged blades (a) and their forced responses (b)

Interestingly, the damaged blades do not themselves exhibit the largest forced response levels, as indicated in Fig. 6-29(b). Furthermore, increasing the mistuning degree of the damaged blades reduces marginally the forced response.

1, 2 and 3 "damaged" blades and others randomly mistuned by ±5%

Mixed mistuning pattern	Normalised forced response			Mixed mistuning pattern	Normalised forced response		
	3EO	6EO	13EO		3EO	6EO	13EO
1 damaged blade, 15%	1.380	1.090	1.410	**3 damaged blades, 15%**	1.330	1.150	1.320
1 damaged blade, 20%	1.380	1.090	1.410	**3 damaged blades, 20%**	1.326	1.165	1.313
1 damaged blade, 40%	1.363	1.164	1.405	**3 damaged blades, 40%**	1.326	1.165	1.311
2 damaged blades, 15%	1.330	1.100	1.360				
2 damaged blades, 20%	1.326	1.165	1.361				
2 damaged blades, 40%	1.326	1.165	1.361				

Table 6-13. Forced response of system with a few “damaged” blades

6.5.2 Sensitivity and robustness assessment

Deterministic analysis of the aforementioned systematically-regulated mistuning patterns provided an indication of their effectiveness as a forced response control strategy. Since the maximum amplitude magnification represents a local maximum in the forced response, it should therefore be sufficiently robust, so that the sensitivity of the system to additional random mistuning about this point should be small. Mistuning sensitivity is usually described as a dependence of forced response magnification of a bladed disc on the degree of mistuning or any other varied parameter. The sensitivity of bladed disc system, $\frac{\partial q}{\partial \alpha_j}$, with respect to the varied parameter can take the form of [77]:

$$\left(K + i\omega C - \omega^2 M\right)\frac{\partial q}{\partial \alpha_j} = \left(\frac{\partial K}{\partial \alpha_j} + i\omega\frac{\partial C}{\partial \alpha_j} - \omega^2\frac{\partial M}{\partial \alpha_j}\right)q, \quad j = 1,...N \tag{6-15}$$

which is obtained by differentiation of the fundamental equation of the forced bladed disc vibration, $\left(K + i\omega C - \omega^2 M\right)\{q\} = \{f\}$, with respect to the *j-th* varied parameter α_j.

As mentioned earlier, the blade amplitudes increase with mistuning strength up to a certain critical level, usually exhibiting a peak forced response at low degrees of mistuning, beyond which a further increase in mistuning causes the forced response to drop and flatten off. This implies that the bladed disc system is highly sensitive to mistuning around the tuned condition, and that increasing the mistuning

may result in a decrease in the sensitivity of forced response, which also justifies the choice of LM as a viable intentional mistuning strategy.

The robustness of the few selected intentionally mistuned patterns is investigated next by examining the variation in the forced response as an additional unintentional random mistuning of ±0.5% is incorporated, which could occur in practice as a result of manufacturing imperfections and/or wear in operation. A further 100 MC simulations were performed in which small random variations in frequency mistuning were projected onto the original intentionally mistuned system. The results for the main intentional mistuning patterns considered with (w) and without (w/o) random mistuning are given in Table 6-14.

Sensitivity and robustness assessment of selected intentional mistuning patterns obtained from 100 random MC simulations of unintentional mistuning from ±0.5% frequency mistuning range									
Mistuning pattern type	Normalised forced response								
	3EO			6EO			13EO		
	w random	w/o random	% diff	w random	w/o random	% diff	w random	w/o random	% diff
Alternate 0.5% / -0.5%	1.938	1.204	60.96%	1.441	1.042	38.29%	1.607	1.179	36.30%
Alternate 2.5% / -2.5%	1.570	1.080	45.37%	1.400	1.01	38.61%	1.820	1.130	61.06%
Alternate 5% / -5%	1.566	1.054	48.58%	1.451	1.015	42.96%	1.781	1.068	66.76%
Alternate 10% / -10%	1.530	1.039	47.26%	1.430	1.02	40.20%	1.860	1.010	84.16%
Alternate 15% / -15%	1.566	1.045	49.77%	1.466	1.037	41.36%	1.866	1.011	84.61%
Alternate 20% / -20%	1.532	1.046	46.47%	1.481	1.042	42.17%	1.932	1.024	88.68%
Alternate 40% / -40%	1.637	1.042	57.10%	1.594	1.044	52.68%	1.996	1.038	92.29%
Harmonic n=1, ±0.5%	1.436	1.020	40.78%	1.531	1.23	24.44%	1.367	1.140	19.91%
Harmonic n=1, ±5%	1.390	1.080	28.70%	1.540	1.29	19.38%	1.370	1.280	7.03%
Harmonic n=1, ±15%	1.221	1.080	13.06%	1.232	1.29	4.50%	1.373	1.280	7.27%
Harmonic n=1, ±20%	1.180	1.170	0.85%	1.230	1.05	17.14%	1.390	1.210	14.88%
Harmonic n=1, ±40%	1.215	1.150	5.65%	1.151	1.05	9.62%	1.218	1.150	5.91%
Linear, ±0.5%	1.725	1.250	38.02%	1.488	1.15	29.39%	1.390	1.210	14.88%
Linear, ±5%	1.390	0.920	51.09%	1.290	0.98	31.63%	1.380	1.180	16.95%
Linear, ±15%	1.221	1.170	4.39%	1.019	0.96	6.17%	1.156	1.130	2.26%
Linear, ±20%	1.150	1.130	1.77%	1.070	0.99	8.08%	1.225	0.980	25.00%
Linear, ±40%	1.083	1.040	4.09%	1.042	1.02	2.20%	1.075	1.010	6.46%
Best pattern, ±0.5%, 3eo	1.783	1.112	60.35%	-	-	-	-	-	-
Worst pattern, ±0.5%, 3eo	1.950	2.020	3.47%	-	-	-	-	-	-
Best pattern, ±15%, 6eo	-	-	-	1.230	1.031	19.30%	-	-	-
Worst pattern, ±15%, 6eo	-	-	-	1.380	1.373	0.51%	-	-	-
Best pattern, ±40%, 6eo	-	-	-	1.143	1.040	9.91%	-	-	-
Worst pattern, ±40%, 6eo	-	-	-	1.371	1.332	2.93%	-	-	-
1 damaged blade, 15%	1.513	1.380	9.64%	1.249	1.090	14.59%	1.469	1.410	4.16%
1 damaged blade, 40%	1.505	1.363	10.42%	1.248	1.164	7.23%	1.469	1.405	4.56%
3 damaged blades, 15%	1.546	1.330	16.24%	1.242	1.150	8.00%	1.456	1.320	10.30%
3 damaged blades, 40%	1.546	1.326	16.59%	1.242	1.165	6.61%	1.456	1.313	10.89%

Table 6-14. Sensitivity and robustness assessment of selected intentional mistuning patterns to ±0.5% additional unintentional mistuning

In the case of alternate mistuning, for 3EO excitation, it can be seen that there is an advantage from increasing the mistuning of high frequency blades, as the maximum forced response obtained from 100 MC simulations is reduced from 1.94

to 1.53. However, for other considered EOs, the LM has an insignificant (6EO) or an adverse effect (13EO), as shown in Figs. 6-30. It can also be seen that the alternate mistuning strategy is not robust for most of the analysed combinations. In particular, for small mistuning patterns, the average difference between the original and the perturbed maximum forced response levels ranges from approximately 36 to 61% depending on the excitation, whereas for the LM patterns, the corresponding difference oscillates between 46 to 92%. Based on the evidence presented for all mistuning ranges considered, it can be concluded that alternate mistuning may not be a robust strategy for maximum forced response control.

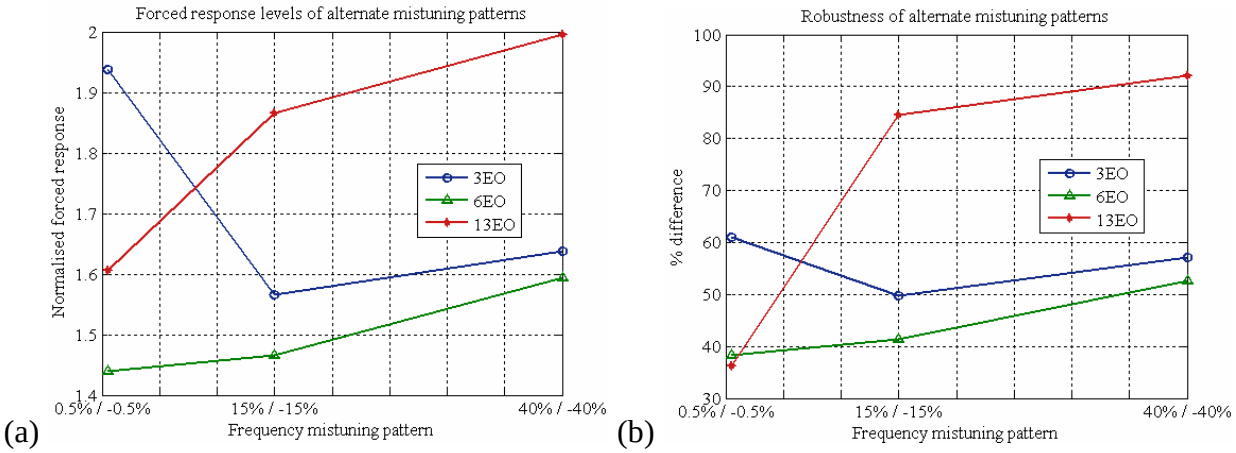

Fig. 6-30. Forced response levels (a) and robustness (b) of the alternate mistuning patterns

For harmonic mistuning patterns, the increase of the mistuning scatter range improves significantly (i.e. reduces) both the maximum forced response levels and their sensitivity to additional mistuning variations, as illustrated in Figs. 6-31. As the mistuning range is amplified, the latter is improved 3-7 times depending on the excitation. Overall, the LM is beneficial for most of the calculated harmonic mistuning cases in mitigating the damaging effects of random mistuning.

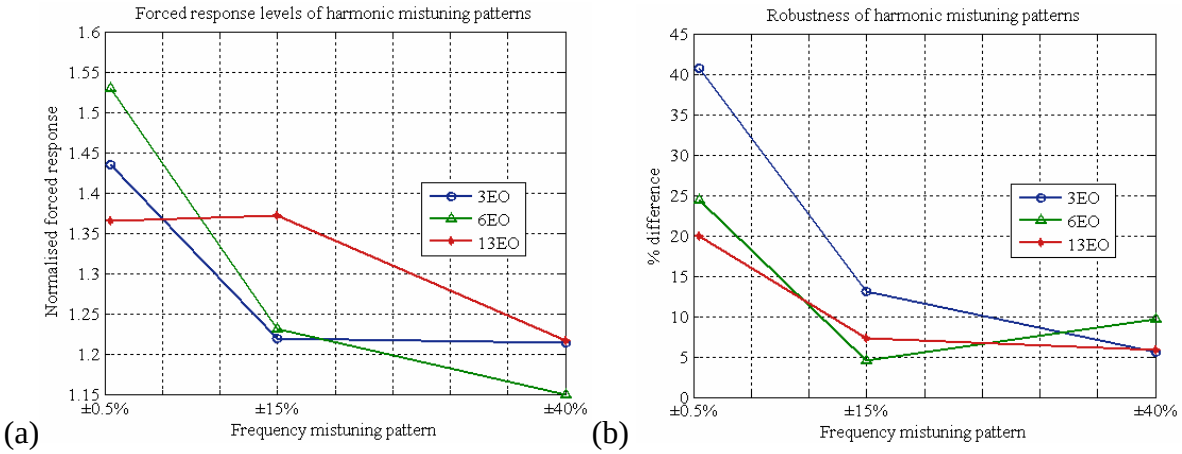

Fig. 6-31. Forced response levels (a) and robustness (b) of the harmonic mistuning patterns

A maximum forced response reduction of 60% from 1.73 to 1.08 and a tenfold robustness improvement are achieved for linear mistuning patterns by increasing the frequency mistuning range from ±0.5% to ±40% for 3EO excitation. Figs. 6-32 demonstrate a corresponding drop in the maximum forced response for 6 and 13EO cases of approx. 43% and 30%, respectively. It is also observed that the difference between the original and the perturbed maximum forced response levels is of the order of 2-8%, whereas a significantly poorer robustness is achieved at lower frequency mistuning ranges, for example, 51% increase after 100 perturbations for ±5% range for 3EO case.

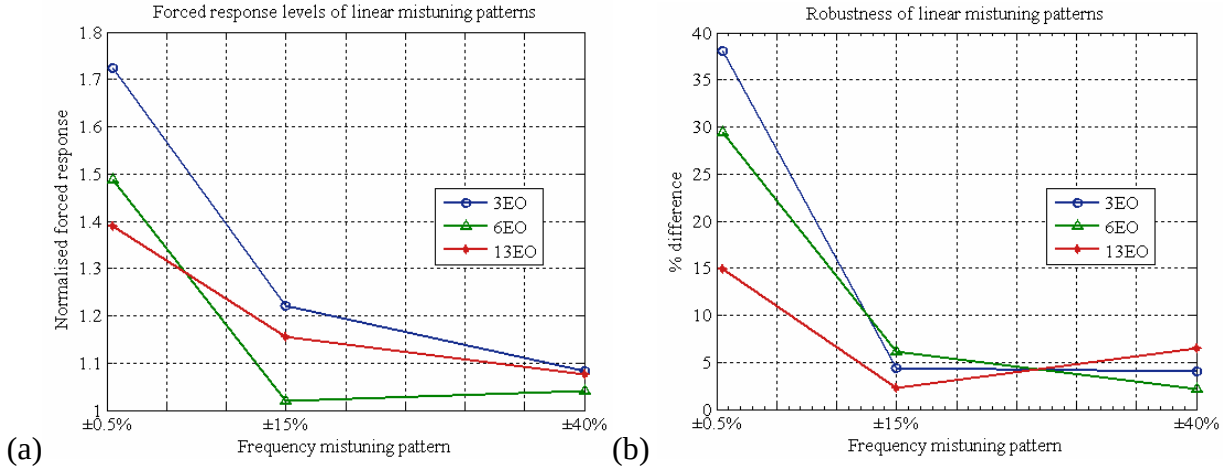

Fig. 6-32. Forced response levels (a) and robustness (b) of the linear mistuning patterns

The sensitivity of the response to additional unintentional mistuning is next assessed for the best and worst mistuning patterns obtained from the study reported in the first part of this Chapter. While a minor change (3-9%) of the maximum forced response levels after 100 random perturbations is obtained for the worst patterns from all considered frequency mistuning ranges, the increase of the latter results in a notably improved robustness of the best mistuning patterns. These results also show the beneficial effects of the LM on maximum forced response levels.

Finally, the sensitivity of the bladed disc assemblies with a few largely mistuned, or ‘damaged’ blades, is determined. The effect of increasing the number of damaged blades from 1 to 3 does not seem to introduce any significant changes in the maximum forced response. However, the mistuning pattern with 1 damaged blade is marginally more robust to small additional mistuning variations of ±0.5%.

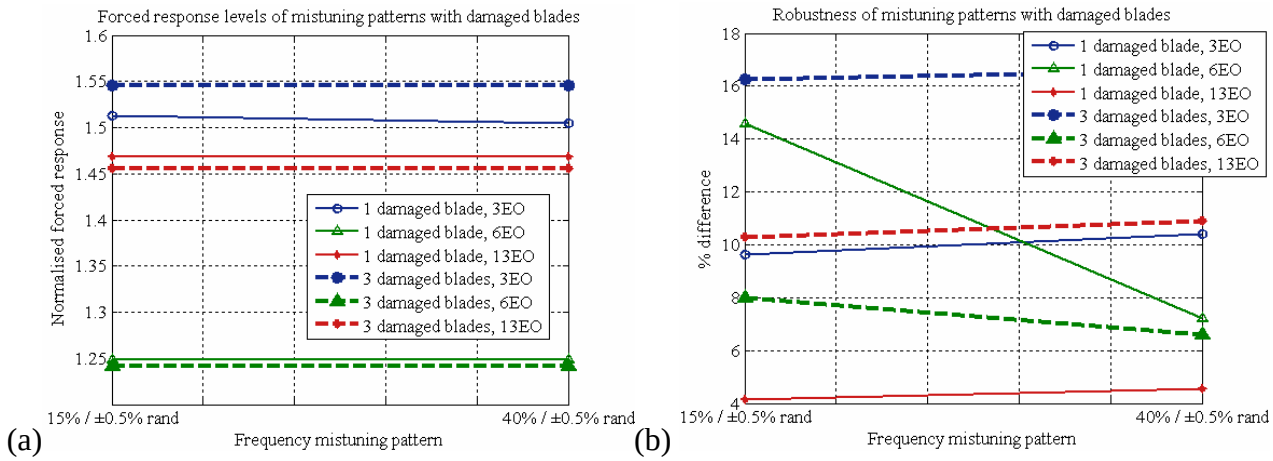

Fig. 6-33. Forced response levels (a) and robustness (b) of the mistuning patterns with damaged blades

In an attempt to find further ways of potential maximum forced response drop and to assess its robustness to random blade positions misplacing, the effects of 100 randomly selected blade rearrangements (or permutations) were tested for (i) the best and worst mistuning patterns and (ii) the combinations of randomly mistuned patterns with damaged blades. From Table 6-15, it can be seen that blade rearrangements lead to a further increase in the maximum forced response levels and a corresponding decrease in the robustness, which is, as for the case of random perturbations in Table 6-14, more severe for the best found mistuning patterns. The maximum forced responses for both worst and best patterns drawn from the LM ranges are more robust to random rearrangements than those corresponding to small mistuning range. As for the random blade rearrangements of the randomly selected mistuning patterns with damaged blades, the change of the maximum forced response levels and robustness depends on the particular engine order excitation analysed.

Effect of 100 random blade rearrangements (permutations) of selected intentional mistuning patterns									
Mistuning pattern type	Normalised forced response								
	3EO			6EO			13EO		
	permuted	original	% diff	permuted	original	% diff	permuted	original	% diff
Best pattern, ±0.5%, 3eo	1.919	1.110	72.87%	-	-	-	-	-	-
Worst pattern, ±0.5%, 3eo	1.751	2.020	13.31%	-	-	-	-	-	-
Best pattern, ±15%, 6eo	-	-	-	1.331	1.031	29.13%	-	-	-
Worst pattern, ±15%, 6eo	-	-	-	1.388	1.373	1.09%	-	-	-
Best pattern, ±40%, 6eo	-	-	-	1.237	1.040	18.95%	-	-	-
Worst pattern, ±40%, 6eo	-	-	-	1.346	1.332	1.05%	-	-	-
1 damaged blade, 15%	1.446	1.380	4.78%	1.520	1.090	39.45%	1.552	1.410	10.07%
1 damaged blade, 40%	1.446	1.363	6.09%	1.522	1.164	30.76%	1.552	1.405	10.46%
3 damaged blades, 15%	1.375	1.330	3.38%	1.378	1.150	19.83%	1.552	1.320	17.58%
3 damaged blades, 40%	1.377	1.326	3.85%	1.371	1.165	17.68%	1.551	1.311	18.31%

Table 6-15. Effect of random blade rearrangements (permutations) of selected intentional mistuning patterns

6.5.3 Discussion of deterministic or “pattern-controlling” large mistuning (LM) intentional mistuning strategy

The sensitivity and robustness of the maximum forced response of selected deterministic LM intentional mistuning patterns to additional unintentional random mistuning, inevitable in practice due to manufacturing imperfections and wear, was investigated in this part of the Chapter. Fundamentally, a high sensitivity of nearly-tuned bladed discs was demonstrated, followed by a relative insensitivity to additional random mistuning after reaching peak forced response levels, all of which indicates prospective benefits from introducing large frequency mistuning. It was shown that it is possible to reduce the maximum forced response levels significantly and to improve the robustness similarly by using the LM concept for some of the considered cases. In particular, linear mistuning patterns based on LM exhibited a significant robustness advantage over other mistuning patterns, in addition to a substantial forced response reduction, which, in combination with the desirable insensitivity, provides predictability and controllability of the maximum forced response. An attempt was made to assess the ‘damage tolerance’ of the bladed disc forced response with a few damaged blades included, and found that the precise extent of the damaged blade frequency deviation has no major influence on the maximum forced response levels or its sensitivity. Furthermore, it was determined that mistuning patterns resulting from blade rearrangements produce more robust forced response characteristics in the case of LM ranges than their smaller mistuning counterparts.

The maximum forced response levels achieved using some examples of the “pattern-controlling” approach are lower than those corresponding to the “scatter-controlling” strategy, although the latter is believed to be more practical. As for the deterministic patterns, there are certain ways to accomplish their wider applicability in practice: examples include use of so-called “pseudo-harmonic” or “pseudo-linear” mistuning, which could include less blade types required to reach the desirable forced response characteristics. These practically-oriented intentional mistuning patterns have been incorporated in the past [68], and might be the most effective maximum forced response control means.

6.5.4 Sensitivity versus statistics

In this Chapter, two commonly-employed tools for uncertainty assessment, (i) statistical analysis and (ii) sensitivity and robustness, have been used. Both methods are appropriate for quantification and control of the blade mistuning problem, and here an attempt is made to clarify their respective functions. From the definition of the mistuning problem, it is known that the uncertainty of the forced response levels (or the 'output') stems from the variability of the blade geometry, material etc characteristics (or the 'input'), as illustrated in a schematic diagram in Fig. 6-34. However, a commonly-encountered large spread of the output is caused predominantly by an insufficient robustness of the design, which has no connection to the stochastic small spread of the input. Thus, a feasible way to resolve the mistuning problem is to control the structural sensitivity of the bladed disc design and to make it robust to additional small mistuning inevitable in practice, which will ensure sufficiently small spread of the output. Fundamentally, the sensitivity analysis contributes to the understanding of the extent to which the input factors affect the forced response of a particular design, consequently providing some guidelines of how to improve the model in order to make it more robust. Statistics' role, on the other hand, is to assess the severity and distribution of the forced response of the bladed disc with an ultimate aim to predict its reliability. Therefore, both of the mentioned uncertainty assessment tools are necessary for a complete analysis of the consequences of the blade mistuning problem.

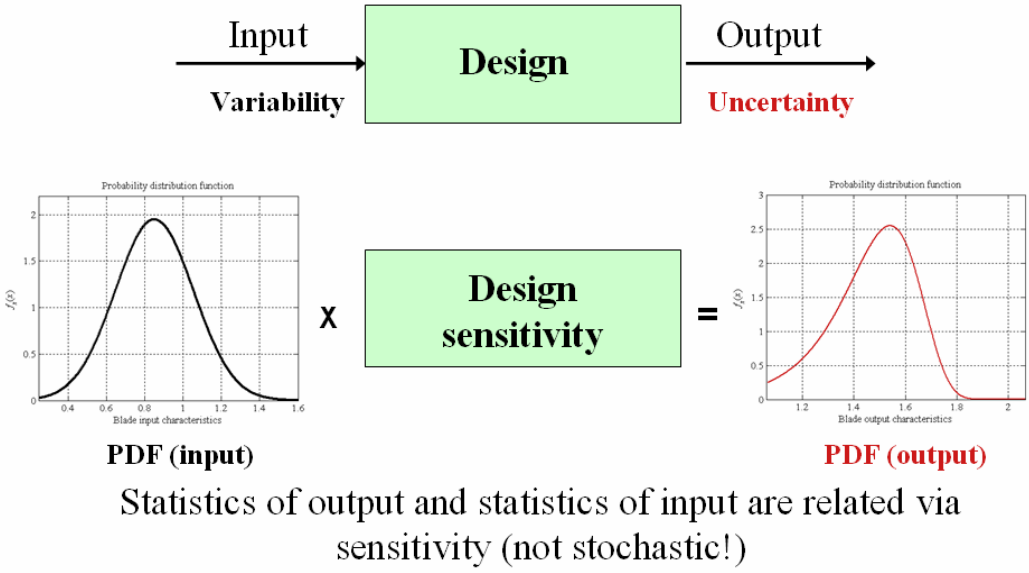

Fig. 6-34. Relation between the statistics of the input and the statistics of the output in relation to blade mistuning problem

6.6 General discussion

The results obtained in this study provide some indications of the effectiveness of a new concept of large mistuning (LM) as a means of maximum forced response reduction and control. Examples are presented which demonstrate that both of the proposed approaches based on LM, the "scatter-controlling" and "pattern-controlling" strategies, result in a substantial improvement of the sensitivity and robustness of the forced response. Nevertheless, the accumulated results could be valid only for the specific bladed disc considered, namely, the industrial fan, and hence, it may be difficult to generalise the results partially, or in whole. Additionally, the focus was put on the first family of modes and three specific engine order excitations, whereas for higher order modes, where frequency veerings between the mode families may occur, and for different engine orders, the effect of increasing the frequency mistuning range may be different. Important, also, could be the interaction of the largely mistuned blades vibrating in one mode and the bladed disc vibrating in another family of modes due to large frequency deviations from the blade-alone natural frequency. Moreover, the effects of damping have not been studied, which may also contribute to the more encouraging conclusions in favour of the LM as a successful intentional mistuning strategy. Furthermore, damping may also have an influence on the sensitivity of the studied mistuning patterns to additional unintentional mistuning.

There is a scope for further work which will establish the trends governing the physics of the studied phenomena of LM and its impact on various designs of bladed discs. Besides, this research work left a handful of general practical questions that could be addressed by carrying out a systematic parametric analysis, which could involve the design of simple bladed disc models in order to capture the underlying characteristics and to contribute to the physical explanations of the reasons behind the commonly-experienced facts and issues surrounding the mistuning problem, such as:

- Why does the forced response of the industrial fan reaches its maximum value at the ±0.5-1.5% frequency mistuning range, whereas for some other bladed discs, the maximum amplification factor is achieved at much higher frequency mistuning ranges?

- Why is the maximum amplification factor for the industrial fan approximately 2, while some other mistuning studies have reported the amplification factors exceeding 4?
- How are the maximum forced response and sensitivity predictions related to the parameter variation, such as the numbers of blades, amount of coupling, rotation speed etc?

Although the mistuning literature provides some evidence of the maximum forced response dependence upon the above-mentioned parameters, there is, nonetheless, scope for future clarifications and improvements in this direction.

It is anticipated that the expansion of the LM and general physics of the maximum forced response study as indicated above will provide reliable characteristics of the LM influence upon the vibration behaviour of a wide range of bladed discs.

6.7 Summary

In this Chapter, novel maximum forced response reduction strategies based on LM have been introduced using an industrial bladed fan disc. Focussing on the statistical analysis, the random or “scatter-controlling” approach has been assessed to reveal the advantages of relaxing the manufacturing tolerances and of extending the typical design acceptance limits. Subsequently, the deterministic or “pattern-controlling” intentional mistuning method demonstrated a substantial maximum forced response reduction and significant improvement in the sensitivity and robustness to the additional unintentional random mistuning by introducing unconventionally large mistuning degrees for bladed discs.

The results from this study show promise in implementing the LM concept into the design of bladed discs as a means of avoiding large forced response levels caused by random mistuning and of ensuring the predictability of the response.

CHAPTER 7

Blade Mistuning Problem Overview: From Lessons Learned To Future Developments, Trends And Philosophy

7.1 Overview

In this Chapter, an attempt is made to present an overview of the blade mistuning problem by discussing the accumulated knowledge from the cases studied in this thesis and the commonly observed facts. The possibilities to generalize from specific examples are considered with an aim to produce a contemporary “mistuning problem map”, from which a range of important factors shaping the patterns of maximum forced response amplification and their mutual interaction are indicated and feasible forced response reduction strategies are discussed. Finally, some thoughts are dedicated to the anticipation of future developments, trends and philosophy of the mistuned bladed disc vibration problems.

7.2 Insights into the blade mistuning problem from lessons learned

7.2.1 A need to improve the fundamental physical model used in the analysis

7.2.1.1 Inclusion of new effects into mistuned system analysis

As discussed in the Chapter 2, recent years have witnessed an increased effort towards development of elaborate FE models for analysis of full-scale industrial bladed discs. Nevertheless, persistent discrepancies in the predictions and measured data continue to stimulate researchers to seek possible physical causes and effects responsible for the observed mismatches. In this thesis, one such effect has been identified in Coriolis forces, which in some cases were shown to have a non-trivial influence on bladed disc dynamics and vibration. More importantly, that example illuminated a few important issues. Firstly, it was found that the inclusion of a previously-neglected effect has a qualitative influence on tuned bladed disc properties, which fundamentally changes formerly established views. Secondly, analysis showed that there is a mutual interaction between the Coriolis forces and blade mistuning, which in combination determine the forced response characteristics. Thirdly, it should be noted that influence of Coriolis forces is particularly significant for specific cases of strong tangential-radial coupling. The evidence and basic principles provided in this study indicate different aspects in which a newly incorporated effect into the analysis could be important, namely, (i) its individual impact on vibration properties, (ii) a combination with a well-established effect and (iii) specific cases for which the considered effect may be of consequence.

7.2.1.2 Physical mistuning characterisation

Another issue that has been raised only recently in Chen [130] 2002 and Feiner et al. [51] 2003 relates to the characterisation of mistuning used in bladed disc analyses. In the past, the most commonly used is blade frequency mistuning, which is not itself a source of mistuning, but a consequence of different mass, stiffness, stagger angle etc combinations. A work reported in Chen [130] 2002 examines the variation of forced response as a result of application of different mistuning elements while matching the natural frequencies of first few mode families to the experimental data. It was found that (i) an inadequate choice of

mistuning elements type and location and the match of natural frequencies of only one mode family of interest could cause a poor correlation of the forced responses, whereas (ii) the match of natural frequencies of several mode families could provide a more accurate forced response prediction within a wide range of frequencies. The appropriate mistuning representation and modelling could be particularly important in the studies of experimental validation of mistuning predictions for realistic practical systems.

7.2.1.3 Regard of the factors of secondary interest

It is a usual practice in bladed disc analyses to make simplifying assumptions about factors of secondary interest when regarding a particular issue. In the study of mutual influence of Coriolis forces and blade mistuning, the conclusions about the maximum forced response amplification were made without a rigorous treatment of damping. In those studies, the damping loss factor was assumed to be 0.003 (or 0.3%), which is within a typical range of 0.1% to 2% for practical bladed discs. In order to observe the influence of damping on maximum forced response levels, the statistical characterisation of forced response was repeated for different damping loss factors.

Influence of proportional damping on the maximum forced response of bladed discs with Coriolis forces and blade mistuning included

Case	Maximum* forced response									
	Damping = 0.1%		Damping = 0.3%		Damping = 1%		Damping = 2%		Damping = 5%	
	with C**	without C	with C	without C	with C	without C	with C	without C	with C	without C
2EO, ±5% freq. mist., γ=0.062†	2.230	1.610	2.460	1.760	2.514	1.847	2.528	1.889	2.420	1.840
2EO, ±5% freq. mist., γ=0.005‡	1.960	1.780	1.810	1.690	1.780	1.673	1.758	1.647	1.700	1.617
5EO, ±5% freq. mist., γ=0.062†	1.755	1.570	1.580	1.460	1.455	1.430	1.380	1.480	1.380	1.365
5EO, ±5% freq. mist., γ=0.005‡	1.500	1.525	1.450	1.440	1.514	1.526	1.604	1.614	1.502	1.507

* Maximum forced responses were obtained from 500 randomly simulated bladed disc configurations
** C denotes "Coriolis"
† indicates strong coupling case
‡ indicates weak coupling case

Table 7-1. Influence of proportional damping on the maximum forced response of bladed discs with Coriolis forces and blade mistuning included

From Table 7-1 and Fig. 7-1, it can be seen that difference between the maximum forced responses calculated with or without Coriolis forces is between ±1 to 40%, depending on the damping loss factor assumed. This further demonstrates the sensitivity of maximum forced response levels on a range of intertwining factors and a need for their careful consideration in attempts to assess accurately the blades' critical amplitudes and their HCF lives.

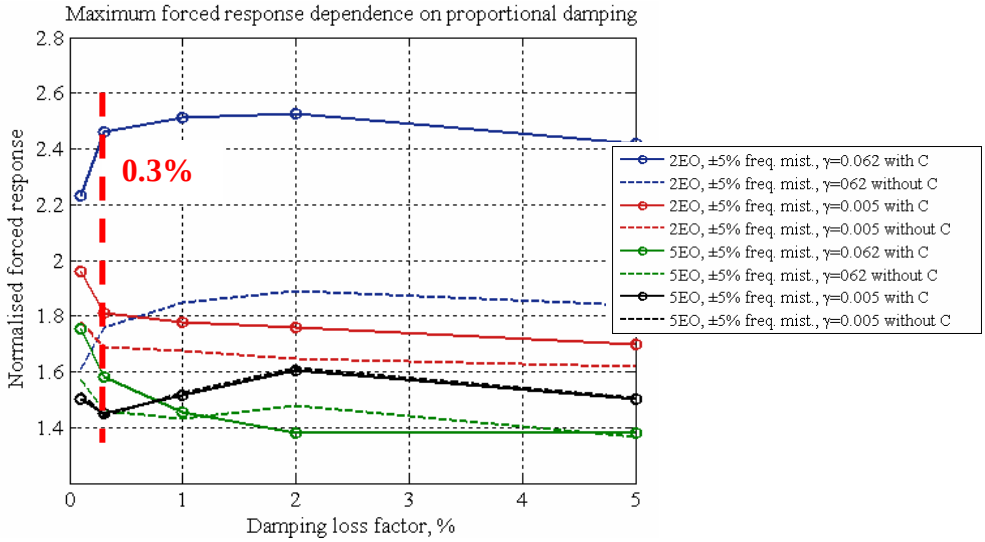

Fig. 7-1. Influence of proportional damping on the maximum forced response of bladed discs with Coriolis forces and blade mistuning included

7.2.2 Benefits of experimental validation

Results gained by extensive observation and experiment have always been powerful tools for validating, modifying and improving existing scientific theories, as well as developing new concepts. The experimental validation study of the effects of Coriolis forces has served as a convincing proof of the significance of influence of these forces on nominally-tuned bladed disc properties and prompted a further study of mutual effects of Coriolis forces and blade mistuning on forced response characteristics. In addition to that, due to the highly flexible nature of the testpiece, a 'convex' shape of the natural frequency split plot has been observed, which is a consequence of simultaneous action of Coriolis and centrifugal forces.

Furthermore, detailed experimental studies could provide explanations for many of the conflicting results published in the mistuning literature and, as a consequence, contribute to a broader view of the blade mistuning problem.

7.2.3 Sensitivity and robustness – a necessary tool for uncertainty assessment

It has been argued in Chapter 6 of this thesis that robust solutions in the presence of random mistuning are sought as a means of providing reliable forced response characteristics. Studies of sensitivity are of great interest due to the

complex nature of the blade mistuning problem with a large number of factors influencing the forced response amplification factors. Sensitivity analysis is also essential in guiding the implementation of design changes necessary for maximum forced response reduction and uncertainty control.

7.3 Development of strategies for maximum forced response control

The design of a bladed disc (the number of blades, amount of coupling …) plays a central role when devising a strategy for maximum mistuned forced response reduction and control. Depending on a design, an intentional mistuning or any other viable strategy is chosen and its sensitivity and robustness is assessed to small random mistuning.

7.4 Mistuning problem map

Fig. 7-2 represents a so-called map of the blade mistuning problem, where some of the most influential factors affecting the maximum forced response amplification of a mistuned bladed disc are indicated. What follows in this brief section is the author's interpretation of conclusions drawn in this thesis and numerous mistuning investigations with regard to the blade mistuning problem.

The most obvious factor responsible for the forced response amplification is mistuning, usually characterised by the degree and arrangement of specific blade properties, which, in combination, affect the maximum magnitude of the forced response. Mistuning is the primary cause of two well established physical mechanisms: natural frequency splitting of double modes and mode localisation or mode distortion. Since the two modes of each mode pair do not occur at the same frequency, they are unable to combine into a pure travelling wave response and thus to superimpose in a manner that can either increase or decrease the forced response amplitudes, depending on the modes interacting and the exact amount of frequency splitting, Ewins [6] 1969. In addition to mistuning, the number of blades has been observed as another factor influencing the critical forced response levels, Whitehead [5] 1966. As the number of blades increases (keeping all other factors constant), a higher number of vibration modes get closer to each other and, subsequently, more energy is transmitted to the worst responding blade.

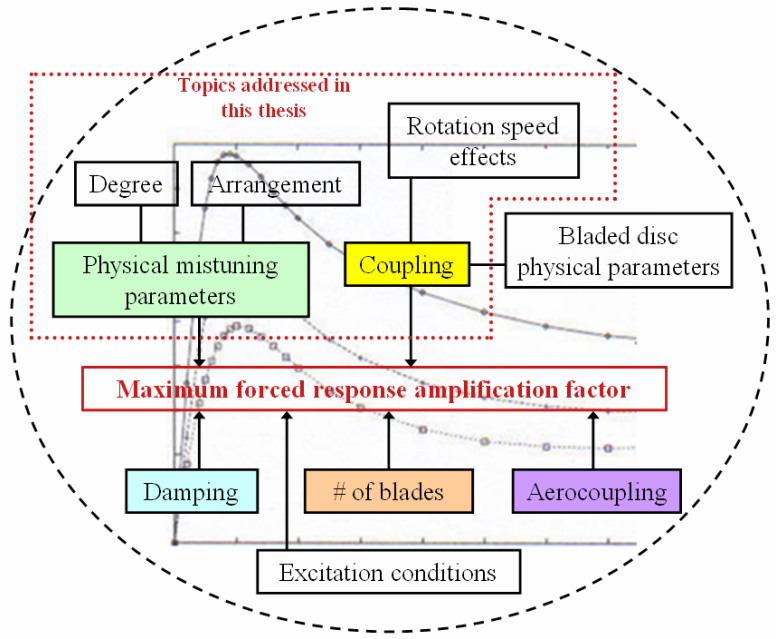

Fig. 7-2. Mistuning problem map

Furthermore, a few studies have shown that the specific location of the peak forced response depends on a ratio of mistuning to coupling strength, rather than the mistuning degree only (Myhre et al. [85] 2003, Rivas-Guerra et al. [65] 2001). The effect of coupling, or the degree of interaction between the blades provided by the disc, can be explained in terms of an energy augmentation mechanism: in order to obtain large amplification levels, the interblade coupling must be weak enough to yield localised modes, but also sufficiently strong so that the blade around which vibrations are being localised can receive energy from adjacent blades. For strongly coupled bladed discs, a larger mistuning strength is required to maintain the same mistuning to coupling ratio, which results in a shift in the peak location of the maximum forced response. Conversely, for weakly coupled bladed discs, as for fan analysed in the Chapter 6, the maximum forced response level was achieved at lower mistuning degrees.

The magnitude and location of the maximum forced response are also affected by rotation effects (Coriolis and centrifugal forces), excitation order, damping and aerocoupling.

The main conclusion from the above is that mistuning can no longer be considered as a sole concern, but rather investigated in combination with other relevant factors in an attempt to provide reliable forced response estimation.

7.5 Where might we go next?

It is difficult to predict how the research on mistuned bladed discs is going to evolve. However, there is a sentiment that more efforts could be directed towards practically-oriented studies, strongly correlated with experimental investigations. Fig. 2-4 in Chapter 2 indicated a few of the possible scenarios addressing practical aspects of mistuned bladed disc vibration. Of particular interest is the provision of guidelines for effective bladed disc measurements and data interpretation and interpolation. Powerful mathematical tools used in treatment of the incomplete data problem could be employed to supply vital information to engine industry practitioners on an every day basis.

Fundamentally, excessive vibration levels confined to few blades of the assembly are undesirable, and will further challenge researchers to seek for new ways of preventing them. While most of studies to date made attempts to resolve the forward mistuning problem, still few efforts exist that have the capability of addressing the inverse problem. In addition to being able to deduce blade mistuning which would ensure acceptable forced response levels, studies could provide means of guaranteeing the acceptable probability of failure as well.

In an attempt to determine bladed disc life and probability of failure, more efficient statistical methods could be developed. In author's opinion, further innovative studies, such as that by Sinha [95] 2005, which used neural networks to establish a correlation between the crucial features of a design and the statistical distribution of forced response, would be beneficial.

Based largely on the research trends of the past few years, the following issues were predominantly on the agenda and will require some further investigation and development: (i) friction damping and prediction of nonlinear vibrations of mistuned bladed discs (Petrov and Ewins [131] 2005, [132] 2006, Koh and Griffin [133] 2006), (ii) the assessment of mistuning sensitivity (Myhre et al. [85] 2003, Baik et al. [89] 2005), and (iii) the inclusion of aerocoupling into mistuned bladed disc analyses (Kielb et al. [46] 2004 and Sladojevic et al. [47] 2005).

Finally, it is important to note that mistuning is a multidisciplinary problem, and its successful "prevention rather than cure" may involve a combination of structural dynamics, rotordynamics and aerodynamics principles.

7.6 Summary

An overview of the blade mistuning problem has been presented in this Chapter, and fundamental factors that affect the maximum forced response amplification have been identified to create a “mistuning problem map”. The insights into the blade mistuning phenomenon from the lessons learned in specific examples in this thesis and historically established facts have been discussed to lead to anticipation of prospective future trends and developments in the field.

CHAPTER 8

Conclusions

"The known is finite, the unknown infinite; intellectually we stand on an islet in the midst of an illimitable ocean of inexplicability. Our business in every generation is to claim a little more land"

Thomas H. Huxley

8.1 Summary and conclusions of the research

It is often the case with research that as many questions are raised as are answered, and the studies described in this thesis are no exception. Nevertheless, in the concluding chapter, it is intended to assess the merit and progress made in this work, which has attempted to gain new insights into the blade mistuning problem. A summary of the research, and the conclusions drawn from it, with regard to the objectives stated in Chapter 1, are presented below.

8.1.1 Identification of "critical outstanding mistuning questions"

The existence of a tremendous amount of literature on blade mistuning, but still the lack of a reliable and straightforward "answer" to the problem, raised doubts concerning the direction of contemporary research efforts. This led to the first

milestone of the thesis – to establish the extent to which the mistuning still remains a problem, resulting in the philosophical debate-style literature review in Chapter 2, which has provided an impetus for new ideas as to how to prevent the blade mistuning problems rather than cure their consequences. Questions have been postulated which seek to address the outstanding mistuning issues that would contribute to a better correlation between theoretical and practical concerns. Provision of solutions to all of these high-level questions was beyond the scope of this thesis, which has concentrated on two main themes: (i) the improvement of the fundamental physical model used in the analysis by including a previously-neglected effect, the Coriolis forces, and assessing its influence on vibration characteristics of mistuned bladed discs, and (ii) the development of practically-oriented strategies for maximum forced response reduction and control based on a new large intentional mistuning concept.

8.1.2 Importance of Coriolis forces in bladed disc analyses

8.1.2.1 Coriolis forces influence on tuned bladed discs and practical implications

For the first time, the effects of Coriolis forces have been included despite their traditional omission in bladed disc analysis, in an effort to represent more realistically and accurately the fundamental physics of the bladed disc model. Contrary to a widely-held belief, it has been found that the Coriolis forces introduce both qualitative and quantitative changes in dynamic properties of tuned bladed discs. When analysed in the absence of Coriolis forces, perfectly-tuned cyclically-symmetric bladed discs are characterized by double modes with identical natural frequencies for each number of nodal diameters. When Coriolis forces are taken into account, these pairs of double modes split into single modes with the natural frequencies of each corresponding to a forward or backward travelling wave for each nodal diameter number. The asymmetry of the velocity-dependent matrix due to the presence of Coriolis forces invokes “right” and “left” eigenvectors, both of which are complex, thus introducing qualitative changes in the mode shapes. Examples have been shown where the order of magnitude of predicted natural frequency splits due to the effects of Coriolis forces can be quite large (0.5% - 9%) for some of the modes with lower numbers of nodal diameters, which are likely to

be in the operating region as contemporary aircraft designs lean towards much faster and lighter engines, meaning higher rotating speeds and increased flexibility. The consequence of large splits is to shift resonance positions on the Campbell diagram for a tuned bladed disc, thereby introducing significant effects on an important design feature, as indicated in Fig. 3-9. Thus, it is compelling, but certainly not rigorous, to hypothesize that the conspicuous absence of Coriolis forces from bladed disc analysis may be a responsible factor for recurring inconsistencies between theoretical predictions and experimental data, and may provide an explanation for some surprising and unexpected occasional failures of bladed discs due to unpredicted resonance conditions, reported for lower nodal diameter modes. Furthermore, it has been established that the order of magnitude of the Coriolis-induced natural frequency splits of the tuned bladed disc can be of the same order as the splits present in typically-mistuned systems, which is believed to have implications on their forced response levels.

8.1.2.2 Experimental validation of the influence of Coriolis forces on tuned bladed discs

The influence of Coriolis forces on a tuned bladed disc has been successfully demonstrated in a process of experimental validation using a carefully-designed testpiece. In order to produce sufficiently clear evidence of Coriolis forces, which are generated when there is simultaneous bladed disc rotation and significant radial and tangential components in blade vibratory displacements, a ‘swept’ testpiece has been designed with blades that lean in the axial direction by 15degrees. This has provided large enough radial components of displacement to allow unambiguous observation of Coriolis forces. A measurement technique using the SLDV and an excitation system comprising an AC magnet have been employed to facilitate the measurements of both the backward and forward travelling waves for mode shapes with predominantly lower numbers of nodal diameters: namely, the 2ND and 3ND modes. Several important conclusions have been drawn. For the 2ND mode pair, being split at rest by 0.36% due to inherent mistuning of the testpiece, the largest measured natural frequency split obtained under rotating conditions was 1.78%, which is unlikely to be due to mistuning, and suggests that Coriolis-splitting is a genuine phenomenon. For the 3ND mode pair, which was unaffected by the inherent mistuning of the testpiece, the corresponding maximum measured split under

rotation was 1.81% (compared with 0% at rest), which also supports the above claim. The predictions and measured data agreed well up to a certain rotation speed, beyond which the predicted natural frequency splits continued to increase almost linearly, whereas the experimentally acquired splits demonstrated a decrease in split magnitudes. The latter was explained by the influence of static deflections resulting from the centrifugal forces induced, which are significant due to the extremely flexible nature of the testpiece. The effect of centrifugal forces was to change the geometry, namely, to reduce the blade sweep angle of the testpiece, and consequently, to diminish the influence of Coriolis forces. The measured data has reassuringly confirmed that the influence of the Coriolis forces is directly dependent upon a precise magnitude of the sweep angle: the higher the sweep angle (and so the radial components of displacement), the more intense the Coriolis forces action becomes, and vice versa. On the other hand, the predictions that did not include the appropriate sweep angle change with rotation speed due to the centrifugal forces, failed to produce a 'convex' shape of the natural frequency split plots. The final attempt to reconcile the predictions with the measurements included repetition of the analysis with the appropriate sweep angle change due to centrifugal forces effects. The concluding comparison of the two sets of results is given in Table 4-3 and Fig. 4-19, from which an excellent agreement between theory and measurement is observed. The experimental validation of the effects of Coriolis forces has provided a convincing confirmation of these forces' non-trivial influence on bladed disc vibration characteristics, has increased confidence in the theoretical model which includes these forces, and has served to identify a crucial design feature stimulating their prominent intensity.

8.1.2.3 Mutual interaction of Coriolis forces and blade mistuning

The mutual interaction of Coriolis forces and blade mistuning has been assessed with an aim to establish whether current mistuned bladed disc analyses should incorporate Coriolis effects in order to represent accurately all the significant factors that affect the forced response levels. In the absence of FE codes capable of undertaking a forced response analysis which includes blade mistuning and Coriolis forces, a simple lumped parameter mass-spring model consisting of four degrees-of-freedom per sector has been developed. The most important feature of this model, compared to earlier versions, is related to the added sector-to-sector cross-coupling

stiffness terms, which simulate the strength of in-plane tangential and radial coupling, necessary for prominent effect of Coriolis forces. A corresponding coupling parameter, γ, has been used as a control parameter to regulate the Coriolis forces' strength: the higher the value of γ, the stronger the effect of Coriolis forces. Fundamentally, the inclusion of Coriolis forces causes the individual frequency response functions to be distinctly different when the Coriolis forces are present compared to their non-Coriolis counterparts, which could provide an explanation for the mismatch sometimes observed between theoretical predictions and experimental data for bladed discs. The influence of increasing frequency mistuning ranges has been studied for bladed discs with the coupling parameter γ spanning from 0.005 to 0.062, demonstrating weak and strong Coriolis forces coupling, respectively. In the latter case, it has been found that the maximum forced response with Coriolis forces included for 2EO can be much higher than that corresponding to mistuned-only system, reaching levels which are 75% greater at a specific mistuning degree. For other excitation cases considered (5EO and 10EO), the impact of Coriolis forces was not as significant. Statistical characterisation of forced response has been obtained based on 500 Monte Carlo simulations of blade frequency mistuning from a typical ±5% range, demonstrating considerable differences in maximum forced responses calculated with and without Coriolis forces for 2EO case. As the coupling parameter γ increased from 0.005 to 0.062, the effects of the Coriolis forces on maximum blade amplitudes increased. Hence, for the same degree of mistuning, the maximum forced response with Coriolis forces included, depicted in Fig. 5-16 over all 500 mistuning patterns for strong coupling case, was higher by approximately 40% than that corresponding to the mistuned-only system. Furthermore, the statistical distributions were also notably different. For 5EO and 10EO, both the maximum forced response levels and their statistical distributions with and without Coriolis forces calculated over 500 mistuning patterns were similar.

The fundamental demonstration of the combined effect of Coriolis forces and blade mistuning has been a highlight of this study in the author's opinion and is believed to be a significant achievement of this thesis, as it addresses an important topic for industry that has not been investigated in the past. The results indicate that despite the fact that in some of the cases considered, the effects of Coriolis forces could be considered as minor compared with typical blade mistuning, their influence certainly cannot be neglected for bladed disc designs with prominent radial

flexibility. Moreover, for such bladed discs, depending on the precise degree of blade mistuning present, the maximum forced response levels with Coriolis forces included can be significantly higher than their mistuned-only counterparts.

The experimental investigation study has contributed to a basic understanding of the mutual interaction of Coriolis forces and deliberately introduced blade mistuning on natural frequency splits of bladed discs. It has been found that for certain designs exhibiting a prominent influence of Coriolis forces, there is a limit of rotation speed up to which addition of blade mistuning contributes significantly to the generated natural frequency split, but beyond which the effect of Coriolis forces 'overtakes' that of mistuning. An important implication of this may be that for certain designs of bladed discs, the commonly observed natural frequency split, customarily accounted for in previous studies as the mistuning-generated effect, may be in fact due to mainly Coriolis forces.

The evidence obtained from both an analysis of a simple model and experimental investigation study suggests that Coriolis forces should be included into mistuned bladed disc analyses, although their exact impact on realistic models is yet to be investigated.

8.1.3 Development of strategies for maximum forced response reduction and control based on new large mistuning concept

A second part of this thesis has been an attempt to test new strategies based on the large mistuning (LM) concept for maximum forced response reduction and control. Two approaches have been introduced and assessed using an industrial bladed fan disc to reveal the advantages of relaxing the manufacturing tolerances and of extending the typical blade mistuning design acceptance limits. The random or "scatter-controlling" approach involved a statistical characterisation of forced response via extensive Monte Carlo simulations for different blade frequency mistuning spanning small to large ranges under several engine order excitations. Although increasing the frequency mistuning range decreased the maximum forced response, the exact amount of this reduction varied depending on the engine order excitation considered, as illustrated in Fig. 6-14. The largest maximum forced response reduction obtained was approximately 33% from 2.0 at ±0.5% frequency mistuning range to 1.3 at ±40% frequency mistuning range for 3EO excitation. The corresponding maximum forced response decreases for 6 and 13EO were 22% and

27%, respectively, demonstrating the benefit from extending the frequency mistuning range.

A rigorous statistical hypothesis analysis based on the Kolmogorov-Smirnov and the Chi-square (Pearson's) goodness-of-fit tests has demonstrated a dependency of forced response statistical distributions on frequency mistuning range. It has been shown that the forced response can be characterised accurately by assuming the Weibull and the extreme value distributions for the frequency mistuning ranges higher than the ±5%, which is in agreement with the past mistuning literature studies (Mignolet et al. [73] 2000, Jones and Cross [76] 2002), although the results from the small frequency mistuning ranges do not conform to any specific statistical distribution. This information could be subsequently used to find the probability that the maximum blade amplitudes will exceed a specified critical value, which is necessary in predictions of failure risks, durability and reliability of bladed disc assemblies. Overall, it has been concluded that random or scatter-controlling LM is a promising approach that, if practically feasible, might be employed as a potentially beneficial forced response diminution strategy.

The deterministic or "pattern-controlling" approach has concentrated on the assessment of sensitivity and robustness to small unavoidable random mistuning of ±0.5% of forced response levels for several intentional mistuning patterns of unconventionally large strengths. It has been demonstrated that sensitivity of forced response is the principal factor in selecting the most efficient mistuning patterns as a way to reduce and regulate the scatter in blades' amplitudes. An increase in frequency mistuning range has been shown to have a beneficial effect on harmonic and linear deliberately-mistuned patterns. In particular, in the case of harmonically-distributed blade variations, the robustness to small unintentional random mistuning has been improved 3-7 times depending on the excitation conditions only by increasing the frequency mistuning range. A maximum forced response reduction of 60% from 1.73 to 1.08 and a tenfold robustness improvement have been achieved for linear mistuning patterns by increasing the frequency mistuning from ±0.5% to ±40% range for 3EO excitation, Fig. 6-32. The sensitivity of forced response obtained from the best and worst mistuning patterns in the first part of Chapter 6 has been assessed initially to additional small mistuning and, subsequently, to random blade rearrangements to show a significantly better robustness for best patterns drawn from LM range, as indicated in Tables 6-14 and 6-15. With an aim to

estimate ‘damage tolerance’ of the bladed disc forced response, a few blades with large mistune have been introduced to demonstrate that forced response levels are almost unaffected by the precise mistuning magnitude of damaged blades. As for random blade rearrangements of the randomly-selected mistuning patterns with damaged blades, the variations of the maximum forced response levels and robustness have been shown to depend on the particular engine order excitation analysed.

Fundamentally, the high sensitivity of nearly-tuned bladed discs has been demonstrated, followed by a relative insensitivity to additional random mistuning after reaching peak forced response levels, which indicates prospective advantages in introducing large frequency mistuning. It has been shown that it is possible to reduce substantially the maximum forced response levels and to improve significantly the robustness by using the LM concept for some of the cases considered. The results indicate that the maximum forced response levels obtained from the “pattern-controlling” approach can be lower than those corresponding to the “scatter-controlling” strategy, although the latter is believed to be more practically-oriented as it does not require blade types of precise mistuning or their specific arrangement on the bladed disc. The wider applicability of the “pattern-controlling” strategy could be achieved by using “pseudo-mistuning” (Castanier et al. [68] 1997), which could include less blade types required to reach the desirable forced response characteristics, thus creating a more practical mistuning. Finally, it should be noted that results presented in this study might be limited to a certain design of bladed discs and considered operating conditions and, subsequently, a more general investigation might be necessary to establish the influence of LM on a wider range of bladed discs than considered here. Nevertheless, encouraging results show promise in implementing the LM concept into the design of bladed discs as a means of preventing very large forced response levels caused by random mistuning and of ensuring the predictability of the response.

8.1.4 Attempts to generalise: past, present and future of the blade mistuning problem

The accumulated knowledge from the issues investigated in this thesis and interpretation of findings from the mistuning studies in the past have been discussed to assess the possibilities to generalise on the blade mistuning problem. Examples

have been shown of how the basic principles demonstrated in this work could be applied to gain insights into other mistuning related questions and to obtain a better apprehension of how to deal efficiently with the problem. One of the conclusions drawn from the mistuning problem map, which showed a multitude of key factors influencing the maximum forced response, has been a compelling need to investigate those factors in combination in efforts to provide reliable vibration characteristics and to prevent excessive forced response levels. The author's view on possible future trends and philosophy of the blade mistuning problem have been also presented, some of which include: (i) the development of practically-oriented studies, strongly correlated with experiments, which could offer guidelines for conducting effective bladed disc measurements and data interpretation; and (ii) provision of means of ensuring acceptable forced response levels and probability of failure by addressing the inverse blade mistuning problem from a statistical viewpoint.

8.2 Main research contributions

A summary of the most prominent contributions of the research reported in this thesis is presented below:

- Identification of "critical outstanding mistuning questions" as a result of philosophical assessment of the persisting blade mistuning problem from a fresh perspective
- A first experience of including previously-neglected effects of Coriolis forces into the analysis of bladed discs in a quest to address the issue of the "real world", or to improve the basic model used in investigations
- Successful experimental validation of the effects of Coriolis forces on tuned bladed disc vibration properties, which served as an indisputable evidence of these forces significant influence
- Original analysis of mutual impact of blade mistuning and Coriolis forces on forced response levels of bladed discs, which fundamentally challenges existing mistuning studies and traditionally established thoughts on the subject
- Development of efficient strategies based on new large mistuning concept, which provide beneficial and practically-oriented ways for maximum forced response reduction and control

- Provision of thorough statistical analysis of forced response characteristics, which could be developed further to predict durability and reliability of bladed disc assemblies.

8.3 Suggestions for future research

Some thoughts on further developments of the research work described in this thesis are outlined below. These can be split into the following four issues:

(i) An assessment of the effects of Coriolis forces on industrial mistuned bladed discs (needs FE codes not yet available);

(ii) An investigation of large mistuning influence on a wider range of bladed disc types;

(iii) A study of the physics of the maximum forced response magnification;

(iv) Analysis of remaining issues postulated in "critical mistuning outstanding questions".

8.3.1 Assessment of the effects of Coriolis forces on industrial mistuned bladed discs

In this thesis, the assessment of mutual influence of Coriolis forces and blade mistuning has been studied using a simple lumped parameter mass-spring model, which enlightened, for the first time, the physics of this complex interaction. No attempt at such an early stage has been made to generalise the results with regard to the realistic bladed discs, which, in author's opinion, is a necessary goal in future. Further work could be carried out initially to determine the quantitative effects of the Coriolis forces on the tuned vibration characteristics of industrial bladed discs that possess significant radial flexibility, and, subsequently, to examine these forces joint influence with typical blade mistuning on forced response levels. The fulfilment of this objective would require the development of an efficient code (not yet available), which could provide correct eigenvalues and eigenvectors and enable the forced response analysis with both Coriolis forces and blade mistuning included of single cyclically-symmetric sector models. Successful completion of this task would determine conclusively the exact impact of Coriolis forces in realistic bladed disc analysis.

8.3.2 Investigation of large mistuning influence on a wider range of bladed discs

A novel concept of LM as a means of maximum forced response reduction and control has been introduced in this thesis and demonstrated by application to an industrial bladed fan disc. It is difficult to generalise the specific acquired results with assurance to a wide range of bladed discs, as the emphasis in this study was placed on a specific bladed disc, the first family of modes and three specific engine order excitations. A potential suggestion for further work could involve assessment of the applicability of the LM approach on higher order modes, where frequency veerings between the mode families may occur, and for different engine orders. Moreover, determination of the benefits, or even possible disadvantages, of LM on several other designs of bladed discs (e.g. with stronger coupling) would be helpful.

8.3.3 Study of the physics of the maximum forced response magnification

A scope for further work has been identified in Chapter 6 in respect to underlying characteristics and physical explanations of the reasons behind the commonly-reported facts surrounding the maximum forced response magnification of bladed discs. This issue could be addressed by carrying out a parametric analysis, which would involve the design of simple bladed disc models in order to capture the relevant physics, fundamentally leading to a vast enrichment of our understanding of the blade mistuning problem and successful means of preventing it.

8.3.4 Analysis of remaining issues postulated in “critical outstanding mistuning questions”

This research effort has been confined to address several issues from the first four groups of the “critical outstanding mistuning questions”, postulated in Chapter 2. The remaining questions could provide feasible projects for future studies, notable among which could be: (i) provision of guidance on how to conduct the bladed disc measurements efficiently and to extrapolate from the measured data to worst case scenarios, (ii) formulation of the inverse mistuning problem to enable the specified forced response levels and probability of failure to be guaranteed with selected blade

mistuning, (iii) development of statistical analysis tools to determine bladed disc durability and risks of failure.

8.4 Epilogue

No matter how elusive the long-standing blade mistuning problem might seem, its successful resolution is believed to be a question of time. Not only the increasingly powerful and accurate computational tools will serve to fulfil this mission, but, fundamentally, it is the attention to detail and filling the gaps in research by identifying and addressing the philosophical questions that will eventually defy the problem.

It is hoped that the work presented in this thesis has been a small contribution towards providing new insights into the blade mistuning problem and possible routes to fathom its 'secrets' and to prevent rather than cure its consequences.

8.5 Publications of thesis work

[1] **Nikolic, M., Petrov, E.P. and Ewins, D.J.**
Coriolis Forces in Forced Response Analysis of Mistuned Bladed Discs
Accepted for publication in ASME Journal of Turbomachinery, paper TURBO-06-1109; previously presented as GT2006-90315 at the ASME TURBO EXPO 2006 Conference in Barcelona, Spain, 8-11 May 2006

[2] **Nikolic, M., Ewins, D.J., Petrov, E.P. and Di Maio, D.**
The Effects of Coriolis Forces on Vibration Properties of Bladed Discs
7th IFToMM Conference on Rotor Dynamics, Vienna, Austria, 25-28 September 2006

[3] **Nikolic, M., Petrov, E.P. and Ewins, D.J.**
Robust Strategies for Forced Response Reduction of Bladed Discs Based on Large Mistuning Concept
Submitted to the ASME TURBO EXPO 2007 Conference in Montreal, Canada, 14-17 May 2007, paper GT2007-27183

REFERENCES

[1] Ewins, D.J., 1991, "The Effects of Blade Mistuning on Vibration Response – A Survey", *IFToMM 4th International Conference on Rotordynamics*, Prague, Czechoslovakia

[2] Srinivasan, A.V., 1997, "Flutter and Resonant Vibration Characteristics of Engine Blades", *ASME Journal of Engineering for Gas Turbines and Power*, Vol. 119, pp. 742-775

[3] Slater, J.C., Minkiewicz, G.R. and Blair, A.J., 1999, "Forced Response of Bladed Disk Assemblies – A Survey", *The Shock and Vibration Digest*, Vol. 31, No. 1, pp. 17-24

[4] Tobias, S.A. and Arnold, R.N., 1957, "The Influence of Dynamical Imperfections on the Vibration of Rotating Disks", *Proceedings of the Institution of Mechanical Engineers, IMechE*, Vol. 171, No. 2, pp. 669-690

[5] Whitehead, D.S., 1966, "Effect of Mistuning on the Vibration of Turbomachine Blades Induced by Wakes", *Journal of Mechanical Engineering Science*, Vol. 8, No. 1, pp. 15-21

[6] Ewins, D.J., 1969, "The Effect of Detuning Upon the Forced Vibration of Bladed Disks", *Journal of Sound and Vibration*, Vol. 9, No. 1, pp. 65-79

[7] Dye, R.C. and Henry, T.A., 1969, "Vibration Amplitudes of Compressor Blades Resulting from Scatter in Blade Natural Frequencies", *ASME Journal of Engineering for Power*, Vol. 91, pp. 182-188

[8] Ewins, D.J., 1973, "Vibration Characteristics of Bladed Disc Assemblies", *Journal of Mechanical Science*, Vol. 12, No. 5, pp. 165-186

[9] Ewins, D.J., 1976, "Vibration Modes of Mistuned Bladed Discs", *ASME Journal of Engineering for Power*, pp. 349-355

[10] El-Bayoumi, L.E., Srinivasan, A.V., 1975, "Influence of Mistuning on Rotor-Blade Vibration",*AIAA Journal*, Vol. 13, No. 4, pp. 460-464

[11] Sogliero, G. and Srinivasan, A.V., 1980, "Fatigue Life Estimates of Mistuned Blades Via a Stochastic Approach", *AIAA Journal*, Vol. 18, No. 3, pp. 318-323

[12] Ewins, D.J., 1980, "Further Studies of Bladed Disc Vibration: Effects of Packeting", *IMechE Conference on Vibrations in Rotating Machinery*, Cambridge, pp. 97-102

[13] Strange, W.A. and MacBain, J.C., 1983, "An Investigation of Dual Mode Phenomena in a Mistuned Bladed Disk", *ASME Journal of Vibration, Acoustics, Stress and Reliability in Design*, Vol. 105, pp. 402-407

[14] Muszynska, A. and Jones, D.I.G., 1983, "On Tuned Bladed Disk Dynamics: Some Aspects of Friction Related Mistuning", *Journal of Sound and Vibration*, Vol. 86, No. 1, pp. 107-128

[15] Ewins, D.J. and Han, Z.S., 1983, "Resonant Vibration Levels of a Mistuned Bladed Disc", *ASME Journal of Vibration, Acoustics, Stress and Reliability in Design*, Vol. 106, No. 2, pp. 211-217

[16] Griffin, J.H and Hoosac, T.M., 1984, "Model Development and Statistical Investigation of Turbine Blade Mistuning", *ASME Journal of Vibration, Acoustics, Stress and Reliability in Design*, Vol. 106, pp. 204-210

[17] MacBain, J.C. and Whaley, P.W., 1984, "Maximum Resonant Response of Mistuned Bladed Disks", *ASME Journal of Vibration, Acoustics, Stress and Reliability in Design*, Vol. 106, No. 2, pp. 218-223

[18] Griffin, J.H. and Sinha, A., 1985, "The Interaction Between Mistuning and Friction in the Forced Response of Bladed Disk Assemblies", *ASME Journal of Engineering for Gas Turbines and Power*, Vol. 107, pp. 205-211

[19] Sinha, A., 1986, "Calculating the Statistics of Forced Response of a Mistuned Bladed Disk Assembly", *AIAA Journal*, Vol. 24, No. 11, pp. 1797-1801

[20] Afolabi, D.H., 1987, "A Note on the Rogue Failure of Turbine Blades", *Journal of Sound and Vibration*, Vol. 122, No. 3, pp. 535-545

[21] Griffin, J.H., 1988, "On Predicting the Resonant Response of Bladed Disk Assemblies", *ASME Journal of Engineering for Gas Turbines and Power*, Vol. 110, pp. 45-50

[22] Crawley, E.F. and Hall, K.C., 1983, "Optimization and Mechanism of Mistuning in Cascades", *ASME Journal of Engineering for Gas Turbines and Power*, Vol. 107, pp. 418-426

[23] Kielb, R.E. and Kaza, K.R.V., 1984, "Effects of Structural Coupling on Mistuned Cascade Flutter and Response", *ASME Journal of Engineering for Gas Turbines and Power*, Vol. 106, pp. 17-24

[24] Imregun, M. and Ewins, D.J., 1984, "Aeroelastic Vibration Analysis of Tuned and Mistuned Bladed Systems", *Proceedings of the 2nd Symposium on Unsteady Aerodynamics of Turbomachines and Propellers*, Cambridge, UK

[25] Dugundji, J. and Bundas, D.J., 1984, "Flutter and Forced Response of Mistuned Rotors Using Standing Wave Analysis", *AIAA Journal*, Vol. 22, No. 11, pp. 1652-1661

[26] Kielb, R.E. and Kaza, K.R.V., 1985, "Vibration and Flutter of Mistuned Bladed Disk Assemblies", *Journal of Propulsion and Power*, Vol. 1, No. 5, pp. 336-344

[27] Basu, P. and Griffin, J.H., 1986, "The Effect of Limiting Aerodynamic and Structural Coupling in Models of Mistuned Bladed Disk Vibration", *ASME Journal of Vibration, Acoustics, Stress and Reliability in Design*, Vol. 108, pp. 132-139

[28] Hoyniak, D. and Fleeter, S., 1986, "Aerodynamic and Structural Detuning of Supersonic Turbomachine Rotors", *Journal of Propulsion and Power*, Vol. 2, No. 2, pp. 161-167

[29] Crawley, E.F., 1988, "Aeroelastic Formulation for Tuned and Mistuned Rotors", AGARDograph No. 298, pp. 19 (1-24)

[30] Singh, M.P. and Ewins, D.J., 1988, "A Probabilistic Analysis of the Mistuned Bladed Turbine Disc", *IMechE Conference on Vibrations in Rotating Machinery*, Edinburgh, pp. 143-150

[31] Sinha, A., Chen, S., 1989, "A Higher Order Technique to Compute the Statistics of Forced Response of a Mistuned Bladed Disk Assembly", *Journal of Sound and Vibration*, Vol. 130, No. 2, pp. 207-221

[32] Petrov, E.P., Sanliturk, K.Y. and Ewins, D.J., 2002, "A New Method for Dynamic Analysis of Mistuned Bladed Disks Based on the Exact Relationship Between Tuned and Mistuned Systems", *ASME Journal of Engineering for Gas Turbines and Power*, Vol. 124, pp. 586-597

[33] Yang, M.-T. and Griffin, J.H., 2001, "A Reduced Order Model of Mistuning Using a Subset of Nominal System Modes", *ASME, Journal of Engineering for Gas Turbines and Power*, Vol. 123, pp. 893-900

[34] Feiner, D.M. and Griffin, J.H., 2002, "A Fundamental Model of Mistuning for a Single Family of Modes", *Proceedings of the ASME TURBO EXPO 2002*, 2002-GT-30425

[35] Kruse, M. and Pierre, C., 1996, "Forced Response of Mistuned Bladed Disks Using Reduced-Order Modelling", AIAA-96-1545, *Proceedings of the 37th AIAA/ASME/ASCE/AHS/ASC Structures, Structural Dynamics, and Materials Conference*, Salt Lake City, Vol. 4, pp. 1938-1950

[36] Bladh, R., Castanier, M.P. and Pierre, C., 2001, "Component-Mode-Based Reduced Order Modeling Techniques for Mistuned Bladed Disks – Part I: Theoretical Models, Part II: Application", *ASME Journal of Engineering for Gas Turbines and Power*, Vol. 123, pp. 89-99, 100-108

[37] Moyroud, F., Fransson, T. and Jacquet-Richardet, G., 2002, "A Comparison of Two Finite Element Reduction Techniques for Mistuned Bladed Disks", *ASME Journal of Engineering for Gas Turbines and Power*, Vol. 124, pp. 942-952

[38] Shapiro, B. and Willcox, K., 2003, "Analysing Mistuning of Bladed Discs by Symmetry and Reduced-order Aerodynamic Modelling", *Journal of Propulsion and Power*, Vol. 19, No. 2, pp. 307-311

[39] Ghiocel, D.M., 2005, "Stochastic Subspace Projection Schemes for Solving Random Mistuning Problems in Jet Engine Bladed-Disks: A New, Fast and Accurate Stochastic Perturbation Matrix Reduced-Order Modeling (SPM ROM) Approach", *10th National Turbine Engine High Cycle Fatigue Conference*, New Orleans, USA

[40] Ayers, J.P., Feiner, D.M. and Griffin, J.H., 2005, "A Reduced Order Model for Transient Analysis of Bladed Disk Forced Response", *Proceedings of the ASME TURBO EXPO 2005*, 2005-GT-68128

[41] Khader, N. and Loewy, R.G., 1990, "Shaft Flexibility Effects on the Forced Response of a Bladed Disk Assembly", *Journal of Sound and Vibration*, Vol. 139, No. 3, pp. 469-485

[42] Jacquet-Richardet, G., Ferraris, G., Rieutord, P., 1996, "Frequencies and Modes of Rotating Flexible Bladed Disc-Shaft Assemblies: A Global Cyclic Symmetry Approach", *Journal of Sound and Vibration*, Vol. 191, No. 5, pp. 901-915

[43] Genta, G. and Tonoli, A., 1996, "A Harmonic Finite Element for the Analysis of Flexural, Torsional and Axial Rotordynamic Behaviour of Discs", *Journal of Sound and Vibration*, Vol. 196, No. 1, pp. 19-43

[44] Chun, S.B. and Lee, C.W., 1996, "Vibration Analysis of Shaft-Blade Disk System by Using Substructure Synthesis and Assumed Modes Method", *Journal of Sound and Vibration*, Vol. 189, No. 5, pp. 587-608

[45] Seinturier, E., Dupont, C., Berthillier, M., Dumas, M., 2002, "A New Aeroelastic Model for Mistuned Bladed Disks", AIAA-2002-1533

[46] Kielb, R.E., Feiner, D.M., Miyakozawa, T. And Griffin, J.H., 2004, "Flutter of Mistuned Bladed Disks and Blisks with Aerodynamic and FMM Structural Coupling", *Proceedings of the ASME TURBO EXPO 2004*, 2004-GT-54315

[47] Sladojevic, I., Petrov, E.P., Sayma, A.I., Imregun, M. and Green, J.S., 2005, "Investigation of the Influence of Aerodynamic Coupling on Response Levels of Mistuned Bladed Discs with Weak Structural Coupling", *Proceedings of the ASME TURBO EXPO 2005*, 2005-GT-69050

[48] Rzadkowski, R. and Drewczynski, M., 2004, "Natural Frequencies and Mode Shapes of Two Mistuned Bladed Discs on the Shaft", *Proceedings of the ASME TURBO EXPO 2004*, 2004-GT-54265

[49] Rzadkowski, R., 1993, "The General Model of Free Vibrations of Mistuned Bladed Discs, Part I: Theory, Part II: Numerical Results", *Journal of Sound and Vibration*, Vol. 173, No. 3, pp. 377-393

[50] Lin, C.C. and Mignolet, M.P., 1996, "Effects of Damping and Damping Mistuning on the Forced Vibration Response of Bladed Disks", *Journal of Sound and Vibration*, Vol. 193, No. 2, pp. 525-543

[51] Feiner, D.M., Griffin, J.H., 2003, "A Completely Experimental Method of Mistuning Identification in Integrally Bladed Rotors", *8th National Turbine Engine High Cycle Fatigue Conference*, Monterey, USA

[52] Judge, J., Pierre, C., Ceccio, S.L., 2002, "Mistuning Identification in Bladed Disks", *Proceedings of the International Conference on Structural Dynamics Modelling*, Madeira, Portugal

[53] Mignolet, M.P., Delor, J.P. and Rivas-Guerra, A., 1999, "Identification of Mistuning Characteristics of Bladed Disks From Free Response Data – Part I, Part II", *ASME Journal of Engineering for Gas Turbines and Power*, Vol. 123, pp. 395-411

[54] Feiner, D.M., Griffin, J.H., 2003, " Mistuning Identification of Bladed Disks Using a Fundamental Mistuning Model – Part I, Part II", *Proceedings of the ASME TURBO EXPO 2003*, 2003-GT-38952, 2003-GT-38953

[55] Lim, S.-H., Pierre, C. and Castanier, M.P., 2004, "Mistuning Identification and Reduced-Order Model Updating for Bladed Disks on a Component Mode Mistuning Technique", *9th National Turbine Engine High Cycle Fatigue Conference*

[56] Feiner, D.M. and Griffin, J.H., 2005, "Identification of Damping Variations in Mistuned Bladed Disks", *10th National Turbine Engine High Cycle Fatigue Conference*

[57] Kruse, M.J., Pierre, C., 1997, "An Experimental Investigation of Vibration Localization in Bladed Disks, Part I, Part II", *Proceedings of the ASME TURBO EXPO 1997*, 1997-GT-501, 1997-GT-502

[58] Pierre, C., Ceccio, S.L., Judge, J., 2000, "Experimental Investigation of Mistuned Bladed Disk Vibration", *5th National Turbine Engine High Cycle Fatigue Conference*, Chandler, Arizona, USA

[59] Judge, J., Pierre, C. and Mehmed, O., 2001, "Experimental Investigation of Mode Localization and Forced Response Amplitude Magnification for a Mistuned Bladed Disk", *ASME Journal of Engineering for Gas Turbines and Power*, Vol. 123, pp. 940-950

[60] Kenyon, J.A., Griffin, J.H., 2003, "Experimental Demonstration of Maximum Mistuned Bladed Disk Forced Response", *Proceedings of the ASME TURBO EXPO 2003*, 2003-GT-38060

[61] Rossi, M.R., Feiner, D.M. and Griffin, J.H., 2005, "Experimental Study of the Fundamental Mistuning Model for Probabilistic Analysis", *Proceedings of the ASME TURBO EXPO 2005*, 2005-GT-68127

[62] Petrov, E.P., Ewins, D.J., 2001, "Analysis of the Worst Mistuning Patterns in Bladed Disc Assemblies", *Proceedings of the ASME TURBO EXPO 2001*, 2001-GT-0292

[63] Kenyon, J.A., Griffin, J.H., Feiner, D.M., 2002, "Maximum Bladed Disk Forced Response from Distortion of a Structural Mode", *Proceedings of the ASME TURBO EXPO 2002*, 2002-GT-30426

[64] Whitehead, D.S., 1998, "The Maximum Factor by Which Forced Vibration of Blade Can Increase Due to Mistuning", *ASME Journal of Engineering for Gas Turbines and Power*, Vol. 120, pp. 115-119

[65] Rivas-Guerra, A. and Mignolet, M.P., 2001, "Local/Global Effects of Mistuning on the Forced Response of Bladed Disks", *Proceedings of the ASME TURBO EXPO 2001*, 2001-GT-0289

[66] Rivas-Guerra, A.J., Mignolet, M.P., 2002, "Maximum Amplification of Blade Response Due to Mistuning: Localization and Mode Shapes Aspects of the Worst Disks", *Proceedings of the ASME TURBO EXPO 2002*, 2002-GT-30323

[67] Xiao, B., Rivas-Guerra, A.J. and Mignolet, M.P., 2004, "Maximum Amplification of Blade Response due to Mistuning in Multi-degree-of-freedom Blade Models", *Proceedings of the ASME TURBO EXPO 2004*, 2004-GT-54030

[68] Castanier, M.P., Pierre, C., 1997, "Consideration on the Benefits of Intentional Blade Mistuning for the Forced Response of Turbomachinery Rotors", *Proceedings of the ASME Aerospace Division*, AD-Vol. 55, pp. 419-425

[69] Castanier, M.P., Pierre, C., 1998, "Investigation of the Combined Effects of Intentional and Random Mistuning on the Forced Response of Bladed Disks", AIAA-98-3720

[70] Pierre, C., Judge, J., Ceccio, S.L., Castanier, M.P., 2002, "Experimental Investigation of the Effects of Random and Intentional Mistuning on the Vibration of Bladed Disks", *7th National Turbine Engine High Cycle Fatigue Conference*, Palm Beach Florida, USA

[71] Shapiro, B., 1998, "Symmetry Approach to Extension of Flutter Boundaries via Mistuning", *Journal of Propulsion and Power*, Vol. 14, No. 3, pp. 354-366

[72] Kenyon, J.A. and Griffin, J.H., 2000, "Intentional Harmonic Mistuning for Robust Forced Response of Bladed Disks", *5th National Turbine Engine HCF Conference*, 2000, Chandler, Arizona, USA

[73] Mignolet, M.P., Hu, W., Jadic, I., 2000, "On the Forced Response of Harmonically and Partially Mistuned Bladed Disks, Part I: Harmonic Mistuning; Part II: Partial Mistuning and Applications", *International Journal of Rotating Machinery*, Vol. 6, No. 1, pp. 29-56

[74] Choi, B.K., Lentz, J., Rivas-Guerra, A.J. and Mignolet, M.P., 2001, "Optimization of Intentional Mistuning Patterns for the Reduction of the Forced Response Effects of Unintentional Mistuning: Formulation and Assessment", *Proceedings of the ASME TURBO EXPO 2001*, 2001-GT-293

[75] Brown, J.M., Beachkofski, B., 2000, "A Phenomenological Investigation of Sequence Effects on Mistuned Rotor Response", *36th AIAA/ASME/SAE/ASEE Joint Propulsion Conference and Exhibit*, Huntsville, AL

[76] Jones, W.J., Cross, C.J., 2002, "Reducing Mistuned Bladed Disk Forced Response Below Tuned Resonant Amplitudes", *7th National Turbine Engine High Cycle Fatigue Conference*, Palm Beach Florida, USA

[77] Petrov, E.P. and Iglin, S., 1999, "Search of the Worst and Best Mistuning Patterns for Vibration Amplitudes of Bladed Disks by the Optimization Methods Using Sensitivity Coefficients", *Engineering Design Optimization, Proceedings of the 1st ASMO UK/ISSMO Conference*, Ilkley, UK

[78] Petrov, E.P., Vitali, R. and Haftka, R.T., 2000, "Optimization of Mistuned Bladed Discs Using Gradient-Based Response Surface Approximations", AIAA-2000-1522

[79] Petrov, E.P., Ewins, D.J., 2002, "Search for the Best Arrangement in Mistuned Bladed Disc Assembly", *7th National Turbine Engine High Cycle Fatigue Conference*, Florida, USA

[80] Ayers, J.P., Feiner, D.M. and Griffin, J.H., 2005, "Reducing Mistuning Effects by Optimally Switching Blades", *10th National Turbine Engine High Cycle Fatigue Conference*, New Orleans, USA

[81] Ottarson, G. and Pierre, C., 1996, "A Transfer Matrix Approach to Free Vibration Localization in Mistuned Blade Assemblies", *Journal of Sound and Vibration*, Vol. 197, No. 5, pp. 589-618

[82] Griffin, J.H., 1990, "A Review of Friction Damping of Turbine Blade Vibration", *International Journal of Turbo and Jet Engines*, No. 7, pp. 297-307

[83] Kaneko, Y., Mase, M., Fujita, K. and Nagashima, T., 1994, "Vibrational Response Analysis of Mistuned Bladed Disk", *JSME International Journal*, Series C, Vol. 37, No. 1, pp. 33-40

[84] Bladh, R., Castanier, M.P. and Pierre, C., 2001, "Effects of Multistage Coupling and Disk Flexibility on Mistuned Bladed Disk Dynamics", *Proceedings of the ASME TURBO EXPO 2001*, 2001-GT-0277

[85] Myhre, M., Moyroud, F., Fransson, T.H., 2003, "Numerical Investigation of the Sensitivity of Forced Response Characteristics of Bladed Disks to Mistuning", *Proceedings of the ASME TURBO EXPO 2003*, 2003-GT-38007

[86] Kenyon, J.A. and Griffin, J.H., 2001, "Forced Response of Turbine Engine Bladed Disks and Sensitivity to Harmonic Mistuning", *Proceedings of the ASME TURBO EXPO 2001*, 2001-GT-0274

[87] Kenyon, J.A., Griffin, J.H. and Kim, N.E., 2004, "Sensitivity of Tuned Bladed Disk Response to Frequency Veering", *Proceedings of the ASME TURBO EXPO 2004*, 2004-GT-53280

[88] Baik, S., Castanier, M.P. and Pierre, C., 2004, "Mistuning Sensitivity Prediction of Bladed Disks Using Eigenvalue Curve Veerings", *9th National Turbine Engine High Cycle Fatigue Conference*

[89] Baik, S., Castanier, M.P. and Pierre, C., 2005, "Some Practical Aspects of Using Reduced-Order Vibration Models for Design of Bladed Disks: Rotation Effects and Power Flow Analysis", *10th National Turbine Engine High Cycle Fatigue Conference*

[90] Wei, S.T. and Pierre, C., 1990, "Statistical Analysis of the Forced Response of Mistuned Cyclic Assemblies", *AIAA Journal*, Vol. 28, No. 5, pp. 861-868

[91] Mignolet, M.P. and Lin, C.C., 1992, "The Combined Closed Form – Perturbation Approach to the Analysis of Mistuned Bladed Disks", *Proceedings of the ASME TURBO EXPO 1992*, 92-GT-125

[92] Cha, D., Sinha, A., 1999, "Statistics of Responses of a Mistuned Bladed Disk Assembly Subjected to White Noise and Narrow Band Excitation", *ASME Journal of Engineering for Gas Turbines and Power*, Vol. 121, pp. 710-717

[93] Bah, M.T., Nair, P.B., Bhaskar, A. and Keane, A.J., 2002, "Statistical Analysis of the Forced Response of Mistuned Bladed Disks Using Stochastic Reduced Basis Methods", AIAA-2002-1534

[94] Sinha, A., 2003, "Computation of the Statistics of Forced Response of a Mistuned Bladed Disk Assembly via Polynomial Chaos", *Proceedings of the ASME TURBO EXPO 2003*, 2003-GT-38961

[95] Sinha, A., 2005, "Statistics of the Peak Maximum Amplitude of the Forced Response of a Mistuned Bladed Disk", *Proceedings of the ASME TURBO EXPO 2005*, 2005-GT-69070

[96] Sanliturk, K.Y., Imregun, M., Ewins, D.J., 1992, "Statistical Analysis of Random Mistuning of Bladed Assemblies", *IMechE Conference on Vibrations in Rotating Machinery*, Bath, pp. 51-58

[97] Griffin, J.H., 1992, "Optimizing Instrumentation When Measuring Jet Engine Blade Vibration", *ASME Journal of Engineering for Gas Turbines and Power*, Vol. 114, pp. 217-221

[98] Xiao, B., Rivas-Guerra, A.J., Mignolet, M.P., 2003, "Identification of the Maximum Responding Blade in Mistuned Bladed Disks", *Proceedings of the ASME TURBO EXPO 2003*, 2003-GT-38966

[99] Wu, M.-C. and Huang, S.-C., 1997, "Modal Analysis of a Rotating Shaft-Disk-Blades System with a Cracked Blade", *Proceedings of the ASME Design Engineering Technical Conferences*, Sacramento, California

[100] Kuang, J. H., Huang, B.W., 1999, "The Effects of Blade Crack on Mode Localization in Rotating Bladed Disks", *Journal of Sound and Vibration*, Vol. 227, No. 1, pp. 85-103

[101] Kim, J. and Ewins, D.J., 2000, "Effect of Crack Locations on the Vibration Characteristics of MDOF Rotor Systems", *Proceedings of the ISMA Conference*, Leuven, Belgium, pp. 259-265

[102] Sanliturk, K.Y. and Imregun, M., 1994, "Vibration Analysis of Mistuned Bladed-Disk Assemblies – Inverse Approach", *AIAA Journal*, Vol. 32, No. 4, pp. 857-865

[103] Capiez-Lernout, E. and Soize, C., 2003, "Specifying Manufacturing Tolerances for a Given Amplification Factor: A Nonparametric Probabilistic Methodology", *Proceedings of the ASME TURBO EXPO 2003*, 2003-GT-38050

[104] Capiez-Lernout, E., Soize, C., Lombard, J.-P., Dupont, C. and Seinturier, E., 2004, "Blade Manufacturing Tolerances Definition for a Mistuned Industrial Bladed Disk", *Proceedings of the ASME TURBO EXPO 2004*, 2004-GT-53356

[105] Goldstein, H., 1980, "Classical Mechanics", Second Edition, Addison Wesley Series in Physics

[106] Loewy, R.G. and Khader, N., 1984, "Structural Dynamics of Rotating Bladed-Disk Assemblies Coupled with Flexible Shaft Motions", *AIAA Journal*, Vol. 22, No. 9, pp. 1319-1327

[107] Crawley, E.F. and Mokadam, D.R., 1984, "Stagger Angle Dependence of Inertial and Elastic Coupling in Bladed Disks", *ASME Journal of Vibration, Acoustics, Stress and Reliability in Design*, Vol. 106, pp. 181-188

[108] Okamoto, S., Sakata, M., Kimura, K., Ohnabe, H., 1995, "Vibration Analysis of a High Speed and Light Weight Rotor System Subjected to a Pitching or Turning Motion, II: A Flexible Rotor System on Flexible Suspensions", *Journal of Sound and Vibration*, Vol. 184, No. 5, pp. 887-906

[109] Wang, W., 1992, "Dynamic Analysis of Flexible Bladed Disk-Shaft Rotor Systems", PhD Thesis, Carleton University Ottawa

[110] Sawicki, J.T. and Genta, G., 2001, "Modal Uncoupling of Damped Gyroscopic Systems", *Journal of Sound and Vibration*, Vol. 244, No. 3, pp. 431-451

[111] Huang, B.W. and Kuang, J.H., 2001, "Mode Localization in a Rotating Mistuned Turbo Disk with Coriolis Effect", *International Journal of Mechanical Sciences*, Vol. 43, pp. 1643-1660

[112] Huang, B.W. and Kuang, J.H., 2001, "The Coupled Longitudinal and Bending Vibrations on Stability in a Cracked Blade-Disk", *Proceedings of the ASME TURBO EXPO 2001*, 2001-GT-0281

[113] Ewins, D.J., 2000, "Modal Testing: Theory, Practice and Application", Second Edition, Research Studies Press

[114] Bucher, I. and Ewins, D.J., 2001, "Modal Analysis and Testing of Rotating Structures", *Philosophical Transactions of the Royal Society*, Vol. 359, pp. 61-96

[115] Meirovitch, L. and Ryland, G., 1979, "Response of Slightly Damped Gyroscopic Systems", *Journal of Sound and Vibration*, Vol. 67, No. 1, pp. 1-19

[116] Meirovitch, L., 1980, "Computational Methods in Structural Dynamics", Sijthoff & Noordhoff

[117] SAMCEF V11.0-06 Manual, 2005, SAMTECH S.A.

[118] Sever, I.A., 2004, "Experimental Validation of Turbomachinery Blade Vibration Predictions", PhD thesis, Imperial College London

[119] Malpede, S.M., 2003, "1D/1E/1F Project Final Report", Internal Report, Imperial College London

[120] Mehdigholi, H., 1991, "Forced Vibration of Rotating Discs and Interaction with Non-rotating Structures", PhD Thesis, Imperial College London

[121] Wildheim, S.J., 1979, "Excitation of Rotationally Periodic Structures", *ASME Journal of Applied Mechanics*, Vol. 46, pp. 878-882

[122] Stanbridge, A.B., Martarelli, M. and Ewins, D.J., 2001, "Rotating Disc Vibration Analysis with a Circular-Scanning LDV", *Proceedings of the IMAC XIX Conference*

[123] Petrov, E.P., Sanliturk, K.Y., Ewins, D.J. and Elliot, R., 2000, "Quantitative Prediction of the Effects of Mistuning Arrangement on Resonant Response of a Practical Turbine Bladed Disc", *5th National Turbine Engine High Cycle Fatigue Conference*, Arizona, USA

[124] Ewins, D.J., 1972, "A Study of the Vibration Modes of a Bladed Turbine Wheel", *IMechE Conference on Vibrations in Rotating Machinery*, London, pp. 170-184

[125] Hahn, G.J. and Shapiro, S.S., 1994, "Statistical models in engineering", John Wiley & Sons

[126] Martinez, W.L. and Martinez, A.R., 2002, "Computational statistics handbook with MATLAB", Chapman & Hall/CRC

[127] Karian, Z.A. and Dudewicz, E.J., 2000, "Fitting statistical distributions: The generalised Lambda distribution and generalised Bootstrap methods", CRC Press, Boca Raton, FL

[128] Sheskin, D.J., 2000, "Handbook of parametric and nonparametric statistical procedures", Second edition, Chapman & Hall/CRC

[129] Bladh, R., Castanier, M. and Pierre, C., 1998, "Reduced Order Modeling and Efficient Forced Response Statistics Prediction for Mistuned Bladed Disks", *3rd National Turbine Engine High Cycle Fatigue Conference*, San Antonio, Texas, USA

[130] Chen, G., 2002, "Model Updating for Mistuning Analysis – Project Report 1", Internal Report, Imperial College London

[131] Petrov, E.P., and Ewins, D.J., 2005, "Effects of Damping and Varying Contact Area at Blade-Disc Joints in Forced Response Analysis of Bladed Disc Assemblies", *Proceedings of the ASME TURBO EXPO 2005*, GT2005-68936

[132] Petrov, E.P., and Ewins, D.J., 2006, "Advanced Modelling of Underplatform Friction Dampers for Analysis of Bladed Disc Vibration", *Proceedings of the ASME TURBO EXPO 2006*, GT2006- 90146

[133] Koh, K.H. and Griffin, J.H., 2006, "Dynamic Behavior of A Spherical Friction Damper and It's Implication to Damper Contact Stiffness", *Proceedings of the ASME TURBO EXPO 2006*, GT2006- 90102

[134] Kabaila, A. and Pulamno, V., 1979, "Analysis of Helicoidal Girders by Stiffness Method", School of Civil Engineering, University of New South Wales, Report UNICIV R-183

APPENDIX A4

A4-1 Features of engine order (EO) excitation

In the review [2], Srinivasan describes the source of excitation of engine bladed discs as “inherently unsteady”, “anything but uniform, either upstream or downstream”, since “the flow entering an engine inlet meets with static obstructions (struts, vanes, etc.), and rotating obstructions (blades) in its path from the inlet to the exhaust”. This type of excitation results from the rotation of a bladed disc past a static force which is not constant circumferentially. Blades experience time-varying forces at speed-dependent frequencies, so that the bladed disc modes can be excited into resonance at certain speeds of rotation.

The angular variation of forcing is usually expressed in terms of a Fourier analysis. It is assumed that n equally spaced obstructions will cause the steady flow to contain a $\cos n\theta$ fluctuation superimposed upon its mean level and, in addition, smaller components of $\cos 2n\theta$, $\cos 3n\theta$ etc, [8]. The $n\theta$ component will excite any mode of the bladed disc which has an n nodal diameter component in its mode shape, and will do so at a frequency equal to $n\Omega$, where Ω is the rotation speed. In the case of a tuned bladed disc, nEO or nth engine order excitation, will only excite the modes with n nodal diameters. For a mistuned system, most modes will be typically excited by any of several engine order excitations, not just one as in the case of a tuned bladed disc. Fig. A4-1 illustrates the envelopes of frequency response functions to several engine order excitations in case of tuned (a) and mistuned (b) bladed disc.

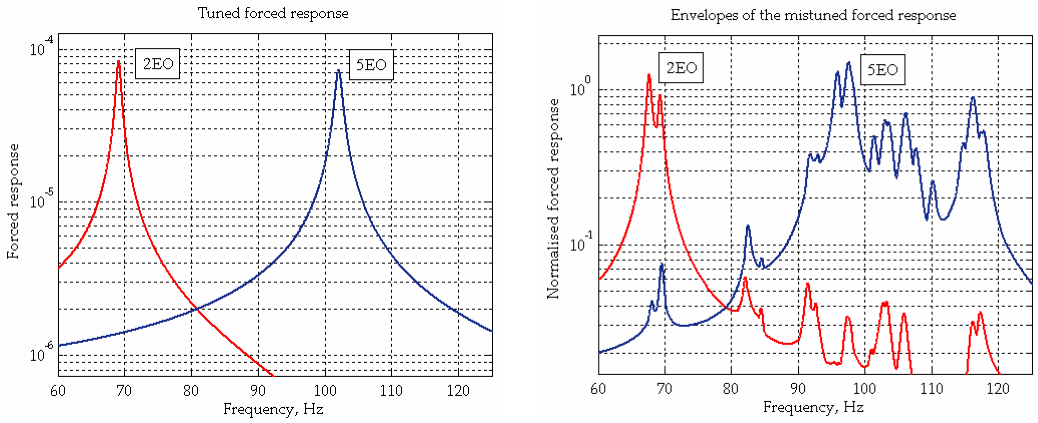

(a) (b)

Fig. A4-1. Forced response under 2 and 5EO of tuned (a) and mistuned (b) bladed disc

APPENDIX A4

A4-2 Results after first bending process – Flat Blisk and Swept Blisk 10deg stationary conditions results

Tables A4-1 and A4-2 and Fig. A4-2 below show the experimental and predicted* results at 0rev/min for the Flat Blisk and Swept Blisk 10degrees testpieces.

Flat Blisk and Swept 10deg measurements natural frequency (Hz) results at 0rev/min									
	Flat (F)				Swept 10deg (S10)				% diff. in aver. measured: F vs. S10
Mode	Freq.1	Freq.2	%Split	Aver.	Freq.1	Freq.2	%Split	Aver.	
0 ND	20.28	-	0.00	20.28	20.50	-	-	20.50	1.08%
1 ND	20.15	20.15	0.00	20.15	20.08	20.08	0.00	20.08	0.35%
2 ND	21.79	21.90	0.50	21.85	21.63	21.72	0.41	21.68	0.78%
3 ND	24.89	24.89	0.00	24.89	24.71	24.71	0.00	24.71	0.72%
4 ND	27.41	27.41	0.00	27.41	27.30	27.30	0.00	27.30	0.40%
5 ND	29.04	29.04	0.00	29.04	28.95	28.95	0.00	28.95	0.31%
6 ND	30.05	30.05	0.00	30.05	30.00	30.00	0.00	30.00	0.17%
7 ND	30.74	30.77	0.10	31.76	30.71	30.71	0.00	30.71	0.15%
8 ND	31.22	31.24	0.06	31.23	31.20	31.20	0.00	31.20	0.10%
9 ND	31.55	31.55	0.00	31.55	31.52	31.57	0.16	31.55	0.02%
10 ND	31.77	31.77	0.00	31.77	31.73	31.73	0.00	31.73	0.13%
11 ND	31.90	31.92	0.06	31.91	31.84	31.84	0.00	31.84	0.22%
12 ND	31.96	31.99	0.09	31.98	31.94	31.94	0.00	31.94	0.11%

Table A4-1. Flat Blisk and Swept Blisk 10degrees measurement results at 0rev/min

Flat Blisk and Swept 10deg predicted natural frequency (Hz) results at 0rev/min				
	Flat		Swept 10deg	
Mode	Freq.	% diff predicted vs. aver. Meas.	Freq.	% diff predicted vs. aver. meas.
0 ND	20.17	0.54%	20.17	1.61%
1 ND	19.83	1.59%	19.81	1.34%
2 ND	21.11	3.39%	21.05	2.91%
3 ND	24.82	0.28%	24.70	0.04%
4 ND	27.62	0.77%	27.44	0.51%
5 ND	29.31	0.93%	29.08	0.45%
6 ND	30.04	0.03%	30.12	0.40%
7 ND	31.09	2.11%	30.81	0.33%
8 ND	31.57	1.09%	31.28	0.26%
9 ND	31.90	1.11%	31.59	0.13%
10 ND	32.12	1.10%	31.80	0.22%
11 ND	32.23	1.00%	31.92	0.25%
12 ND	32.28	0.94%	31.96	0.06%

Table A4-2. Flat Blisk and Swept Blisk 10degrees predicted results at 0rev/min

* "Predicted" refers to SAMCEF code predicted data

Experimental results demonstrate that natural frequencies of some of the Flat Blisk modes are split by between 0.06-0.50% due to inherent mistuning of the bladed disc, although most of them are double (tuned). The natural frequencies have not changed very much after the first bending process, where the largest difference with the Flat Blisk is approx 1.1%. The predicted natural frequencies at 0rev/min compare well with those measured, with the average difference less than 1.6% for most of the modes for both blisks.

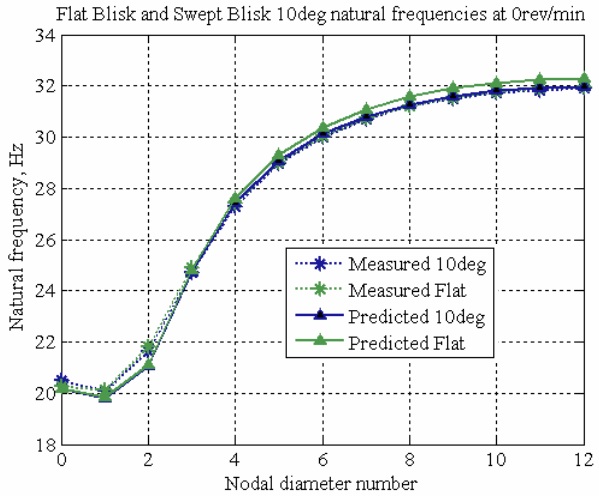

Fig. A4-2. Flat Blisk and Swept Blisk 10deg natural frequencies at rest

A4-3 Results after first bending process – Flat Blisk and Swept Blisk 10deg rotating conditions results

Experimental backward and forward modes natural frequencies have been obtained for Flat Blisk and Swept Blisk 10degrees configurations in the case of first 2ND mode pair for rotation speeds from 270rev/min to 900rev/min and 270rev/min to 450rev/min, respectively. Table A4-3 shows the rotating conditions results for the Flat Blisk from measurements and predicted data, which include the effects of Coriolis forces. As expected, the predictions demonstrate no split of tuned system natural frequencies due to Coriolis forces at any rotation speed, whereas the measured data indicate a small natural frequency split, generated by a small amount of mistuning inherently present in the testpiece.

Table A4-4 and Figs. A4-3 present the Flat Blisk and Swept Blisk 10degrees first 2ND natural frequency results.

Flat Blisk – Measured and predicted natural frequency (Hz) results first 2ND mode pair, 270-900rev/min								
	1.Measurements			2. Predictions				
Speed (rev/min)	BW (Hz)	FW (Hz)	% Split	BW (Hz)	FW (Hz)	% Split	Freq. No Cor	% diff. 1.& 2.
0	**21.79**	**21.90**	**0.50**	**21.11**	**21.11**	**0.00**	**21.11**	**-**
270	22.47	22.5	0.13	21.78	21.78	0.00	21.78	-
300	22.61	22.67	0.26	-	-	0.00	-	-
330	22.78	22.84	0.26	22.10	22.10	0.00	22.10	-
360	22.94	23.03	0.39	-	-	0.00	-	-
390	23.15	23.23	0.34	22.48	22.48	0.00	22.48	-
420	23.35	23.45	0.43	-	-	0.00	-	-
450	23.57	23.67	0.42	22.92	22.92	0.00	22.92	-
600	24.90	24.99	0.36	24.24	24.24	0.00	24.24	-
900	28.19	28.33	0.49	27.64	27.64	0.00	27.64	-
2500	-	-	-	53.30	53.30	0.00	53.30	-

Table A4-3. Flat Blisk measured and predicted results for the first 2ND mode pair

Swept Blisk 10deg – Measured and predicted natural frequency (Hz) results first 2ND mode pair, 270-450rev/min								
	1.Measurements			2. Predictions				
Speed (rev/min)	BW (Hz)	FW (Hz)	% Split	BW (Hz)	FW (Hz)	% Split	Freq. No Cor	% diff. 1.& 2.
0	**21.63**	**21.72**	**0.41**	**21.05**	**21.05**	**0.00**	**21.05**	**-**
270	22.23	22.42	0.85	21.62	21.78	0.76	21.70	10.59%
300	22.38	22.58	0.89	21.76	21.94	0.84	21.85	5.62%
330	22.53	22.74	0.92	21.91	22.11	0.92	22.01	0.00%
360	22.68	22.91	1.00	22.08	22.29	0.99	22.19	1.00%
390	22.84	23.11	1.17	22.27	22.50	1.07	22.38	8.55%
420	23.05	23.32	1.16	22.46	22.71	1.14	22.59	1.72%
450	23.25	23.53	1.19	22.67	22.94	1.18	22.80	1.00%
2500	-	-	-	51.46	53.34	3.52	52.39	-

Table A4-4. Swept Blisk 10deg measured and predicted results

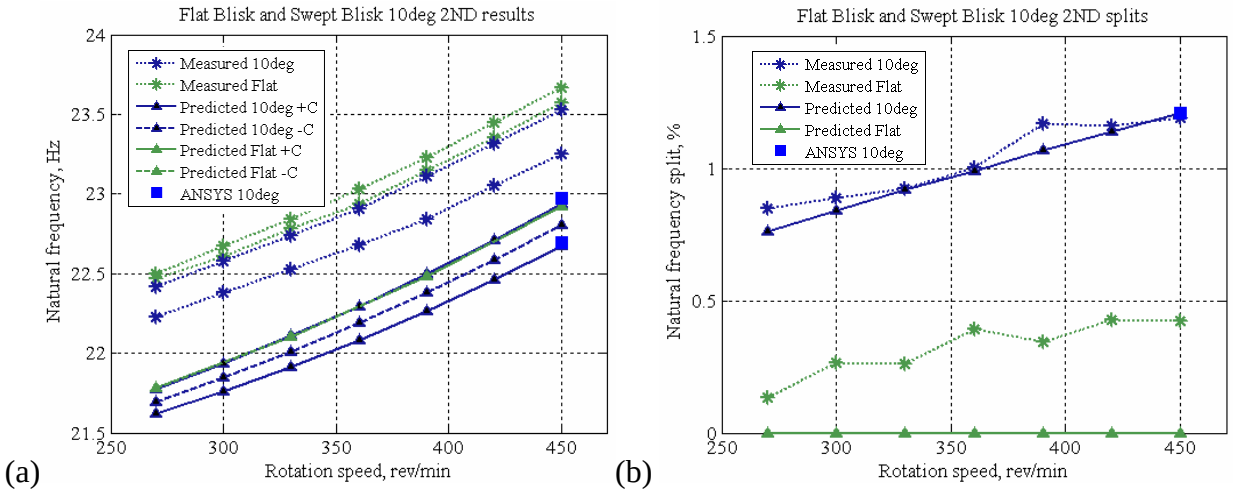

(a) (b)

Fig. A4-3. Flat Blisk and Swept Blisk 10deg first 2ND mode pair rotating conditions results: natural frequencies (a) and their splits (b)

It is immediately obvious that the measured natural frequencies are slightly higher compared with those predicted, even though a simple theoretical model updating procedure has been carried out by modifying the material properties. The emphasis of this work is on natural frequency splits rather than on specific natural frequencies, and, thus, no further attempts have been made to make any further improvements of the theoretical model.

Predicted and measured natural frequencies splits agree well, indicating a steady increase of the measured split for Swept Blisk 10deg from 0.85% at 270rev/min to 1.19% at 450rev/min, as shown in Table A4-5, which demonstrates a summary of the most important results from the above Tables. With the aim of brief numerical code verification, in addition to the SAMCEF predictions, ANSYS results for the Swept Blisk 10deg including both Coriolis and centrifugal forces were acquired at 450rev/min. The difference between the SAMCEF and ANSYS predicted natural frequency splits is 0.01%, which shows that two codes based on the same theory, predict very close natural frequency separations due to Coriolis forces. A disadvantage of using the ANSYS code compared to SAMCEF is the necessity of analysing a whole bladed disc model (in ANSYS) as opposed to a single cyclic sector (in SAMCEF), which dramatically increases the computation time.

		2ND mode pair	
	Speed, rev/min	Measured Split, %	Predicted Split, %
Flat Blisk	0	0.50%	0.00%
	270	0.13%	0.00%
	360	0.39%	0.00%
	450	0.42%	0.00%
	600	0.36%	0.00%
	900	0.49%	0.00%
Swept Blisk	0	0.41%	0.00%
10deg	270	0.85%	0.76%
	360	1.00%	0.99%
	450	1.19%	1.18%

Table A4-5. Selected Flat Blisk and Swept Blisk 10deg results

At this stage, it is still difficult to establish beyond any question whether the measured natural frequency split is due to Coriolis forces or inherent mistuning, as the first 2ND mode pair was found to be mistuned at 0rev/min by 0.5%. Thus, a subsequent additional blade sweeping to 15degrees will serve to clarify this issue and to provide a definitive answer.

A4-4 Results after second bending process

Swept Blisk 10deg and Swept Blisk 15deg measurements natural frequency (Hz) results at 0rev/min									
	Swept 10deg (S10)				Swept 15deg (S15)				% diff. in average measured: S10 vs. S15
Mode	Freq.1	Freq.2	%Split	Aver.	Freq.1	Freq.2	%Split	Aver.	
0 ND	20.50	-	-	20.50	20.49	-	-	20.49	0.05%
1 ND	20.08	20.08	0.00	20.08	20.02	20.18	0.79	20.10	0.10%
2 ND	21.63	21.72	0.41	21.68	21.60	21.68	0.36	21.64	0.19%
3 ND	24.71	24.71	0.00	24.71	24.70	24.70	0.00	24.70	0.04%
4 ND	27.30	27.30	0.00	27.30	27.31	27.31	0.00	27.31	0.04%
5 ND	28.95	28.95	0.00	28.95	28.97	28.97	0.00	28.97	0.07%
6 ND	30.00	30.00	0.00	30.00	30.04	30.04	0.00	30.04	0.13%
7 ND	30.71	30.71	0.00	30.76	30.76	30.76	0.00	30.76	0.00%
8 ND	31.20	31.20	0.00	31.20	31.24	31.24	0.00	31.24	0.13%
9 ND	31.52	31.57	0.16	31.55	31.57	31.57	0.00	31.57	0.06%
10 ND	31.73	31.73	0.00	31.73	31.77	31.77	0.00	31.77	0.13%
11 ND	31.84	31.84	0.00	31.84	31.94	31.94	0.00	31.94	0.31%
12 ND	31.94	31.94	0.00	31.94	32.22	32.22	0.00	32.22	0.88%

Table A4-6. Swept Blisk 10deg and Swept Blisk 15deg measurement results at 0rev/min

Swept Blisk 10deg and Swept Blisk 15deg predicted natural frequency (Hz) results at 0rev/min				
	Swept 10deg		Swept 15deg	
Mode	Freq.	% diff predicted vs. aver.meas.	Freq.	% diff predicted vs. aver.meas.
0 ND	20.17	1.61%	20.42	0.34%
1 ND	19.81	1.34%	20.15	0.25%
2 ND	21.05	2.91%	21.34	1.39%
3 ND	24.7	0.04%	24.94	0.97%
4 ND	27.44	0.51%	27.60	1.06%
5 ND	29.08	0.45%	29.19	0.76%
6 ND	30.12	0.40%	30.17	0.43%
7 ND	30.81	0.33%	30.83	0.23%
8 ND	31.28	0.26%	31.27	0.10%
9 ND	31.59	0.13%	31.57	0.00%
10 ND	31.8	0.22%	31.77	0.00%
11 ND	31.92	0.25%	31.88	0.19%
12 ND	31.96	0.06%	31.91	0.96%

Table A4-7. Swept Blisk 10deg and Swept Blisk 15deg predicted results at 0rev/min

Flat Blisk – Measured and predicted natural frequency (Hz) results								
first 3ND mode pair, 270-1300rev/min								
	1.Measurements			2. Predictions				
Speed (rev/min)	BW (Hz)	FW (Hz)	% Split	BW (Hz)	FW (Hz)	% Split	Freq. No Cor	% diff. 1.& 2.
0	**24.89**	**24.89**	**0.00**	**24.82**	**24.82**	**0.00**	**24.82**	**-**
270	25.52	25.53	0.04	25.45	25.45	0.00	25.45	-
330	-	-	-	25.76	25.76	0.00	25.76	-
390	-	-	-	26.12	26.12	0.00	26.12	-
450	26.60	26.62	0.08	26.54	26.54	0.00	26.54	-
600	-	-	-	27.80	27.80	0.00	27.80	-
700	28.89	28.92	0.10	28.79	28.79	0.00	28.79	-
800	-	-	-	29.90	29.90	0.00	29.90	-
900	-	-	-	31.10	31.10	0.00	31.10	-
1000	32.50	32.57	0.22	32.39	32.39	0.00	32.39	-
1100	-	-	-	33.76	33.76	0.00	33.76	-
1200	-	-	-	35.19	35.19	0.00	35.19	-
1300	-	-	-	36.68	36.68	0.00	36.68	-

Table A4-8. Flat Blisk measured and predicted results for the first 3ND mode pair

Swept Blisk 15deg – Measured and predicted natural frequency (Hz) results								
first 2ND mode pair, 270-900rev/min								
	1.Measurements			2. Predictions				
Speed (rev/min)	BW (Hz)	FW (Hz)	% Split	BW (Hz)	FW (Hz)	% Split	Freq. No Cor	% diff. 1.& 2.
0	**21.60**	**21.68**	**0.36**	**21.34**	**21.34**	**0.00**	**21.34**	**-**
270	22.11	22.38	1.21	21.78	22.13	1.64	21.95	35.54%
300	22.26	22.55	1.29	21.89	22.30	1.81	22.09	40.31%
330	22.36	23.70	1.50	22.03	22.47	1.96	22.25	30.67%
360	22.54	22.86	1.40	22.17	22.66	2.15	22.42	53.57%
390	22.69	23.06	1.61	22.33	22.86	2.30	22.60	42.86%
420	22.89	23.24	1.51	22.51	23.08	2.46	22.79	62.91%
450	23.07	23.47	1.70	22.69	23.30	2.61	23.00	53.53%
510	23.54	23.90	1.51	23.10	23.79	2.91	23.44	94.00%
600	24.23	24.67	1.78	23.79	24.61	3.34	24.20	87.64%
700	26.16	26.60	1.65	24.67	25.64	3.77	25.15	55.23%
800	26.17	26.58	1.54	25.65	26.76	4.15	26.20	116.15%
900	27.51	27.77	0.95	26.71	27.98	4.54	27.34	377.89%

Table A4-9. Swept Blisk 15deg measured and predicted results for the first 2ND mode pair

Swept Blisk 15deg – Measured and predicted natural frequency (Hz) results first 3ND mode pair, 270-1300rev/min								
	1.Measurements			2. Predictions				
Speed (rev/min)	BW (Hz)	FW (Hz)	% Split	BW (Hz)	FW (Hz)	% Split	Freq. No Cor	% diff. 1.& 2.
0	**24.70**	**24.70**	**0.00**	**24.94**	**24.94**	**0.00**	**24.94**	**-**
270	25.17	25.40	0.91	25.34	25.69	1.36	25.51	49.45%
300	25.24	25.61	1.05	25.46	25.85	1.51	25.65	43.81%
330	25.39	25.73	1.32	25.58	26.01	1.65	25.80	25.00%
360	25.5	25.93	1.66	25.72	26.19	1.79	25.96	78.31%
390	25.67	26.04	1.42	25.88	26.38	1.90	26.13	33.81%
420	25.84	26.22	1.45	26.04	26.59	2.07	26.31	42.76%
450	25.99	26.43	1.67	26.22	26.81	2.20	26.51	31.74%
480	26.20	26.64	1.65	26.41	27.04	2.33	26.72	41.21%
510	26.41	26.88	1.75	26.61	27.28	2.46	26.94	40.57%
540	26.64	27.13	1.81	26.82	27.53	2.58	27.17	42.54%
570	26.85	27.37	1.75	27.04	27.79	2.70	27.41	54.29%
600	27.07	27.54	1.71	27.27	28.07	2.85	27.67	66.67%
630	27.31	27.79	1.73	27.52	28.35	2.91	27.93	68.21%
660	27.56	28.06	1.78	27.77	28.65	3.07	28.20	72.47%
700	27.90	28.40	1.76	28.12	29.06	3.23	28.58	83.52%
800	28.86	29.28	1.43	29.07	30.15	3.58	29.61	150.35%
900	29.98	30.48	1.64	30.11	31.34	3.96	30.72	141.46%
1000	31.16	31.66	1.58	31.23	32.62	4.26	31.92	169.62%
1100	32.50	32.95	1.37	32.42	33.97	4.56	33.19	232.85%
1200	33.95	34.37	1.22	33.67	35.39	4.86	34.52	298.36%
1300	35.46	35.87	1.14	34.97	36.87	5.15	35.91	351.75%

Table A4-10. Swept Blisk 15deg measured and predicted results for the first 3ND mode pair

APPENDIX A5

A5-1 Description of basis of the lumped parameter mass model stiffness matrix incorporating cross-coupling stiffnesses

The lumped parameter mass model introduced in Chapter 5 presents an extension to its previous version, developed by Dye and Henry [7] 1969, by adding disc-to-disc and blade-to-disc cross-coupling stiffness terms, kdd_{xy} and kbd_{xy}, respectively, necessary for a demonstration of the effect of Coriolis forces. The following paragraphs describe the formation of representative sectors of the disc-to-disc and blade-to-disc stiffness matrices expressing this original feature.

For the sake of clarity, a 3-sector disc-only model, depicted in Fig. 5-1, is considered first with added disc-to-disc cross-coupling terms.

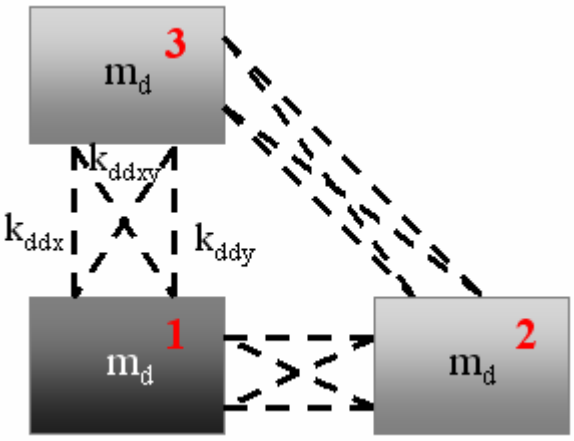

Fig. A5-1. 3-sector disc model example of disc-to-disc cross-coupling

The stiffness matrix for this simple system can be easily derived and is expressed as:

$$\begin{Bmatrix} F_{x1} \\ F_{y1} \\ F_{x2} \\ F_{y2} \\ F_{x3} \\ F_{y3} \end{Bmatrix} = \begin{bmatrix} k_{11}+k_{22} & k_{12} & k_{13} \\ k_{21} & k_{22}+k_{33} & k_{23} \\ k_{31} & k_{32} & k_{33}+k_{11} \end{bmatrix} \begin{Bmatrix} x_1 \\ y_1 \\ x_2 \\ y_2 \\ x_3 \\ y_3 \end{Bmatrix} \tag{A5-1}$$

Thus, the stiffness matrix connecting disc sector 1 to disc sector 2 is:

$$\begin{Bmatrix} F_1 \\ F_2 \end{Bmatrix} = \left[K_{c\_12} \right] \begin{Bmatrix} q_1 \\ q_2 \end{Bmatrix} = \begin{bmatrix} k_{11} & k_{12} \\ k_{21} & k_{22} \end{bmatrix} \begin{Bmatrix} q_1 \\ q_2 \end{Bmatrix} \tag{A5-2}$$

where $q_{1,2}=\begin{Bmatrix}x\\y\end{Bmatrix}_{1,2}$, $F_{1,2}=\begin{Bmatrix}F_x\\F_y\end{Bmatrix}_{1,2}$ and $k_{11}=\begin{bmatrix}kdd_x & kdd_{xy}\\ kdd_{yx} & kdd_y\end{bmatrix}$, $\underset{(2\times2)}{k_{11}}$ is a symmetric positive matrix, $kdd_{yx}=kdd_{xy}$.

Analogously, the stiffness matrix connecting disc sector 1' to its blade sector 2', shown in Fig. A5-2, can be written as:

$$\begin{Bmatrix}F_{1'}\\F_{2'}\end{Bmatrix}=\left[K_{c\_1'2'}\right]\begin{Bmatrix}q_{1'}\\q_{2'}\end{Bmatrix}=\begin{bmatrix}k_{1'1'} & k_{1'2'}\\ k_{2'1'} & k_{2'2'}\end{bmatrix}\begin{Bmatrix}q_{1'}\\q_{2'}\end{Bmatrix} \tag{A5-3}$$

where $q_{1',2'}=\begin{Bmatrix}x\\y\end{Bmatrix}_{1',2'}$, $F_{1',2'}=\begin{Bmatrix}F_x\\F_y\end{Bmatrix}_{1',2'}$ and $k_{1'1'}=\begin{bmatrix}kbd_x & kbd_{xy}\\ kbd_{yx} & kbd_y\end{bmatrix}$, $\underset{(2\times2)}{k_{1'1'}}$ is also a symmetric positive matrix, $kbd_{yx}=kbd_{xy}$.

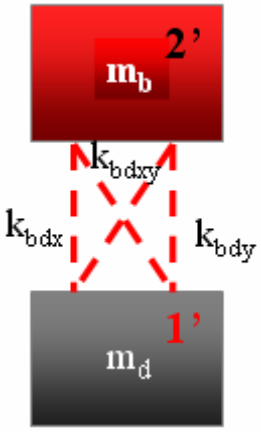

Fig. A5-2. Blade-to-disc cross-coupling

One possible way to express the sector cross-coupling in both cases is (Kabaila and Pulmano [134] 1979):

$$\begin{aligned}\left[K_{c\_12}\right]&=\begin{bmatrix}k_{11} & k_{12}\\ k_{21} & k_{22}\end{bmatrix}=\begin{bmatrix}k_{11} & k_{11}R^T\\ Rk_{11} & Rk_{11}R^T\end{bmatrix}\\ \left[K_{c\_1'2'}\right]&=\begin{bmatrix}k_{1'1'} & k_{1'2'}\\ k_{2'1'} & k_{2'2'}\end{bmatrix}=\begin{bmatrix}k_{1'1'} & k_{1'1'}R^T\\ Rk_{1'1'} & Rk_{1'1'}R^T\end{bmatrix}\end{aligned} \tag{A5-4}$$

where the transformation matrix is

$$R=\begin{bmatrix}\cos\alpha & \sin\alpha\\ -\sin\alpha & \cos\alpha\end{bmatrix} \tag{A5-5}$$

For the sake of convenience, a "coupling parameter", or parameter for the radial-tangential coupling, γ, is related to α, so that:

$$\alpha=\pi-\gamma \tag{A5-6}$$

Hence, using the standard trigonometric identities:

$$\begin{aligned}\cos(\pi-\gamma) &= -\cos\gamma \\ \sin(\pi-\gamma) &= \sin\gamma\end{aligned} \tag{A5-7}$$

the transformation matrix becomes

$$R = -\begin{bmatrix}\cos\gamma & -\sin\gamma \\ \sin\gamma & \cos\gamma\end{bmatrix} \tag{A5-8}$$

As mentioned above, the choice of the form of $\left[K_{c\_12}\right]$ and $\left[K_{c\_1'2'}\right]$ is not unique, but was found to satisfy the case with no disc-to-disc coupling ($\alpha=\pi$ or $\gamma=0$ and $kdd_{xy}=kdd_{yx}=0$), in which:

$$\left[K_{c\_12}\right] = \begin{bmatrix} kdd_x & 0 & -kdd_x & 0 \\ 0 & kdd_y & 0 & -kdd_y \\ -kdd_x & 0 & kdd_x & 0 \\ 0 & -kdd_y & 0 & kdd_y \end{bmatrix} \tag{A5-9}$$

as $k_{11} = \begin{bmatrix} kdd_x & 0 \\ 0 & kdd_y \end{bmatrix}$ and $R = \begin{bmatrix} -1 & 0 \\ 0 & -1 \end{bmatrix}$.

The total stiffness matrix of the system is obtained by summation of the corresponding disc-to-disc and blade-to-disc stiffness matrices.

APPENDIX A5

A5-2 Results for deliberately-mistuned 2gr/1gr Swept Blisk 15deg testpiece for the first 2ND mode pair

2ND results							
Speed (rev/min)	Measured Freq. (Hz) BW	Measured Freq. (Hz) FW	Measured Split, %	Predicted Freq. (Hz) BW	Predicted Freq. (Hz) FW	Predicted Split, %	Predicted Freq. (Hz) without C
0	21.44	21.54	0.44%	21.13	21.13	0.00%	21.13
60	21.45	21.57	0.53%	21.12	21.20	0.39%	21.16
120	21.53	21.68	0.67%	21.17	21.34	0.78%	21.25
180	21.66	21.84	0.82%	21.28	21.53	1.16%	21.41
270	21.96	22.21	1.13%	21.56	21.94	1.71%	21.75
360	22.40	22.69	1.28%	21.96	22.47	2.24%	22.21
450	NA	NA	-	22.49	23.12	2.74%	22.80
480	NA	NA	-	22.68	23.36	2.89%	23.02
540	NA	NA	-	23.12	23.88	3.20%	23.49
600	NA	NA	-	23.59	24.44	3.49%	24.01
660	NA	NA	-	24.11	25.05	3.76%	24.57
720	NA	NA	-	24.66	25.69	4.02%	25.17
780	NA	NA	-	25.25	26.38	4.27%	25.81
840	NA	NA	-	25.87	27.09	4.51%	26.47

Note: sinθtheta mistuning does not split 2ND mode pair

Table A5-1. Deliberately-mistuned 2gr/1gr Swept Blisk 15deg measured and predicted 2ND natural frequency splits

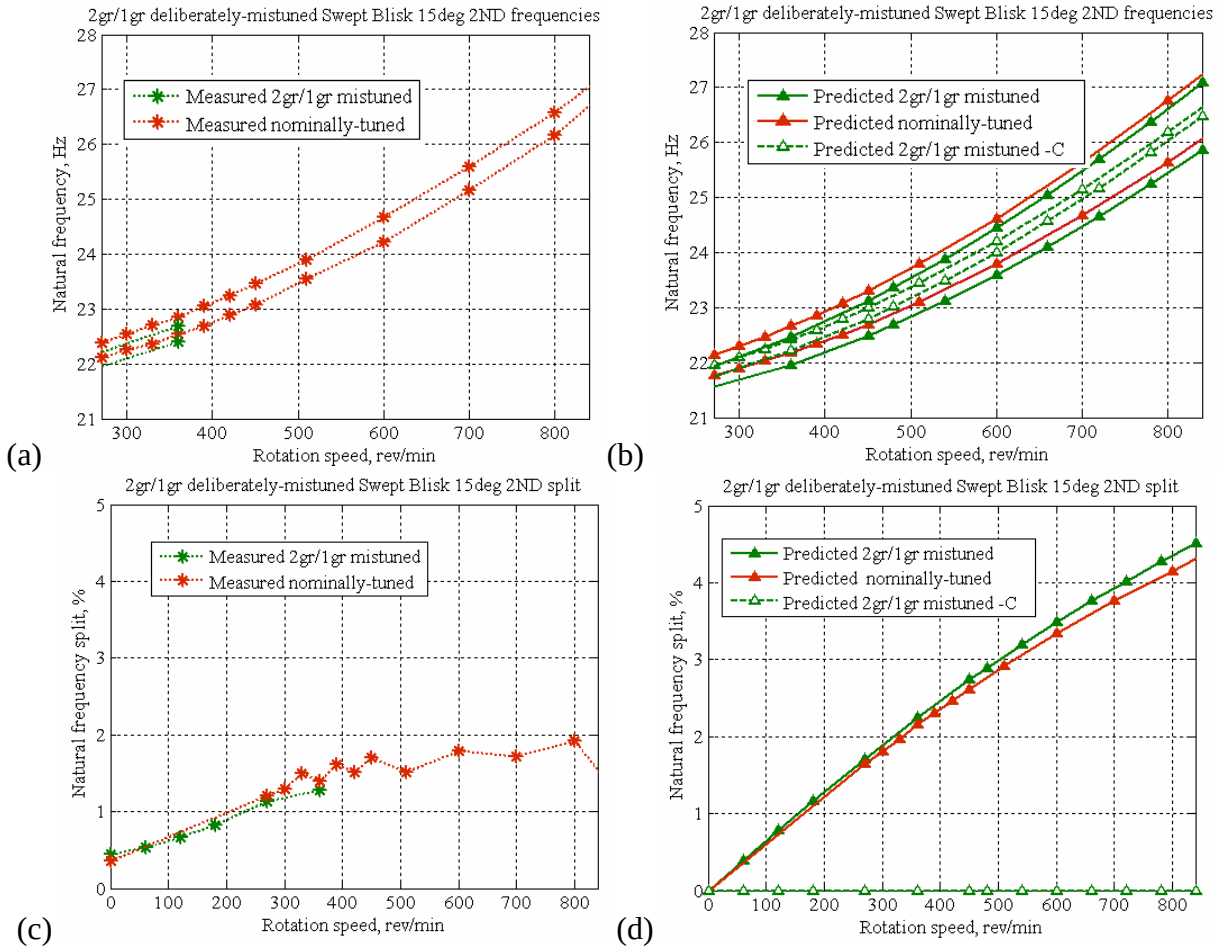

Fig. A5-3. Deliberately-mistuned 2gr/1gr Swept Blisk 15deg rotating conditions natural frequencies (a,b) and their splits (c,d) for first 2ND mode pair

APPENDIX A6-1

Fig. A6-1a – Dependency of forced response on frequency mistuning range - 3EO results

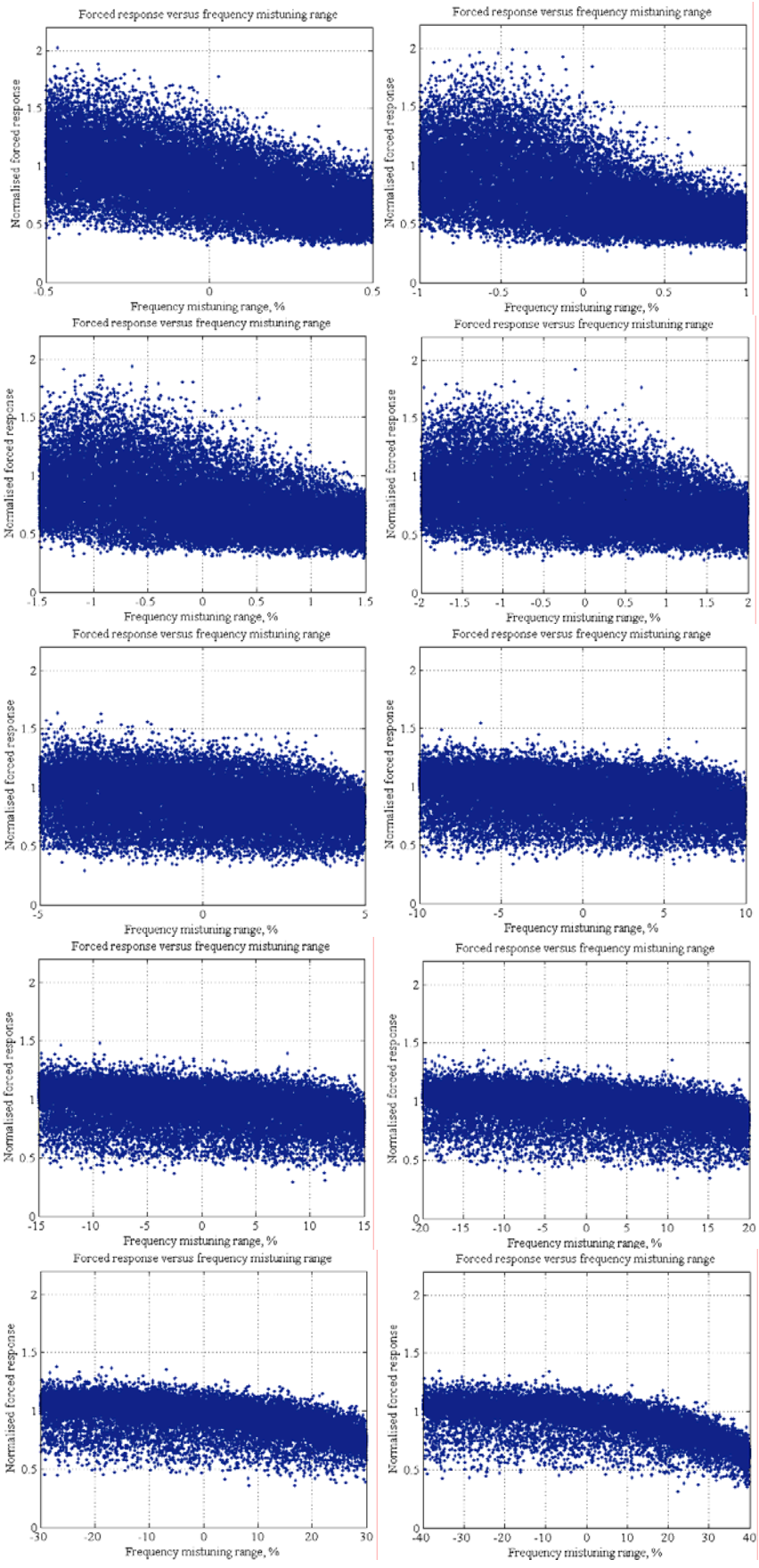

Fig. A6-1b – Dependency of forced response on frequency mistuning range - 6EO results

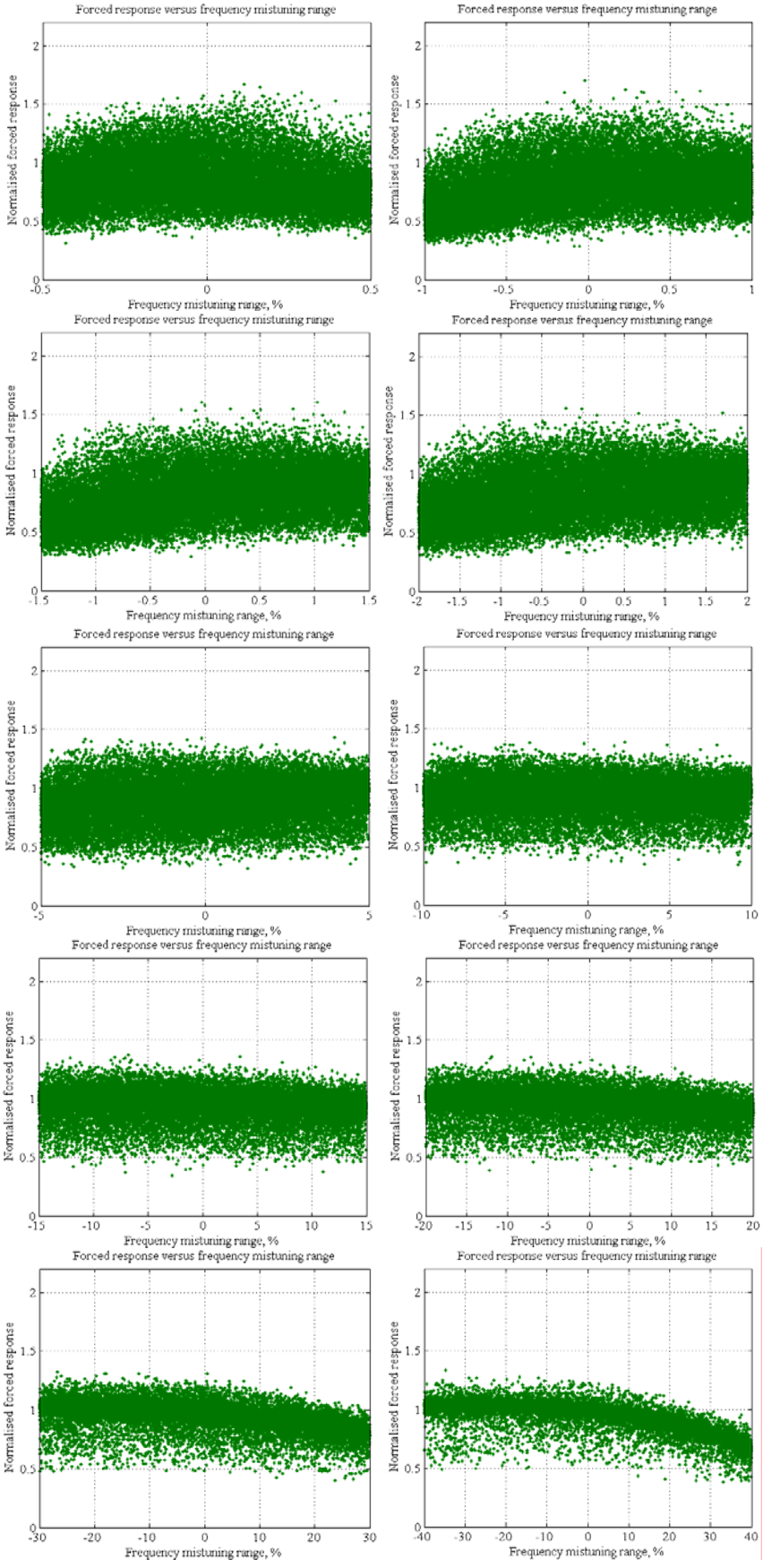

Fig. A6-1c – Dependency of forced response on frequency mistuning range - 13EO results

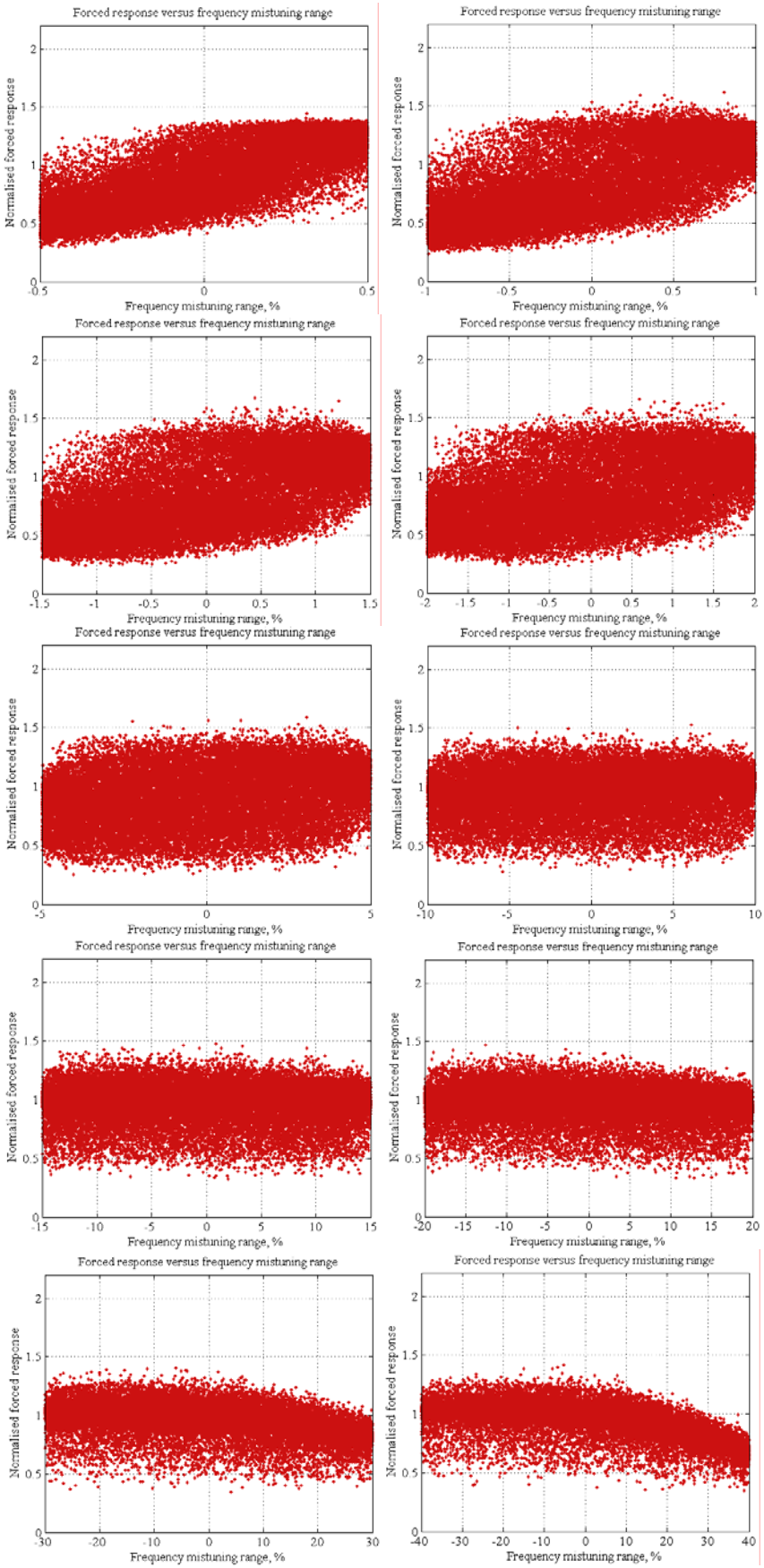

APPENDIX A6-2

Description of hypothetical theoretical distributions

The Gaussian distribution is the most frequently used theoretical function as an approximation to diverse physical phenomena. The theoretical justification for role of the Gaussian distribution is the central limit theorem concerned with large samples. Although this distribution may have some serious drawbacks in representing a certain range of physical variables, in general, it provides a substantially fair model for a random variable when: (i) there is a strong tendency for the variable to take a central value; (ii) positive and negative deviations from the central value are equally likely; and (iii) the frequency of deviations falls off rapidly as the deviations become larger.

The Gaussian probability density function is given as:

$$f\left(x;\mu,\sigma\right)=\frac{1}{\sigma\sqrt{2\pi}}\exp\left[-\frac{\left(x-\mu\right)^2}{2\sigma^2}\right] \tag{A6-1}$$

where $-\infty < x < \infty,\ -\infty < \mu < \infty,\ \sigma > 0$, μ and σ are location and scale parameters respectively, which can be shown to represent the mean and standard deviation of the Gaussian distribution, respectively. All "bell-shape curves" are symmetric about the mean and have the same shape – that is, the distribution has no shape parameter.

The Gaussian cumulative density function is determined as:

$$F\left(x;\mu,\sigma\right)=\int_{-\infty}^{x} f\left(z\right)dz=\Phi\left(\frac{x-\mu}{\sigma}\right)+\frac{1}{2} \tag{A6-2}$$

where $\Phi\left(y\right)$ is the Laplace's integral obtained from the tables.

If two independent variables y_1 and y_2 are independent from each other and normally distributed with equal variance and zero mean, then the variable $x=\sqrt{y_1^2+y_2^2}$ will follow the Rayleigh probability density function:

$$f\left(x;\sigma\right)=\begin{cases}\dfrac{x}{\sigma^2}\exp\left[-\dfrac{x^2}{2\sigma^2}\right], & x\geq 0,\ \ \sigma>0,\\ 0 & \textit{elsewhere}\end{cases} \tag{A6-3}$$

where σ is the scale parameter.

The Rayleigh cumulative distribution can be evaluated as:

$$F(x;\sigma)=\begin{cases}1-\exp\left[-\dfrac{x^2}{2\sigma^2}\right], & x\geq 0\\ 0 & \textit{elsewhere}\end{cases} \tag{A6-4}$$

The Gamma distribution is used to describe random variables bounded at one end. Its probability density function is:

$$f(x;\eta,\lambda)=\begin{cases}\dfrac{\lambda^{\eta}}{\Gamma(\eta)}x^{\eta-1}\exp(-\lambda x), & x\geq 0,\ \ \lambda>0,\ \ \eta>0\\ 0 & \textit{elsewhere}\end{cases} \tag{A6-5}$$

where η is the shape parameter, λ is the scale parameter and $\Gamma(\eta)$ is the well known Gamma function:

$$\Gamma(\eta)=\int_0^{\infty}x^{\eta-1}\exp(-x)\,dx \tag{A6-6}$$

Many phenomena that cannot be justified theoretically as Gamma variates have been found empirically to be well approximated by this model. The wide assortment of Gamma distribution shapes accounts for its recurrent use.

The Gamma cumulative distribution is known as the "incomplete Gamma function" and is formulated as:

$$F(x;\eta,\lambda)=\begin{cases}\dfrac{\lambda^{\eta}}{\Gamma(\eta)}\displaystyle\int_0^{x}t^{\eta-1}\exp(-\lambda t)\,dt, & x\geq 0\\ 0 & \textit{elsewhere}\end{cases} \tag{A6-7}$$

The Beta distribution is typically used to model the distribution of order statistics. Because of its many shapes, it is often employed to represent a large number of physical variables whose values are restricted to an identifiable interval, for example, the processes with natural lower and upper limits. The Beta probability density function is defined as:

$$f(x;\gamma,\eta)=\begin{cases}\dfrac{\Gamma(\gamma+\eta)}{\Gamma(\gamma)\Gamma(\eta)}x^{\gamma-1}(1-x)^{\eta-1}, & 0\leq x\leq 1,\ \ \gamma>0,\ \ \eta>0\\ 0 & \textit{elsewhere}\end{cases} \tag{A6-8}$$

where γ and η both affect the distribution shape.

The Beta cumulative distribution is known as the "incomplete Beta function":

$$F\left(x;\gamma,\eta\right)=\begin{cases}0, & x<0\\ \dfrac{\Gamma\left(\gamma+\eta\right)}{\Gamma\left(\gamma\right)\Gamma\left(\eta\right)}\displaystyle\int_0^x t^{\gamma-1}\left(1-t\right)^{\eta-1}dt, & 0\le x\le 1,\\ 1, & x>1\end{cases} \tag{A6-9}$$

When $\gamma=\eta=1$, the Beta distribution reduces to:

$$f\left(x;1,1\right)=\begin{cases}1, & 0\le x\le 1,\\ 0 & elsewhere\end{cases} \tag{A6-10}$$

In generalising this probability density function to the interval $\left(\vartheta_1,\vartheta_2\right)$, we obtain:

$$f\left(x;\vartheta_1,\vartheta_2\right)=\begin{cases}\dfrac{1}{\vartheta_2-\vartheta_1}, & \vartheta_1\le x\le\vartheta_2,\\ 0 & elsewhere\end{cases} \tag{A6-11}$$

which is the uniform or rectangular distribution, whose probability density function is a horizontal line.

The uniform cumulative density function is given by:

$$F\left(x;\vartheta_1,\vartheta_2\right)=\begin{cases}0, & x<\vartheta_1\\ \dfrac{x-\vartheta_1}{\vartheta_2-\vartheta_1}, & x\in\left[\vartheta_1,\vartheta_2\right]\\ 1, & x>\vartheta_2\end{cases} \tag{A6-12}$$

The Weibull distribution is one of the most widely used lifetime distributions in reliability engineering. It is a versatile distribution that can take on the characteristics of other types of distributions, based on the value of the shape parameter. The Weibull probability density function is defined as follows

$$f\left(t;\eta,\sigma\right)=\begin{cases}\dfrac{\eta}{\sigma}\left(\dfrac{t}{\sigma}\right)^{\eta-1}\exp\left[-\left(\dfrac{t}{\sigma}\right)^{\eta}\right], & t\ge 0,\ \ \sigma>0,\ \ \eta>0,\\ 0 & elsewhere\end{cases} \tag{A6-13}$$

where σ is the scale parameter and η is the shape parameter.

The cumulative Weibull distribution is obtained as:

$$F\left(t;\eta,\sigma\right)=\int_0^t\frac{\eta}{\sigma}\left(\frac{y}{\sigma}\right)^{\eta-1}\exp\left[-\left(\frac{y}{\sigma}\right)^{\eta}\right]dy=1-\exp\left[-\left(\frac{t}{\sigma}\right)^{\eta}\right],\quad t\ge 0 \tag{A6-14}$$

Failure of the system may often be connected to the extreme phenomena that reside in the tails of probability distributions associated with either the smallest or largest values. The precise statistical distribution of these extreme events depends on the sample size and the nature of initial distribution. A sufficiently large sample size

permits use of general asymptotic distributions results for both maximum and minimum values that rely on some limited assumptions concerning the initial distribution [17]. The extreme value distributions are customarily considered to comprise the following distribution families:

1. Type I asymptotic distribution or the "Gumbel-type distribution";
2. Type II asymptotic distribution or the "Frechet-type distribution";
3. Type III asymptotic distribution or the "Weibull-type distribution".

Of all these families, the Type I is the most commonly referred to in association with the extreme values, and will be used in this study. A Type I asymptotic distribution for maximum (minimum) values is the limiting model as the sample size n approaches infinity for the distribution of maximum (minimum) of n independent values from initial distribution whose right (left) tail is unbounded and which is the "exponential type" for increasing (decreasing) values: that is, the initial cumulative distribution function approaches unity with increasing values at least as rapidly as the exponential distribution function. The probability density functions for the Type I asymptotic distributions for the largest and smallest values respectively, which are the mirror images of one another, are defined as:

$$f\left(t;\mu,\sigma\right)=\frac{1}{\sigma}\exp\left[-\frac{1}{\sigma}\left(t-\mu\right)-e^{-\frac{1}{\sigma}(t-\mu)}\right],\quad -\infty<t<\infty,\ -\infty<\mu<\infty,\ \sigma>0 \quad \text{(A6-15)}$$

$$f\left(t;\mu,\sigma\right)=\frac{1}{\sigma}\exp\left[\frac{1}{\sigma}\left(t-\mu\right)-e^{\frac{1}{\sigma}(t-\mu)}\right],\quad -\infty<t<\infty,\ -\infty<\mu<\infty,\ \sigma>0 \quad \text{(A6-16)}$$

The values of the largest and smallest element Type I asymptotic probability density functions and the corresponding cumulative probability distributions respectively are:

$$F\left(y;0,1\right)=\exp\left[-e^{-y}\right]\quad \textit{and}\quad F\left(y\right)=1-\exp\left[-e^{-y}\right] \qquad \text{(A6-17)}$$

where the standardised variate is $y=\dfrac{\left(t-\mu\right)}{\sigma}$.

APPENDIX A6-3

Table A6-3 – Statistical hypothesis tests results for forced response characteristics obtained for all blades over 1,000 bladed discs

Frequency mistuning range and EO	Goodness-of-fit test analysis, 26,000 samples				
	Best-fit distribution	Test statistic	Cutoff	Conclusion	Goodness-of-fit test
±0.5%, 3EO	Gamma	2.62	1.63	NA	Kolmogorov-Smirnov
	"	399.00	53.40	NA	Chi-square
±0.5%, 6EO	Gamma	3.12	1.63	NA	Kolmogorov-Smirnov
	"	301.30	42.60	NA	Chi-square
±0.5%, 13EO	Weibull	10.90	1.63	NA	Kolmogorov-Smirnov
	"	6060.00	53.50	NA	Chi-square
±1.0%, 3EO	Gamma	8.44	1.63	NA	Kolmogorov-Smirnov
	"	1770.00	53.50	NA	Chi-square
±1.0%, 6EO	Gamma	3.64	1.63	NA	Kolmogorov-Smirnov
	"	327.00	53.50	NA	Chi-square
±1.0%, 13EO	Weibull	10.70	1.63	NA	Kolmogorov-Smirnov
	"	5310.00	53.40	NA	Chi-square
±1.5%, 3EO	Gamma	5.32	1.63	NA	Kolmogorov-Smirnov
	"	898.00	52.20	NA	Chi-square
±1.5%, 6EO	Gaussian	4.36	1.63	NA	Kolmogorov-Smirnov
	"	630.00	52.20	NA	Chi-square
±1.5%, 13EO	Weibull	9.68	1.63	NA	Kolmogorov-Smirnov
	"	3980.00	53.50	NA	Chi-square

Frequency mistuning range and EO	Goodness-of-fit test analysis, 26,000 samples				
	Best-fit distribution	Test statistic	Cutoff	Conclusion	Goodness-of-fit test
±2.0%, 3EO	Gamma	3.35	1.63	NA	Kolmogorov-Smirnov
	"	445.00	82.20	NA	Chi-square
±2.0%, 6EO	Gaussian	4.00	1.63	NA	Kolmogorov-Smirnov
	"	582.00	53.40	NA	Chi-square
±2.0%, 13EO	Weibull	8.35	1.63	NA	Kolmogorov-Smirnov
	"	2710.00	53.50	NA	Chi-square
±5.0%, 3EO	Weibull	3.85	1.63	NA	Kolmogorov-Smirnov
	"	619.00	49.60	NA	Chi-square
±5.0%, 6EO	Weibull	2.21	1.63	NA	Kolmogorov-Smirnov
	"	319.00	52.20	NA	Chi-square
±5.0%, 13EO	Weibull	5.64	1.63	NA	Kolmogorov-Smirnov
	"	1100.00	53.50	NA	Chi-square
±10.0%, 3EO	Weibull	3.65	1.63	NA	Kolmogorov-Smirnov
	"	692.00	48.30	NA	Chi-square
±10.0%, 6EO	Weibull	9.00	1.63	NA	Kolmogorov-Smirnov
	"	2080.00	50.90	NA	Chi-square
±10.0%, 13EO	Extreme	4.14	1.63	NA	Kolmogorov-Smirnov
	"	1110.00	49.60	NA	Chi-square
±15.0%, 3EO	Extreme	4.37	1.63	NA	Kolmogorov-Smirnov
	"	1580.00	46.90	NA	Chi-square
±15.0%, 6EO	Extreme	12.50	1.63	NA	Kolmogorov-Smirnov
	"	5370.00	48.30	NA	Chi-square
±15.0%, 13EO	Weibull	6.97	1.63	NA	Kolmogorov-Smirnov
	"	1060.00	52.20	NA	Chi-square

Frequency mistuning range and EO	Goodness-of-fit test analysis, 26,000 samples				
	Best-fit distribution	Test statistic	Cutoff	Conclusion	Goodness-of-fit test
±20.0%, 3EO	Weibull	4.00	1.63	NA	Kolmogorov-Smirnov
	"	1280.00	46.90	NA	Chi-square
±20.0%, 6EO	Weibull	10.60	1.60	NA	Kolmogorov-Smirnov
	"	4250.00	45.60	NA	Chi-square
±20.0%, 13EO	Weibull	8.10	1.60	NA	Kolmogorov-Smirnov
	"	1530.00	49.60	NA	Chi-square
±30.0%, 3EO	Extreme	6.20	1.60	NA	Kolmogorov-Smirnov
	"	2090.00	48.30	NA	Chi-square
±30.0%, 6EO	Weibull	9.36	1.60	NA	Kolmogorov-Smirnov
	"	3180.00	45.60	NA	Chi-square
±30.0%, 13EO	Weibull	6.61	1.60	NA	Kolmogorov-Smirnov
	"	1460.00	49.60	NA	Chi-square
±40.0%, 3EO	Extreme	11.40	1.60	NA	Kolmogorov-Smirnov
	"	4650.00	49.60	NA	Chi-square
±40.0%, 6EO	Extreme	13.80	1.60	NA	Kolmogorov-Smirnov
	"	5730.00	48.30	NA	Chi-square
±40.0%, 13EO	Extreme	7.94	1.60	NA	Kolmogorov-Smirnov
	"	2990.00	46.90	NA	Chi-square

APPENDIX A6-4

Table A6-4 – Statistical hypothesis tests results for maximum forced response characteristics obtained for each bladed disc

Frequency mistuning range and EO	Goodness-of-fit test analysis, 1,000 samples				
	Best-fit distribution	Test statistic	Cutoff	Conclusion	Goodness-of-fit test
±0.5%, 3EO	Gamma	1.16	1.63	A	Kolmogorov-Smirnov
	"	21.48	32.00	A	Chi-square
±0.5%, 6EO	Gamma	1.10	1.63	A	Kolmogorov-Smirnov
	"	29.33	34.81	A	Chi-square
±0.5%, 13EO	Gamma	0.67	1.63	A	Kolmogorov-Smirnov
	"	22.23	30.58	A	Chi-square
±1.0%, 3EO	Gamma	0.94	1.63	A	Kolmogorov-Smirnov
	"	41.73	36.19	NA	Chi-square
±1.0%, 6EO	Gamma	1.29	1.63	A	Kolmogorov-Smirnov
	"	47.69	30.58	NA	Chi-square
±1.0%, 13EO	Gamma	2.39	1.63	NA	Kolmogorov-Smirnov
	"	79.07	29.14	NA	Chi-square
±1.5%, 3EO	Gamma	1.50	1.63	A	Kolmogorov-Smirnov
	"	38.83	33.41	NA	Chi-square
±1.5%, 6EO	Gamma	1.31	1.63	A	Kolmogorov-Smirnov
	"	34.20	32.00	NA	Chi-square
±1.5%, 13EO	Gamma	1.79	1.63	NA	Kolmogorov-Smirnov
	"	95.01	30.58	NA	Chi-square

Frequency mistuning range and EO	Goodness-of-fit test analysis, 1,000 samples				
	Best-fit distribution	Test statistic	Cutoff	Conclusion	Goodness-of-fit test
±2.0%, 3EO	Gamma	0.97	1.63	A	Kolmogorov-Smirnov
	"	24.84	32.00	A	Chi-square
±2.0%, 6EO	Gamma	1.12	1.63	A	Kolmogorov-Smirnov
	"	29.45	33.41	A	Chi-square
±2.0%, 13EO	Gamma	1.67	1.63	NA	Kolmogorov-Smirnov
	"	98.12	33.41	NA	Chi-square
±5.0%, 3EO	Gamma	1.65	1.63	NA	Kolmogorov-Smirnov
	"	90.11	32.00	NA	Chi-square
±5.0%, 6EO	Gamma	1.19	1.63	A	Kolmogorov-Smirnov
	"	39.67	34.81	NA	Chi-square
±5.0%, 13EO	Gamma	0.59	1.63	A	Kolmogorov-Smirnov
	"	21.03	33.41	A	Chi-square
±10.0%, 3EO	Gamma	2.36	1.63	NA	Kolmogorov-Smirnov
	"	117.59	26.22	NA	Chi-square
±10.0%, 6EO	Gamma	1.54	1.63	A	Kolmogorov-Smirnov
	"	53.14	34.81	NA	Chi-square
±10.0%, 13EO	Gamma	1.07	1.63	A	Kolmogorov-Smirnov
	"	33.13	32.00	NA	Chi-square
±15.0%, 3EO	Gamma	2.43	1.63	NA	Kolmogorov-Smirnov
	"	127.02	27.69	NA	Chi-square
±15.0%, 6EO	Gamma	0.76	1.63	A	Kolmogorov-Smirnov
	"	33.42	33.41	NA	Chi-square
±15.0%, 13EO	Gamma	1.88	1.63	NA	Kolmogorov-Smirnov
	"	72.77	33.41	NA	Chi-square

Frequency mistuning range and EO	Goodness-of-fit test analysis, 1,000 samples				
	Best-fit distribution	Test statistic	Cutoff	Conclusion	Goodness-of-fit test
±20.0%, 3EO	Gamma	2.20	1.63	NA	Kolmogorov-Smirnov
	"	132.55	29.19	NA	Chi-square
±20.0%, 6EO	Gamma	1.14	1.63	A	Kolmogorov-Smirnov
	"	45.92	33.41	NA	Chi-square
±20.0%, 13EO	Gamma	1.27	1.63	A	Kolmogorov-Smirnov
	"	49.26	32.00	NA	Chi-square
±30.0%, 3EO	Gamma	1.55	1.63	A	Kolmogorov-Smirnov
	"	75.29	29.14	NA	Chi-square
±30.0%, 6EO	Gamma	2.11	1.63	NA	Kolmogorov-Smirnov
	"	119.80	33.41	NA	Chi-square
±30.0%, 13EO	Gamma	0.83	1.63	A	Kolmogorov-Smirnov
	"	29.77	33.41	A	Chi-square
±40.0%, 3EO	Gamma	1.87	1.63	NA	Kolmogorov-Smirnov
	"	124.67	30.58	NA	Chi-square
±40.0%, 6EO	Gamma	2.72	1.63	NA	Kolmogorov-Smirnov
	"	183.70	29.14	NA	Chi-square
±40.0%, 13EO	Gamma	1.66	1.63	NA	Kolmogorov-Smirnov
	"	45.74	32.00	NA	Chi-square

APPENDIX A6-5

Table A6-5 – Statistical hypothesis tests results for mean forced response characteristics obtained for each bladed disc

Frequency mistuning range and EO	Goodness-of-fit test analysis, 1,000 samples				
	Best-fit distribution	Test statistic	Cutoff	Conclusion	Goodness-of-fit test
±0.5%, 3EO	Gamma	0.62	1.63	A	Kolmogorov-Smirnov
	"	11.44	33.41	A	Chi-square
±0.5%, 6EO	Beta	0.85	1.63	A	Kolmogorov-Smirnov
	"	27.93	32.00	A	Chi-square
±0.5%, 13EO	Beta	0.64	1.63	A	Kolmogorov-Smirnov
	"	10.87	27.69	A	Chi-square
±1.0%, 3EO	Gamma	0.72	1.63	A	Kolmogorov-Smirnov
	"	12.19	32.00	A	Chi-square
±1.0%, 6EO	Gaussian	0.66	1.63	A	Kolmogorov-Smirnov
	"	15.32	33.91	A	Chi-square
±1.0%, 13EO	Beta	0.83	1.63	A	Kolmogorov-Smirnov
	"	10.23	33.91	A	Chi-square
±1.5%, 3EO	Gamma	0.43	1.63	A	Kolmogorov-Smirnov
	"	19.22	30.56	A	Chi-square
±1.5%, 6EO	Beta	0.59	1.63	A	Kolmogorov-Smirnov
	"	17.07	32.00	A	Chi-square
±1.5%, 13EO	Beta	0.63	1.63	A	Kolmogorov-Smirnov
	"	17.08	36.19	A	Chi-square
±2.0%, 3EO	Gaussian	0.49	1.63	A	Kolmogorov-Smirnov
	"	20.00	32.00	A	Chi-square
±2.0%, 6EO	Gamma	0.58	1.63	A	Kolmogorov-Smirnov
	"	23.24	34.81	A	Chi-square
±2.0%, 13EO	Beta	0.49	1.63	A	Kolmogorov-Smirnov
	"	15.20	34.81	A	Chi-square
±5.0%, 3EO	Beta	0.85	1.63	A	Kolmogorov-Smirnov
	"	12.96	33.41	A	Chi-square
±5.0%, 6EO	Beta	0.44	1.63	A	Kolmogorov-Smirnov
	"	6.83	32.00	A	Chi-square
±5.0%, 13EO	Beta	0.86	1.63	A	Kolmogorov-Smirnov
	"	26.44	36.19	A	Chi-square
±10.0%, 3EO	Beta	0.67	1.63	A	Kolmogorov-Smirnov
	"	12.60	32.00	A	Chi-square
±10.0%, 6EO	Beta	0.54	1.63	A	Kolmogorov-Smirnov
	"	12.37	30.58	A	Chi-square
±10.0%, 13EO	Gaussian	0.95	1.63	A	Kolmogorov-Smirnov
	"	26.49	36.19	A	Chi-square
±15.0%, 3EO	Beta	0.87	1.63	A	Kolmogorov-Smirnov
	"	18.93	30.58	A	Chi-square
±15.0%, 6EO	Beta	1.04	1.63	A	Kolmogorov-Smirnov
	"	23.09	33.41	A	Chi-square
±15.0%, 13EO	Beta	0.86	1.63	A	Kolmogorov-Smirnov
	"	22.86	32.00	A	Chi-square

Frequency mistuning range and EO	Goodness-of-fit test analysis, 1,000 samples				
	Best-fit distribution	Test statistic	Cutoff	Conclusion	Goodness-of-fit test
±20.0%, 3EO	Beta	0.74	1.63	A	Kolmogorov-Smirnov
	"	14.60	33.41	A	Chi-square
±20.0%, 6EO	Beta	0.76	1.63	A	Kolmogorov-Smirnov
	"	20.69	33.41	A	Chi-square
±20.0%, 13EO	Gaussian	0.88	1.63	A	Kolmogorov-Smirnov
	"	28.29	33.41	A	Chi-square
±30.0%, 3EO	Gaussian	0.87	1.63	A	Kolmogorov-Smirnov
	"	22.71	33.41	A	Chi-square
±30.0%, 6EO	Gaussian	0.97	1.63	A	Kolmogorov-Smirnov
	"	25.18	36.19	A	Chi-square
±30.0%, 13EO	Gaussian	1.34	1.63	A	Kolmogorov-Smirnov
	"	28.90	33.41	A	Chi-square
±40.0%, 3EO	Gaussian	1.02	1.63	A	Kolmogorov-Smirnov
	"	16.28	30.58	A	Chi-square
±40.0%, 6EO	Gaussian	0.87	1.63	A	Kolmogorov-Smirnov
	"	26.23	36.19	A	Chi-square
±40.0%, 13EO	Gaussian	0.98	1.63	A	Kolmogorov-Smirnov
	"	22.07	32.00	A	Chi-square

APPENDIX A6-6

Table A6-6 – Statistical hypothesis tests results for minimum forced response characteristics obtained for each bladed disc

Frequency mistuning range and EO	Goodness-of-fit test analysis, 1,000 samples				
	Best-fit distribution	Test statistic	Cutoff	Conclusion	Goodness-of-fit test
±0.5%, 3EO	Gamma	0.89	1.63	A	Kolmogorov-Smirnov
	"	27.86	34.81	A	Chi-square
±0.5%, 6EO	Beta	0.57	1.63	A	Kolmogorov-Smirnov
	"	8.98	30.58	A	Chi-square
±0.5%, 13EO	Gamma	0.49	1.63	A	Kolmogorov-Smirnov
	"	18.45	33.41	A	Chi-square
±1.0%, 3EO	Beta	0.37	1.63	A	Kolmogorov-Smirnov
	"	11.33	33.41	A	Chi-square
±1.0%, 6EO	Gaussian	0.61	1.63	A	Kolmogorov-Smirnov
	"	10.51	34.81	A	Chi-square
±1.0%, 13EO	Gamma	0.78	1.63	A	Kolmogorov-Smirnov
	"	20.57	33.41	A	Chi-square
±1.5%, 3EO	Gaussian	0.75	1.63	A	Kolmogorov-Smirnov
	"	23.95	34.81	A	Chi-square
±1.5%, 6EO	Gaussian	0.81	1.63	A	Kolmogorov-Smirnov
	"	22.38	36.19	A	Chi-square
±1.5%, 13EO	Gamma	0.51	1.63	A	Kolmogorov-Smirnov
	"	17.45	36.19	A	Chi-square

Frequency mistuning range and EO	Goodness-of-fit test analysis, 1,000 samples				
	Best-fit distribution	Test statistic	Cutoff	Conclusion	Goodness-of-fit test
±2.0%, 3EO	Beta	0.48	1.63	A	Kolmogorov-Smirnov
	"	17.32	36.19	A	Chi-square
±2.0%, 6EO	Gaussian	0.79	1.63	A	Kolmogorov-Smirnov
	"	19.19	36.19	A	Chi-square
±2.0%, 13EO	Gaussian	0.81	1.63	A	Kolmogorov-Smirnov
	"	15.70	33.41	A	Chi-square
±5.0%, 3EO	Gamma	0.65	1.63	A	Kolmogorov-Smirnov
	"	15.59	34.81	A	Chi-square
±5.0%, 6EO	Beta	0.98	1.63	A	Kolmogorov-Smirnov
	"	35.13	36.19	A	Chi-square
±5.0%, 13EO	Gaussian	0.75	1.63	A	Kolmogorov-Smirnov
	"	23.10	36.19	A	Chi-square
±10.0%, 3EO	Gaussian	1.03	1.63	A	Kolmogorov-Smirnov
	"	30.49	36.19	A	Chi-square
±10.0%, 6EO	Gaussian	0.56	1.63	A	Kolmogorov-Smirnov
	"	21.97	36.19	A	Chi-square
±10.0%, 13EO	Gaussian	0.58	1.63	A	Kolmogorov-Smirnov
	"	27.08	34.81	A	Chi-square
±15.0%, 3EO	Gamma	0.88	1.63	A	Kolmogorov-Smirnov
	"	25.49	32.00	A	Chi-square
±15.0%, 6EO	Gaussian	0.84	1.63	A	Kolmogorov-Smirnov
	"	26.12	34.81	A	Chi-square
±15.0%, 13EO	Gamma	0.56	1.63	A	Kolmogorov-Smirnov
	"	21.04	34.81	A	Chi-square

Frequency mistuning range and EO	Goodness-of-fit test analysis, 1,000 samples				
	Best-fit distribution	Test statistic	Cutoff	Conclusion	Goodness-of-fit test
±20.0%, 3EO	Weibull	1.21	1.63	A	Kolmogorov-Smirnov
	"	65.97	37.57	NA	Chi-square
±20.0%, 6EO	Gamma	1.04	1.63	A	Kolmogorov-Smirnov
	"	26.69	37.57	A	Chi-square
±20.0%, 13EO	Gaussian	0.68	1.63	A	Kolmogorov-Smirnov
	"	18.03	36.19	A	Chi-square
±30.0%, 3EO	Weibull	1.07	1.63	A	Kolmogorov-Smirnov
	"	43.14	37.57	NA	Chi-square
±30.0%, 6EO	Weibull	1.34	1.63	A	Kolmogorov-Smirnov
	"	60.78	37.57	NA	Chi-square
±30.0%, 13EO	Beta	0.86	1.63	A	Kolmogorov-Smirnov
	"	43.90	37.57	NA	Chi-square
±40.0%, 3EO	Extreme	0.99	1.63	A	Kolmogorov-Smirnov
	"	46.24	33.41	NA	Chi-square
±40.0%, 6EO	Extreme	1.19	1.63	A	Kolmogorov-Smirnov
	"	67.02	36.19	NA	Chi-square
±40.0%, 13EO	Weibull	0.53	1.63	A	Kolmogorov-Smirnov
	"	19.28	33.41	A	Chi-square